

LEVEL #

(12)

ADA 079620

DDC  
RECEIVED  
JUN 16 1990  
A

STATEMENT N

Approved for public release;  
Distribution Unlimited

### COVER MOTIF

The illustrations on the cover highlight significant developments and issues affecting current interest and understanding of near-millimeter wave propagation phenomena.

- Gaut and Reifstein empirical correction term to account for the discrepancy between calculated and measured  $H_2O$  absorption for frequencies below 1000 GHz.
- First published spectrum of atmospheric transmission at near-millimeter wavelengths—H. Alastair Gebbie, *Phys. Rev.*, 1957.
- Weather chart station symbol indicating meteorological conditions which motivate consideration of near-millimeter remote sensing for military applications.
- $H_2O$  phase diagram descriptive of the atmospheric saturation conditions occurring in weather scenarios of interest.
- Equation for the combustion of white phosphorus. The pentoxide formed is extremely hygroscopic, generating dense clouds of smoke capable of screening military targets from weapon systems operating in the visible and infrared.

LEVEL

(12)

UNCLASSIFIED

SECURITY CLASSIFICATION OF THIS PAGE (When Data Entered)

REPORT DOCUMENTATION PAGE		READ INSTRUCTIONS BEFORE COMPLETING FORM	
1. AUTHOR NUMBER <b>(14)</b> HDL-SR-79-8- <del>4701-1</del>	2. GOVT ACCESSION NO.	3. RECIPIENT'S CATALOG NUMBER	
4. TITLE (and Subtitle) <b>(6)</b> Near-Millimeter Wave Technology Base Study: Volume I Propagation and Target/ Background Characteristics	5. TYPE OF REPORT & PERIOD COVERED <b>(9)</b> Special Report		
6. AUTHOR(s) <b>(10)</b> Stanley M. Kulpa Edward A. Brown	7. CONTROLLING OFFICE NAME AND ADDRESS DA: <b>(11)</b> IL161162AH44		
8. PERFORMING ORGANIZATION NAME AND ADDRESS Harry Diamond Laboratories 2800 Powder Mill Road Adelphi, MD 20783	9. PROGRAM ELEMENT, PROJECT, TASK AREA & WORK UNIT NUMBERS Program Ele: 6.11.02.A		
11. CONTROLLING OFFICE NAME AND ADDRESS U.S. Army Materiel Development and Readiness Command Alexandria, VA 22333  Defense Advanced Research Projects Agency Arlington, VA 22209	10. REPORT DATE <b>(11)</b> November 1979		
	12. NUMBER OF PAGES 163		
	13. SECURITY CLASS. (of this report) UNCLASSIFIED		
14. DISTRIBUTION STATEMENT (of this Report) <b>(12)</b> Approved for public release; distribution unlimited. <b>(170)</b>			
17. DISTRIBUTION STATEMENT (of the abstract entered in Block 20, if different from Report)			
18. SUPPLEMENTARY NOTES Prepared as a result of the Near-Millimeter Wave Technology Base Study Panel, co-chaired by Drs. Kulpa and Brown at HDL during 1977, and jointly sponsored by USADARCOM and DARPA. HDL Project: A44732			
19. KEY WORDS (Continue on reverse side if necessary and identify by block number) Near-millimeter Propagation Remote sensing Submillimeter Atmosphere Transmission Millimeter wave Target signatures EHF Far infrared Background signatures XIR			
20. ABSTRACT (Continue on reverse side if necessary and identify by block number) This study is a comprehensive summary of the Near-Millimeter Wave (100 to 1000 GHz) technology base and its potential applications. The state of the art is reviewed, and technology gaps are identified. Volume I contains the results of that portion of the Study devoted to the analysis of various factors influencing atmospheric propagation and target/background signatures. Comparison is made between theoretical predictions and limited experimental data in several key areas. Topics discussed include clear air absorption, the ef-			

REC'D  
JAN 30 1980  
RECEIVED  
A

DD FORM 1 JAN 73 1473 EDITION OF 1 NOV 65 IS OBSOLETE

UNCLASSIFIED

SECURITY CLASSIFICATION OF THIS PAGE (When Data Entered)

163050

y/B

**UNCLASSIFIED**

SECURITY CLASSIFICATION OF THIS PAGE(When Data Entered)

ffects of atmospheric particulates (rain, fog, clouds, etc.), turbulence, measurement techniques, and the signature characteristics of a variety of targets and backgrounds at near-millimeter (NMM) wavelengths. A summary is given of research thrusts which would be useful in establishing a more reliable data base for evaluating near-millimeter wave systems applications. Also included is a list of facilities and organizations actively involved in this technology, plus a comprehensive reference list of current and historical literature pertinent to the material in this volume.

RE: HDL-SR-79-8, Classified References,  
Distribution Unlimited-  
No Change per Mr. Stanley M. Kulpa,  
HDL

Accession For	
NTIS GRA&I	<input checked="" type="checkbox"/>
DWG TAB	<input type="checkbox"/>
Unannounced	<input type="checkbox"/>
Justification	<input type="checkbox"/>
By	
Date	
Availability Codes	
Dist.	Avail and/or special
A	

**UNCLASSIFIED**

SECURITY CLASSIFICATION OF THIS PAGE(When Data Entered)

## ACKNOWLEDGEMENTS

The near-millimeter wave community of scientists and engineers will, for some time to come, owe a very special debt of gratitude to James A. Bender of the U.S. Army Materiel Development and Readiness Command and Stephen Zakanycz of the Defense Advanced Research Projects Agency. Their foresight, timeliness, strong support, and constant encouragement have been responsible for the planning and establishment of a major new R&D thrust in near-millimeter wave (NMMW) technology. The scientific and military impact of their efforts will surely exceed present conceptualizations, as has been the case each time man has moved into a relatively unexplored portion of the electromagnetic spectrum.

On behalf of the United States Army Materiel Development and Readiness Command and the Defense Advanced Research Projects Agency, the editors wish to express their sincere appreciation to the members of the NMMW Propagation and Target/Background Characteristics Subpanel. This group of individuals, under the able Chairmanship of Dominick A. Giglio, comprised some of the best talent available in the United States. The Army is most grateful to them, for their time, efforts, and patience.

Finally, it may be noticed that the carefully chosen motif for the cover of this report contains the first near-millimeter wave atmospheric transmission data as reported by H. Alastair Gebbie in *Physical Review*, 1957. Distance precluded Professor Gebbie's participation in the study panel meetings. However, the editors were most fortunate to have the opportunity for numerous discussions with Professor Gebbie and his colleagues, both in the United States and at Professor Gebbie's laboratory in England.

## PREFACE

The desire to "see" through limited visibility environments such as fogs, clouds, and smokes has recently motivated substantial interest in that portion of the electromagnetic spectrum having wavelengths near 1 mm. This region appears to offer an attractive compromise between the high resolution capabilities of infrared radiation and the low loss propagation characteristics of microwaves. The technology base for such millimeter/submillimeter wavelengths is, however, extremely limited.

In early 1977, the U.S. Army Materiel Development and Readiness Command (DARCOM) and the Defense Advanced Research Projects Agency (DARPA) provided support to the Harry Diamond Laboratories for a comprehensive study of the status and projected future of millimeter/submillimeter technology. With this goal in mind, the editors organized a study panel consisting of 50 scientists and engineers, from government, industry, and academia. Each of these individuals was carefully chosen on the basis of his recognized contributions to the technology.

The full panel and several subpanels met numerous times over a nine month period. Their first task, of course, was to define and bound the assigned investigation. In this regard, it was clear from the outset that two, historically distinct camps of individuals existed—those working in millimeter wave technology, and those working in submillimeter wave technology. Those with millimeter wave experience were approaching the 1 mm region technology mainly from an electronics viewpoint, whereas those with submillimeter wave experience were approaching from an optics viewpoint. Obviously, it was important to clearly define the spectral region of interest for the panel. Since the panel was requested to examine specifically that portion of the millimeter/submillimeter region wherein the technology was in its very early stages, those areas having had more significant past funding,

and thus closer to the stage of engineering development, were deemphasized. Thus, it was decided that the panel's efforts would be focused on that region bounded by the atmospheric "windows" at 100 and 1000 GHz (3 to 0.3 mm). This portion of the spectrum excluded, for example, the more developed 30-GHz region and was felt to represent the compromise between optics and microwaves mentioned earlier.

The editors, by analogy to the designation of various infrared bands, coined the name "near-millimeter" to designate that portion of the spectrum of interest. Several advantages accrued from the use of this new terminology. First, it formalized the acceptability of a common meeting ground for optics and electronics, thus encouraging a constructive interchange between millimeter and submillimeter proponents. Second, it eliminated the dual "millimeter/submillimeter" designation so frequently used to describe that region around 300 GHz. Third, it constituted a fundamental frequency band designation in powers of 10 which blended nicely with similar designations of other portions of the spectrum.

Having bounded their assigned task in terms of frequency, the "Near-Millimeter Wave Technology Base Study Panel" organized into three subpanels:

- I. Propagation and Target/Background Characteristics
- II. Components
- III. Applications

Reports were prepared in each of these areas by members of the panel. These in turn have been supplemented by considerable additional material compiled from visits, conversations, and further review of current literature by the editors.

The final output of this study effort is presented in a four-volume set, plus an executive summary. This first volume (I) deals primarily with propagation effects and target/background signatures. A Selected Bibliography, following Chapter VIII, complements the literature references found at the end of each chapter. Volume II deals with components, and Volume III deals with specific applications of the technology. A fourth volume contains classified

information relevant to the preceding three volumes. It is hoped that these volumes will be found to be useful as a general reference for researchers, system designers, and program managers whose interests extend into that portion of the spectrum wherein standard electronic and optical techniques truly overlap.

*Stanley M. Kulpa  
Edward A. Brown*

**DARCOM/DARPA**  
**NEAR-MILLIMETER WAVE TECHNOLOGY BASE STUDY**  
**VOLUME I. PROPAGATION AND TARGET/BACKGROUND**  
**CHARACTERISTICS**

**Stanley M. Kulpa and Edward A. Brown, Editors**  
**Dominick A. Giglio, Subpanel Chairman**

**Subpanel Members**

**Dominick A. Giglio, CM/CCM Center, U.S. Army Electronics Research and Development Command, Chairman**

**Edward Altshuler, U.S. Air Force, Rome Air Development Center**

**Darrell E. Burch, Ford Aeronutronic Division**

**S. Anthony Clough, U.S. Air Force Geophysical Laboratory**

**William L. Gamble, U.S. Army Missile Research and Development Command**

**Bobby D. Guenther, U.S. Army Missile Research and Development Command**

**David C. Hogg, National Oceanic and Atmospheric Administration**

**James P. Hollinger, Naval Research Laboratory**

**Robert G. Humphrey, Harry Diamond Laboratories, U.S. Army Electronics Research and Development Command**

**Robert Rohde, Night Vision and Electro-Optics Laboratory, U.S. Army Electronics Research and Development Command**

**Gwynn H. Suits, Environmental Research Institute of Michigan**

**Mary S. Tobin, Harry Diamond Laboratories, U.S. Army Electronics Research and Development Command**

**Kenneth O. White, Atmospheric Sciences Laboratory, U.S. Army Electronics Research and Development Command**

**Stephen Zakanycz, Defense Advanced Research Projects Agency**

**"The interest of the Navy and other services in this field is so great that the generation, propagation, and detection of such waves are the subject of an expanding research program in the Department of Defense today."**

**Rear Admiral R. Bennett, ONR  
Symposium on Millimeter Waves  
Polytechnic Institute of Brooklyn  
31 March 1959**

**"Now is the time for you workers in the field to come out of hiding and be counted! All is forgiven!"**

**Leonard R. Weisberg, OUSDRE  
Proceedings of the Sixth DARPA/Tri-Service  
Millimeter Wave Conference  
29 November 1977**

## CONTENTS

	Page
I INTRODUCTION AND OVERVIEW .....	1
II PROPAGATION THROUGH THE CLEAR ATMOSPHERE .....	31
III PROPAGATION IN THE PRESENCE OF NATURALLY OCCURRING PARTICULATES .....	53
IV ADDITIONAL METEOROLOGICAL INFORMATION .....	75
V PROPAGATION IN SMOKE AND CHAFF .....	83
VI TARGETS AND BACKGROUNDS .....	85
VII MEASUREMENT TECHNIQUES AND CAPABILITIES .....	125
VIII CONCLUDING REMARKS .....	145
IX SELECTED BIBLIOGRAPHY .....	153

**CHAPTER I.—INTRODUCTION AND OVERVIEW**

**by Stanley M. Kulpa and Edward A. Brown**

## CONTENTS

	Page
I-1. CLEAR ATMOSPHERE EFFECTS .....	5
I-2. HYDROMETEOR EFFECTS .....	11
I-3. TURBULENCE EFFECTS .....	19
I-4. ANTENNA EFFECTS .....	25
LITERATURE CITED .....	26

It is the intent of this chapter to provide material which complements and somewhat expands the areas discussed in the following chapters. Since the various other chapters were completed, the editors have had the opportunity to discuss and review considerable additional material. Important highlights of this material are presented in this chapter, with numerous recent references otherwise not found in the text. By presenting the additional material, the editors hope to provide an up-to-date volume which will be interesting, informative, and valuable for the newcomers to near-millimeter wave technology as well as for those whose expertise in NMMW propagation and signature effects exceeds that of the editors.

### 1-1. CLEAR ATMOSPHERE EFFECTS

The near-millimeter portion of the electromagnetic spectrum, as originally defined by the editors, spans the region bounded by the atmospheric "windows" at 100 and 1000 GHz. Near sea level, the principal molecular absorbers in this region are  $H_2O$  and  $O_2$ . The oxygen lines centered at 60 and 118 GHz add to the water absorption spectrum which is composed of numerous lines extending into the infrared. When one attempts to compare the limited experimental data for atmospheric  $H_2O$  with existing theories, it is found that, invariably, measured absorption in the window regions exceeds theory. In an excellent review article, Waters<sup>1</sup> discusses this situation in detail. Figure 1-1 shows, for example, the predicted and measured values in the region near the 22- and 183-GHz lines. Both the Van Vleck-Weisskopf and the Gross line shapes fail to give adequate absorption, except near line center. A similar situation is found for other windows, for example, 345 and 415 GHz, etc, in the water absorption spectrum. The discrepancy between the Gross line-shape predictions and measurements appears, within 10 percent, to be describable by a correction term which is proportional to the

<sup>1</sup>J. W. Waters, *Absorption and Emission by Atmospheric Gases, Methods of Experimental Physics*, vol. 12, Part B, Ch 2.3, M. L. Meeks, Ed., Academic Press (1976).

square of the frequency. Gaut and Reifstein<sup>2</sup> proposed an empirical correction term,  $\Delta a_v$ , of the form

$$\Delta a_v = 4.69 \times 10^{-4} \left( \frac{300}{T} \right)^{2.1} \left( \frac{P}{1000} \right) \nu^2 \text{ (dB/km)}. \quad (1)$$

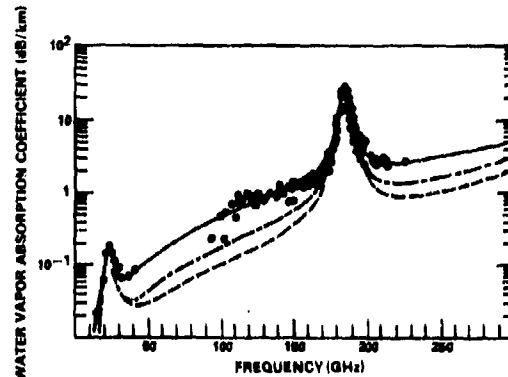


Figure 1-1. Comparison of calculated and measured water-vapor absorption;  $\rho_{H_2O} = 7.5 \text{ g/m}^3$ ,  $T = 300 \text{ K}$ , and  $P = 1013 \text{ mbar}$ . Van Vleck-Weisskopf line shape (---), Gross line shape (— · — ·), Gross line shape with added empirical correction (—), measured values ( $\bullet$ ).

As shown in figure 1-1, this added term, for 300 K and 1000 mbar pressure, yields close agreement with measured values. In fact, as shown in figure 1-2, the discrepancy between measured points and calculated absorption closely follows the empirical correction term (solid line in the figure) throughout the near-millimeter region. The validity of this term at other temperatures and pressures has, however, not been tested experimentally.

The "excess" absorption, sometimes referred to as anomalous absorption, bears a striking similarity to the IR continuum absorption as discussed by Carlon.<sup>3,4</sup> Its origin is not currently understood. A possible source<sup>1</sup> of discrepancy

<sup>2</sup>N. E. Gaut and E. C. Reifstein, III, *Environmental Research and Technology Report 13*, Lexington, MA (1971).

<sup>3</sup>H. R. Carlon, *Phase Transition Changes in the Molecular Absorption Coefficient of Water in the Infrared: Evidence for Clusters*, *Applied Optics*, vol. 17, no. 20 (15 October 1978), 3192-3193.

<sup>4</sup>H. R. Carlon, *Molecular Interpretation of the IR Water Vapour Continuum: Comments*, *Applied Optics*, vol. 17, no. 20 (15 October 1978), 3193-3195.

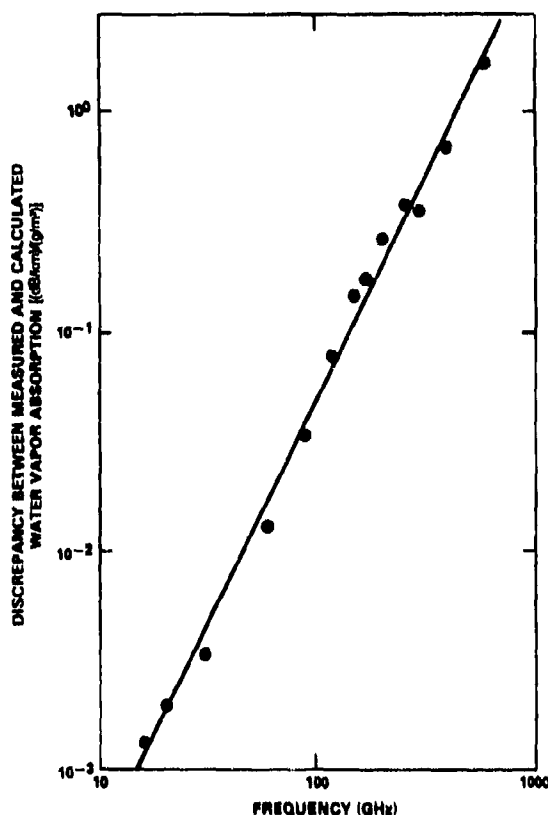


Figure I-2. Discrepancy between measured and calculated (Gross line shape) atmospheric water vapor absorption. Solid line is the empirical correction term for a water vapor density of  $1 \text{ g/m}^3$ .  $T = 300 \text{ K}$ ,  $P = 1000 \text{ mbar}$ .

between the measured and calculated absorption values may depend upon the impact assumption used in deriving the collision line shapes. Instantaneous collisions are assumed, thus neglecting any effects that occur within the duration of the time of the collision. Figure I-2, however, suggests that this assumption may be responsible for the excess absorption that is observed. This may be seen through the following arguments. Ben-Reuven<sup>6</sup> has shown that the absorption should be proportional to  $\nu^2$  multiplied by the Fourier transform of the autocorrelation function of the dipole moments. Figure I-2 therefore implies that

<sup>6</sup>A. Ben-Reuven, *Advances in Atomic and Molecular Physics*, vol. 5 (1969), 201.

this transform is constant over a frequency range of at least  $10^{12} \text{ Hz}$ . Thus, an excess dipole moment may exist for a time shorter than typical collision times of  $10^{-12} \text{ s}$ .

Figure I-3 shows the results of chamber absorption measurements by Llewellyn-Jones, Knight, and Gebbie at 213 GHz.<sup>4</sup> An excess component with quadratic water vapor pressure dependence is clearly evident, which strongly suggests an interaction involving more than one water molecule. The temperature dependence of this quadratic factor (fig. I-4) is considerably larger than that predicted for equilibrium dimers.<sup>4</sup> An explanation for this is being sought in terms of non-equilibrium species. In general, as discussed by Carlon,<sup>4</sup> the temperature and pressure dependence of water vapor absorption may be considered more complex than that predicted for monomer species. It seems that aside from line shape changes for explaining the excess absorption, polymolecular or cluster-type phenomena may be important, especially for low-temperature, high humidity conditions.

Field measurements in the near-millimeter region are extremely few in number. Of the data shown in figures I-1 to -4, only those points in figure I-1 near 183 GHz are field data, whereas the remainder are results from laboratory measurements. Those points near 183 GHz are the results of numerous workers, with attempts to reduce the data to common meteorological conditions. Other field studies which highlight some of the important propagation issues are best discussed in terms of either horizontal- or vertical-looking measurements.

Hogg's and Westwater's recent horizontal studies at 70 and 80 GHz<sup>7,8</sup> the results of which

<sup>4</sup>H. R. Carlon, *Molecular Interpretation of the IR Water Vapour Continuum: Comments*, *Applied Optics*, vol. 17, no. 20 (15 October 1978), 3193-3195.

<sup>4</sup>D. T. Llewellyn-Jones, R. J. Knight, and H. A. Gebbie, *Absorption by Water Vapour at  $7.1 \text{ cm}^{-1}$  and its Temperature Dependence*, *Nature*, vol. 274 (August 1978), 876-878.

<sup>7</sup>E. R. Westwater and D. C. Hogg, *Evidence for the Quadratic Dependence on Water Vapor of the Microwave Absorption Coefficient of Moist Air*, presented at the URSI-National Radio Science Meeting, Boulder, CO (January 1978).

<sup>8</sup>D. C. Hogg, *Measurements of 70- and 80-GHz Attenuation by Water Vapor on a Terrestrial Path*, presented at the URSI-National Radio Science Meeting, Boulder, Co (January 1978).

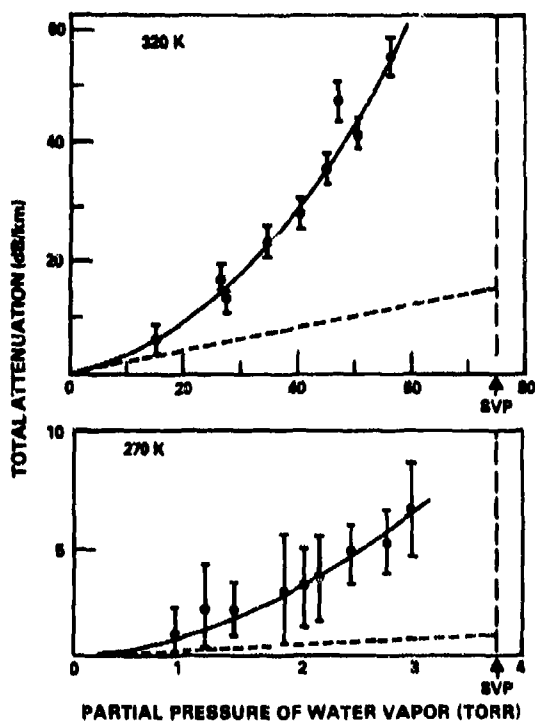


Figure I-3. Measured 213-GHz water vapor absorption dependence on the partial pressure of water vapor plus 700 torr of nitrogen. The dashed line corresponds to monomer predictions.

are shown in figure I-5, strongly support the evidence of a square-law dependence on water vapor content. If, in fact, one attempts to describe the data with a linear fit, the resultant absorption for zero humidity is not consistent with the remaining oxygen absorption.

Gebbie et al.<sup>9,10,\*</sup> have reported horizontal path measurements which indicate considerable structure in the absorption windows (fig. I-6). They have concluded that their field measure-

<sup>9</sup>R. J. Emery, P. Moffat, R. A. Bohlander, and H.A. Gebbie, *Measurements of Anomalous Absorption in the Wavenumber Range 4 cm<sup>-1</sup> - 15 cm<sup>-1</sup>*, *Journal of Atmospheric and Terrestrial Physics*, vol. 37 (1975), 587-594.

<sup>10</sup>R. J. Emery, A. Zavody, and H. A. Gebbie, *Further Measurements of Anomalous Atmospheric Absorption in the Range 4 cm<sup>-1</sup> - 15 cm<sup>-1</sup>*, *Journal of Atmospheric and Terrestrial Physics* (submitted for publication).

\*H. A. Gebbie, private communication (February 1978).

ments indicate an absorption, in excess of the monomer contribution, which

- (1) Is variable in both strength and spectral distribution,
- (2) Does not appear to depend in any simple way on the standard meteorological variables of temperature or water vapor density,
- (3) Is strongest at high levels of saturation and appears to be particularly so when liquid water or ice is present along with vapor in or near the absorbing path,
- (4) For a given amount of water, increases rapidly with decreasing temperature, and
- (5) Generally shows greater anomalous absorption than laboratory measurements.

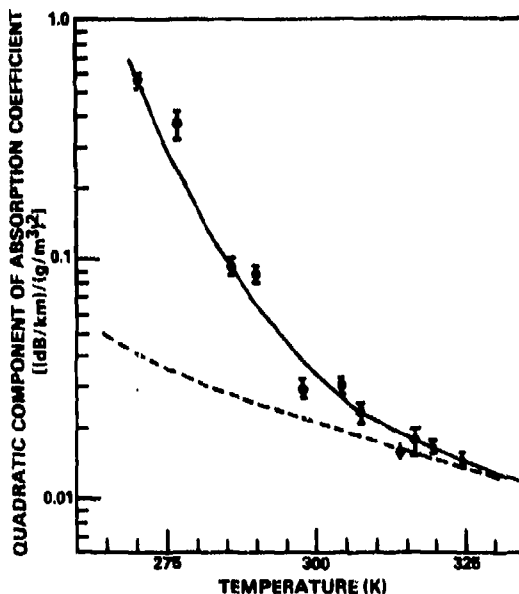


Figure I-4. Measured temperature dependence of quadratic water-vapor absorption components at 213 GHz. The dashed line refers to predicted absorption of equilibrium dimers having a binding energy of 0.16 eV.

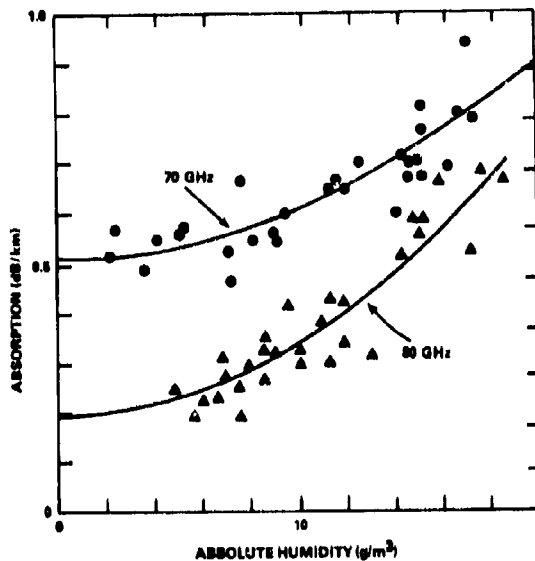


Figure I-5. Measured dependence of terrestrial path (1.5 km) absorption on absolute humidity.

Some of these phenomena may be attributable to the difficulty of absolute calibration and to the fact that extremely long integration times were used in performing the Fourier transform spectroscopy. It is generally agreed that during these times (of about 20 to 30 min), local meteorological conditions can change considerably and thus account for the lack of reproducibility. What are important, however, are the strong absorption increases which consistently become more apparent at low temperatures and near saturation. After all, it is these very conditions which will prevail in a foggy European environment wherein near-millimeter waves are postulated to be useful for remote sensing.

When investigating the different results reported for vertical propagation effects, one finds a situation quite similar to that of the horizontal studies. Figure I-7 shows the results of

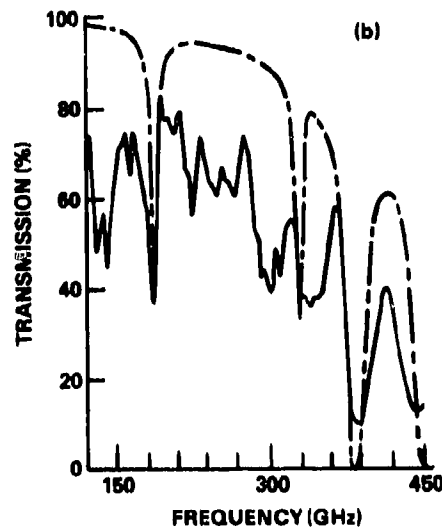
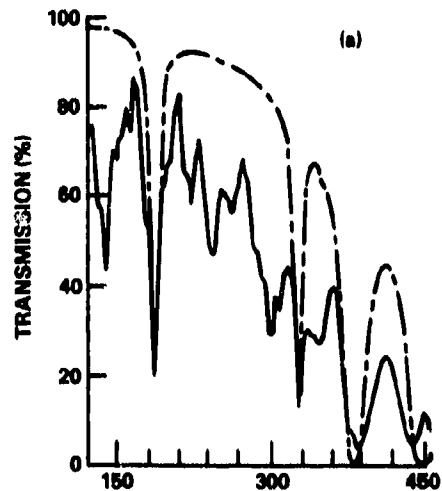


Figure I-6. Atmospheric transmission over a 216-m path; (a) mean temperature of 9 C, relative humidity = 95 percent, 1.85-mm precipitable water, (b) mean temperature of 2 C, relative humidity = 82 percent, 1.0-mm precipitable water. (---) indicates calculated monomer spectrum in both cases.

zenith opacity calculations reported in Waters review.<sup>1</sup> For comparison, Gebbie's et al transmission measurement above Mauna Kea<sup>11</sup> is shown in figure I-8, together with predicted values. Again, one may note the "excess," structured absorption in the atmospheric windows. As for the horizontal experiments, controversy over these results centers about the absolute calibration techniques used and the long integration times (30 min) required for adequate signal recovery.

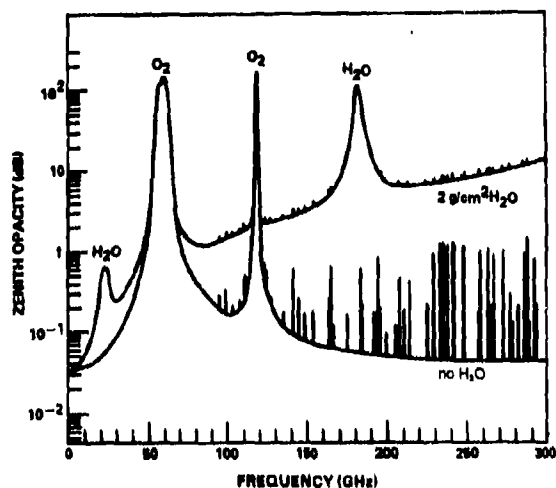


Figure I-7. Atmospheric zenith opacity from sea level calculated with water vapor, oxygen, and ozone absorption contributions. Model utilizes 1962 Standard Atmosphere, Gross line shapes, and empirical correction term. Curve including water effects assumes a 10-g/m<sup>2</sup> surface density with 2-km scale height. The narrow lines most apparent for the case of no water are attributable to ozone.

<sup>1</sup>J. W. Waters, *Absorption and Emission by Atmospheric Gases, Methods of Experimental Physics*, vol. 12, Part B, Ch 2.3, M. L. Meeks, Ed., Academic Press (1976).

<sup>11</sup>P. H. Moffat, R. A. Bohlander, W. R. Macrae, and H. A. Gebbie, *Atmosphere Absorption between 4 and 30 cm<sup>-1</sup> Measured Above Mauna Kea*, *Nature*, vol. 269 (October 1977), 676-677.

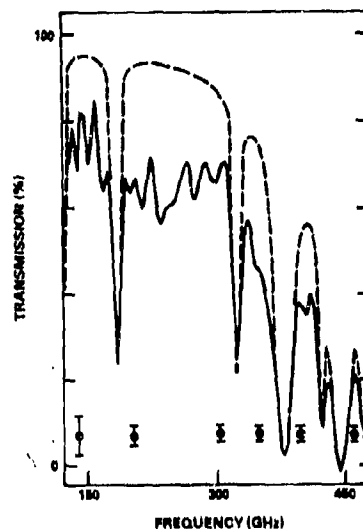


Figure I-8. Atmospheric transmission measured at Mauna Kea, zenith angle, 55 deg. Solid curve represents nine-day average with mean water vapor content of 1.9-mm precipitable water in path. Dashed curve is theoretically predicted absorption. Displaced error bars represent a standard deviation of noise on the spectra.

Recently, Hills et al<sup>12</sup> have begun to report on their Fourier transform measurements of absolute absorption and emission in the range of 100 to 1000 GHz. Using liquid helium-cooled detectors and very careful calibration procedures, they have obtained typical vertical measurements, such as that shown in figure I-9.\* The absence of structured absorption in these experiments is striking. Hills feels that his

<sup>12</sup>R. E. Hills, A. S. Webster, D. A. Alston, P. L. R. Morse, C. C. Zammitt, D. H. Martin, D. P. Rice, and E. I. Robson, *Absolute Measurements of Atmospheric Emission and Absorption in the Range 100 - 1000 GHz*, reported at the Third International Conference on SMM Waves (April 1978); published in *Infrared Physics*, vol. 18, no. 5/6 (1978), 819-825.

\*R. E. Hills, Mullard Radio Astronomy Observatory, Cambridge, England, private communication (December 1978).

measurements are generally consistent (see fig. I-10) with the predictions as discussed in Waters' article. These calculations, it should be remembered, utilize the Gross line shape and the empirical  $\nu^2$  correction term discussed earlier. It should also be mentioned that relatively short integration times ( $\sim 6$  min) were possible in these experiments, thus reducing the effects of meteorological variability.

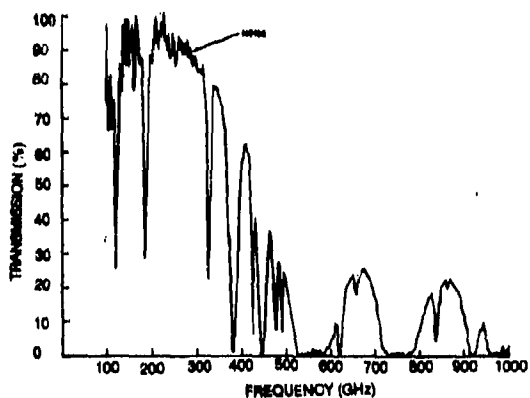


Figure I-9. Zenith transmission spectrum measured by Hills et al at Tenerife (3-GHz resolution, linear apodization, 6-min integration time).

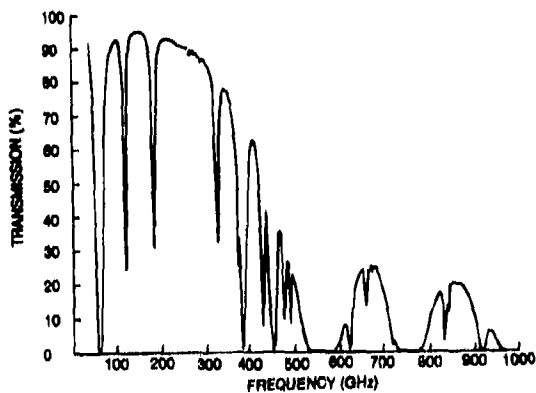


Figure I-10. Zenith transmission spectrum at Tenerife as calculated by Hills et al. Calculations include the effects of  $O_2$ ,  $H_2O$ , and  $O_3$  with Gross line shapes and the empirical correction term. Altitude 2.4 km, water content 1 mm, scale height 2 km, and results smoothed to 3-GHz resolution.

Only a few single-frequency measurements have been reported on zenith opacity in the near-millimeter wave region.<sup>12-14</sup> In an attempt to correlate measured absorption with the total precipitable water content along the vertical path, the assumption is often made that the content is linearly proportional to the surface humidity. As discussed in Waters' and Wrixon,<sup>14</sup> such an assumption can be of limited validity. Since, however, real-time simultaneous measurements of condensed water have not yet been made, the surface density correlation is often used. Ideally, the method of choice would be to use dual-channel radiometry for real-time measurement of vapor and condensed water along the observation path.

Plambeck's<sup>13</sup> 225-GHz measurements from a 1-km site elevation are shown in figure I-11. From that height, theory predicts zenith absorption,  $A$ , whose dependence on the surface water vapor density,  $q$ , varies as

$$A(\text{dB}) = 0.50 q \quad (2)$$

Figure I-11 shows a reasonably good correlation with this prediction if the observations through cloud and rain cover are excluded.

For observations from sea level, the theory predicts

$$A(\text{dB}) = 0.54 q \quad (3)$$

<sup>12</sup>J. W. Waters *Absorption and Emission by Atmospheric Gases, Methods of Experimental Physics*, vol. 12, Part B, Ch 2.3, M. L. Meeks, Ed., Academic Press (1976).

<sup>13</sup>R. L. Plambeck, *Measurements of Atmospheric Attenuation near 225 GHz: Correlation with Surface Water Vapor Density*, IEEE Transactions on Antennas and Propagation, vol. AP-26 (September 1978), 737-738.

<sup>14</sup>G. T. Wrixon and R. W. McMillan, *Measurements of Earth-Space Attenuation at 230 GHz*, IEEE Transactions on Microwave Theory and Techniques, vol. MTT-26, no. 6 (June 1978), 434-439.

<sup>15</sup>F. I. Shimabukuro and E. E. Epstein, *Attenuation and Emission of the Atmosphere at 3.3 mm*, IEEE Transactions on Antennas and Propagation, vol. AP-18 (1970), 485.

<sup>16</sup>A. V. Sokolov, E. V. Sukhonin, and I. A. Iskhakov, *Attenuation of Radio Waves at Wavelengths from 0.45 to 4.0 mm in the Earth's Atmosphere through the Slant Paths*, presented at the Second International Conference on SMM Waves, San Juan (December 1976).

Wron and McMillan<sup>14</sup> have, however, found that 30-GHz clear sky attenuation measurements from Holmdel, NJ, yield

$$A(\text{dB}) = 0.35 q \quad (4)$$

The source of this discrepancy is not clear, though it may be related to the surface water vapor correlation as discussed earlier.

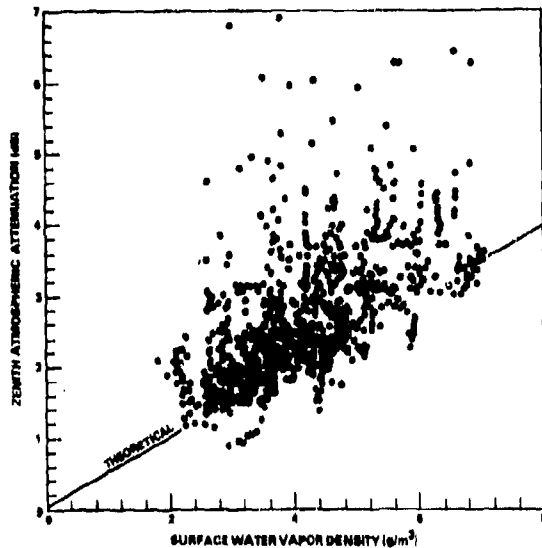


Figure I-11. Zenith opacity measured near 225 GHz versus surface water density. Much of the scatter is due to fluctuations in the distribution of water vapor within the atmosphere, but most points lying more than 1 dB above the theoretical curve were obtained when looking through heavy cumulus clouds or rain showers. The theoretical curve was calculated as described by Waters, using a 1-km site elevation and a 2-km scale height for the water distribution in the atmosphere.

<sup>14</sup>G. T. Wron and R. W. McMillan, Measurements of Earth-Space Attenuation at 230 GHz, IEEE Transactions on Microwave Theory and Techniques, vol. MTT-26, no. 6 (June 1978), 434-439.

It is interesting<sup>15</sup> that, at 225 GHz, the contribution from the empirical  $v^2$  correction term required to match theory and experiment is approximately 85 percent of the total absorption. The importance of understanding the physical origin of this term should, therefore, be clear.

Figures I-12<sup>16</sup> and -13<sup>16</sup> show additional zenith absorption measurements near the 100- and 1000-GHz boundaries of the near-millimeter region. In both figures, the best straight-line fit to the data is indicated.

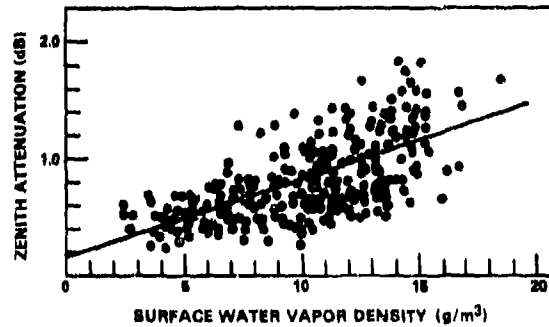


Figure I-12. Zenith opacity measured at 90 GHz versus surface water vapor density. Straight line is  $a(\text{dB}) = 0.17 + 0.06 q(\text{g/m}^3)$ .

## I-2. HYDROMETEOR EFFECTS

As discussed earlier, near-millimeter wave technology is of interest primarily since near-millimeter waves seem to offer the potential of being able to "see" through fogs, clouds, and

<sup>15</sup>R. L. Plambeck, Measurements of Atmospheric Attenuation near 225 GHz: Correlation with Surface Water Vapor Density, IEEE Transactions on Antennas and Propagation, vol. AP-26 (September 1978), 737-738.

<sup>16</sup>F. I. Shimabukuro and E. E. Epstein, Attenuation and Emission of the Atmosphere at 3.3 mm, IEEE Transactions on Antennas and Propagation, vol. AP-18 (1970), 485

<sup>16</sup>A. V. Sokolov, E. V. Sukhonin, and I. A. Iskhakov, Attenuation of Radio Waves at Wavelengths from 0.45 to 4.0 mm in the Earth's Atmosphere through the Slant Paths, presented at the Second International Conference on SMM Waves, San Juan (December 1978).

smoke. Basically, fogs and clouds consist of condensed water droplets or ice crystals suspended in a medium of high relative humidity and, frequently, low temperatures. It should be recalled that these conditions are similar to those under which our understanding of clear air propagation is probably the poorest. Thus, for properly interpreting measurements in a given meteorological environment one is left with the important problem of separating the attenuation effects of water vapor near saturation conditions and those of precipitating water liquid or ice.

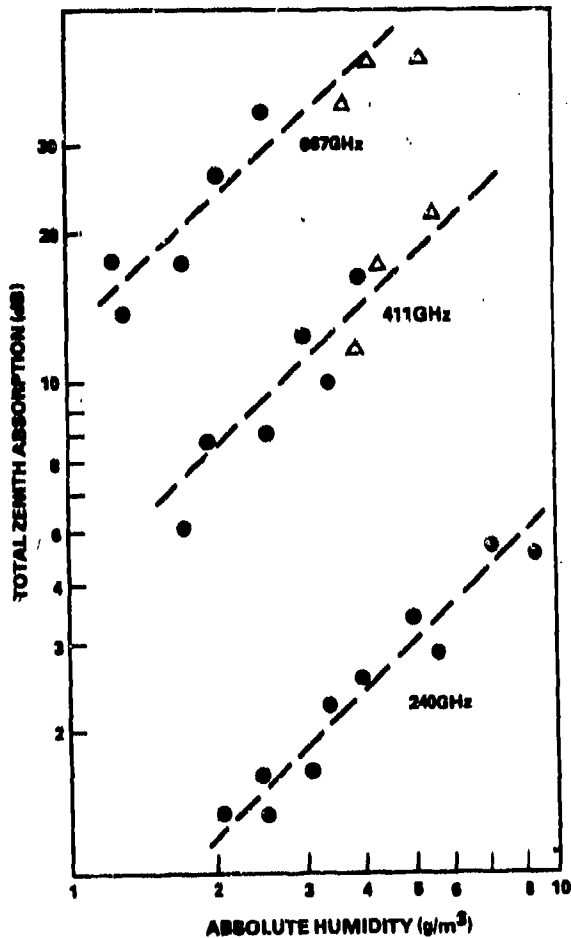


Figure I-13. Zenith opacity measured at 240, 411, and 667 GHz versus surface water density. Dotted points measured by solar transmission and triangle points measured by atmospheric emission.

Experimental fog and cloud data in the NMMW portion of the spectrum are almost nonexistent. Richard et al.<sup>17</sup> at the Ballistic Research Laboratories (BRL) have performed fog measurements over a 725-m land path and compared those (fig. I-14) with Robinson's measurements at 35 GHz.<sup>18</sup> In both cases, apparatus was not available to properly characterize the fog by particle density and size distributions. Instead, the fogs were described by transmissometer measurements of visibility accurate to  $\pm 10$  percent. As can be seen from the figure, there is a considerable scatter of data points when characterizing the fog by its visibility. This is not surprising since, at near-millimeter wavelength, when drop sizes are small compared with the wavelength, the attenuation is not very sensitive to the drop size whereas, at optical wavelength, it is very sensitive to drop size. In both the 35- and the 140-GHz cases, the attenua-

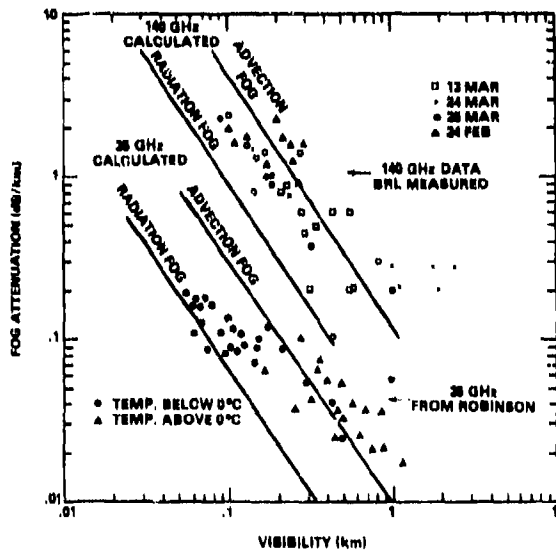


Figure I-14. Measured and calculated fog attenuation at 35 and 140 GHz.

<sup>17</sup>V. W. Richard, J. E. Kammerer, and R. G. Reitz, 140-GHz Attenuation and Optical Visibility Measurements of Fog, Rain, and Snow, U. S. Army Ballistic Laboratories Memorandum Report ARBRL-MR-2800 (December 1977).

<sup>18</sup>N. P. Robinson, Measurements of the Effect of Rain, Snow, and Fogs on 8.6-mm Radar Echoes, Proc. IEE, London, vol. 203B (September 1955), 709-714.

tions measured are larger than that predicted for radiation fogs which more commonly occur over land paths.

It is important to recognize that throughout this discussion of reported measurements of attenuation by hydrometeors (fogs, clouds, rain, snow, and hail), no meteorological measurements have been made to allow separation of absorption effects due to water vapor, liquid, and ice along the propagation path. What is normally reported is the "additional" attenuation apparently due to the hydrometeors, thus neglecting vapor absorption effects which, as discussed earlier, become particularly confusing near saturation. Another problem discussed briefly in Chapter III centers about the dielectric constant data of water and ice for use in theoretical predictions of attenuation. There is significant variability<sup>17</sup> in these data, particularly for temperatures lower than 20 C and for the higher frequencies.

Emery, Zavody, and Gebbie<sup>10</sup> have recently performed broadband fog attenuation measurements using the Fourier transform system discussed earlier. Results of these measurements are shown in figures I-15 and -16. As for the clear air spectra, structured spectral features which do not match predictions are seen in the window regions. The level of structure was observed to correlate with fog density on a number of occasions, an example of which is shown in figure I-16. Three consecutive measured spectra are shown in conditions where the fog density was slowly increasing. Structure in the window region is clearly seen to be building up with the fog density. Aside from these features, the overall attenuation levels at 230, 345, and 415 GHz appear to be very substantial.

<sup>10</sup>R. J. Emery, A. Zavody, and H. A. Gebbie, *Further Measurements of Anomalous Atmospheric Absorption in the Range  $4\text{ cm}^{-1} - 15\text{ cm}^{-1}$* , *Journal of Atmospheric and Terrestrial Physics* (submitted for publication).

<sup>17</sup>V. W. Richard, J. E. Kammerer, and R. G. Reitz, *140-GHz Attenuation and Optical Visibility Measurements of Fog, Rain, and Snow*, U.S. Army Ballistic Research Laboratories Memorandum Report, ARBRL-MR-2800 (December 1977).

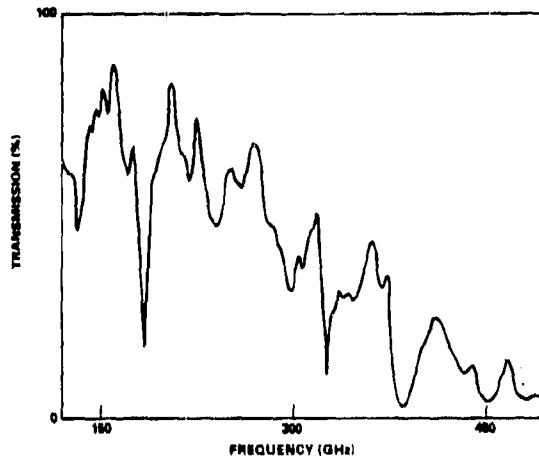


Figure I-15. Broadband Fourier transform measurements of fog transmission. Visibility approximately 50 m, 216-m path, Temp = 283 K, relative humidity = 95 percent. (Data obtained from H. A. Gebbie, private communication, 1978).

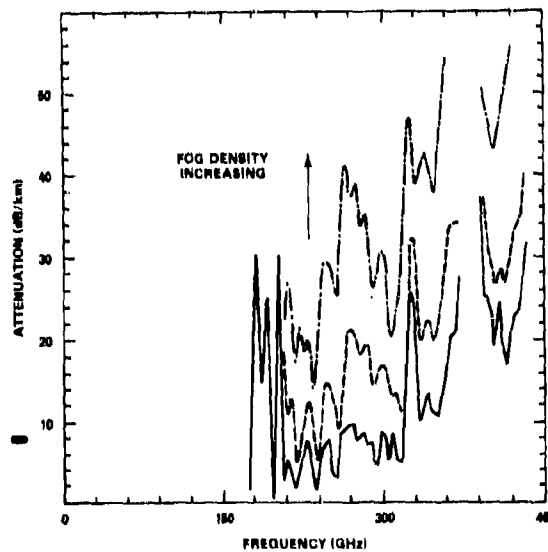


Figure I-16. Broadband Fourier transform measurements through an evolving fog. (Data obtained from H. A. Gebbie, private communication, May 1978).

The data are very limited for characterizing NMMW attenuation effects in clouds. The Soviets<sup>16,19</sup> have reported on a number of zenith cloud attenuation measurements using atmospheric emission and solar absorption techniques. The results of measurements of the average attenuation values at 75 GHz are given in figure I-17 as dots, for six days with continuous cloudiness from April to June 1976. The crosses relate to molecular zenith absorption values calculated for a cloudless standard atmosphere. The cloud attenuation is therefore taken to be the difference between the dot and cross on a particular day. On 11 and 12 May 1976, in the presence of high stratus and undeveloped cumulus clouds, the attenuation at 75 GHz is negligible. On 10 May, in the presence of low continuous cloudiness with fractus stratus and cumulus clouds, the attenuation reached 4 dB. On 29 April and 2 and 7 June, in the presence of stratus-cumulus and stratus clouds, the attenuation was approximately 1.5 dB.

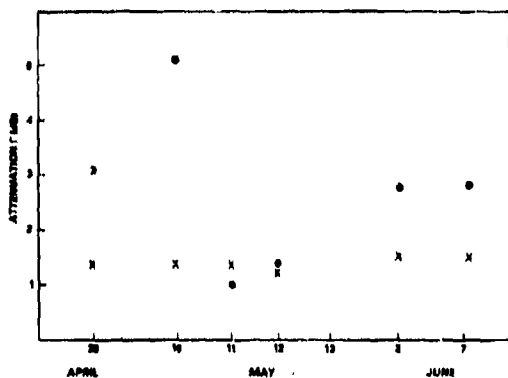


Figure I-17. Zenith cloud attenuation measurements at 75 GHz. Dots are the measured total zenith atmospheric attenuation values for six days with continuous cloudiness in April-June 1976. The crosses represent the calculated contribution from a cloudless atmosphere.

<sup>16</sup>A. V. Sokolov, E. V. Sukhonin, and I. A. Iskhakov, Attenuation of Radio Waves at Wavelengths from 0.45 to 4.0 mm in the Earth's Atmosphere Through the Slant Paths, presented at the second International Conference on SMM Waves, San Juan (December 1976).

<sup>19</sup>L. I. Fidozev, SMM Atmospheric Research in the USSR, presented at the Third International Conference on SMM Waves, Gulliford, England (April 1978).

Correlation of the single-cloud type of attenuation with frequency is a difficult task. In the same reports referenced above,<sup>16,19</sup> the Soviets have attempted to analyze their measurements so as to provide some feeling for this correlation. Table I-1 lists their results for 75, 238, 411, and 667 GHz.

TABLE I-1. MEASURED ZENITH ATTENUATION  $\Gamma$  (dB) IN CLOUDS<sup>a, b</sup>

Cloud type	Frequency (GHz)			
	75	238	411	667
Alto cumulus	—	0.16	0.6	1.9
Stratus	—	0.16	—	1.5
Cumulus	1.2	1.75	10.1	17.5
Cumulus congestus	3	8.7	27	51.0

<sup>a</sup>A. Sokolov, Sukhonin, and Iskhakov, Second International Conference on SMM Waves, San Juan (December 1976).

<sup>b</sup>L. I. Fidozev, SMM Atmospheric Research in the USSR, Third International Conference on SMM Waves, Gulliford, England (April 1978).

The reliability of such data is difficult to estimate because of the complexity of unfolding the varying meteorological conditions as discussed earlier. The significant thing to notice is the increasing attenuation with frequency and that the largest attenuations for NMMW occur for cumulus clouds.

A number of theoretical and experimental efforts have gone into the study of rain attenuation in the NMMW portion of the spectrum. Such studies are extremely important since rain may very likely be the principal limiting factor to obtaining "all-weather" NMMW systems. Unlike the situation at lower frequencies, it is not possible to accurately predict the attenuation from knowledge of rain rates alone because, at NMMW frequencies, the drop size distribution is far more important in the calculation.<sup>20</sup> Perspective on this situation may be gained by referring to figure I-18, which shows expected attenuation as a function of frequency as calculated by

<sup>20</sup>R. L. Olsen and D. V. Rogers, The  $nR^b$  Relation in the Calculation of Rain Attenuation, IEEE Transaction on Antennas and Propagation, vol. AP-26, no. 2 (March 1978), 318-329.

Llewellyn-Jones and Zavody.<sup>21</sup> They performed comparison measurements at 110 and 890 GHz and found an attenuation ratio of

$$\frac{\alpha_{890}}{\alpha_{110}} \approx 1.25 \pm 0.02 \quad (5)$$

In figure I-18,<sup>21</sup> only the Joss distribution for drizzle (very small drops) would predict an attenuation of 890 GHz significantly greater than at 110 GHz. Since the experiment was performed in summer thundershowers of about 5 to 30 mm/hr, it is unlikely that this distribution predominated, thus indicating the importance of measurement of actual drop size distribution for comparison of experiment and theory.

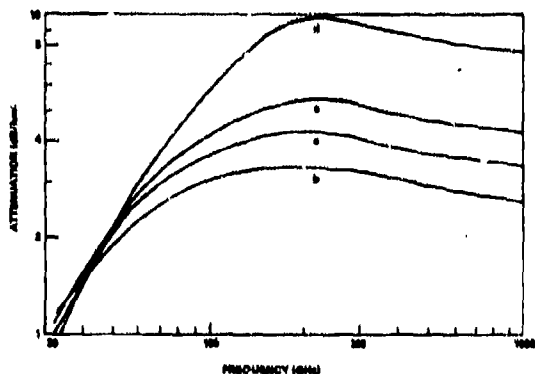


Figure I-18. Calculated rain attenuation for various drop size distributions at a rainfall rate of 5 mm/hr. (a) Laws and Parsons, (b) Joss thunderstorm, (c) Joss widespread, and (d) Joss drizzle.

Additional attenuation comparison studies performed at 36 and 110 GHz by Zavody and Harden<sup>22</sup> again clearly indicate the sensitivity to drop size distribution as well as drop shape. In both the above experiments, it should be mentioned that the path lengths were relatively short (200 m), thus, it is hoped, circumventing any question as to uniformity of rain rate along the

<sup>21</sup>D. T. Llewellyn-Jones and A. M. Zavody, Rainfall Attenuation at 110 and 890 GHz, *Electronics Letters*, vol. 7, no. 12 (1971), 321-322.  
<sup>22</sup>A. M. Zavody and B. N. Harden, Attenuation/Rain Rate Relationships at 36 and 110 GHz, *Electronics Letters*, vol. 12 (1976), 422-424.

path. Ho, Mavroukoulakis, and Cole,<sup>23</sup> on the other hand, have recently made 36- and 110-GHz comparison measurements along a 4-km path with rain rate measured near the receiver end. They find that the measured ratio for attenuations at these two frequencies is consistent with calculations based on the Laws-Parsons distribution. This is particularly true for attenuations exceeding about 3 dB/km at 110 GHz and 1.5 dB/km at 36 GHz. In this range,

$$\frac{\alpha_{110}}{\alpha_{36}} \approx 2.5 \quad (6)$$

In a recent report from the Netherlands, Keizer, Sneider, and de Haan<sup>24</sup> have made detailed studies (vertical polarization) of rain attenuation at 94 GHz on a 1000-m terrestrial path. Simultaneously, the rain drop size distribution was measured with a distrometer, and the rainfall intensity was recorded with three rapid-response rain gauges spaced 500 m apart. Using the actually measured rain drop size distribution and assuming spherical raindrops, the attenuation caused by the rain was calculated with the aid of Mie's scattering theory for water spheres. Figure I-19 shows the measured and calculated attenuations along with predictions based upon various drop size distributions. Figure I-20 expresses, in detail, the agreement between the measured attenuation and that calculated from the actually measured drop size distribution. It can be seen that the agreement between the theory and experiment is very satisfactory.

In a closely related Canadian study at 74 GHz, Kharadly, McNichol, and Peters<sup>25</sup> also demonstrate the importance of proper rain characterization. They conclude that without measured drop size distributions and rapid, path-average rain rates, it is not possible to make consistently accurate studies of rain effects. This is

<sup>23</sup>K. L. Ho, N. D. Mavroukoulakis, and R. S. Cole, Rain Induced Attenuation at 36 GHz and 110 GHz, *IEEE Transactions on Antennas and Propagation*, vol. AP-26 (November 1978), 873-875.

<sup>24</sup>W. P. M. N. Keizer, J. Sneider, and C. D. de Haan, Rain Attenuation Measurements at 94 GHz: Comparison of Theory and Experiment, NATO AGARD (Conference Proceedings No. 245 (February 1979)).

<sup>25</sup>M. M. Kharadly, J. D. McNichol, and J. B. Peters, Measurement of Attenuation Due to Rain at 74 GHz, NATO AGARD Conference Proceedings No. 245 (February 1979).

particularly evident from figure I-21 where their attenuation measurements during the time interval  $T_1$  are seen to dip to significantly lower values than during the interval  $T_2$ , the corresponding peak rain rates being comparable. The vertical component of wind velocity measured at the transmitter/receiver site, during  $T_1$ , was generally upward with peak values up to 2 m/s; during  $T_2$ , it was generally downward with peak values of 1 m/s. This affects the instantaneous concentration of smaller drops in the signal path and thus the attenuation.

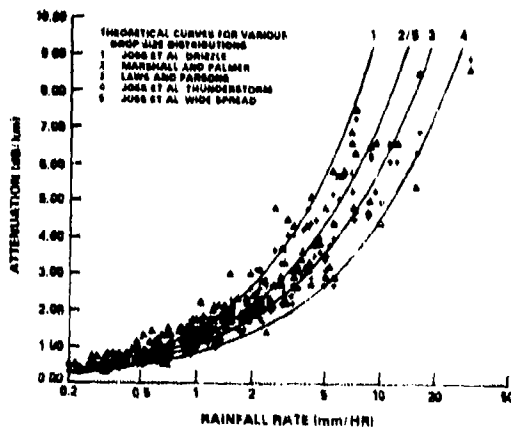


Figure I-19. Measured ( $\Delta$ ) and calculated (+) 94-GHz attenuation versus rainfall rate. Calculated values derived from measured rain drop size distribution. Path length, 1 km.

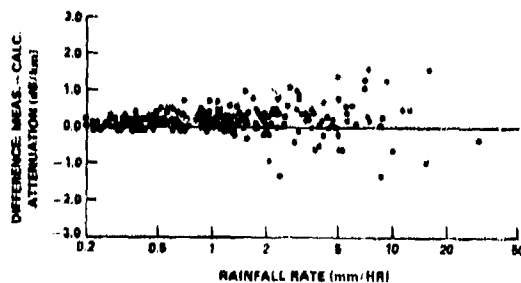


Figure I-20. Difference between measured and calculated rain attenuation at 94 GHz.

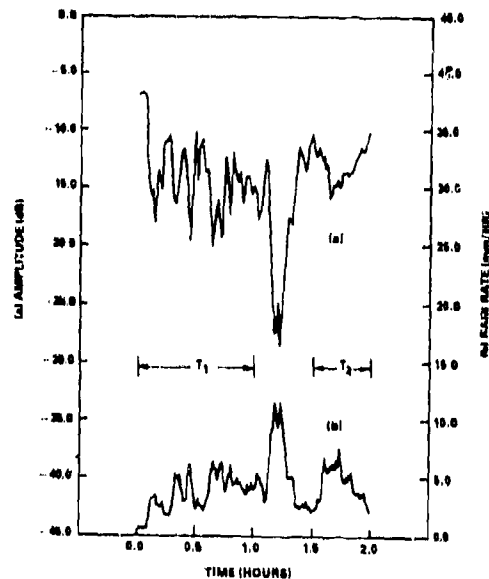


Figure I-21. Relative 74-GHz transmitted signal level and path-average rain rate versus time. Path length, 1 km.

Richard et al.<sup>17</sup> have measured rain attenuation at 140 GHz together with rainfall rate and optical visibility. Interestingly, even over their relatively short path length (700 m), the three distributed rain gauges often showed differences of up to four to one. Their attenuation measurements were performed when all three gauges gave close agreement, thus somewhat assuring a uniform rain rate. Figure I-22 shows their measurements correlated with rate. The scatter observed is roughly consistent with values spanning the various types of distributions, as shown in figure I-19. Figure I-23 shows the correlation of the 140-GHz attenuation and rain visibility measurements. The large scatter of the data indicates a weak relationship. As discussed earlier, this stems from the fact that the

<sup>17</sup>V. W. Richard, J. E. Kammerer, and R. G. Reitz, 140-GHz Attenuation and Optical Visibility Measurements of Fog, Rain, and Snow. U.S. Army Ballistic Research Laboratories Memorandum Report, ARBRL-MR-2800 (December 1977).

140-GHz attenuation strongly depends on the total water, whereas the optical visibility is more affected by the small droplets.

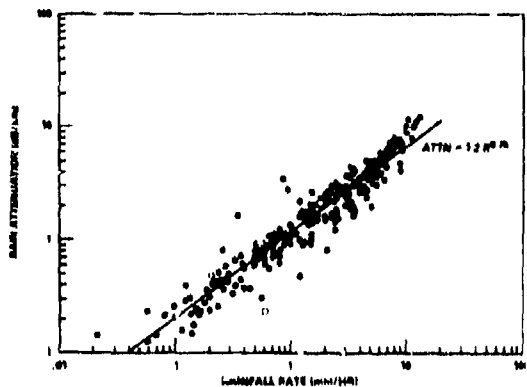


Figure I-22. Measured attenuation at 140-GHz versus rainfall rate.

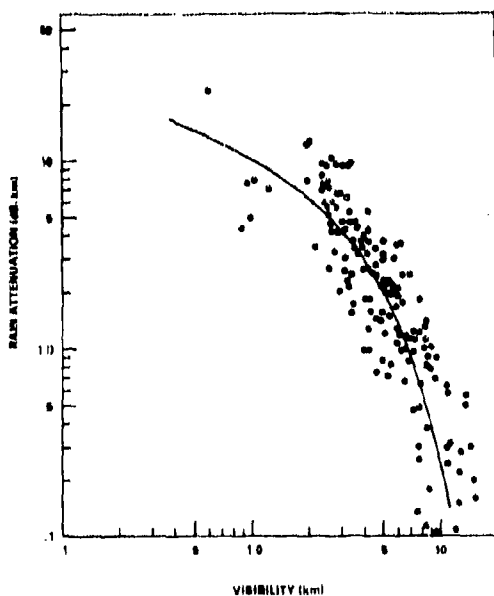


Figure I-23. Measured attenuation at 140 GHz versus visibility.

So far, the discussion of rain effects has centered on near-horizontal propagation paths. Except for some widely varying measurements at 75 GHz reported by Sokolov et al.,<sup>16</sup> no zenith or slant path rain measurements have been found. Such measurements are obviously necessary to assess the "all-weather" penetration capabilities. (In such an evaluation, attention must also be given to the often neglected fact that cloud attenuation will also be present with that of the rain.)

Richard and Kammerer of BRL have performed<sup>16</sup> rain backscatter amplitude and fluctuation measurements simultaneously at 10, 35, 70, and 95 GHz with pulse radars for both linear and circular polarization. This rather comprehensive report discusses, among other things, a particularly significant experimental verification of the expected decrease in rain backscatter above 70 GHz. The experiment verifies the long-standing theoretically predicted capability of radar to "see" a target of given size above rain clutter better at 95 GHz than at 70 or 35 GHz when the same antenna size is used. No further backscatter measurements were found for frequencies higher in the NMMW band.

Finally, in the discussion of hydrometeor effects on NMMW propagation, it is important that some attention be given to the condensation and precipitation effects on antennas. No published data have been found for condensation effects, which one would expect to become increasingly serious with increasing frequency. The BRL 140-GHz tests<sup>17</sup> have shown, however, that rain falling on the lucite window in front of the

<sup>16</sup>A. V. Sokolov, E. V. Sukhanin, and I. A. Ikhakov, *Attenuation of Radio Waves at Wavelengths from 0.45 to 4.0 mm in the Earth's Atmosphere through the Slant Paths*, presented at the Second International Conference on 5MM Waves, San Juan (December 1976).

<sup>17</sup>V. W. Richard and J. E. Kammerer, *Rain Backscatter Measurements and Theory at Millimeter Wavelengths*, U.S. Army Ballistic Research Laboratories Report No. 1838 (October 1975).

receiving antenna can cause large and variable attenuation. Measured attenuation of this wetted window versus rainfall rate is shown in figure I-24.

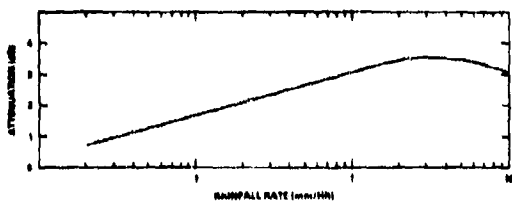


Figure I-24. Attenuation effects due to rainfall on a lucite window in front of receiving antenna used in 140-GHz measurements of figure I-22.

Keizer et al<sup>24</sup> realized from the beginning of their 94-GHz experiment that rain on the antenna or its cover represented a serious problem. Therefore, tunnel housings were used to shield their antennas. However, in order to see to what extent water on antennas and radomes can degrade the accuracy of measurements, a series of artificial wetting tests were carried out on one of the 1.2-m Cassegrain antennas. Table I-2 summarizes these measurements.

TABLE I-2. WETTING TESTS ON 1.2-m CASSEGRAIN ANTENNA AT 94 GHz

Condition	Decrease in antenna gain (dB)
Whole antenna wet	3.0 to 5.8
Only radome on feed horn wet	1.8 to 3.5
Only subreflector wet	1.4 to 2.1
Only main reflector wet	0.3 to 0.9
Only Teflon sheet in front of antenna wet	0.6 to 1.0

<sup>24</sup>V. W. Richard, J. E. Kammerer, and R. G. Reitz, 140-GHz Attenuation and Optical Visibility Measurements of Fog, Rain, and Snow. U.S. Army Ballistic Research Laboratories Memorandum Report, ARBRL-MR-2800 (December 1977).

<sup>25</sup>W. P. M. N. Keizer, J. Sijder, and C. D. de Haan, Rain Attenuation Measurements at 94 GHz: Comparison of Theory and Experiment, NATO AGARD Conference Proceedings No. 245 (February 1979).

Clearly, water on reflector antennas and radomes can cause considerable losses. A wet Teflon radome is seen to introduce much less degradation than complete wetting of the antenna and, therefore, radomes can be a useful solution for long propagation links where high rain attenuations will be encountered. However, for short links, even the use of a radome may leave the losses unacceptably high, thus requiring complete shielding of the antenna.

Richard et al<sup>27</sup> have performed 140-GHz attenuation measurements in wet snows and compared these with other frequency measurements as shown in figure I-25 (rate equivalent of 1 mm/hr liquid). Shown also on this figure are 1 mm/hr rain attenuation estimates obtained by averaging a number of calculations by different authors.<sup>28</sup> Snow attenuation is between 2.5 and 5 times greater than rain attenuation for all the frequencies measured. In general, this is due to the large, more irregular shapes of the snow precipitation and the fact that higher concentrations exist for the snow due to the low fall velocities. The attenuation of snow very strongly depends on the moisture state of the snowflakes. Lammers<sup>27</sup> reports that the measured attenuation of very dry snow at 53 GHz is only one-sixth the attenuation of rain. It can be expected that when it is very cold and the snow is dry, the attenuation will be very low, less than an equivalent rain attenuation.

Hail is encountered much less frequently than rain or snow and its duration is relatively short. Aganbekyan et al<sup>28</sup> have reported single scattering calculations for hails of varying

<sup>27</sup>V. W. Richard and J. E. Kammerer, Rain Backscatter Measurements and Theory at Millimeter Wavelengths U.S. Army Ballistic Research Laboratories Report No. 1838 (October 1975).

<sup>28</sup>U. Lammers, Investigations of the Effects of Precipitation on MM-Wave Propagation, Doctoral-Engineering Dissertation, Technik Universität Berlin, D 83 (1965), Translation by U.S. Army STC-HT-23-0298-75, Defense Intelligence Agency Task No. T741801 (1975).

<sup>29</sup>K. A. Aganbekyan, V. P. Blyarin, A. Yu. Vrazhetovskiy, A. O. Izyumov, A. V. Sokolov, and E. V. Sukhonin, The Propagation of Submillimeter, Infrared, and Visible Waves in the Earth's Atmosphere, Rasprostraneniye Radiovoln, Institut Radiotekhniki i Elektroniki, published by Nauka (1973), 187-227.

diameters and intensities, taking the complex index of refraction of ice to be  $m = 1.78 - 0.0024i$ . An example of these calculations is given in table I-3.

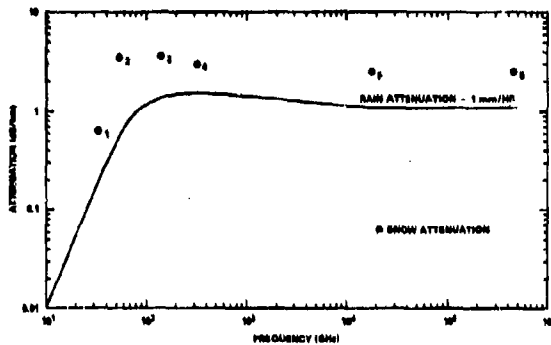


Figure I-25. Measured snow attenuations as a function of frequency. Snowfall rate of 1 mm (liquid)/hr. (1) Robinson (1955), (2) Lammers (1967), (3) BRL, (4) Babkin et al (1970), and (5) Sokolov (1970). Comparison curve shown for equivalent rainfall.

TABLE I-3. ATTENUATION IN HAIL WITH INTENSITY OF HAIL  $J = 10$  mm/hr (equivalent water)

From Aganbekyan et al, Institut Radiotekhniki i Elektroniki, published by Nauka (1975).

Hail particle diameter (mm)	Attenuation (dB/km)	
	$\lambda = 1.0$ mm	0.1 mm
2.5	2.7	2.0
5.0	0.9	0.6
10.0	0.4	0.4

No experimental data have been found in the literature, and therefore relatively little can definitely be said about hail. Obviously, hail attenuation will not depend strongly on wavelength, since the sizes of hailstones often significantly exceed  $\lambda$  in the near-millimeter region.

### I-3. TURBULENCE EFFECTS

The effects of atmospheric turbulence on NMMW propagation have only recently begun to receive attention. Frequently, one finds that such effects have been minimized because of simple extrapolation from optical studies. Such simple extensions of very complex theoretical results which are based on numerous assumptions are of questionable validity and are therefore worthy of more detailed analysis and experiment.

Articles by Fante,<sup>29</sup> Davis,<sup>30</sup> Lawrence,<sup>31</sup> and Yura<sup>32</sup> provide very nice reviews of the physical basis for various effects of atmospheric turbulence. The effects can include beam steering, image dancing, beam spreading, image blurring, intensity fluctuations, and phase fluctuations. Basically, the effects of turbulence on propagation are determined by the refractive index fluctuations along the atmospheric path. These fluctuations are, in general, functions of the position,  $\vec{r}$ , and time,  $t$ , so that the index of refraction,  $n$ , can be written as

$$n(\vec{r}, t) = 1 + n_1(\vec{r}, t), \quad (7)$$

where  $n_1$  is the fluctuation in the index of refraction. It is possible to assume that the temporal dependence of  $n_1$  is due mainly to a net transport of the inhomogeneities of the medium as a whole past the line of sight (winds) so that

$$n_1(\vec{r}, t) = n_1(\vec{r} - v(t)t), \quad (8)$$

<sup>29</sup>R. L. Fante, *Electromagnetic Beam Propagation in a Turbulent Media*, Proc. IEEE, vol. 63, no. 12 (1975), 1669-1692.

<sup>30</sup>J. I. Davis, *Consideration of Atmospheric Turbulence in Laser Systems Design*, Applied Optics, vol. 5, no. 1 (January 1966), 139-147.

<sup>31</sup>R. S. Lawrence, *A Review of the Optical Effects of Clear Turbulent Atmosphere*, SPIE, vol. 75 (1976), 2-8.

<sup>32</sup>H. T. Yura, *An Elementary Derivation of Phase Fluctuations of an Optical Wave in the Atmosphere*, SPIE, vol. 75 (1976), 9-15.

where  $v(\vec{r})$  is the local "wind" velocity. This assumption, known as the Taylor's frozen-flow hypothesis,<sup>29</sup> appears to hold in most practical cases of interest. Assuming homogeneous and isotropic conditions, the Kolmogorov model<sup>32</sup> has been used to describe the index variations. Within a particular range of separation,  $r_1$  and  $r_2$ , the model yields

$$\langle (n(\vec{r}_1) - n(\vec{r}_2))^2 \rangle = C_n^2 |\vec{r}_1 - \vec{r}_2|^{2/3} \quad (9)$$

where the brackets denote an ensemble average and  $C_n^2$  is called the index structure constant. The separation range for validity of this model (often referred to as the inertial subrange) is  $l_0 \ll |\vec{r}_1 - \vec{r}_2| \ll L_0$ , where  $L_0$  and  $l_0$  are called the outer and inner scales of turbulence, respectively.  $L_0$  and  $l_0$  may be thought of as the approximate maximum and minimum of the eddy sizes. In the atmosphere,  $l_0$  ranges from a millimeter to a centimeter and  $L_0$  for horizontal propagation in the lower atmosphere is about one-third the height above the ground. For separations larger than  $L_0$ , the mean square index fluctuation levels off to a value of the order  $C_n^2 L_0^{2/3}$  whereas, for separation less than  $l_0$ , viscosity effects cause a very rapid decrease in index fluctuations. Given this basic model, one can go on to quantify the various effects mentioned above.

Some of the important aspects of such calculations for NMM wavelengths are best discussed first in terms of intensity fluctuations. A theoretical description<sup>33</sup> requires consideration of the problem in two separate domains dependent upon the size of the outer scale of the turbulence compared to the first Fresnel zone along the propagation path of length  $R$ . These two cases are when  $L_0 < \sqrt{\lambda R}$  or  $L_0 > \sqrt{\lambda R}$ . Most rough assessments of turbulence effects in NMM waves are based on Tatarski's calculations, valid for the case  $L_0 > \sqrt{\lambda R}$ . If, however, one has a propagation range, say of 2 km with  $\lambda = 1$  mm,  $\sqrt{\lambda R} \approx 1.4$  m. With a vehicle-mounted antenna

<sup>29</sup>R. L. Fante, *Electromagnetic Beam Propagation in a Turbulent Media*, Proc. IEEE, vol. 63, no. 12 (1975), 1669-1692.

<sup>32</sup>H. T. Yura, *An Elementary Derivation of Phase Fluctuations of an Optical Wave in the Atmosphere*, SPIE, vol. 75 (1976), 9-15.

at a height,  $h$ , of 2 m, one expects<sup>34</sup>  $L_0$  to be of the order of  $h/3$  or 0.7 m, and thus in the domain where  $L_0 < \sqrt{\lambda R}$ . In addition, except for some aperture averaging estimates,<sup>30</sup> most simple calculations (plane waves) have ignored the fact that the transmitting and receiving apertures contemplated for use in tactical NMM systems have diameters of the order of 0.5 to 1 m. Thus, antenna near-field effects may be important at wavelengths of 1 mm.

No simple quantitative models of amplitude fluctuations have been found for either the case of  $L_0 < \sqrt{\lambda R}$  or for antenna near-field operations. However, the Tatarski calculations, for a plane wave with  $L_0 > \sqrt{\lambda R}$  shows the variance of the log-intensity fluctuations,  $\sigma^2$ , to be

$$\sigma^2 = \left\langle \left( 10 \log_{10} \frac{I}{I_0} \right)^2 \right\rangle = 23.39 C_n^2 k^{7/6} R^{11/6} \text{ (dB)}^2 \quad (10)$$

where  $k = 2\pi/\lambda$ . Worst-case estimates<sup>31</sup> for  $C_n^2$  are usually made on the basis of optical measurements wherein  $C_n^2 \approx 6 \times 10^{-13} \text{ m}^{-2/3}$  for strong turbulence. For this situation, equation (10) predicts minimal intensity variations for the wavelengths and ranges of interest for tactical operations wherein  $L_0 > \sqrt{\lambda R}$ . With, for example,  $\lambda = 1$  mm and a range of 2 km,  $\sigma^2 \approx 0.4$  (dB<sup>2</sup>). Under similar limitations, it is also found<sup>34</sup> that calculated phase fluctuation effects across the receiver aperture are negligible for antennas of reasonable size for tactical applications.

In utilizing optical constants for obtaining estimates of near-millimeter wave turbulence effects, one must realize that optical turbulence is

<sup>30</sup>J. I. Davis, *Consideration of Atmospheric Turbulence in Laser Systems Design*, Applied Optics, vol. 5, no. 1 (January 1966), 139-147.

<sup>31</sup>V. I. Tatarski, *Wave Propagation in a Turbulent Medium* (Translated from the Russian by R. A. Silverman), McGraw-Hill Book Co., Inc., New York (1961).

<sup>32</sup>R. S. Lawrence and J. W. Strohbach, *A Survey of Clear-Air Propagation Effects Relevant to Optical Communications*, Proceedings of IEEE, vol. 58, no. 10 (October 1970), 1523-1545.

<sup>33</sup>F. F. Hall, Jr., *Index of Refraction Structure Parameter in the Real Atmosphere—An Overview*, OSA Topical Meeting on Propagation Through Turbulence, Rain and Fog, Paper TuC1 (9 to 11 August 1977).

<sup>34</sup>J. Gallagher et al., *Application of Submillimeter Wave Gigawatt Sources*, Georgia Institute of Technology, Final Report GT/FSS, Project No. A-1717 (1975).

principally dependent upon atmospheric temperature fluctuations and that varying water vapor effects are negligible. For near-millimeter wavelengths, however, water vapor contributions to the index of refraction become important. Brown<sup>37</sup> has shown, figure 1-26, that for microwaves ( $\sim 10$  GHz), statistical variations in water vapor below 8 km can produce values of  $C_n^2$  that are more than two orders of magnitude larger than for the corresponding optical case ( $C_{nc}^2$ ). Thus, estimates, for example, of  $\sigma^2$  based on optical constants may be in serious error. Armand et al<sup>38</sup> have looked at fluctuation effects near the 920- $\mu$ m water line and found that, on the absorption center, the amplitude fluctuations (dB) were approximately five times lower than in the 980- $\mu$ m window. Kanevskii<sup>39</sup> however, has done theoretical analyses which indicate that under certain conditions, dependent upon the range and outer scale turbulence condition, opposite and more intense effects are possible.

From the brief discussion thus far it should be clear that an understanding of the effects of turbulence on NMMW propagation will require considerable theoretical and experimental effort. Aside from the Soviet work discussed above, it is only recently that other workers have begun the experiments so necessary in this area. Ho, Cole, and Mavroukoulakis have recently published

a series of papers<sup>40-44</sup> discussing their work on amplitude fluctuations at 36 and 110 GHz along a terrestrial path. They have compared the two regions  $L_0 > \sqrt{\lambda R}$  and  $L_0 < \sqrt{\lambda R}$  and the applicability of Tatarski's theoretical predictions to millimeter wavelengths.

The comparison study was conducted over a 4-km path using 0.5-m antennas approximately 50 m above ground. Figures 1-27 and 1-28 summarize their results for  $L_0 > \sqrt{\lambda R}$  and  $L_0 < \sqrt{\lambda R}$ , respectively. One-dimensional temperature spectra, measured by a fast response sensor, were taken for two purposes. First, to obtain an estimate of the outer scale of turbulence and second, to ascertain whether or not the Kolmogorov 2/3 spatial power law model discussed earlier was valid. It should be recalled that the temperature fluctuations of the sensor are caused by wind flow of the turbulence eddy packets. For a given wind speed, the temperature spectrum<sup>44</sup> gives a good estimate of the refractive

<sup>37</sup>W. D. Brown, *A Model for the Refractive Index Structure Constant at Microwave Frequencies*, Sandia Laboratories Report SAND 76-0593 (February 1977).

<sup>38</sup>N. A. Armand, A. O. Izyumov, and A. V. Sokolov, *Fluctuations of Submillimeter Waves in a Turbulent Atmosphere*, *Radio Engineering and Electronic Physics*, vol. 14, no. 10 (1971), 1259-1266.

<sup>39</sup>M. D. Kanevskii, *The Problem of the Influence of Absorption on Amplitude Fluctuations of Submillimeter Radio Waves in the Atmosphere*, *Izvestiya Vysshikh Uchebnykh Zav. Radiofizika*, vol. 15, no. 12 (December 1972), 1939-1940.

<sup>40</sup>K. L. Ho, N. D. Mavroukoulakis, and R. S. Cole, *Wavelength Dependence of Scintillation Fading at 110 and 36 GHz*, *Electronics Letters*, vol. 13, no. 7 (31 March 1977), 181-183.

<sup>41</sup>K. L. Ho, R. S. Cole, and N. D. Mavroukoulakis, *The Effect of Wind Velocity on the Amplitude Scintillations of Millimetre Radio Waves*, *Journal of Atmospheric and Terrestrial Physics*, vol. 40 (1978), 443-448.

<sup>42</sup>R. S. Cole, K. L. Ho, and N. D. Mavroukoulakis, *The Effect of the Outer Scale Turbulence and Wavelength on Scintillation Fading at Millimeter Wavelengths*, *IEEE Transactions on Antennas and Propagation*, vol. AP-26 (September 1978), 712-715.

<sup>43</sup>K. L. Ho, N. D. Mavroukoulakis, and R. S. Cole, *Determination of the Atmospheric Refractive Index Structure Parameter from Refractivity Measurements and Amplitude Scintillation Measurements at 36 GHz*, *Journal of Atmospheric and Terrestrial Physics*, vol. 40 (1978), 745-747.

<sup>44</sup>N. D. Mavroukoulakis, K. L. Ho, and R. S. Cole, *Temporal Spectra of Atmospheric Amplitude Scintillations at 110 GHz and 36 GHz*, *IEEE Transactions on Antennas and Propagation*, vol. AP-26 (November 1978), 875-877.

<sup>45</sup>D. T. Gjessing, A. G. Kjellass, and E. Golton, *Small Scale Atmospheric Structure Deduced from Measurements of Temperature, Humidity, and Refractive Index*, *Boundary-Layer Meteorol.* (1972), 475.

index spectrum and size of the outer scale. Figures I-27(a) and I-28(a) show the results of the measurements. Given a measured wind speed and frequency of the slope change in the spectra, one derives the outer scale of the turbulence. It is interesting that even at the 50-m height of the measurement,  $L_0$  was found on occasion to average as low as 2 m. The measured  $-5/3$  frequency dependence of the fluctuations is consistent with what is predicted by Tatarski<sup>23</sup> on the basis of the Kolmogorov spatial model.

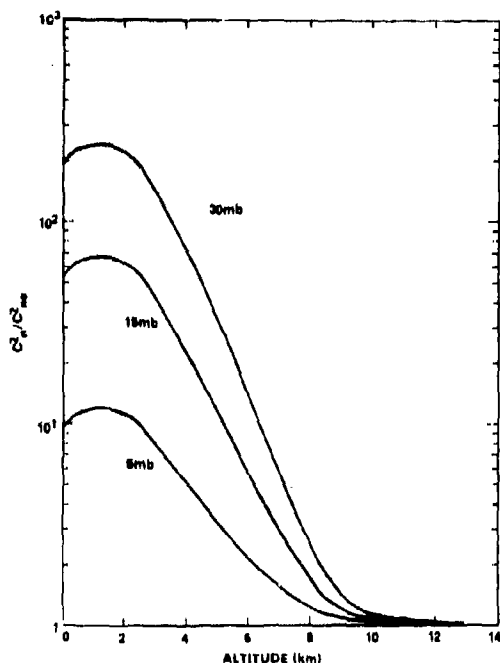


Figure I-26. Theoretical ratio of refractive index structure constants at radar ( $\sim 10$  GHz) and optical frequencies versus altitude with sea-level water vapor pressure as a parameter.

Figures I-27(b) and I-28(b) show a comparison of the measured variances of log-amplitude fluctuations at 36 and 110 GHz as a function of time. It is clear that fluctuations at the different frequencies were very well correlated. Assume for the moment that, on the

<sup>23</sup>V. I. Tatarski, *Wave Propagation in a Turbulent Medium* (Translated from the Russian by R. A. Silverman), McGraw-Hill Book Co., Inc., New York (1961).

average, figure I-28(b) indicates  $\sigma_{10}^2 \sim 3 \times 10^{-2}$  dB<sup>2</sup>. This implies intensity fluctuations of the order of 0.2 dB. In recent battlefield, near-ground propagation studies, Snider et al<sup>44</sup> have observed significantly greater power fluctuations of the order of  $\pm 2$  dB and attributed these to clear air turbulence.\* It may be, however, that the wide antenna beamwidths in these measurements result in the inclusion of some multipath effects.

Figures I-27(c) and I-28(c) plot the measured 110- and 36-GHz fluctuation ratios. The mean value for  $L_0 > \sqrt{\lambda R}$  is approximately 3.83, whereas for  $L_0 < \sqrt{\lambda R}$  the mean is 9.81. As discussed earlier, the theory for the fluctuations in the  $L_0 > \sqrt{\lambda R}$  domain should vary as  $k^{7/6}$ . This is consistent with the measured ratio. For  $L_0 < \sqrt{\lambda R}$ , Tatarski predicts a  $k$  dependence which is quadratic. Again this is consistent with figure I-28(c).

For  $L_0 > \sqrt{\lambda R}$ , the closed form expression for the fluctuations as discussed earlier allows one to calculate  $C_n^2$  from the measured data. Ho et al<sup>45</sup> performed simultaneous millimeter wave fluctuation measurements and X-band refractivity measurements of  $C_n^2$ . These two techniques yielded—over a one-hour period—respective average values of  $C_n^2$  of  $0.25 \times 10^{-14} \text{ m}^{-2/3}$  and  $0.32 \times 10^{-14} \text{ m}^{-2/3}$ . Thus, it appears that when  $L_0 > \sqrt{\lambda R}$ , millimeter fluctuation measurements can provide a rather good measurement of  $C_n^2$ .

The question of the spectral content of the amplitude fluctuations is important since the fluctuations generally might be expected to occur in the low audio range and thus could conceivably interfere with such things as servo-mechanism tracking loops which operate in the audio region. Mavrokoukoulakis<sup>46</sup> have

<sup>44</sup>K. L. Ho, N. D. Mavrokoukoulakis, and R. S. Cole, *Determination of the Atmospheric Refractive Index Structure Parameter from Refractivity Measurements and Amplitude Scintillation Measurements at 36 GHz*, *Journal of Atmospheric and Terrestrial Physics*, vol. 40 (1978), 745-747.

<sup>45</sup>D. E. Snider, J. C. Wiltsie, and R. W. McMillan, *The Effects of Atmospheric Turbulence and Adverse Weather on Near Ground 94- and 140-GHz Systems*, MIRADCOM Workshop on Millimeter and Sub-millimeter Atmospheric Propagation Applicable to Radar and Missile Systems (March 1979).

\*Editor's Note: also see 1979 Wiltsie et al reference in Selected Bibliography (Ch IX).

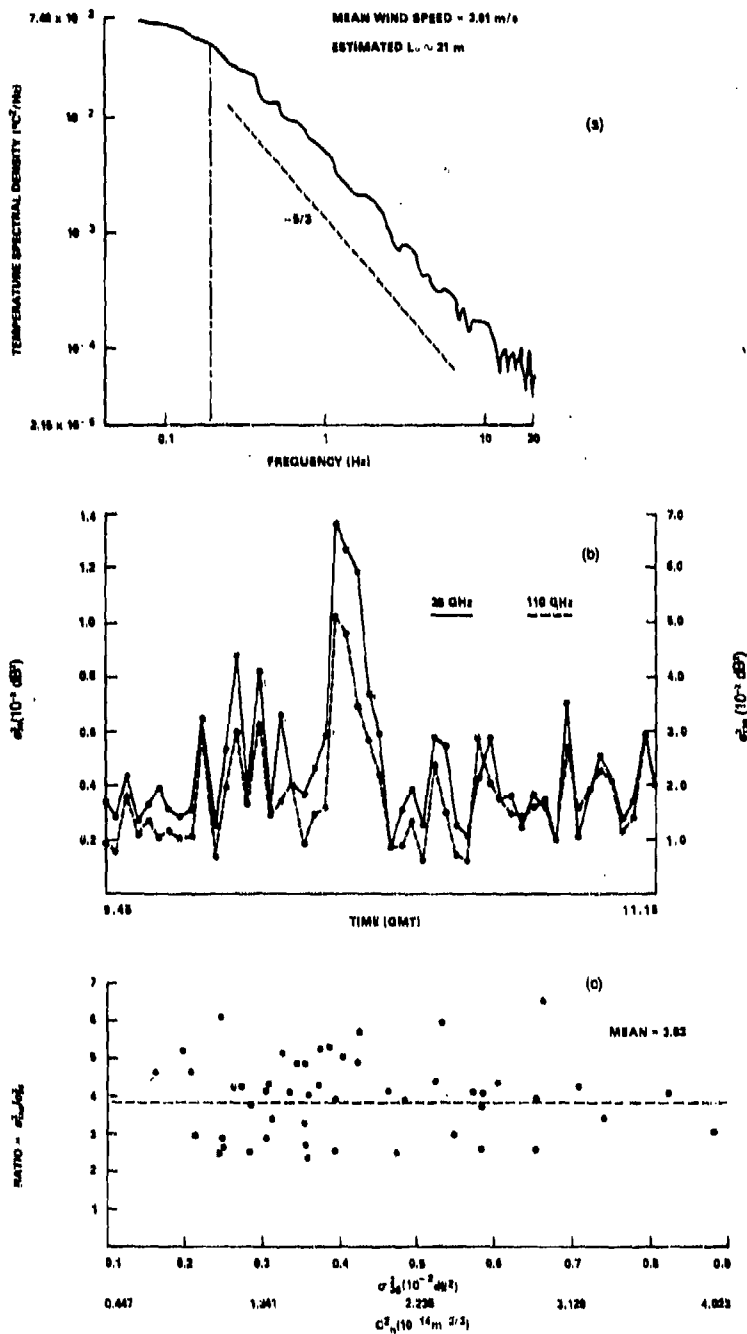


Figure 1-27. Characteristics of atmospheric turbulence and its effects on amplitude fluctuations of 36- and 110-GHz signals,  $L_0 > \sqrt{\lambda R}$ . (a) Measured temperature spectral density, (b) variance of log-amplitude fluctuations, (c) ratio of the variances of log-amplitude fluctuations as a function of the 36-GHz variance and the refractive index structure constant.

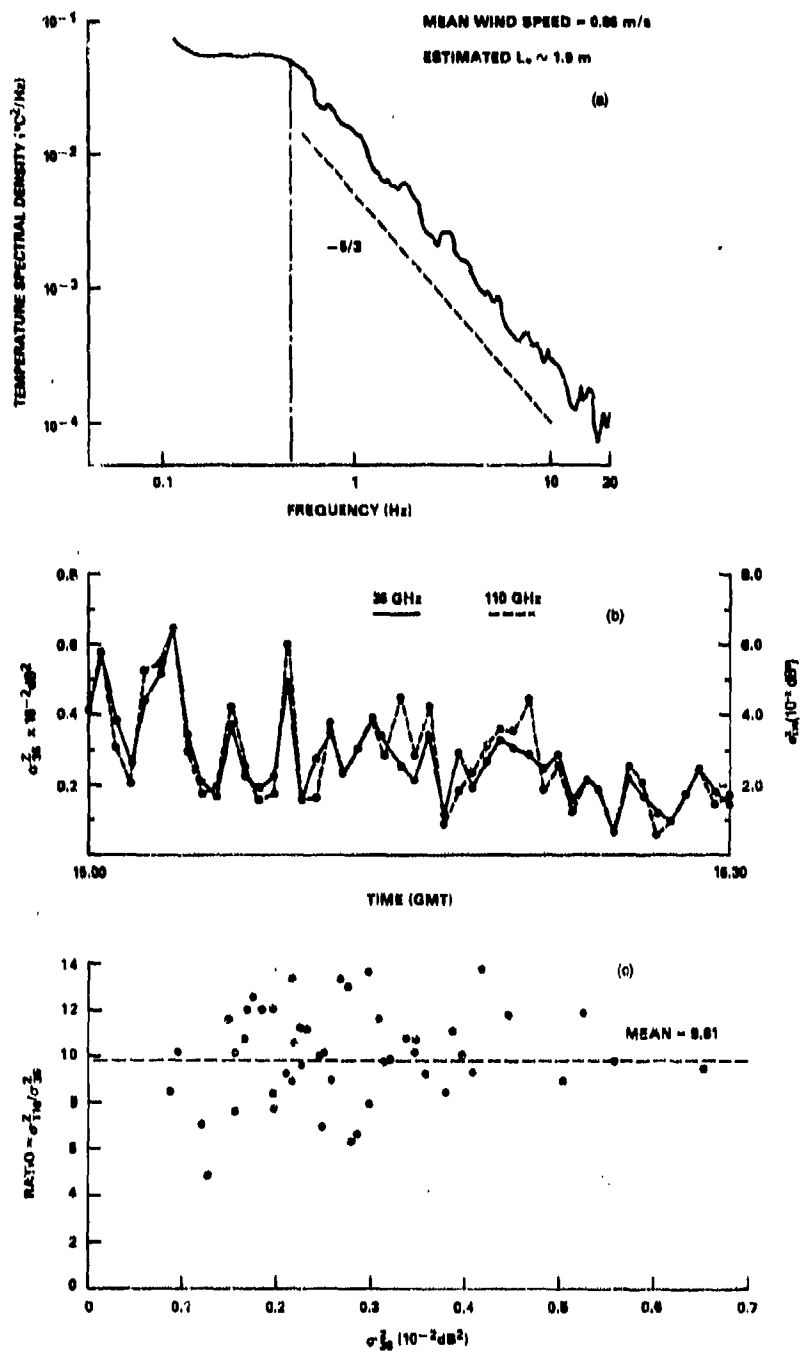


Figure I-28. Characteristics of atmospheric turbulence and its effects on amplitude fluctuations of 36- and 110-GHz signals,  $L_0 < \sqrt{\lambda R}$ . (a) Measured temperature spectral density, (b) variance of log-amplitude fluctuations, and (c) ratio of the variances of log-amplitude fluctuations as a function of the 36-GHz variance.

found spectral dependencies at 36 and 110 GHz, as shown in figure I-29.<sup>44</sup> The  $-8/3$  power law roll-off is consistent with Tatarski's theory, as discussed by Ishimaru<sup>47</sup> and Fante.<sup>29</sup>

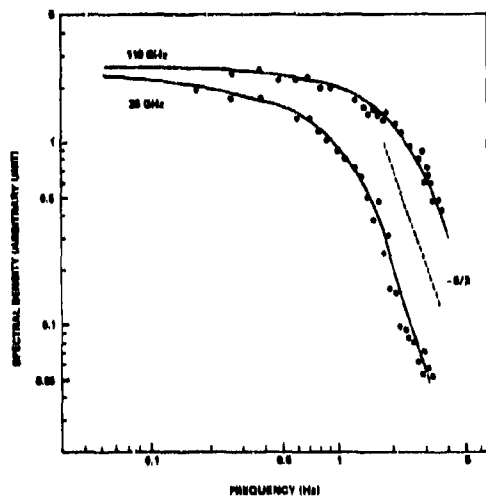


Figure I-29. Frequency spectra of the amplitude fluctuations at 110 and 36 GHz.

#### I-4. ANTENNA EFFECTS

A word is appropriate as to the performance of accurate, absolute propagation measurements. Such measurements, of course,

are very difficult and thus one very frequently finds that data presented and discussed in an absolute fashion are, in reality, quite dependent on a host of experimental conditions. In this regard, there particularly appears to be little concern given to the area of antenna effects—pattern shapes, near-field phenomena, etc. For example, at wavelengths of about 1 mm and antenna apertures of 0.5 m, the near-field region extends out to approximately  $R = 2D^2/\lambda = 500$  m. McGee at BRL (1978 data, private communication) has noticed that the fluctuation amplitudes observed in his measurements near 100 GHz seem to be dependent on near-field phenomena. There have been some recent theoretical efforts by Haworth et al<sup>48</sup> and vW. Welsbeck<sup>49</sup> to study such effects. However, no conclusive results have yet been reached, except that it is clear that some attention must be given to antenna effects.

<sup>29</sup>R. L. Fante, *Electromagnetic Beam Propagation in a Turbulent Media*, Proc. IEEE, vol. 63, no. 12 (1975), 1669-1692.

<sup>44</sup>N. D. Makrokokoulakis, K. L. Ho, and R. S. Cole, *Temporal Spectra of Atmospheric Amplitude Scintillations at 110 GHz and 36 GHz*, IEEE Transactions on Antennas and Propagation, vol. AP-26 (November 1978), 875-877.

<sup>47</sup>A. Ishimaru, *Temporal Frequency Spectra of Multi-Frequency Waves in a Turbulent Atmosphere*, IEEE Transactions on Antennas and Propagation, vol. AP-20 (1972), 10-19.

<sup>48</sup>D. P. Haworth, N. J. McEwan, and P. A. Watson, *Effect of Rain in the Near Field of an Antenna*, Electronics Letters, vol. 14, no. 4 (16 February 1978), 94-96.

<sup>49</sup>vW. Welsbeck, *Regenechos bei Nahbereichsimpulsradaranlagen*, A.E.U. band 30, heft II (1976), 429.

## CHAPTER I.—LITERATURE CITED

1. J. W. Waters, *Absorption and Emission by Atmospheric Gases*, *Methods of Experimental Physics*, vol. 12, Part B, Ch 2.3, M. L. Meeks, Ed., Academic Press (1976).
2. N. E. Gaut and E. C. Reifstein, III, *Environmental Research and Technology Report 13*, Lexington, MA (1971).
3. H. R. Carlon, *Phase Transition Changes in the Molecular Absorption Coefficient of Water in the Infrared: Evidence for Clusters*, *Applied Optics*, vol. 17, no. 20 (15 October 1978), 3192-3193.
4. H. R. Carlon, *Molecular Interpretation of the IR Water Vapour Continuum: Comments*, *Applied Optics*, vol. 17, no. 20 (15 October 1978), 3193-3195.
5. A. Ben-Reuven, *Advances in Atomic and Molecular Physics*, vol. 5 (1969), 201.
6. D. T. Llewellyn-Jones, R. J. Knight, and H. A. Gebbie, *Absorption by Water Vapour at 7.1 cm<sup>-1</sup> and its Temperature Dependence*, *Nature*, vol. 274 (August 1978), 876-878.
7. E. R. Westwater and D. C. Hogg, *Evidence for the Quadratic Dependence on Water Vapor of the Microwave Absorption Coefficient of Moist Air*, presented at the URSI-National Radio Science Meeting, Boulder, CO (January 1978).
8. D. C. Hogg, *Measurements of 70- and 80-GHz Attenuation by Water Vapor on a Terrestrial Path*, presented at the URSI-National Radio Science Meeting, Boulder, CO (January 1978).
9. R. J. Emery, P. Moffat, R. A. Bohlander, and H. A. Gebbie, *Measurements of Anomalous Absorption in the Wavenumber Range 4 cm<sup>-1</sup> - 15 cm<sup>-1</sup>*, *Journal of Atmospheric and Terrestrial Physics* vol. 37 (1975), 587-594.
10. R. J. Emery, A. Zavody, and H. A. Gebbie, *Further Measurements of Anomalous Atmospheric Absorption in the Range 4 cm<sup>-1</sup> - 15 cm<sup>-1</sup>*, *Journal of Atmospheric and Terrestrial Physics* (submitted for publication).
11. P. H. Moffat, R. A. Bohlander, W. R. Macrae, and H. A. Gebbie, *Atmospheric Absorption between 4 and 30 cm<sup>-1</sup> Measured Above Mauna Kea*, *Nature*, vol. 269 (October 1977), 676-677.
12. R. E. Hills, A. S. Webster, D. A. Alston, P. L. R. Morse, C. C. Zammit, D. H. Martin, D. P. Rice, and E. I. Robson, *Absolute Measurements of Atmospheric Emission and Absorption in the Range 100 -- 1000 GHz*, reported at the Third International Conference on SMM Waves (April 1978); published in *Infrared Physics*, vol. 18, no. 5/6 (1978), 819-825.
13. R. L. Plambeck, *Measurements of Atmospheric Attenuation near 225 GHz: Correlation with Surface Water Vapor Density*, *IEEE Transactions on Antennas and Propagation*, vol. AP-26 (September 1978), 737-738.
14. G. T. Wrixon and R. W. McMillan, *Measurements of Earth-Space Attenuation at 230 GHz*, *IEEE Transactions on Microwave Theory and Techniques*, vol. MTT-26, no. 6 (June 1978), 434-439.

CHAPTER I.—LITERATURE CITED (Cont'd)

15. F. I. Shimabukuro and E. E. Epstein, Attenuation and Emission of the Atmosphere at 3.3 mm, IEEE Transactions on Antennas and Propagation, vol. AP-18 (1970), 485.
16. A. V. Sokolov, E. V. Sukhonin, and I. A. Iskhakov, Attenuation of Radio Waves at Wavelengths from 0.45 to 4.0 mm in the Earth's Atmosphere through the Slant Paths, presented at the Second International Conference on SMM Waves, San Juan (December 1976).
17. V. W. Richard, J. E. Kammerer, and R. G. Reitz, 140-GHz Attenuation and Optical Visibility Measurements of Fog, Rain, and Snow, U.S. Army Ballistic Research Laboratories Memorandum Report, ARBRL-MR-2800 (December 1977).
18. N. P. Robinson, Measurements of the Effect of Rain, Snow, and Fogs on 8.6-mm Radar Echoes, Proc. IEE, London, vol. 203B (September 1955), 709-714.
19. L. I. Fidoosev, SMM Atmospheric Research in the USSR, presented at the Third International Conference on SMM Waves, Guildford, England (April 1978).
20. R. L. Olsen and D. V. Rogers, The  $\sigma^0$  Relation in the Calculation of Rain Attenuation, IEEE Transaction on Antennas and Propagation, vol. AP-26, no. 2 (March 1978), 318-329.
21. D. T. Llewellyn-Jones and A. M. Zavody, Rainfall Attenuation at 110 and 890 GHz, Electronics Letters, vol. 7, no. 12 (1971), 321-322.
22. A. M. Zavody and B. N. Harden, Attenuation/Rain Rate Relationships at 36 and 110 GHz, Electronics Letters, vol. 12 (1976), 422-424.
23. K. L. Ho, N. D. Mavroukoulakis, and R. S. Cole, Rain Induced Attenuation at 36 GHz and 110 GHz, IEEE Transactions on Antennas and Propagation, vol. AP-26 (November 1978), 873-875.
24. W. P. M. N. Kelzer, J. Snieder, and C. D. de Haan, Rain Attenuation Measurements at 94 GHz: Comparison of Theory and Experiment, NATO AGARD Conference Proceedings no. 245 (February 1979).
25. M. M. Kharadly, J. D. McNichol, and J. B. Peters, Measurement of Attenuation Due to Rain at 74 GHz, NATO AGARD Conference Proceedings no. 245 (February 1979).
26. V. W. Richard and J. E. Kammerer, Rain Backscatter Measurements and Theory at Millimeter Wavelengths, U.S. Army Ballistic Research Laboratory Report no. 1838 (October 1975).
27. U. Lammers, Investigations of the Effects of Precipitation on MM-Wave Propagation, Doctoral-Engineering Dissertation, Technik Universitat Berlin, D 83 (1965), Translation by U.S. Army HSTC-HT-23-0298-75, Defense Intelligence Agency Task No. T741801 (1975).
28. K. A. Aganbekyan, V. P. Bisyarin, A. Yu. Zrazhevsky, A. O. Izyumov, A. V. Sokolov, and E. V. Sukhonin, The Propagation of Submillimeter, Infrared, and Visible Waves in the Earth's Atmosphere, Rasprostraneniye Radiovoln, Institut Radiotekhniki i Elektroniki, published by Nauka (1975), 187-227.
29. R. L. Fante, Electromagnetic Beam Propagation in a Turbulent Media, Proc. IEEE, vol. 63, no. 12 (1975), 1669-1692.

CHAPTER I.—LITERATURE CITED (Cont'd)

30. J. I. Davis, Consideration of Atmospheric Turbulence in Laser Systems Design, *Applied Optics*, vol. 5, no. 1 (January 1966), 139-147.
31. R. S. Lawrence, A Review of the Optical Effects of Clear Turbulent Atmosphere, *SPIE*, vol. 75 (1976), 2-8.
32. H. T. Yura, An Elementary Derivation of Phase Fluctuations of an Optical Wave in the Atmosphere, *SPIE*, vol. 75 (1976), 9-15.
33. V. I. Tatarski, Wave Propagation in a Turbulent Medium (Translated from the Russian by R. A. Silverman), McGraw-Hill Book Co., Inc., New York (1961).
34. R. S. Lawrence and J. W. Strohbehn, A Survey of Clear-Air Propagation Effects Relevant to Optical Communications, *Proceedings of IEEE*, vol. 58, no. 10 (October 1970), 1523-1545.
35. F. F. Hall, Jr., Index of Refraction Structure Parameter in the Real Atmosphere—An Overview, *OSA Topical Meeting on Propagation through Turbulence, Rain and Fog*, Paper TuC1 (9 to 11 August 1977).
36. J. J. Gallagher et al, Application of Submillimeter Wave Gigawatt Sources, Georgia Institute of Technology, Final Report GT/EES, Project No. A-1717 (1975).
37. W. D. Brown, A Model for the Refractive Index Structure Constant at Microwave Frequencies, Sandia Laboratories Report SAND 76-0593 (February 1977).
38. N. A. Armand, A. O. Izyumov, and A. V. Sokolov, Fluctuations of Submillimeter Waves in a Turbulent Atmosphere, *Radio Engineering and Electronic Physics*, vol. 14, no. 10 (1971), 1259-1266.
39. M. D. Kanevskii, The Problem of the Influence of Absorption on Amplitude Fluctuations of Submillimeter Radio Waves in the Atmosphere, *Izvestiya Vysshikh Uchebnykh Zav. Radiofizika*, vol. 15, no. 12 (December 1972), 1939-1940.
40. K. L. Ho, N. D. Mavroukoulakis, and R. S. Cole, Wavelength Dependence of Scintillation Fading at 110 and 36 GHz, *Electronics Letters*, vol. 13, no. 7 (31 March 1977), 181-183.
41. K. L. Ho, R. S. Cole, and N. D. Mavroukoulakis, The Effect of Wind Velocity on the Amplitude Scintillations of Millimetre Radio Waves, *Journal of Atmospheric and Terrestrial Physics*, vol. 40 (1978), 443-448.
42. R. S. Cole, K. L. Ho, and N. D. Mavroukoulakis, The Effect of the Outer Scale Turbulence and Wavelength on Scintillation Fading at Millimeter Wavelengths, *IEEE Transactions on Antennas and Propagation*, vol. AP-26 (September 1978), 712-715.
43. K. L. Ho, N. D. Mavroukoulakis, and R. S. Cole, Determination of the Atmospheric Refractive Index Structure Parameter from Refractivity Measurements and Amplitude Scintillation Measurements at 36 GHz, *Journal of Atmospheric and Terrestrial Physics*, vol. 40 (1978), 745-747.
44. N. D. Mavroukoulakis, K. L. Ho, and R. S. Cole, Temporal Spectra of Atmospheric Amplitude Scintillations at 110 GHz and 36 GHz, *IEEE Transactions on Antennas and Propagation*, vol. AP-26 (November 1978), 875-877.

CHAPTER I.—LITERATURE CITED (Cont'd)

45. D. T. Gjessing, A. G. Kjellass, and E. Golton, Small Scale Atmospheric Structure Deduced from Measurements of Temperature, Humidity, and Refractive Index, *Boundary-Layer Meteorol* (1972), 473.
46. D. E. Snider, J. C. Wiltse, and R. W. McMillan, The Effects of Atmospheric Turbulence and Adverse Weather on Near Ground 94- and 140-GHz Systems, *MIRADCOM Workshop on Millimeter and Submillimeter Atmospheric Propagation Applicable to Radar and Missile Systems* (March 1979).
47. A. Ishimaru, Temporal Frequency Spectra of Multi-Frequency Waves in a Turbulent Atmosphere, *IEEE Transactions on Antennas and Propagation*, vol. AP-20 (1972), 10-19.
48. D. P. Haworth, N. J. McEwan, and P. A. Watson, Effect of Rain in the Near Field of an Antenna, *Electronics Letters*, vol. 14, no. 4 (16 February 1978), 94-96.
49. vW. Wiesbeck, Regenechos bei Nahbereichsimpulsradaranlagen, *A.E.U.* band 30, heft II, (1976), 429.

**CHAPTER II.—PROPAGATION THROUGH THE CLEAR ATMOSPHERE**

**by Darrell E. Burch and S. Anthony Clough**

## CONTENTS

	Page
II-1. INTRODUCTION.....	35
II-1.1 Background and Summary .....	35
II-1.2 Gaseous Composition of the Atmosphere .....	35
II-1.3 Absorption Parameters and Line-by-Line Calculations .....	37
II-2. HORIZONTAL ATTENUATION AT LOW ALTITUDES .....	39
II-3. HORIZONTAL ATTENUATION AT HIGH ALTITUDES .....	42
II-4. VERTICAL ATTENUATION .....	43
II-5. ANOMALOUS ABSORPTION.....	45
II-6. ACCURACY AND ASSUMPTIONS MADE IN CALCULATIONS.....	46
LITERATURE CITED .....	50

## II-1. INTRODUCTION

### II-1.1 Background and Summary

Most of the attenuation of NMM wavelength radiation by the clear atmosphere near sea level is due to the absorption lines of  $H_2O$  and  $O_3$ . Additional very weak absorption results from the rotational lines of  $CO$ ,  $N_2O$ , and  $O_2$ . In the lower atmosphere, the absorption by these gases at any wavelength is usually much less than the absorption by  $H_2O$ . In the upper atmosphere, where the  $H_2O$  density is very low and collisional broadening of the lines is slight, one of these minor constituents may produce most of the attenuation at a given wavelength.

The spectral curves of  $H_2O$  attenuation versus wavenumber given in sections II-2, -3, and -4 of this chapter are based on a combination of theory and experimental results obtained by many workers. Air Force Geophysical Laboratory (AFGL) scientists<sup>1</sup> have compiled and stored on magnetic tape the essential parameters of all the significant atmospheric absorption lines at all frequencies up through the infrared. These line parameters served as the basis for calculated values of attenuation. Following a procedure similar to that employed by Burch,<sup>2</sup> we have added an "empirical continuum" to the theoretical values to bring about agreement with experimental results in the atmospheric windows. Although this procedure lacks a rigorous theoretical basis, the results probably represent all the accumulated  $H_2O$  attenuation data in as simple and as accurate a form as is possible at this time. Data on the other gases ( $O_2$ ,  $CO$ ,  $N_2O$ , and  $O_3$ ) that absorb in the NMMW region are based strictly on the line-by-line calculations.

<sup>1</sup>R. A. McClatchey, V. S. Benedict, S. A. Clough, D. E. Burch, R. F. Calfee, K. Fox, L. A. Rothman, and J. S. Garing, *AFGL Atmospheric Absorption Line Parameters Compilation*, Air Force Cambridge Research Laboratory AFCRL-TR-73-0096 (January 1973).

<sup>2</sup>D. E. Burch, *Absorption of Infrared Radiation Energy by  $CO_2$  and  $H_2O$ . III. Absorption by  $H_2O$  between  $0.5$  and  $36\text{ cm}^{-1}$  ( $278\text{ }\mu\text{m}$  to  $2\text{ cm}$ )*, *Journal of Optical Society of America*, vol. 58 (1958), 1382-1394.

The methods used in the calculation are described and most of the absorption parameters are defined later in this section. Because of the dominance of the  $H_2O$  absorption, this gas is treated separately. Contributions by the other gases are then included. Horizontal attenuation at low altitudes is discussed in section II-2. The effects of decreased pressure and  $H_2O$  density at high altitudes are illustrated in the discussion of section II-3. Five NMM windows have been investigated further in order to determine the attenuation as a function of altitude from the top of the atmosphere down to various altitudes. Results of these calculations are presented in section II-4.

Section II-5 deals briefly with possible anomalous absorption by  $H_2O$ , particularly when the vapor is near saturation. Uncertainties in the results are discussed in section II-6.

### II-1.2 Gaseous Composition of the Atmosphere

Approximately 99.97 percent of the dry (no  $H_2O$  vapor) air in the lower atmosphere consists of  $N_2$ , 78.09 percent;  $O_2$ , 20.95 percent; and Ar, 0.93 percent. Several permanent constituents make up the remaining 0.03 percent. The gases that contribute significantly to attenuation in the NMMW region are listed in table II-1, along with their average concentrations and densities. The values given in the table are based on the 1962 U. S. Standard Atmosphere<sup>3,4</sup> and have been used in the calculations that are discussed below. For the present purposes,  $O_2$ ,  $N_2O$ , and  $CO$  can be considered uniformly mixed throughout the atmosphere. The concentration of  $O_3$  is highly variable in the lower atmosphere and is always much lower than it is at altitudes between approximately 10 and 30 km.

<sup>3</sup>S. L. Valley, *Handbook of Geophysics and Space Environments* AFCRL (1965).

<sup>4</sup>R. A. McClatchey, R. W. Fenn, J. E. A. Selby, F. E. Volz, and J. S. Garing, *Optical Properties of the Atmosphere (Revised)*, AFCRL-71-0279 Environmental Research Papers, No. 354 (10 May 1971).

TABLE II-1. ABUNDANCES OF ATMOSPHERIC GASES THAT ABSORB IN THE NEAR-MILLIMETER REGION

Gas species	Altitude (km)	Total pressure (atm)	Concentration (molecules/cm <sup>3</sup> )	Relative concentration by volume <sup>a</sup>
O <sub>3</sub>	0	1.00	$5.34 \times 10^{16}$	20.95 percent
	4	0.61	$3.57 \times 10^{16}$	
	16	0.102	$7.25 \times 10^{17}$	
N <sub>2</sub> O	0	1.00	$7.12 \times 10^{13}$	0.28 ppm
	4	0.61	$4.76 \times 10^{13}$	
	16	0.102	$9.67 \times 10^{11}$	
CO	0	1.00	$1.91 \times 10^{13}$	0.075 ppm
	4	0.61	$1.28 \times 10^{13}$	
	16	0.102	$2.59 \times 10^{11}$	
O <sub>2</sub>	0	1.00	$6.78 \times 10^{11}$	0.027 ppm
	4	0.61	$5.77 \times 10^{11}$	
	16	0.102	$3.01 \times 10^{12}$	
H <sub>2</sub> O <sup>b</sup>	(See figure II-2, relating H <sub>2</sub> O concentration to altitude)			
	0	1.00	$1.98 \times 10^{17} = 5.91 \text{ g/m}^3$	
	4	0.61	$3.69 \times 10^{16} = 1.10 \text{ g/m}^3$	
	16	0.102	$2.04 \times 10^{15} = 6.1 \times 10^{-4} \text{ g/m}^3$	

<sup>a</sup>Concentrations for all gases except H<sub>2</sub>O correspond to H<sub>2</sub>O-free air.

<sup>b</sup>Concentrations given for H<sub>2</sub>O correspond to the 1962 U.S. Standard Atmosphere. Other H<sub>2</sub>O concentrations employed in the calculations are indicated in the text. 1 gm H<sub>2</sub>O/m<sup>3</sup> corresponds to  $3.35 \times 10^{16}$  molecules/cm<sup>3</sup>.

Figure II-1 provides a convenient means of determining H<sub>2</sub>O vapor density from data on temperature and relative humidity. If the vapor density is required in molecules of H<sub>2</sub>O per cm<sup>3</sup>, it can be found by multiplying  $3.35 \times 10^{16}$  by the density in g/m<sup>3</sup>.

The concentration of H<sub>2</sub>O is highly variable in time, altitude, and geographical location. Several different model atmospheres have been derived and used by various groups. Figure II-2 shows plots of H<sub>2</sub>O vapor density versus altitude for three such atmospheric models. Of the three models, the most representative single model is the 1962 U. S. Standard. The other two are more representative of extreme conditions.

Tabulated data have been plotted for altitudes separated by 1 km, and the points have been connected by straight lines.

As originally published,<sup>3</sup> the 1962 U. S. Standard Atmosphere did not include H<sub>2</sub>O. However, an H<sub>2</sub>O distribution derived by Sissenwine<sup>4</sup> has been added to the standard and is given in an Air Force Cambridge Research Laboratory (AFCLR) report. Tabulated data on the Tropical and Subarctic Winter Models also appear in this same report.

<sup>3</sup>S. L. Valley, *Handbook of Geophysics and Space Environments*, AFCLR (1965).

<sup>4</sup>N. Sissenwine, D. D. Grantham, and H. A. Salemla, *Humidity Up to the Mesopause*, AFCLR-68-0550 (1968).

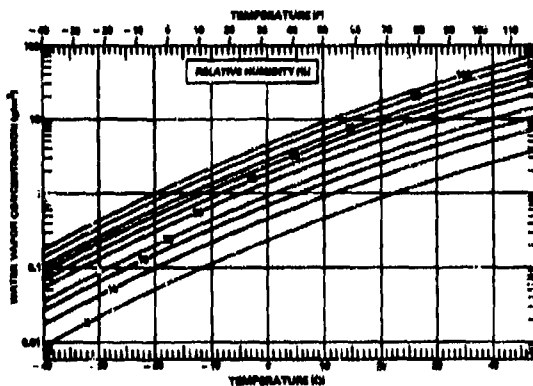


Figure II-1. Plots of H<sub>2</sub>O concentration versus temperature for various percentages of relative humidity.

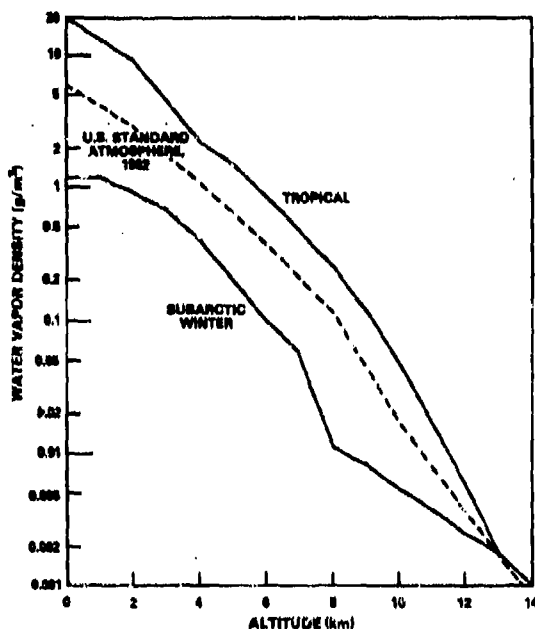


Figure II-2. Plots of water vapor density versus altitude for three atmospheric models.

### II-1.3 Absorption Parameters and Line-by-Line Calculations

The transmittance of a gas sample at a single frequency is given by an exponential equation of the form

$$\tau = I/I_0 = \exp(-uK) = \exp(-NLK). \quad (1)$$

$I$  is the radiant power level transmitted through the medium of interest, and  $I_0$  is the power level that would be observed with no attenuation. Workers in different areas define the quantities corresponding to  $u$  and  $K$  in different ways, but they must be defined in such a way that the product  $uK$  is dimensionless. The AFGL line parameters<sup>1</sup> are based on a system of units commonly used in the infrared which defines  $u$  as the number of absorbing molecules in a square cm cross section of the optical path. The quantity  $u$  is, therefore, equal to the density  $N$ , molecules/cm<sup>3</sup> times the path length  $L$  in cm. It follows that the absorption coefficient (cross section per molecule)  $K$  has the units of cm<sup>2</sup> molecules<sup>-1</sup>.

Workers in the millimeter region traditionally have not characterized atmospheric propagation in terms of transmittance; instead, they express it in terms of attenuation measured in decibels (dB). The attenuation  $A$  in dB is defined by

$$A(\text{dB}) = 10 \log (I_0/I) = -10 \log \tau. \quad (2)$$

Combining equations (1) and (2) gives

$$A(\text{dB}) = -10 \log \tau = -4.34 \ln \tau = 4.34 NLK. \quad (3)$$

It is frequently convenient to express the density of the absorbing gas in mass per unit volume rather than number of molecules per unit volume. If  $K$  is to be retained with units of cm<sup>2</sup> molecules<sup>-1</sup>,  $N$  must be replaced by  $q/m$ , where  $q$  is the density in g/cm<sup>3</sup> and  $m$  is the mass of each molecule, found by dividing the molecular weight by Avogadro's Number ( $6.02 \times 10^{23}$  molecules per gram molecular weight). In many of the calculations discussed below,  $q$  is expressed in g/m<sup>3</sup>,  $L$  is in km, and the attenuation coefficient is in dB/km.

Equation (3) can then be rewritten as

$$A_L(\text{dB/km}) = A(\text{dB})/L(\text{km}) \quad (4)$$

$$= \frac{4.34 \times 10^6 (\text{cm/km})q(\text{g/m}^3)10^{-6}(\text{m}^3/\text{cm}^3)K(\text{cm}^2/\text{molecule})}{m(\text{g/molecule})}$$

<sup>1</sup>R. A. McClatchey, W. S. Benedict, S. A. Clough, D. E. Lurch, R. F. Calfee, K. Fox, L. A. Rothman, and J. S. Garing, AFGL Atmospheric Absorption Line Parameters Compilation, Air Force Cambridge Research Laboratory AFGL-TR-73-0096 (January 1973).

With the units as defined, this equation reduces to the following when the absorbing gas is H<sub>2</sub>O (molecular wt = 18.0 and m = 2.99 × 10<sup>-23</sup> g/molecule).

$$A_L(\text{dB/km}) = 1.45 \times 10^{23} qK \quad (\text{for H}_2\text{O}) \quad (5)$$

The absorption coefficient K as defined is unambiguous and has the important advantage of being independent of the density of the absorbing gas. On the other hand, it involves the use of numbers with large exponents and is somewhat difficult to relate to lengths and densities normally used. Use of the quantity A<sub>L</sub> has the disadvantage that it is necessary to specify the density for which it is defined. This quantity has the advantage, however, that the total attenuation by a path of known length can be calculated from it quite easily.

For convenience in comparing different values of attenuation by H<sub>2</sub>O, we define an additional quantity A<sub>L</sub><sup>\*</sup> as the value of A<sub>L</sub> for an H<sub>2</sub>O density of 1 g/m<sup>3</sup>.

$$A_L^* = A_L(\text{dB/km})/q(\text{g/m}^3) \quad (6)$$

A path length of 1 km (10<sup>5</sup> cm) through an atmosphere with an H<sub>2</sub>O density of 1 g/m<sup>3</sup> corresponds to an absorber thickness of 0.1 g/cm<sup>2</sup>, or to 0.1 precipitable cm of liquid H<sub>2</sub>O. The units of g/cm<sup>2</sup> and precipitable cm of liquid H<sub>2</sub>O are commonly used by infrared workers.

The AFGL line-parameters tape includes the intensity S<sub>0,i</sub> (sometimes called strength), center position ν<sub>i</sub>, and half-width α<sub>0,i</sub> of each absorption line of significance for atmospheric attenuation from the infrared to the microwave region. Also included is other information that is required to calculate the strengths and half-widths at temperatures other than the reference temperatures. Data are included for the permanent atmospheric gases: N<sub>2</sub>, O<sub>2</sub>, CO<sub>2</sub>, H<sub>2</sub>O, N<sub>2</sub>O, CO, CH<sub>4</sub>, and O<sub>3</sub>. Only five of these, H<sub>2</sub>O, O<sub>2</sub>, CO, N<sub>2</sub>O, and O<sub>3</sub> absorb significantly in the NMMW region and are considered below.

In a calculation typical of those discussed below, the theoretical absorption coefficient (K = ∑k<sub>i</sub> cm<sup>2</sup>molecules<sup>-1</sup>) is computed by summing the calculated portion of the absorption coefficient due to each individual absorption line centered in the microwave, near-millimeter and infrared regions of the spectrum below 6000 GHz. Similar calculations are made for many wavelengths, with the intervals between adjacent wavelengths small enough to retain all of the spectral structure. This requires that the spacing be no more than about 1/4 the half-width of the narrowest lines. Values of the attenuation coefficient, A<sub>L</sub>, for a particular H<sub>2</sub>O density q are computed from the calculated values of K by the use of equation (5). Values of A<sub>L</sub> for CO, N<sub>2</sub>O, O<sub>2</sub>, and O<sub>3</sub> are calculated similarly by using standard densities of these gases.

Curves of transmittance for a given value of u can be obtained by applying equation (1) to the computed values of K. If two or more gas species (such as H<sub>2</sub>O + O<sub>2</sub> + CO) contribute to the absorption at a given wavenumber, the combined transmittance τ is equal to the product of the individual transmittances.

A very important parameter in the transmittance calculation is the shape assumed for the absorption lines. Different shapes have been proposed for NMM lines, particularly for those of H<sub>2</sub>O, the major absorber. All the calculations represented below are based on a modified version of the Van Vleck-Weisskopf line shape that is included in the following expression for the absorption coefficient

$$k_i = \frac{\nu_i [1 - \exp(-h\nu_i/kT)]}{\nu_i [1 - \exp(-h\nu_i/kT)]} \left(\frac{T_0}{T}\right)^d S_{0,i} e^{\left(\frac{E^*}{kT_0} - \frac{E^*}{kT}\right)} \cdot \frac{1}{\pi} \left[ \frac{\alpha_i}{(\nu - \nu_i)^2 + \alpha_i^2} + \frac{\alpha_i}{(\nu + \nu_i)^2 + \alpha_i^2} \right] \quad (7)$$

The line intensity S<sub>0,i</sub> corresponds to the reference temperature T<sub>0</sub> (293 K). The

value of  $S_{O,i}$  at any given temperature  $T$  is essentially independent of  $\alpha_i$  (the half width of the line), and thus independent of total pressure  $P$ . The center of the line is given by  $\nu_i$  and the point of calculation by  $\nu$ .  $E^*$  is the energy of the lower state involved in the transition. If  $E^*$  is large,  $S_{O,i}$  increases rapidly with increasing temperature. Planck's constant and Boltzmann's constant are represented by  $h$  and  $k$ , respectively. The constant  $d = 1.5$  for  $H_2O$  and  $O_2$  and  $1$  for the other molecules considered here.

The line shape represented by equation (7) has the obvious drawback that the integral  $\int k_i d\nu$  is infinite if the integration is carried out over all wavenumbers. This results because  $k_i$  approaches a constant value when  $\nu \gg \nu_i$ . In the NMMW region, this is not a problem because  $\nu$  is never large and is less than the values of  $\nu_i$  for many of the lines that contribute to the absorption. In the calculations represented below, only the  $H_2O$  lines for which  $\nu_i \leq 6000$  GHz were included.

In the NMMW region, Doppler broadening of absorption lines is negligible for the present applications. Therefore, line broadening is due solely to collisions of the absorbing molecules with other molecules. The half-width  $\alpha_i$  of a line when the gas is at total pressure  $P$  (atm) is given approximately by

$$\alpha_i = \alpha_{O,i} (T_0/T)^{0.4} (P/P_0) \quad (8)$$

where  $P_0 = 1$  atm, and  $\alpha_{O,i}$  is the half-width at half maximum of the line at the reference conditions. Values of  $\alpha_{O,i}$  listed on the AFGL tape are based on the assumption that all the collisions of the absorbing molecules are with  $N_2$  molecules. Thus, self-broadening produced by collisions of the absorbing molecules with other molecules of the same species is excluded. This assumption probably does not lead to significant error in the attenuation calculations for  $O_2$ ,  $CO$ , and  $N_2O$  because of the very low concentrations of these gases. Errors of several percentage points may be introduced by this simplifying assumption in the calculations for  $H_2O$  and  $O_3$ . These possible errors are discussed in more detail in section II-6.

The modified Van Vleck-Weisskopf line shape represented by equation (7) is one of the few shapes that have been suggested for  $H_2O$  absorption lines in the infrared and NMMW regions. Unfortunately, none of the proposed shapes lead to theoretical results that agree well with experimental results. In the "windows" between the strong  $H_2O$  lines, the experimental attenuation is generally greater than the theoretical value by as much as 25 to 150 percent. The method of accounting for this discrepancy is discussed, along with the results in section II-2.

Although none of the theoretical shapes is completely adequate, one feature is common to all of them and is consistent with experimental results obtained in the infrared and NMMW regions. In the wings of a line where  $|\nu - \nu_i| \gg \alpha$ , the value of  $k_i$  is proportional to  $\alpha$ , which, in turn, is proportional to pressure (see eq (7) and (8)). Thus, in a window region that is well separated from any lines that contribute significantly, the total absorption coefficient  $K$  due to all of the lines is also proportional to pressure. It follows from the above discussion that  $A_L$ , the attenuation in dB/km, is proportional to  $qP$ , the product of the density of the absorbing gas and the total pressure. At most of the altitudes of interest, the densities of  $O_2$ ,  $N_2O$  and  $CO$  are proportional to  $P$ ; thus, the attenuation by the wings of the lines of any of these gases varies as  $P^2$  and consequently decreases rapidly with increasing altitude. In general, the attenuation by  $H_2O$  decreases even more rapidly with increasing altitude because of the rapid decrease in  $q_{H_2O}$ .

## II-2. HORIZONTAL ATTENUATION AT LOW ALTITUDES

The method described in the previous section has been used to calculate the theoretical attenuation by  $H_2O$  at zero altitude for the  $H_2O$  density ( $5.91$  g/m<sup>3</sup>) represented by figure II-2 for the 1962 U. S. Standard Atmosphere. The calculated values were then compared with the

experimental results obtained by many different workers. In most cases, the experimental data are based on a different  $H_2O$  density and had to be adjusted to represent a density of  $5.91 \text{ g/m}^3$ . No adjustments were made for the differences between the gas temperatures.

In general, there is excellent agreement in the positions of the line centers; intensities and line widths also appear to agree well, although these two parameters cannot be checked as accurately as the positions. Serious discrepancies occur between the experimental and theoretical attenuation coefficients in the windows between the strong lines. The relatively high experimental values imply that either (a) the theoretical line shapes do not predict enough wing absorption or (b) there is an additional source of absorption. Dimers consisting of two  $H_2O$  molecules joined together have been suggested as a possible additional source of absorption. Dimers and other possible sources of anomalous absorption are discussed further in section II-6. Rather than attempt the very difficult task of determining the exact absorption mechanism, we have used a combined theoretical-experimental approach to obtain spectral curves of attenuation that are realistic and adaptable to a variety of atmospheric conditions.

In order to bring about agreement between calculated and experimental data, we have added an "empirical continuum" to the values calculated theoretically on the basis of the line parameters. Curve A of figure II-3 represents the calculated values after the empirical continuum, represented by curve B, has been added. The data points shown in figure II-3 represent several sets of workers, and in many cases a single data point represents the average of many original data points. Many apparently reliable data by various other workers necessarily have been omitted. The results of different workers are generally in good agreement if the data were obtained under well-controlled conditions. The data illustrated by the points between  $14 \text{ cm}^{-1}$  and  $34 \text{ cm}^{-1}$  are based on laboratory data of

Burch.<sup>2</sup> These data agree favorably with the other limited data available from laboratory and field measurements. Other data represented in figure II-3 are by Ryadov and Furashov,<sup>6</sup> Frenkel and Woods,<sup>7</sup> Straiton and Tolbert,<sup>8</sup> and Dryagin, et al.<sup>9</sup>

A bibliography by Guenther et al.<sup>10</sup> references many other papers and reports on NMMW propagation.

Most of the discrepancy between the theoretical and the experimental results is probably due to the lack of knowledge about the shapes of the extreme wings of collision-broadened  $H_2O$  lines. Many very strong  $H_2O$  lines centered at frequencies above the NMMW region contribute to the absorption in the NMM windows. The shapes of these distant lines must be known if their contributions are to be calculated accurately.

The theoretical contributions by all the lines centered below  $200 \text{ cm}^{-1}$  ( $6000 \text{ GHz}$ ) were included in the calculations. Other calculations performed at a different time indicated that there is a negligible contribution to NMMW absorption by the extreme wings of  $H_2O$  lines centered above  $6000 \text{ GHz}$ . In fact, most of the calculated NMMW attenuation by  $H_2O$  results from lines centered below  $1200 \text{ GHz}$  ( $\lambda > 0.25 \text{ mm}$ ). The separate use of the empirical continuum curve is

<sup>2</sup>D. E. Burch, *Absorption of Infrared Radiant Energy by  $CO_2$  and  $H_2O$ . III. Absorption by  $H_2O$  between  $0.5$  and  $36 \text{ cm}^{-1}$  ( $278 \mu\text{m}$  to  $2 \text{ cm}$ )*, *Journal of the Optical Society of America*, vol. 58 (1958), 1382-1394.

<sup>6</sup>Ya. V. Ryadov and R. I. Furashov, *Investigation of the Spectrum of Radiowave Absorption by Atmospheric Water Vapor in the 1.15 to 1.5-mm Range*, *Radio Physics and Quantum Electronics*, vol. 15, no. 10 (October 1974), 1124-1128.

<sup>7</sup>L. Frenkel and D. Woods, *The Microwave Absorption by  $H_2O$  Vapor and Its Mixtures with Other Gases Between 100 and 300 GHz*, *Proceedings of the IEEE*, vol. 54 (1966), 498-505.

<sup>8</sup>A. W. Straiton and C. W. Tolbert, *Anomalies in the Absorption of Radio Waves by Atmospheric Gases*, *Proceedings of the IRE*, vol. 48 (1960) 898.

<sup>9</sup>Yu. A. Dryagin, A. G. Kislyakov, L. M. Kukin, A. I. Naumov, and L. I. Fedoseyev, *Measurements of Atmospheric Absorption of Radiowaves in 1.36- to 3.0-mm Range*, *Izvestiya VUZ Radiophysics*, vol. 9, no. 6 (1966), 624-627.

<sup>10</sup>B. D. Guenther, J. S. Bennett, W. L. Gamble, and R. L. Harman, *Submillimeter Research: A Propagation Bibliography*, U.S. Army Missile Command, Technical Report RR-77-3 (November 1976).

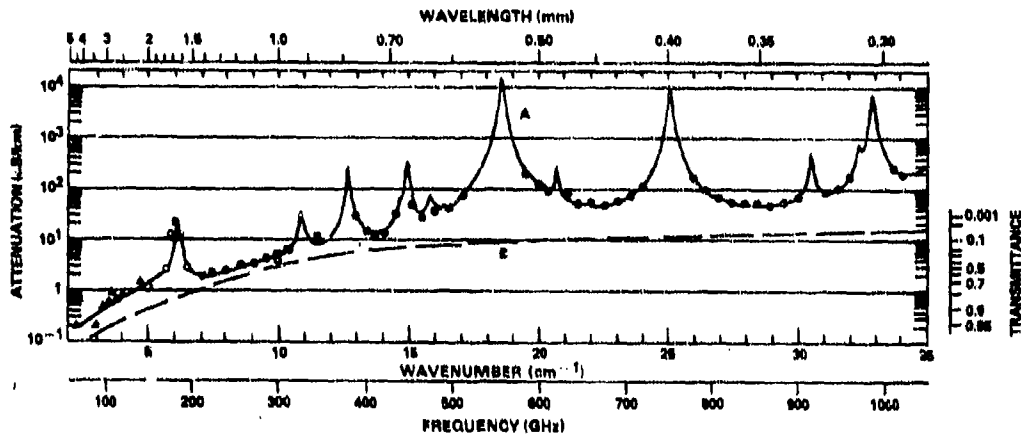


Figure II-3. Spectral plots of the attenuation by atmospheric  $H_2O$  at sea level. Curve A represents a combination of theoretical and experimental results for an  $H_2O$  density of  $5.91 \text{ g/m}^3$ . Curve B corresponds to an empirical continuum that is added to theoretical results to provide agreement with the experimental results represented by the data points (superscript numerals represent literature references of Chapter II). ●, Burch;<sup>1</sup> ■, Ryadov and Furshov;<sup>2</sup> ○, Frenkel and Woods;<sup>3</sup> ▲, Stratton and Tolbert;<sup>4</sup> and ▼, Dryagin et al.<sup>5</sup> The transmittance scale on the right-hand side corresponds to a 1 km path.

not intended to imply that such a continuum exists as a result of some separate absorption mechanism. It is, however, interesting, that values represented by this smooth curve do represent the difference between experimental and theoretical results. As indicated above, this "extra" absorption may be due to unpredictably high absorption by the wings of lines, or to dimers, or to other sources that are not yet understood. If a line shape other than the modified Van Vleck-Weisskopf shape had been used, the values represented by the empirical continuum would be slightly different. But a continuum is still required to produce agreement between experimental results and theoretical results based on any of the widely used line shapes.

The  $H_2O$  vapor density ( $5.91 \text{ g/m}^3$ ) on which figure II-3 is based corresponds to approximately 46-percent relative humidity at 15 C (59 F). The actual density may vary in extreme cases from as low as approximately  $0.2 \text{ g/m}^3$  in very cold, dry air to as high as 30 or

$40 \text{ g/m}^3$  in hot, humid air. To a first approximation, the attenuation by a fixed atmospheric path length at a fixed pressure and temperature may be taken proportional to the  $H_2O$  density. The deviation from this simple, linear relationship for high  $H_2O$  vapor densities is discussed in section II-6 and Chapter I.

Curve A of figure II-4 applies to low altitudes where the pressure is near 1 atm. This curve is based on the same  $H_2O$  density ( $5.91 \text{ g/m}^3$ ) as the corresponding curve in figure II-3. However, the contributions by  $O_3$ ,  $O_2$ , CO, and  $N_2O$  are also included in the curve of figure II-4. Of these four gases, only  $O_3$  makes a significant contribution for low-altitude atmospheric paths. The  $O_3$  contribution represented by the bottom curve is also much less than that by  $H_2O$  except over a few narrow spectral intervals. Thus, the two curves labelled A in figures II-3 and II-4 are quite similar. The only significant influence on curve A by the  $O_3$  in the NMMW region is near  $2.5 \text{ mm}$  ( $4 \text{ cm}^{-1}$ ). Very minor effects can be observed near  $14$  and  $16 \text{ cm}^{-1}$ .

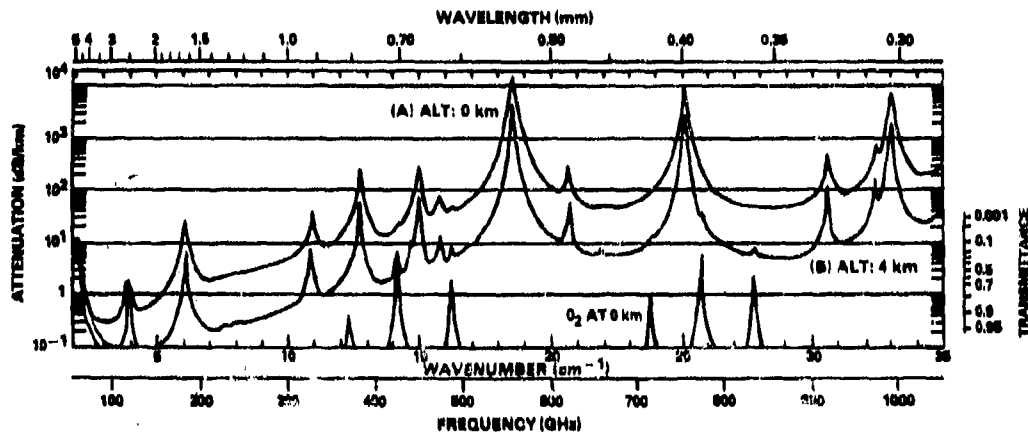


Figure II-4. Spectral plots of the attenuation by the 1962 U.S. Standard Atmosphere at sea level and 4-km altitude. The water vapor density is  $5.91 \text{ g/m}^3$  at sea level and  $1.10 \text{ g/m}^3$  at 4-km altitude. Concentrations of other gases are given in table II-1. The lower curve represents  $\text{O}_2$  only at sea level.

For comparison, the attenuation for this same model absorption is approximately 0.2 dB/km in the  $10\text{-}\mu\text{m}$  window<sup>11,12</sup> and less than 0.1 dB/km near  $3.8 \mu\text{m}$ .<sup>13</sup>

### II-3. HORIZONTAL ATTENUATION AT HIGH ALTITUDES

Curve B of figure II-4 corresponds to a horizontal path at a 4-km altitude where the total pressure of the 1962 U.S. Standard Atmosphere is 0.61 atm. In obtaining curve B, the appropriate temperature ( $-11 \text{ C}$ ) and  $\text{H}_2\text{O}$  density ( $1.10 \text{ g/m}^3$ ) were used to calculate the line contribution. The amount of empirical continuum added to the theoretical values was 0.11 times the value given by curve B of figure II-3. The constant 0.11 was based on the assumption

that the required empirical continuum is proportional to the product of total pressure and  $\text{H}_2\text{O}$  density ( $0.61 (1.10/5.91) = 0.11$ ). No accounting was made for the different temperature in computing the continuum.

The important difference in the attenuation curve for a 4-km altitude is the decrease by more than a factor of 10 in the attenuation in the window regions. A few very weak  $\text{H}_2\text{O}$  lines and the  $\text{O}_2$  lines also make an observable, but small, influence on the curve for the higher altitude.

Figure II-5 shows calculated spectral attenuation curves for the 1962 U.S. Standard Atmosphere at a 16-km altitude where the total pressure is only 0.1 atm. All the absorbing gases have been included with the concentrations given in table II-1. Comparison of figure II-5 with figures II-3 and II-4 reveals two major differences. First, the average attenuation is much lower in the window regions between the strong  $\text{H}_2\text{O}$  lines. This, of course, is due to the combination of lower total pressure and lower  $\text{H}_2\text{O}$  density. Second, there is much more structure in the spectrum. The lines of all of the gases

<sup>11</sup>D. E. Burch, *Semi-Annual Technical Report: Investigation of the Absorption of Infrared Radiation by Atmospheric Gases*, Contract No. F19628-69-C-0263. Aeronutronic-Ford Publication U-4784 (January 1970).

<sup>12</sup>R. E. Roberts, J. E. Selby, and L. M. Biberman, *Infrared Continuum Absorption by Atmospheric Water Vapor in 8-12- $\mu\text{m}$  Window*, *Applied Optics*, vol. 15, no. 9 (September 1976), 2085-2090.

<sup>13</sup>R. W. Watkins and K. O. White, *Water-Vapor-Continuum Absorption Measurements (3.5-4.0- $\mu\text{m}$ ) Using HDO-Depleted Water*, *Optics Letters*, vol. 1, no. 1 (July 1977), 31-32.

are narrower, because of the reduced collision broadening at the low pressure. Because of the greatly reduced amount of  $H_2O$  absorption, the lines of  $O_2$ ,  $O_3$ ,  $CO$ , and  $N_2O$  can be observed.

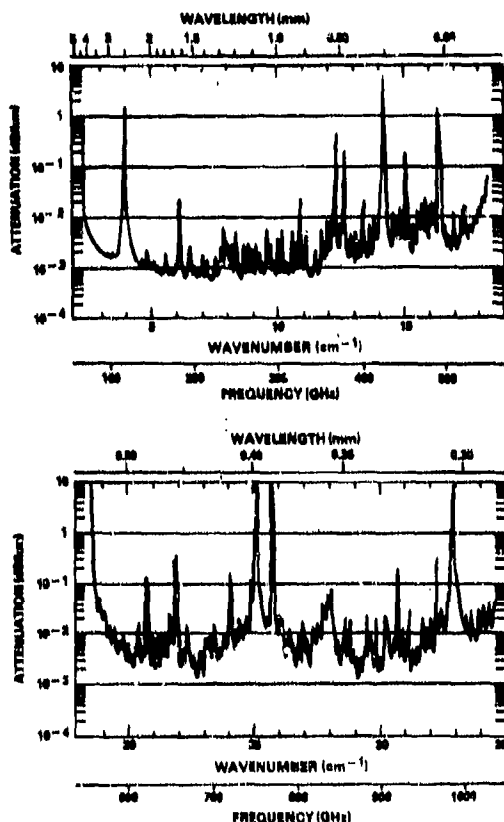


Figure II-5. Spectral plot of calculated horizontal attenuation at 16-km altitude. No empirical continuum for  $H_2O$  has been added to theoretical values. All permanent atmospheric gases have been included.

The average broadband attenuation is quite low for long atmospheric paths at high altitudes. Only a few decibels of broadband attenuation are predicted for paths of as much as 100 km. If a monochromatic source is to be used over very long paths in the upper atmosphere, particular attention must be paid to the possible wavelength coincidence of the source and the absorption lines.

#### II-4. VERTICAL ATTENUATION

It is necessary to calculate the vertical attenuation on the basis of the assumed vertical distributions of the gases and on the known dependence of attenuation on pressure and temperature.

The most accurate calculation of the vertical attenuation would require dividing the atmosphere into several layers. The appropriate temperature, pressure, and gas concentrations would be applied to each layer, and the attenuation would be calculated. Spacings between the adjacent wavenumbers where calculations are made would necessarily be very small in order to preserve the spectral structure. At very high altitudes, the pressures are low and the absorption lines are very narrow. Thus, the spectral interval between points must be much narrower than is required for calculations of lower atmospheric attenuation. After the appropriate calculations have been made for each layer, the attenuations by successive layers are added together to yield the combined attenuation.

Calculations of the type just described for the entire NMMW region are very expensive and beyond the scope of the present study. In addition, the accuracy of such calculations would be limited because of the lack of knowledge about line shapes, effects of temperature change, and possible anomalous absorption. However, by making a few simplifying assumptions, it is possible to perform some zenith attenuation calculations with an accuracy that may be adequate for many applications. Although errors of several percent may be introduced by making the assumptions, the results may be as accurate as the assumed atmospheric composition.

Figure II-6 shows the results of calculations of the vertical attenuation in five different windows. The center of each window is indicated, and the interval over which each curve applies is given in the legend. The width of each interval is chosen so that the attenuation coefficient varies within approximately  $\pm 10$  percent

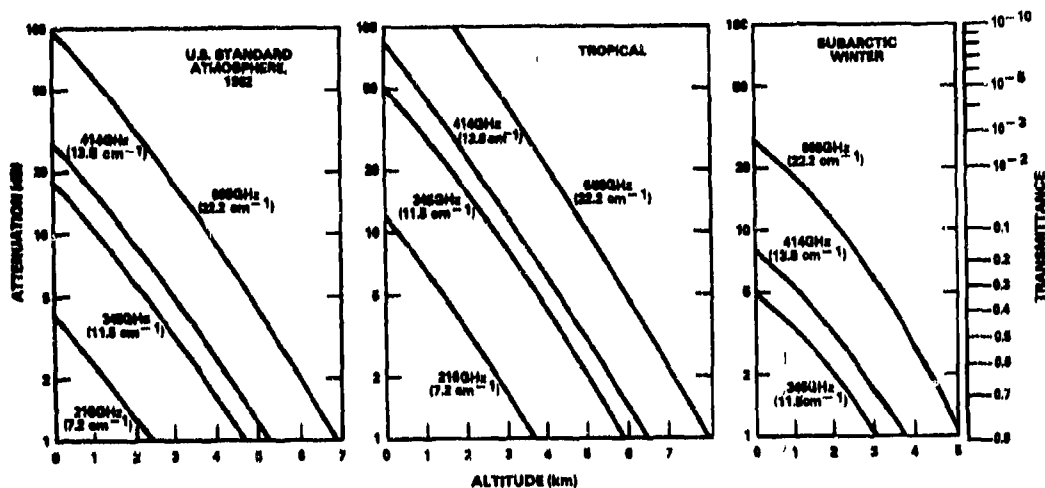


Figure II-6. Plots of calculated zenith attenuation versus altitude. Curves represent attenuation by water vapor from top of atmosphere down to altitude indicated by abscissa. Each curve is valid over the approximate spectral interval as follows:  $22.2 \text{ cm}^{-1}$ ,  $22.3$  to  $23.2 \text{ cm}^{-1}$  ( $0.471$  to  $0.431 \text{ mm}$ ) and  $27.2$  to  $29.7 \text{ cm}^{-1}$  ( $0.368$  to  $0.337 \text{ mm}$ );  $13.8 \text{ cm}^{-1}$ ,  $13.5$  to  $14.1 \text{ cm}^{-1}$  ( $0.74$  to  $0.71 \text{ mm}$ );  $11.5 \text{ cm}^{-1}$ ,  $11.2$  to  $11.9 \text{ cm}^{-1}$  ( $0.89$  to  $0.84 \text{ mm}$ );  $7.2 \text{ cm}^{-1}$ ,  $6.7$  to  $7.8 \text{ cm}^{-1}$  ( $1.49$  to  $1.28 \text{ mm}$ ).

of the nominal value used in the calculations. As can be seen in figure II-3, the attenuation is very nearly the same in the  $22.2 \text{ cm}^{-1}$  window as in the  $28.5 \text{ cm}^{-1}$  window. Therefore, the  $22.2 \text{ cm}^{-1}$  curve also applies to the  $28.5 \text{ cm}^{-1}$  window.

Each curve corresponds to a relatively wide band at any wavenumber within the interval indicated. Because of the fine structure in the attenuation curves that results from the narrow lines, the attenuation may be much greater at a particular wavelength than is indicated. The average attenuation over an interval wider than approximately  $0.1 \text{ cm}^{-1}$  is not affected greatly by these narrow lines, which may produce relatively large attenuation coefficients at the line centers.

Three different atmospheric models have been assumed. The Tropical Model Atmosphere is intended to be typical of the tropics; therefore, even higher humidity than that assumed for the calculations may be encountered. The resulting attenuation would then be correspondingly higher. Similarly, the Subarctic Model Atmosphere does not represent the lowest

possible humidity, but it is typical of the geographical location and climate implied by the name.

From results of calculations of lower atmospheric attenuation by  $\text{O}_2$ ,  $\text{O}_3$ ,  $\text{N}_2\text{O}$ , and  $\text{CO}$ , we have shown that the combined broadband attenuation by these gases in the five atmospheric windows considered is less than 1 dB for the entire path from ground level to the top of the atmosphere. For the applications of primary interest, this small amount of attenuation is of no concern. Therefore, no contribution by these four gases has been included in the results illustrated in figure II-6.  $\text{H}_2\text{O}$  is the only absorbing gas considered. The maximum possible error introduced by neglecting the other four gases is less than 0.5 dB for altitudes above 4 km and less than 1 dB for any altitude.

Data on total pressure  $P$  and  $\text{H}_2\text{O}$  vapor density  $q$  were compiled for each of the three atmospheric models (see fig. II-2). The average values of  $P$ ,  $q$ , and the product  $qP$  were determined for each 1-km-thick layer from 0- to

15-km altitude. It was assumed that the attenuation coefficient  $A_L$  is proportional to the product  $\rho P$  in accordance with the discussion of section II-1.3. For example, from figure II-3 we see that the average attenuation coefficient  $A_L$  in the 22.2  $\text{cm}^{-1}$  window is approximately 50 dB/km for  $\rho = 5.9 \text{ g/m}^3$ . The attenuation in a given window by each atmospheric layer was found by multiplying the average value of  $\rho P$  by 0.169 ( $= 1/5.9$ ) times the average value of  $A_L$  from figure II-3. Values of the attenuation of successive layers were then added.

This method of calculation ignores any influence of changing temperature in the atmosphere. Infrared data<sup>14</sup> on the absorption by the extreme wings of  $\text{H}_2\text{O}$  indicate that the absorption increases rapidly with decreasing temperature. No existing theories on line shape adequately predict this observed behavior. It seems likely that the effect of temperature on the wing absorption in the NMMW region also cannot as yet be predicted reliably. Thus, a sophisticated calculation of zenith attenuation that is based on the theoretical line shapes could very well produce results that are no more reliable than those obtained in this relatively simple manner.

If the temperature dependence is the same in the NMMW region as in the infrared, the values indicated by figure II-6 are more likely to be low than high. It seems likely that the true values are more than 50 to 100 percent higher than those indicated for the high altitudes where the temperatures are lowest. The expected error is less (25 to 50 percent) for altitudes below approximately 3 km.

The calculated attenuation in the Tropical and 1962 U.S. Standard Atmospheres from a 0-km altitude to the top of the atmosphere is approximately equal to that of a 2-km path at 0-km

<sup>14</sup>D. E. Burch, D. A. Gryvnak, and G. H. Piper, *Infrared Absorption by  $\text{H}_2\text{O}$  and  $\text{N}_2\text{O}$*  AFCRL-TR-73-0530 (July 1973).

altitude.<sup>15</sup> For the Subarctic Winter Model, the corresponding equivalent horizontal path is somewhat longer, approximately 2.7 km.

## II-5. ANOMALOUS ABSORPTION

Workers at Appleton Laboratory in Slough, England (see references 6, 9, 10, and 11 in Chapter I) have published a series of letters and papers that present experimental evidence of anomalous  $\text{H}_2\text{O}$  absorption that is not predicted theoretically for the simple  $\text{H}_2\text{O}$  monomer (single  $\text{H}_2\text{O}$  molecule). Emery et al<sup>16</sup> discuss the experimental methods and present spectral data in the 4 to 15  $\text{cm}^{-1}$  (120 to 450 GHz) region. The amount of this anomalous absorption is difficult to relate quantitatively to  $\text{H}_2\text{O}$  density and temperature, the two parameters on which it is expected to depend most strongly. In general, the absorption is much more prevalent when the  $\text{H}_2\text{O}$  vapor is near saturation. It has been suggested that other  $\text{H}_2\text{O}$  molecular complexes in addition to the dimer are the source of this absorption. Lack of equilibrium between the different complexes could account for the inability of the experimenters to obtain reproducible results.

The strongest maximum in the anomalous absorption occurs near 13  $\text{cm}^{-1}$ . At this position, the anomalous portion of the absorption coefficient was found to be more than 45 dB/km for a laboratory sample with  $T = 25.5 \text{ C}$ , relative humidity, 80 percent, and  $\text{H}_2\text{O}$  vapor density of 19  $\text{g/m}^3$ . Smaller peaks were observed near 8.5, 9.0, 10.2, and 11.2  $\text{cm}^{-1}$ . The relative heights of the peaks were not reproducible and were quite

<sup>15</sup>R. W. McMillan, J. J. Gallagher, and A. M. Cook, *Calculations of Antenna Temperature, Horizontal Path Attenuation, and Zenith Attenuation Due to Water Vapor in the Frequency Band 150-700 GHz*, *IEEE Trans. Microwave Theory and Techniques*, vol. MTT-25, no. 6 (June 1977), 485-488.

<sup>16</sup>R. J. Emery, P. Moffat, R. A. Bohlander, and H. A. Gebbie, *Measurements of Anomalous Atmospheric Absorption in the Wavenumber Range 4  $\text{cm}^{-1}$  - 15  $\text{cm}^{-1}$* , *Journal of Atmospheric and Terrestrial Physics*, vol. 37 (1975), 587-594.

different for samples in a multi-pass cell than for open air samples. These data point out the need to consider the spectral structure of the anomalous absorption as well as that of the  $H_2O$  monomer when selecting the wavelength of operation for any near-millimeter system.

Calculated values of attenuation based on the curves of figures II-3 through II-6 may be optimistically low under conditions that are conducive to anomalous absorption. There is an obvious need for additional research designed to bring about a better understanding of this problem.

## II-6. ACCURACY AND ASSUMPTIONS MADE IN CALCULATIONS

Several assumptions were made in calculating the attenuation values given in previous sections. The most important assumptions involve (1) the modified Van Vleck-Weisskopf line shape, (2) the validity of an empirical continuum to account for the difference between the experimental and theoretical attenuation, (3) the lack of a dependence of  $H_2O$  wing absorption on temperature, (4) neglecting self-broadening by  $H_2O$ , and (5) exclusion of anomalous absorption in atmospheric applications. Each of these assumptions was made because of the lack of reliable data to account properly for the effect involved. This sub-section deals with these assumptions and the expected errors that result in calculations.

Burch<sup>3</sup> has shown that experimental data on  $H_2O$  attenuation cannot be predicted accurately over the entire NMMW region by a single theoretical line shape. The disagreement between theory and experiment is worst in the windows where the nearest lines are several half-widths away. Burch and his co-workers<sup>14</sup> at

Ford-Aeronutronic have also found evidence that the shapes of self-broadening infrared lines of  $H_2O$  are different from  $N_2$ -broadened lines. Workers<sup>17</sup> in the same laboratory have also found that the same is true for  $CO_2$  absorption lines. The major differences in the shapes of both  $CO_2$  and  $H_2O$  lines occur in the extreme wings. In view of the inability to predict infrared absorption by a single, relatively simple line shape, it is not surprising that the same problem exists in the NMMW region.

Equation (8) for the half-width of absorption lines is based on the assumption that all the collisions of the absorbing molecules are either with molecules of  $N_2$ , or that the collisions with other molecules have exactly the same broadening effect as a like number of  $N_2$  molecules. This assumption is valid when the absorbing gas is mixed very dilutely with  $N_2$ ; collisions of two molecules of the absorbing gas species are then negligible. When dealing with air, it would be better to relate the half-widths to a mixture of one fifth  $O_2$  and four fifths  $N_2$ . The broadening ability of  $O_2$  is approximately the same as that of  $N_2$  in the infrared. The same is probably true in the NMMW region; therefore, only small errors are introduced by treating  $N_2$  as the only significant non-absorbing broadening gas and using a pressure equal to the sum of the  $O_2$  and  $N_2$  partial pressures.

The most serious potential errors in ignoring all broadening except that by  $N_2$  arise from the self-broadening of  $H_2O$  lines. Partial pressures of  $H_2O$  seldom exceed 3 or 4 percent of the total pressure in air. However, collisions of absorbing  $H_2O$  molecules with other  $H_2O$  molecules are much more effective than  $H_2O$ - $N_2$  collisions. Line broadening data on  $H_2O$  lines throughout much of the infrared indicate that the broadening by a given number of  $H_2O$  molecules is equivalent to approximately five times as many  $N_2$  molecules. Liebe and Dillon<sup>18</sup> have

<sup>14</sup>D. E. Burch, *Absorption of Infrared Radiant Energy by  $CO_2$  and  $H_2O$ . III. Absorption by  $H_2O$  between 0.5 and 36  $cm^{-1}$  (278  $\mu m$  to 2 cm).* *Journal of the Optical Society of America*, vol. 58 (1958), 1382-1394.

<sup>14</sup>D. E. Burch, D. A. Gryunak, and G. H. Pifer, *Infrared Absorption by  $H_2O$  and  $N_2O$* , AFCRL-TR-73-0503 (July 1973).

<sup>17</sup>D. E. Burch, D. A. Gryunak, R. R. Patty, and C. E. Bartky, *Absorption of Infrared Radiant Energy by  $CO_2$  and  $H_2O$ . IV. Shapes of Collision-Broadened  $CO_2$  Lines*, *Journal of the Optical Society of America*, vol. 59 (1969), 267-280.

<sup>18</sup>H. J. Liebe and T. A. Dillon, *Accurate Foreign-Gas-Broadening Parameters of the 22-GHz  $H_2O$  Line from Refraction Spectroscopy*, *Journal of Chemical Physics*, vol. 50 (1969), 727-732.

demonstrated that this same ratio between self-broadening and  $N_2$  broadening also applies to the  $0.71 \text{ cm}^{-1}$  (22 GHz) and  $6.1 \text{ cm}^{-1}$  (183 GHz)  $H_2O$  lines. Thus, it is probably safe to assume that the same ratio applies throughout the NMMW region.

It follows that the half-width of an  $H_2O$  line is more accurately given by the following equation than by equation (9) for a mixture of  $H_2O$  in  $N_2$ .

$$\alpha = \left(\frac{T_0}{T}\right)^{0.2} \left[ \frac{\alpha_0}{P_0} (PN_2 + 5PH_2O) \right] - \left(\frac{T_0}{T}\right)^{0.2} \left[ \frac{\alpha_0}{P_0} (P + 4PH_2O) \right] \quad (9)$$

The half-width of the  $H_2O$  line is equal to  $\alpha_0$  when the  $H_2O$  is mixed very dilutely ( $PH_2O \ll PN_2$ ) in 1 atm of  $N_2$  at temperature  $T_0$ . The total pressure,  $H_2O$  partial pressure, and  $N_2$  partial pressure are indicated by  $P$ ,  $PH_2O$ , and  $PN_2$ , respectively. Under a quite humid condition,  $PH_2O$  could be as high as 0.04 atm. This leads to a 16-percent increase in  $\alpha$  for  $P = 1$  atm over its value if  $PH_2O$  were negligible.

Self-broadening of  $H_2O$  lines also influences the absorption in atmospheric windows by another mechanism that may be more important than the change in  $\alpha$ . This results from the apparent difference between the shape of the wings of a self-broadened line and that of an  $N_2$ -broadened line. The absorption by pure  $H_2O$  and by  $H_2O + N_2$  has been investigated extensively in many narrow windows throughout the infrared. Of special interest are windows in which much of the observed absorption is due to  $H_2O$  lines centered more than about 10 or 20  $\text{cm}^{-1}$  from the point of measurement. In all such windows, the influence of self-broadening is more than five times the influence on  $N_2$ -broadening by the same number of  $N_2$

molecules. Burch<sup>2</sup> has found that this is also true for the  $22 \text{ cm}^{-1}$  and  $28 \text{ cm}^{-1}$  windows. We conclude from all of these data that the proper ratio for line widths is approximately 5:1, and that the wings of a self-broadening  $H_2O$  line absorb more than the wings of the same  $H_2O$  line if it is broadened to the same width by  $N_2$ . Note that, by definition, the half-width relates only to the center portion of a line and not to the wings. Two lines of the same intensity are said to have a different shape if they absorb differently in the wings when their half-widths are equal.

The combined influence of self-broadening due to changes in the half-widths and the shapes may be much greater than would ordinarily be expected because of the low concentration of  $H_2O$ . All the discussion in sections II-2, -3, and -4 is based on the absorption coefficient  $K$  being independent of the  $H_2O$  density  $\rho$ , and  $A_1$ , therefore being directly proportional to  $\rho$  (see eq (4)). The self-broadening may increase the values of  $K$  enough to cause the attenuation to be considerably higher for high  $H_2O$  density than would be predicted from the equations based on data obtained at lower densities. For example, if  $\rho \approx 30 \text{ g } H_2O/m^3$  ( $PH_2O \approx 0.04 \text{ atm}$ ) the calculated attenuation in the  $22 \text{ cm}^{-1}$  and  $28 \text{ cm}^{-1}$  windows may be low by as much as 20 to 40 percent. This error due to self-broadening could be even greater in the lower wavenumber windows; it is unlikely that it would be less than 20 percent.

All the calculations discussed in sections II-2, -3, and -4 are also based on the assumption that the only influence of changing temperature on  $K$  is that due to the change in  $\alpha$  (see eq (8)). Again, data on infrared windows indicate that this assumption is not completely valid; it is also probably not entirely valid in the NMMW region. In general, the wing absorption decreases

<sup>2</sup>D. E. Burch, Absorption of Infrared Radiant Energy by  $CO_2$  and  $H_2O$ . III. Absorption by  $H_2O$  between 0.5 and  $36 \text{ cm}^{-1}$  ( $279 \mu\text{m}$  to 2 cm), *Journal of Optical Society of America*, vol. 56 (1968), 1383-1394.

with increasing temperature at a faster rate than is predicted by simple line-shape equations. This unexplained temperature dependence is more pronounced for self-broadening than for  $N_2$ -broadening. High  $H_2O$  densities necessarily occur with high temperatures. Therefore, the temperature effect may partially cancel the self-broadening effect discussed in the previous paragraph.

Available data in the microwave and millimeter regions were not generally obtained under conditions that were controlled well enough to provide much information on the influences of temperature or self-broadening. Data at 3.8 and 4.3 mm by Crawford and Hogg (see description of technique in Chapter VII) do indicate an increase in the attenuation per km per unit density ( $A_l$  as defined in eq (6)) with increasing  $H_2O$  density. This could be explained in terms of self-broadening. Unfortunately,  $O_2$  absorbs at these two wavelengths, and the  $H_2O$  attenuation was determined by subtracting the  $O_2$  attenuation from the measured total attenuation. Variations in temperature undoubtedly produced variations in the amount of  $O_2$  attenuation, which, in turn, increased the uncertainty in the  $H_2O$  measurements.

It seems likely that the Van Vleck-Weisskopf line shape included as a factor in equation (7) is valid for both self-broadening and  $N_2$  broadening within a few-tenths of a  $cm^{-1}$ , or even a few  $cm^{-1}$ , from the line centers. The influences of both self-broadening and  $N_2$  broadening must, of course, be accounted for in calculating  $\alpha$ . Most of the deviation from the simple shape probably occurs beyond 1  $cm^{-1}$  from the line center; this deviation depends strongly on temperature and is different for self-broadening than for  $N_2$  broadening. The use of the empirical continuum discussed in section II-2 has some physical basis in that it could represent the "extra" absorption due to the extreme wings of very distant lines as well as that due to deviations from the Van Vleck-Weisskopf shape. Proper use of the empirical continuum requires that the portions due to self-broadening and  $N_2$

broadening be known. The temperature dependence must also be known.

The extra absorption not predicted by theory has been attributed by some workers to dimers. This source of absorption has also been used to explain the large ratio between the effects of self-broadening and  $N_2$  broadening in windows. Dimers may be responsible for some of this absorption, but it is unlikely that they are responsible for it at every wavelength where it has been observed. Infrared lines of several gases have been shown to have different shapes for self-broadening than for  $N_2$  broadening. It is reasonable to expect that the same is true in the NMMW region. Absorption by the wings of self-broadening  $H_2O$  lines has the same dependence on  $H_2O$  partial pressure as does absorption by dimers. The absorption per unit length at a fixed temperature is proportional to  $(P_{H_2O})^2$ . This similar dependence makes it very difficult to determine experimentally which type of absorption is being observed.

The anomalous absorption below 15  $cm^{-1}$  that has been observed by the group at Appleton Laboratory contains distinct absorption features that are not produced by adding a continuum to theoretical spectra of the  $H_2O$  monomer. It has not been possible to relate this anomalous absorption quantitatively to  $H_2O$  density and temperature although it is most prominent at high relative humidities. Ryadov and Furashov<sup>4</sup> have studied  $H_2O$  attenuation between 5.5 and 6.5  $cm^{-1}$ , a portion of the region where the Appleton Laboratory group observed distinct anomalous absorption minima and maxima. Ryadov and Furashov did not observe any structure; therefore, it is difficult to determine under what conditions the anomalous absorption is important. Under conditions of very high relative humidity, the total attenuation including anomalous absorption might well be much greater in the 7.2 and 11.5  $cm^{-1}$  windows than is predicted by figures II-3 through II-6.

<sup>4</sup>Ya. V. Ryadov and N. I. Furashov, *Investigation of the Spectrum of Radiowave Absorption by Atmospheric Water Vapor in the 1.15 to 1.5-mm Range*, *Radio Physics and Quantum Electronics*, vol. 15, no. 10 (October 1974), 1124-1128.

The curves labelled A in figures II-3 and II-4 are based on results of many different experiments carried out under many conditions. Therefore, the uncertainties in the attenuation coefficients in the windows are difficult to estimate. Those presented for the 22 and 28  $\text{cm}^{-1}$  windows are probably accurate to 15 or 20 percent. Values presented for lower wavenumbers are more uncertain because the data were obtained under less-controlled conditions. Of course, the application of these results to the real atmosphere is subject to the additional uncertainty in the atmospheric composition. Self-broadening in atmospheric paths with high  $\text{H}_2\text{O}$  density may produce 20 to 30 percent more attenuation than

would be calculated by assuming that the attenuation is directly proportional to  $\text{H}_2\text{O}$  density.

The curves of zenith attenuation by  $\text{H}_2\text{O}$  in figure II-6 are based on the curves of figures II-3 and II-4 and are subject to the same errors. Additional errors undoubtedly arise because of the differences in  $\text{H}_2\text{O}$  density and temperature in the upper atmosphere. These variations may not be accounted for properly. Values of total zenith attenuation may be in error by as much as 50 to 100 percent at high altitudes; the errors are probably less than 25 to 50 percent at low altitudes.

## CHAPTER II.—LITERATURE CITED

- (1) R. A. McClatchey, W. S. Benedict, S. A. Clough, D. E. Burch, R. F. Calfee, K. Fox, L. A. Rothman, and J. S. Garing, *AFCRL Atmospheric Absorption Line Parameters Compilation*, Air Force Geophysical Laboratories AFCRL-TR-73-0096 (January 1973).
- (2) D. E. Burch, *Absorption of Infrared Radiant Energy by CO<sub>2</sub> and H<sub>2</sub>O. III Absorption by H<sub>2</sub>O between 0.9 and 36 cm<sup>-1</sup> (278 μm to 3 cm)*, *Journal of the Optical Society of America*, vol. 58 (1968), 1383-1394.
- (3) S. L. Valley, *Handbook of Geophysics and Space Environments*, Air Force Cambridge Research Laboratory (AFCRL) (1965).
- (4) R. A. McClatchey, R. W. Fenn, J. E. A. Selby, F. E. Voiz, and J. S. Garing, *Optical Properties of the Atmosphere (Revised)*, AFCRL-71-0279, *Environmental Research Papers*, No. 354 (10 May 1971).
- (5) N. Sissenwinn, D. D. Grantham, and H. A. Salemla, *Humidity Up to the Mesopause*, AFCRL-68-0553 (1962).
- (6) Ya. V. Ryadov and N. I. Furashov, *Investigation of the Spectrum of Radiowave Absorption by Atmospheric Water Vapor in the 1.15 to 1.5-mm Range*, *Radio Physics and Quantum Electronics*, vol. 15, no. 10 (October 1974), 1124-1128.
- (7) L. Frenkel and D. Woods, *The Microwave Absorption by H<sub>2</sub>O Vapor and Its Mixtures with Other Gases Between 100 and 300 GHz*, *Proceedings of the IEEE*, vol. 54 (1966), 493-505.
- (8) A. W. Stralton and C. W. Tolbert, *Anomalies in the Absorption of Radio Waves by Atmospheric Gases*, *Proceedings of the IRE*, vol. 48 (1960), 898.
- (9) Yu. A. Dryagin, A. G. Kislyakov, L. M. Kukin, A. I. Naumov, and L. I. Fedoseyev, *Measurements of Atmospheric Absorption of Radiowaves in 1.36- to 3.0-mm Range*, *Izvestiya VUZ Radiophysica*, vol. 9, no. 6 (1966), 624-627.
- (10) B. D. Guenther, J. S. Bennett, W. L. Gamble, and R. L. Hartman, *Submillimeter Research: A Propagation Bibliography*, U.S. Army Missile Command, Technical Report RR-77-3 (November 1976).
- (11) D. E. Burch, *semi-Annual Technical Report: Investigation of the Absorption of Infrared Radiation by Atmospheric Gases*, Contract No. F19628-69-C-0263, Aeronutronic-Ford Publication U-4784 (January 1970).
- (12) R. E. Roberts, J. E. Selby, and L. M. Biberman, *Infrared Continuum Absorption by Atmospheric Water Vapor in 8-12-μm Window*, *Applied Optics*, vol. 15, no. 9 (September 1973), 2035-2090.
- (13) R. W. Watkins and K. O. White, *Water-Vapor Continuum Absorption Measurements (3.5-4.0-μm) Using HDO-Depleted Water*, *Optics Letters*, vol. 1, no. 1 (July 1977), 31-32.
- (14) D. E. Burch, D. A. Gryvnak, and G. H. Piper, *Infrared Absorption by H<sub>2</sub>O and N<sub>2</sub>O*, AFCRL-TR-73-0530 (July 1973).
- (15) F. W. McMillan, J. J. Gallagher, and A. M. Cook, *Calculations of Antenna Temperature, Horizontal Path Attenuation, and Zenith Attenuation Due to Water Vapor in the Frequency Band 150-700 GHz*, *IEEE Trans. Microwave Theory and Techniques*, vol. MTT-25, no. 6 (June 1977), 484-488.

CHAPTER II.—LITERATURE CITED (Cont'd)

- (16) R. J. Emery, P. Moffat, R. A. Bohlander, and H. A. Gebbie, Measurements of Anomalous Atmospheric Absorption in the Wavenumber Range  $4\text{ cm}^{-1}$  -  $15\text{ cm}^{-1}$ , *Journal of Atmospheric and Terrestrial Physics*, vol. 37 (1975), 587-594.
- (17) D. E. Burch, D. A. Gryvnak, R. R. Patty, and C. E. Bartky, Absorption of Infrared Radiant Energy by  $\text{CO}_2$  and  $\text{H}_2\text{O}$ . IV. Shapes of Collision-Broadened  $\text{CO}_2$  Lines, *Journal of the Optical Society of America*, vol. 39, (1969), 267-280.
- (18) H. J. Liebe and T. A. Dillon, *Journal of Chemical Physics*, Accurate Foreign-Gas-Broadening Parameters of the 22-GHz  $\text{H}_2\text{O}$  Line from Refraction Spectroscopy, vol. 50 (1969), 727-732.

**CHAPTER III.—PROPAGATION IN THE PRESENCE OF NATURALLY  
OCCURRING PARTICULATES**

**by William L. Gamble**

## CONTENTS

	Page
III-1. INTRODUCTION .....	57
III-2. FOG AND HAZE .....	60
III-2.1 General Characteristics .....	60
III-2.2 Near-Millimeter Wave Attenuation in Fog .....	62
III-3. RAIN AND SNOW .....	66
III-3.1 General Characteristics .....	66
III-3.2 Attenuation in Rain and Snow .....	66
III-3.3 Backscattering in Rain .....	67
III-4. DUST .....	68
III-5. CLOUDS .....	69
LITERATURE CITED .....	73

### III-1. INTRODUCTION

The extinction of radiation by particles is a very old and well-developed field of physics, and for the purposes of radar, is very well understood. The difficulties arise because of the lack of precise data characterizing scattering media, such as the shape of dust particles, the degree of asphericity of rain droplets, particle size distributions and temperatures, and the refractive indices of the particles.

The exact relationships for the extinction of electromagnetic radiation by small particles were first obtained by Mie in the early 1900's and many subsequent treatments of the subject are available. Notable among these are Stratton<sup>1</sup> and Van de Hulst.<sup>2</sup> An excellent treatise of the general subject has been edited by Kerr.<sup>3</sup>

The particular effect of atmospheric particulates which is most important depends on the kind of system under consideration. For monostatic radar systems, backscattering from aerosols limits the contrast between beam on and off target and often the range at which a target can be detected and tracked. Wide-angle scattering and absorption remove power from the beam and will limit either range, where no contrast problem occurs, or the signal-to-noise ratio, where one does occur. Forward scattering normally shows up as an attenuation mechanism where flood-illuminated targets against a non-cluttered background are being encountered. It attenuates by spreading the beam and hence reducing the power density of the illuminating beam. Forward scattering could have more serious effects on systems where high angular resolution is of paramount importance. Wide-angle scattering aside from attenuation would be most serious in designator systems, since a seeker might not be able to track effectively.

<sup>1</sup>J. A. Stratton, *Electromagnetic Theory*, McGraw-Hill Book Company, New York (1941), 554-573.

<sup>2</sup>H. C. Van de Hulst, *Light Scattering by Small Particles*, John Wiley and Sons, New York (1957).

<sup>3</sup>D. E. Kerr, ed., *Propagation of Short Radio Waves*, McGraw-Hill Book Company, New York, Ch 7-8 (1951).

Attenuation (often called extinction) is normally broken down into absorption and scattering. The cross sections appropriate to these quantities are defined as follows for individual particles.

- Scattering cross section

$$C_{sca} = \frac{\text{Power scattering into } 4\pi \text{ steradians}}{\text{Incident power density}} \quad (1a)$$

- Absorption cross section

$$C_{abs} = \frac{\text{Power absorbed as heat}}{\text{Incident power density}} \quad (1b)$$

- Extinction or attenuation cross section

$$C_{ext} = C_{abs} + C_{sca} \quad (1c)$$

- Backscattering cross section for the scattering region in the far field of the antenna

$$C_{bcs} = \frac{\text{Backscattered power}}{\text{Incident power density}} \quad (1d)$$

These four quantities are normally complex functions of the shape, size, dielectric properties of the particle, and the frequency of the incident radiation. Following normal practice,<sup>2</sup> the normalized cross sections or efficiencies,  $Q$ , can be expressed in the following manner for homogeneous spherical particles:

$$Q_{bcs} = \frac{C_{bcs}}{\pi D^2/4} = \frac{1}{\chi^2} \left[ \sum_{n=1}^{\infty} (-1)^n (2n+1)(A_n - B_n) \right]^2 \quad (2a)$$

$$Q_{sca} = \frac{C_{sca}}{\pi D^2/4} = \frac{2}{\chi^2} \sum_{n=1}^{\infty} (2n+1)(|A_n|^2 + |B_n|^2) \quad (2b)$$

$$Q_{ext} = \frac{C_{ext}}{\pi D^2/4} = \frac{2}{\chi^2} \text{Re} \left[ \sum_{n=1}^{\infty} (2n+1)(A_n + B_n) \right] \quad (2c)$$

$$Q_{abs} = \frac{C_{abs}}{\pi D^2/4} = Q_{ext} - Q_{sca} \quad (2d)$$

where  $D$  is the particle diameter and  $\chi = \pi D/\lambda$ ;  $A_n$  and  $B_n$  are the coefficients of the  $n^{\text{th}}$  electric and magnetic modes given by

$$A_n = \frac{\chi j_n(\chi) [\beta]_n(\beta)' - m [\chi]_n(\chi) [\beta]_n(\beta)'}{\chi h_n(\chi) [\beta]_n(\beta)' - m [\chi]_n(\chi) [\beta]_n(\beta)'} \quad (3a)$$

$$B_n = \frac{[\chi]_n(\chi) [\beta]_n(\beta)' - m \chi j_n(\chi) [\beta]_n(\beta)'}{[\chi h_n(\chi) [\beta]_n(\beta)' - m \chi h_n(\chi) [\beta]_n(\beta)']} \quad (3b)$$

where  $m$  is the complex refractive index of the particle,  $\beta = am$ ,  $j_n$  is the  $n^{\text{th}}$  order spherical Bessel function of the first kind, and  $h_n(z) = j_n(z) + i(-1)^{n-1} y_{n-1}(z)$  is the  $n^{\text{th}}$  order spherical Bessel function of the third kind. The prime denotes differentiation with respect to the argument.  $\text{Re}$  denotes real part of.

For particles small compared to the wavelength, the Rayleigh approximation is valid and only the first term in the series need be retained. The cross sections then reduce to

$$C_{\text{bcs}} = \frac{\pi^2 |K|^2 D^6}{\lambda^4} \quad (4a)$$

$$C_{\text{scs}} = \frac{2\pi^2 |K|^2 D^6}{3\lambda^4} \quad (4b)$$

$$C_{\text{abs}} = \frac{\pi^2 D^3 \text{Im}(-K)}{\lambda} \quad (4c)$$

where  $K = (m^2 - 1)/(m^2 + 2)$ ;  $\text{Im}$  means imaginary part of. The complex index of refraction,  $m$ , is defined as

$$m = v - ix \quad (5)$$

$x$  is related to the bulk absorption coefficient,  $\xi$ , in the medium by

$$x = \frac{4\pi d}{\lambda} \quad (6)$$

The power in a collimated beam is reduced by  $e^{-\xi l}$  after transversing a path length  $l$  in a medium with a bulk absorption  $\xi$ . The term  $\text{Im}(-K)$  in equation (4c) is expressed in terms of  $v$  and  $x$  as

$$\text{Im}(-K) = \frac{6vx}{(v^2 + x^2)^2 + 4(v^2 - x^2 + 1)} \quad (7)$$

This should not be confused with the volume-scattering coefficient of an assemblage of such particles suspended in air.

If radiation impinges on a medium of index of refraction,  $n$ , where  $|n - 1|$  is small and in which is suspended a distribution of particles of index of refraction,  $m$ , separated by distances large compared to their diameters and the wavelength, then the cross sections characterizing the medium are as follows.

The reflectivity or backscatter cross section per unit volume (backscatter coefficient),  $\eta$ , and the attenuation coefficient,  $\gamma$ , are evaluated essentially by summing the effect over all particles in the illuminated volume. Thus,

$$\eta = \int_{D_{\text{min}}}^{D_{\text{max}}} N(D) C_{\text{bcs}}(D) dD \quad (8)$$

where  $N(D)dD$  is the number of particles per unit volume with diameters between  $D$  and  $D + dD$ . The attenuation  $\gamma$  (dB/unit of path length) is

$$\gamma = 4.343 \int_{D_{\text{min}}}^{D_{\text{max}}} N(D) C_{\text{ext}}(D) dD \quad (9)$$

In the Rayleigh scattering region, where  $\pi D/\lambda \ll 1$ , attenuation is due mainly to absorption, i. e.,  $C_{\text{ext}} \approx C_{\text{abs}}$ . The expressions (4) appropriate to the Rayleigh regime, can be substituted into expressions (8) and (9), yielding,

$$\eta = \frac{\pi^2 |K|^2}{\lambda^4} \int D^2 N(D) dD \quad (10)$$

$$\gamma = 4.343 \frac{\pi^2 \text{Im}(-K)}{\lambda} \int D^2 N(D) dD \quad (11)$$

$\int D^2 N(D) dD$  is just the total volume of particles per unit volume divided by  $\pi/6$  so that (11) reduces to

$$\gamma = 81.66 \frac{\text{Im}(-K)}{\lambda} V_p \quad (12)$$

where  $V_p$  is the total volume of particulate matter per unit volume.  $\gamma$  has the units of dB/(unit for measuring  $\lambda$ ). If the particulate matter has a density of  $\rho$  (g/cm<sup>3</sup>) and if  $V_p$  is expressed in m<sup>3</sup>/m<sup>3</sup>, one can write

$$\gamma = 81.66 \frac{\text{Im}(-K)}{\lambda} \frac{W}{\rho} \text{ (dB/km)} \quad (13)$$

for  $\lambda$  in millimeters.  $W$  is the mass of particles in grams per cubic meter of aerosol. Note that  $\rho = 1$  g/cm<sup>3</sup> for water. This is an extremely important equation, yielding the aerosol attenuation of near-millimeter wave in the Rayleigh limit. The expression will be valid regardless of the shape of dust or smoke particles as long as the condition ( $\lambda \gg$  largest particle dimension) holds.

For particles very large compared to the wavelength it is interesting to note another important limiting case. This is where  $x \rightarrow \infty$  or where  $D \gg \lambda$ . This is called the optical limit, as distinguished from the Rayleigh or small particle limit. In the optical regime, the shape of particles is of obvious crucial importance and it turns out that for spherical particles

$$\gamma_{\text{ext}} = 4.343 \frac{\pi}{4} \int D^2 N(D) dD \quad (14a)$$

or

$$\gamma_{\text{ext}} = 8.686\pi \int R^2 N(R) dR \quad (14b)$$

$$= 8.686 \sum_{\substack{\text{all particles} \\ \text{unit volume}}} (\text{individual particle cross-sectional areas}) \quad (14c)$$

This result means that large particles attenuate beams or remove twice as much power from a beam as would be expected from a simple summing of their geometrical cross sections. This effect is a consequence of the diffraction around such particles.

It is also well known that particles have a maximum extinction cross section of four times their geometrical cross sections when  $x = 1$ .

For spherical homogeneous particles with diameters comparable to the wavelength, the Mie scattering theory is very well developed and demonstrably correct. There is some information available on particle-size distributions typical of rain and fogs for making predictions as to the attenuation and backscattering characteristics during such conditions.

The current major source of uncertainty about the attenuation effects due to atmospheric condensed water is in the temperature dependence of the refractive index. Diermendjian,<sup>4</sup> Rozenberg,<sup>5</sup> Lukes,<sup>6</sup> and Ray,<sup>7</sup> have made relatively recent critical surveys of this subject. Rozenberg and Ray have tabulated the temperature and frequency dependence based on a modification of the Debye theory and the best available data, but errors may be substantial except in the long wavelength part of the near millimeter range. Diermendjian and Lukes concluded that the room temperature data of Davies et al<sup>8</sup> are quite reliable. Diermendjian considered the available data at other temperatures so

<sup>4</sup>D. Diermendjian, *Far Infrared and Submillimeter Wave Attenuation by Clouds and Rain*, Rand Corporation Report AD-A021-947 (April 1975).

<sup>5</sup>V. I. Rozenberg, *Scattering and Attenuation of Electromagnetic Radiation by Atmospheric Particles*, Hydrometeorological Press, Leningrad, USSR (1972).

<sup>6</sup>G. D. Lukes, *Penetrability of Haze, Fog, Clouds, and Precipitation by Radiant Energy over the Spectral Range 0.1 Micron to 10 Centimeters*, The Center for Naval Analyses of the University of Rochester, Report No. 61 (May 1968).

<sup>7</sup>P. S. Ray, *Broadband Complex Refractive Indices of Ice and Water*, *Applied Optics*, vol. 11 (1972), 1839.

<sup>8</sup>M. Davies, G. W. F. Pardoe, J. Chamberlain, and H. A. Gebbie, *Submillimeter- and Millimeter-wave Absorption of Some Polar and Non-polar Liquids Measured by Fourier Transform Spectroscopy*, *Transactions of the Faraday Society*, vol. 66 (1970), 273.

unreliable that he made his rain and fog attenuation calculations using room temperature (24 C) refractive indices in spite of his knowledge that rain and cloud droplets are substantially cooler than this. In spite of this uncertainty, Rozenberg's tabulation probably illustrates the trends which are interesting and important. Figure III-1 is a plot of  $\nu$  and  $\kappa$  versus temperature for the indicated wavelengths. The rather large increase in  $\nu$  for the longer wavelength has the effect of increasing the backscattering and attenuation from scattering due to small particles at high temperatures in rain. Of more importance is the decrease in  $\kappa$  with decreasing temperature at 0.8 mm. This has the effect of substantially decreasing the losses due to absorption by small droplets of liquid water at colder temperatures. It should be emphasized that under most conditions, absorption, not scattering, is the dominant attenuation mechanism at these wavelengths. The factor  $\text{Im}(-K)$  is plotted in figure III-2 for  $\lambda = 0.8$  mm and  $\lambda = 3$  mm. It can be seen that for temperatures higher than about -5 C, the temperature dependence is opposite for these two wavelengths. The absorption at 0.8 mm increases with increasing temperature while that for 3 mm increases with decreasing temperature. The scattering coefficient, however, varies only ~20 percent over the same range, so that any significant temperature dependence in the scattering is buried in whatever role temperature might play in a particle-size distribution or in the details of the Mie series. Generally,  $\nu$  increases significantly at the longer millimeter and centimeter wavelengths while remaining relatively constant for short millimeter and submillimeter wavelengths. It should be noted that the above discussion pertains to supercooled water and not to ice.

The temperature at which an ice fog forms from a water fog depends on particle sizes<sup>9</sup> and other factors, such as purity. Generally, it appears to be in the range of -30 to -40 C for droplets in the 1 to 10  $\mu\text{m}$  range. Figure III-3 (from Dierrnendjian) shows the optical constants

<sup>9</sup>B. J. Mason, *Cloud Physics*, 2nd edition, Clarendon Press (1971).

of water and ice which he considers to be the most reliable available. Figure III-4 is the same for ice (from Ray). It can be seen that each set of data for  $\kappa$  (ice) tends toward negligible values in the near-millimeter wave region. The real part,  $\nu$ , is not large and, therefore, one would anticipate negligible NMMW attenuation in an ice fog.

Figure III-5 is a plot from Lukes<sup>4</sup> of the number density versus droplet radius for a number of different meteorological conditions ranging from haze to very heavy rain. In can be seen from this that scattering will be a more important factor for rain than for fogs at NMM wavelengths.

## III-2. FOG AND HAZE

### III-2.1 General Characteristics

The meteorological conditions referred to as fog and haze are generally different only in intensity. Both conditions are caused by suspended liquid water droplets near the earth's surface. The particle-size distribution and concentrations are roughly as illustrated in figure III-5. The condition is called a fog or a haze, depending on whether visibility is less or greater than a kilometer, respectively.

As is discussed by Middleton,<sup>10</sup> visibility is loosely defined as that distance at which large dark objects can be discerned against the horizon during daylight by human observers.

Fogs are roughly characterized as being advection or radiation, depending on the meteorological conditions causing their formation. Advection fogs generally form when saturated air moves over water or terrain at a lower temperature. This causes cooling and hence the condensation or small water droplets. Radiation

<sup>4</sup>G. D. Lukes, *Penetrability of Haze, Fog, Clouds and Precipitation by Radiant Energy over the Spectral Range 0.1 Microns to 10 Centimeters*, The Center for Naval Analyses of the University of Rochester, Report No. 61 (May 1968).

<sup>10</sup>W. E. K. Middleton, *Vision Through the Atmosphere*, University of Toronto Press (1963).

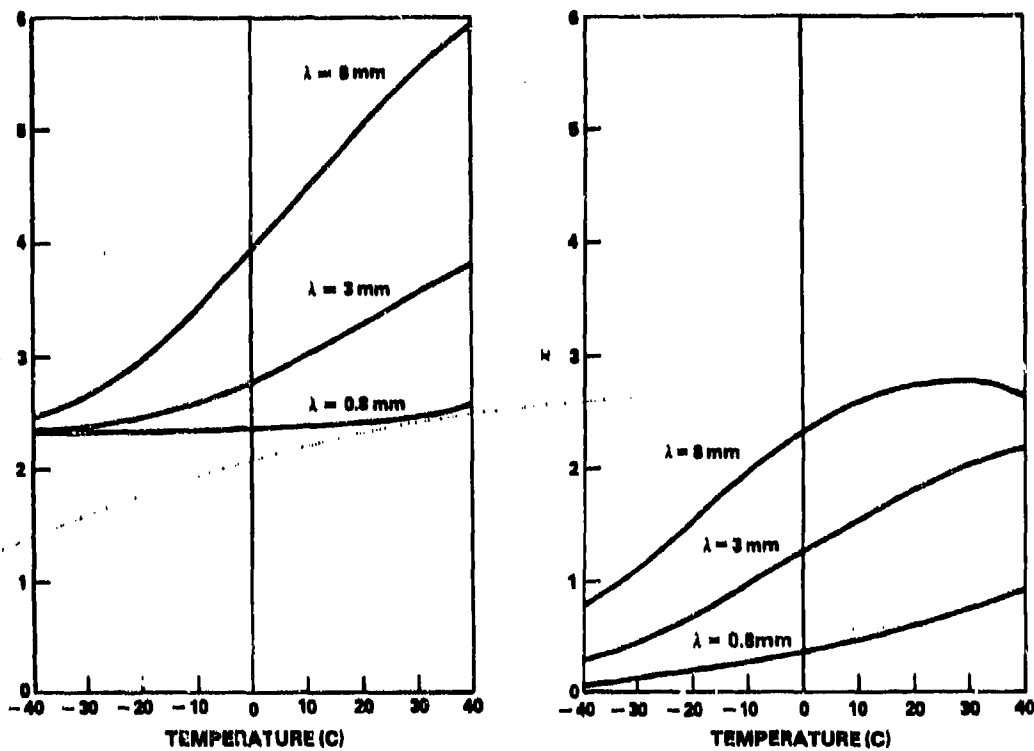


Figure III-1. Variation of  $\nu$  and  $\kappa$  with temperature for  $\lambda = 8, 3,$  and  $0.8$  mm, according to Rozenberg, *Scattering and Attenuation of Electromagnetic Radiation by Atmospheric Particles*, Hydrometeorological Press, Leningrad, USSR (1972).

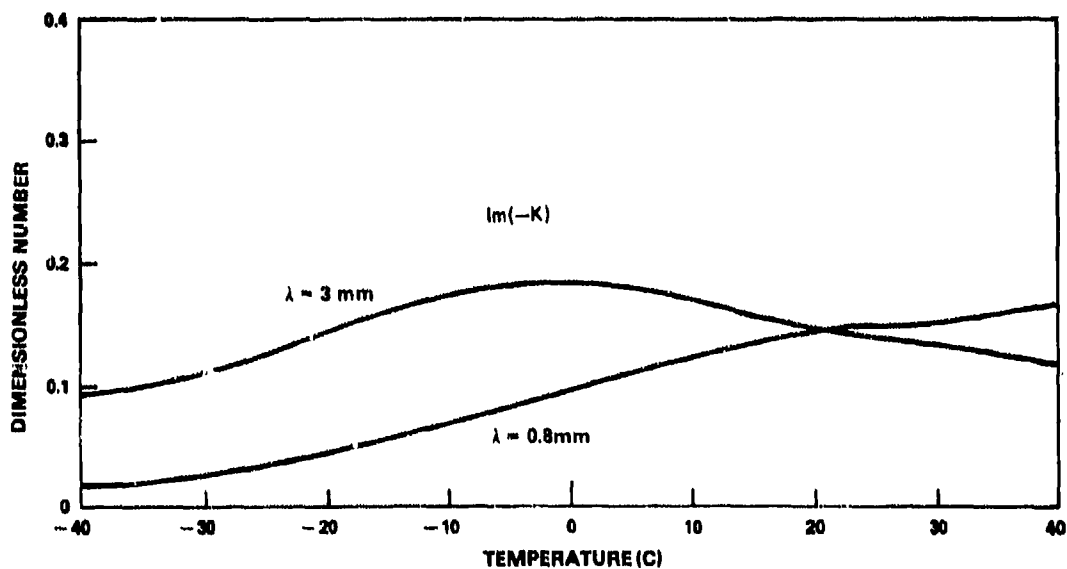


Figure III-2. Variation of  $\text{Im}(-K)$  with temperature at  $\lambda = 3$  and  $0.8$  mm using data shown in figure III-1.

fogs are caused by the rapid cooling of land or water after sunset. This causes a fog if the surface atmosphere was near saturation at the temperature of the surface during sunshine. Other types of fogs are identifiable and it should be emphasized that, very often, several of the established mechanisms may contribute simultaneously to the formation of any given fog. Figure III-6 is a plot visibility versus liquid water content characteristic of the two kinds of fogs.<sup>11</sup>

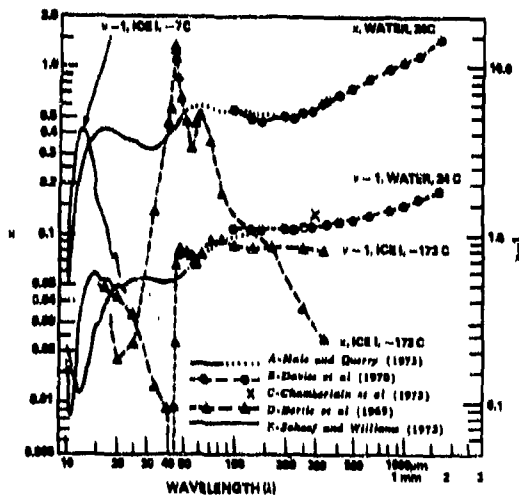


Figure III-3. Optical constants of water as used by Diermendjian, *Far Infrared and Submillimeter Wave Attenuation by Clouds and Rain*, Rand Corporation, AD-021-947 (1975).

Predictability of fog<sup>12</sup> is an important factor. The frequency of occurrence, severity, and duration of those meteorological conditions causing severely restricted visibility (such as fog, haze, and low-lying clouds) are very sensitive functions of geographic location. This discussion will be restricted to that of the central North Atlantic Treaty Organization (NATO) front or to West Germany. Figures III-7, -8, and -9 are reproduced from the U.S.

<sup>11</sup> R. G. Eldridge, *Haze and Fog Aerosol Distribution*, *Journal of Atmospheric Science*, vol. 23 (1966), 608.

<sup>12</sup> O. Eissenwanger, *On the Duration of Widespread Fog and Low Ceiling in Central Europe and Some Aspects of Predictability*, Missile Research and Development Command TR-RR-73-9 (1 August 1973).

Army Field Manual FM100-5 and show in a self-explanatory way the conditions in West Germany. Generally, one in every three mornings, visibility will be less than 1 km in the fall and winter. Note also that fog is infrequent in the summer and relatively infrequent in the spring.

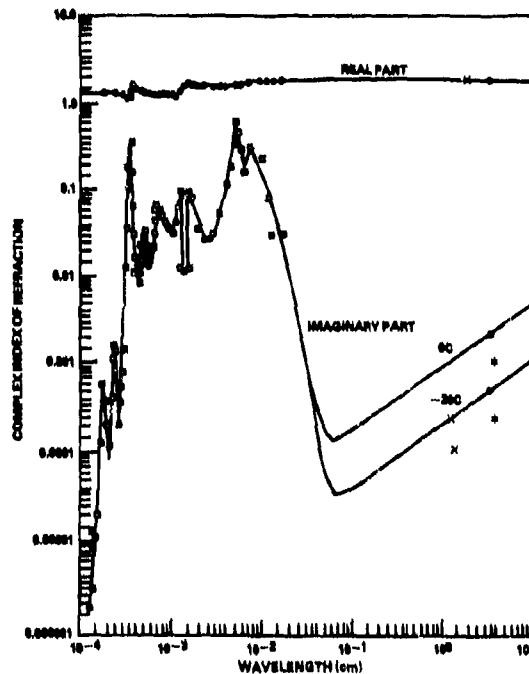


Figure III-4. Optical constants of ice according to Kay, *Applied Optics*, vol. 11 (1972), 1839.

### III-2.2 Near-Millimeter Wave Attenuation in Fog

Figure III-10 is a plot from Diermendjian, based on full Mie calculations of extinction versus wavelength for three cloud particle-distribution models and for two rain models. The models used in the calculations for this figure are as follows (liquid temperature = 24 C).

Cloud C.1--fair weather cumulus, mode radius  $r_c = 4 \mu\text{m}$ , droplet density  $N = 100/\text{cm}^3$ , liquid content  $q_L = 0.067 \text{ g/m}^3$

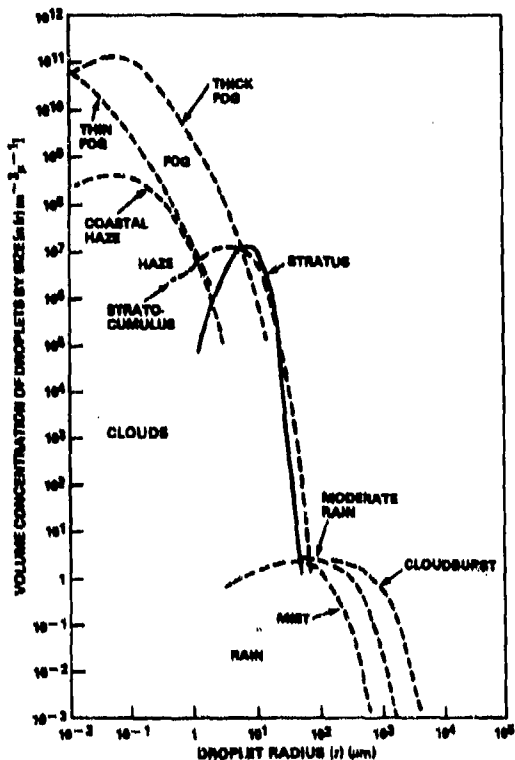


Figure III-5. Volume concentration of water droplet by size, (counted in 1- $\mu$ m intervals of droplet radius). Lukes, *The Center for Naval Analyses of the University of Rochester, Report 61 (May 1968)*.

The climate of Germany is generally cold and wet. Although there are sunny warm days in summer and snow conditions in winter, the predominant climate is a low overcast with rain.

This chart shows the mean temperatures for the four seasons in Germany. While the temperature means do not appear to be particularly severe, US forces must be well equipped and trained to operate for extended periods in cold weather and snow.

This chart shows the mean rainfall that can be expected in Germany. This is particularly significant in late fall and early spring when the snow begins to melt, the ground thaws, and spring rainfall occurs. During this period, cross country wheeled vehicle trafficability will be seriously impaired.

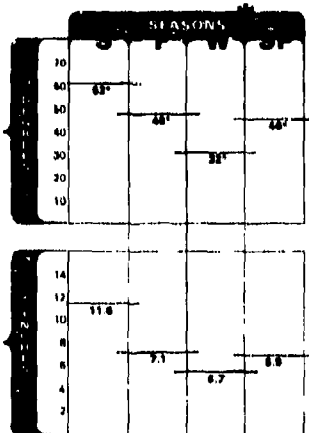
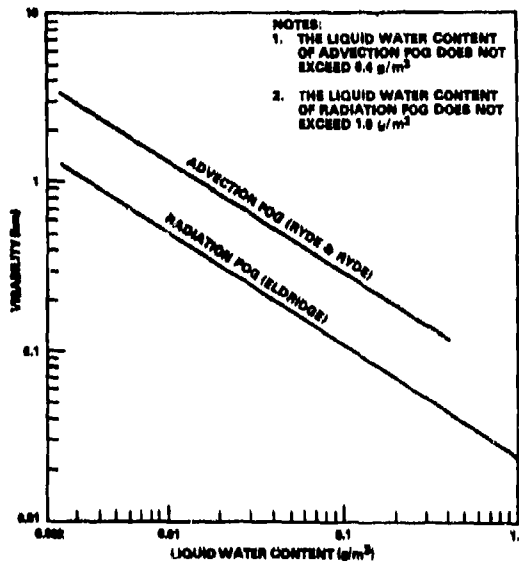


Figure III-7. Seasonal average temperature and precipitation in West Germany, adapted from U.S. Army Field Manual FM100-5, Operations.

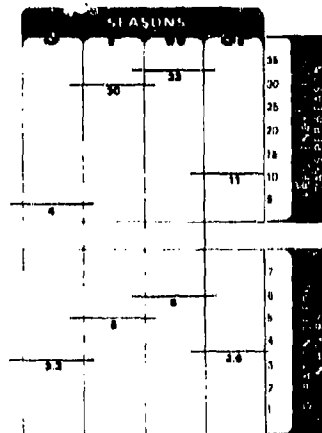


- NOTES:  
 1. THE LIQUID WATER CONTENT OF ADVECTION FOG DOES NOT EXCEED 0.4 g/m<sup>3</sup>  
 2. THE LIQUID WATER CONTENT OF RADIATION FOG DOES NOT EXCEED 1.8 g/m<sup>3</sup>

Figure III-6. Correlation of visibility in fog with liquid water content. R. G. Eldridge, *Journal of Atmospheric Science*, vol. 123 (1966).

☀	SUMMER 20 JUNE	20 SEPTEMBER
🍂	FALL 21 SEPTEMBER	20 DECEMBER
❄	WINTER 21 DECEMBER	19 MARCH
🌸	SPRING 20 MARCH	19 JUNE

Fall, winter, and early spring are featured by frequent fog which lies heavily on the land and often does not lift until midday. Frequency and duration of morning fog are as follows:



Approximately 1 out of 3 mornings during the fall and winter, US forces will have less than 1 km visibility.

Figure III-8. Seasonal average occurrence and duration of fog in West Germany, adapted from U.S. Army Field Manual FM100-5, Operations.

The cloud layer over Western Europe is typically low and scudding on westerly winds. The average ceilings (more than 50% cloud cover) expressed as a percentage for three month periods in West Germany are:

NO CEILING	29.7%	33.9%	26.1%	19.7%
3000 PLUS	49.2	54.2	45.3	41.2
1800-3000	3.9	3.4	4.9	9.9
1000-1800	5.4	3.3	6.2	5.9
500-1000	6.3	5.8	5.6	14.1
UNDER 500	6.3	4.4	14.4	19.8
AVERAGE	9.3	6.7	14.5	17.1

The incidence of ceilings less than 500 feet is markedly increased when coupled with fog as in this chart.

Figure III-9. Seasonal cloud cover statistics in West Germany, adapted from U.S. Army Field Manual FM100-5, Operations.

Cloud C.5—stratus or nimbostratus,  $r_c = 6 \mu\text{m}$ ,  $N = 100/\text{cm}^3$ ,  $q_L = 0.297 \text{ g/m}^3$

Cloud C.6—large droplet stratus/nimbostratus,  $r_c = 20 \mu\text{m}$ ,  $N = 0.1/\text{cm}^3$ ,  $q_L = 0.025 \text{ g/m}^3$

Rain-10—10 mm/hr rain rate

Rain-50—50 mm/hr rain rate

Cloud C.5 is essentially equivalent to a fog of roughly 100-m visibility.

Figure III-11 shows experimental data of attenuation versus visibility at 140 GHz ( $\lambda \sim 2 \text{ mm}$ ), which is in rough agreement with Diermendjian's calculation when corrected for molecular absorption.

It should be remembered that the lack of reliable data on the temperature dependence of the dielectric constants of liquid

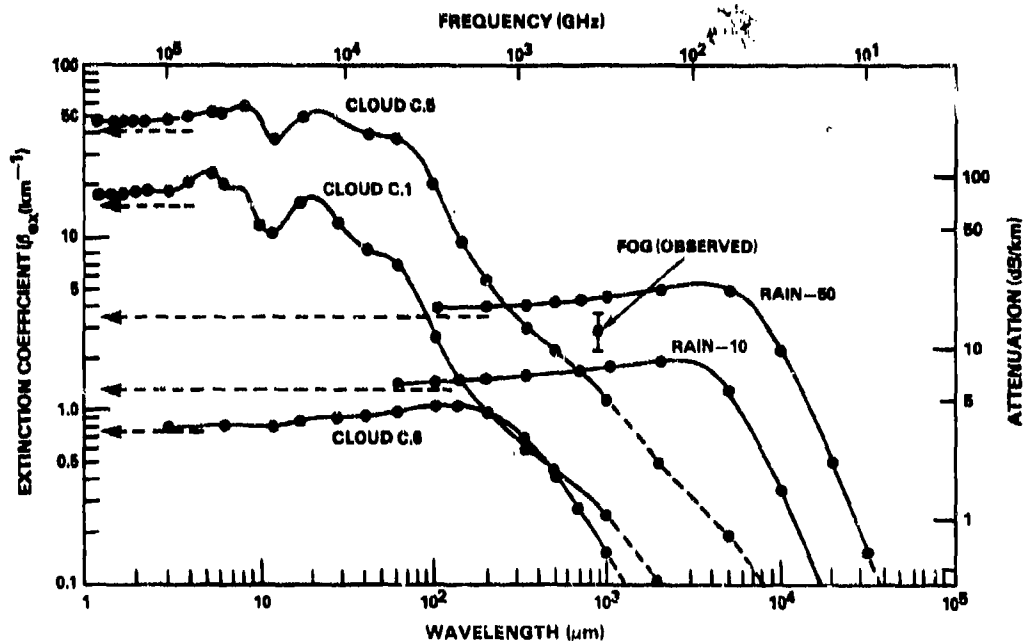


Figure III-10. Theoretical extinction coefficients according to three cloud models and two precipitation models. An experimental measurement made at MIRADCOM during a 100-m visibility fog at 0.89 mm has been added for comparison. D. Diermendjian, Rand Corporation AD-A021-947 (April 1975).

water droplets as a function of temperature renders data such as that from Diemendjian uncertain by as much as a factor of 2. This is especially true for wavelengths less than 2 mm where both Rozenberg and Ray agree that the imaginary part of the refractive index drops significantly as the temperature drops.

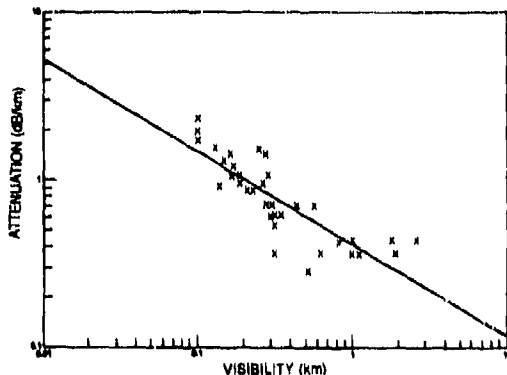


Figure III-11. Plot of 140-GHz one-way attenuation in fog versus visibility. D. G. Bauer et al, Ballistic Research Laboratories, Interim Memorandum Report 538 (January 1977).

Since fog is by far the most frequent condition causing severely restricted visibility in Europe, it is worthwhile to estimate the total attenuation of NMMW radiation during fog (including absorption due to water vapor and oxygen). Water vapor will be near saturation during fog so that a knowledge of the temperatures at which fogs occur is sufficient for such an estimation. Essenwanger\* has determined that 80 percent of fogs in Western Europe occur with an absolute humidity less than  $7.5 \text{ g/in}^3$  and that only 7 percent of such fogs occur when the relative humidity is greater than  $9.4 \text{ g/m}^3$ .

Figure III-12 is a set of curves for various NMM wavelengths showing estimated

\*O. M. Essenwanger, Estimation of the Temperature During Fog in Europe, Missile Research and Development Command (in press).  
 †Editor's Note: see reference 7 in Chapter VIII for recent measurements.

total attenuation during radiation fogs of 100-m visibility. A few comments are necessary about the validity of this figure. The water/vapor contribution was calculated by linear extrapolation of absolute humidity and with no attempt to correct for any other temperature effects. The fog contribution was calculated in the Rayleigh limit assuming the liquid water temperature to be 24 C. The values for the vapor may be low by possibly as much as 50 percent while the liquid water part is overestimated by possibly 50 percent. Adequate data do not exist to substantially reduce the uncertainty in such calculations.

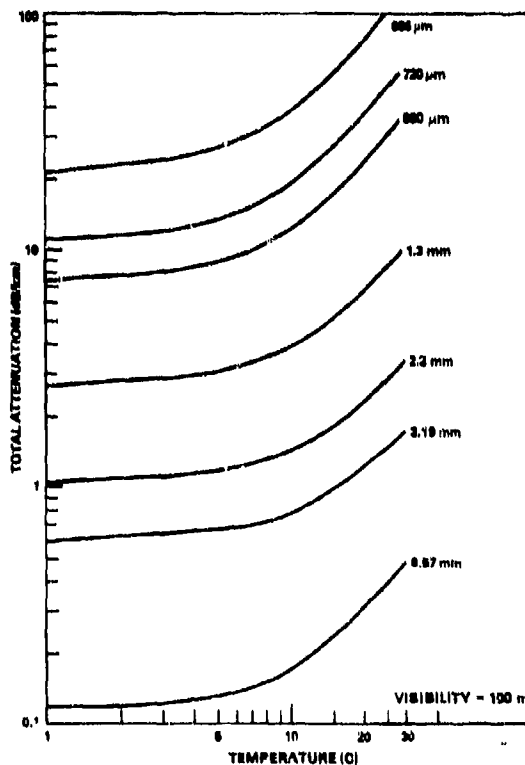


Figure III-12. Estimated total attenuation versus temperature at various wavelengths during a 100-m visibility radiation fog.

Measurements made at BRL<sup>13</sup> of total attenuation in fog at 140 GHz (2.15 mm) are shown in figure III-11. It can be seen that there is substantial agreement with figure III-12 at a temperature of around 13 C.

A substantial amount of data relevant to fog and haze can be found in section III-5 of this report.

### III-3. RAIN AND SNOW

#### III-3.1 General Characteristics

Table III-1 (from Lukes) illustrates the spectra of rain particles over a wide range of rain rates.

The dominant NMMW attenuation mechanism ranges from absorption for mist to scattering for the heavier rain rates. It should be emphasized that scattering is not negligible, even for mist and drizzle. It should also be noted that absorption is the most important mechanism for the lighter rains so that the temperature of the liquid water is important as is the prevailing temperature during rainfall. It is reasonable to assume that the atmosphere will be nearly saturated with water vapor during rains of reasonably long duration.

Seasonal precipitation as well as the temperature at which it occurs in Western Germany is shown in figure III-7. Table III-2 shows the number of days annually at five locations in West Germany when rain and snow will be encountered.\*† It is well known that heavy rains (rate > 4 mm/hr) are very rare and are of short duration.

<sup>13</sup>D. G. Bauer, R. A. McGee, J. E. Know, and H. B. Wallace, 140-GHz Beamrider Feasibility Experiment, Ballistic Research Laboratories, Interim Memorandum Report No. 538 (January 1977).

\*H. Duftel, Missile Research and Development Command (private communication).  
†Editor's Note: West German climatological information gathered from a broader and more current data base is being prepared for publication; R. G. Humphrey and W. H. Pepper, Standards for Environmental Conditions, preliminary data to be published by the Harry Diamond Laboratories.

It can be concluded that statistically, heavy rain is not a major limiting factor for ground-to-ground systems, but is a serious problem for ground-to-air and air-to-ground systems because of the cloud cover which usually accompanies the rain.

While the occurrence of snow is much less than rain, its effect on ground-to-ground visibility is much more serious.

#### III-3.2 Attenuation in Rain and Snow

Attenuation data in rain are very scarce throughout the NMMW region and this is especially true at the shorter wavelengths. From a look at figure III-10 one can see that the attenuation due to rain is roughly independent of wavelength from the visible through the NMMW range. It has been generally found that the attenuation of millimeter waves in rain is roughly proportional to the rain rate. Figure III-13 is a plot of attenuation at 140 GHz (2.1 mm) from Bauer et al.<sup>13</sup> which adequately illustrates the roughly linear dependence of attenuation on rain rate.

Figure III-14 shows data taken at 0.96 mm by Sokolov et al.<sup>14</sup> Note that the agreement is only fair, but a lack of information as to the temperatures and other factors precludes any serious analysis.

The attenuation of NMMW radiation in snow will depend strongly on how wet the snow is and hence on the temperature at which it is falling. The dominant mechanism will certainly be scattering in dry snow and perhaps also in wet snow. Figure III-15, taken from Richard<sup>15</sup> is a compendium of the relevant experimental data.

<sup>14</sup>A. V. Sokolov and Ye. V. Sukhorin, Attenuation of Submillimeter Radio Waves in Rain, *Radio Engineering and Electronic Physics*, vol. 15, no. 12 (1970), 2167.

<sup>15</sup>V. V. Richard, Low Angle Tracking at Millimeter Wavelengths, TTCF Ad-Hoc Study Group 102, Electro-Optical Low Angle Tracking (December 1976).

TABLE III-1. RAIN: NUMBER OF WATER DROPLETS PER CUBIC METER FOR SEVEN RAIN INTENSITIES

Interval of drop sizes (r in $\mu\text{m}$ )	Mist (0.05-mm per hr)	Drizzle (0.25-mm per hr)	Light rain (1-mm per hr)	Moderate rain (4-mm per hr)	Heavy rain (16-mm per hr)	Excessive rain (40-mm per hr)	Cloudburst (100-mm per hr)
3 to 10	6	6	6	6	6	6	6
10 to 20	13	13	13	13	13	13	13
20 to 50	51	51	51	51	51	51	51
50 to 100	69	80	85	90	92	92	95
100 to 200	51	85	106	146	160	163	187
200 to 300	10	26	54	87	110	128	160
300 to 400	2	9	24	45	75	95	138
400 to 500	0.5	3	11	27	50	69	115
500 to 600	0.1	1	5	15	32	50	95
600 to 700	-	0.3	2	8	20	35	80
700 to 800	-	0.1	1	4	13	23	65
800 to 900	-	-	0.4	2	8	16	52
900 to 1000	-	-	0.2	1	6	11	41
1000 to 1500	-	-	0.3	2	13	26	110
1500 to 2000	-	-	-	0.1	2	4	32
2000 to 2500	-	-	-	-	0.1	1	10
2500 to 3000	-	-	-	-	-	0.1	3
3000 to 3500	-	-	-	-	-	-	1
3500 to 4000	-	-	-	-	-	-	0.2
Total	203	274	359	501	651	783	1249

### III-3.3 Backscattering in Rain

Under some conditions,<sup>16</sup> systems operating in the NMMW region could be limited by backscattering. There are only scant experimental backscattering data at NMM wavelengths. Figure III-16 shows the dependence of measured backscattering cross section at several millimeter wavelengths versus rain rate.<sup>16</sup> These data are for summer rains in the

Orlando, FL, area. One should note that the backscattering coefficient is smaller at 3 mm (95 GHz) than at 4.2 mm (70 GHz).

Figure III-17, also taken from Richard,<sup>16</sup> represents a fit of Miescattering calculations to the BRL data as a function of frequency. Note the predicted slight advantage of shorter wavelengths. It should be emphasized, however, that this may not be true with the detailed particle-size distributions typical of Western Europe.

<sup>16</sup>V. W. Richard, *Millimeter Wave Radar Applications to Weapon System*, Memorandum Report No. 2631, Ballistic Research Laboratories (June 1976).

**TABLE III-2. AVERAGE ANNUAL PRECIPITATION CLIMATOLOGY/WEST GERMANY**

Five locations Measured	Total <sup>a</sup>	N <sub>RR</sub> <sup>b</sup>	N <sub>SS</sub> <sup>c</sup>	Percent
Bitburg	26 in.	159 days	25 days	(16)
Frankfurt	25	146	11	(8)
Fulda	31	187	36	(19)
Stuttgart	26	157	16	(10)
Berlin	22	153	12	(8)

<sup>a</sup>Total: Annual total precipitation in in.

<sup>b</sup>N<sub>RR</sub>: Number of days with precipitation  $\geq 0.01$  in.

<sup>c</sup>N<sub>SS</sub>: Number of days with snowfall  $\geq 0.1$  in.

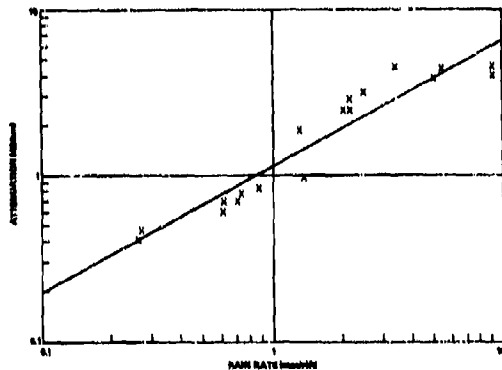


Figure III-13. 140-GHz rain attenuation versus rain rate. D. G. Bauer et al, Ballistic Research Laboratories, Interim Memorandum Report 538 (January 1977).

### III-4. DUST

Naturally occurring dust storms are not a problem in Europe in the sense of causing attenuation of NMMW radiation. According to Hinds and Hordale<sup>17</sup> visibility is reduced to less than a kilometer only once every 10 years. BRL<sup>13</sup> has shown that at 2.1 mm (140 GHz), sufficient dust to severely attenuate near-infrared and optical links caused no measurable attenuation at NMM wavelengths. This dust was generated by vehicular traffic.

<sup>13</sup>D. G. Bauer, R. A. McGee, J. E. Know, and H. B. Wallace, 140-GHz Beamrider Feasibility Experiment, Ballistic Research Laboratories, Interim Memorandum Report No. 538 (January 1977).

<sup>17</sup>B. D. Hinds and G. D. Hordale, Boundary Layer Dust Occurrence IV, Atmospheric Dust Over Selected Geographic Areas, USA Electronic Command ECOM-DR-77-3 (June 1977).

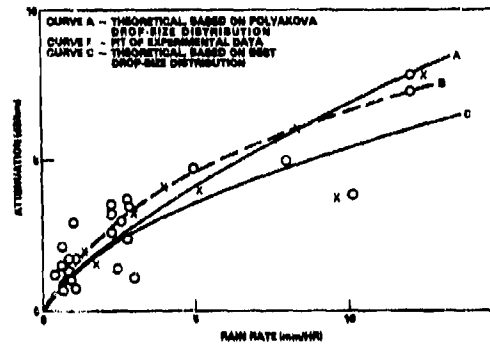


Figure III-14. Comparison of theoretical and experimental dependence of attenuation on the rain intensity at 0.96-mm wavelength. A. V. Sokolov and Ye. V. Sukhonin, *Radio Engineering and Electronic Physics*, vol. 15, no. 12 (1970), 2167.

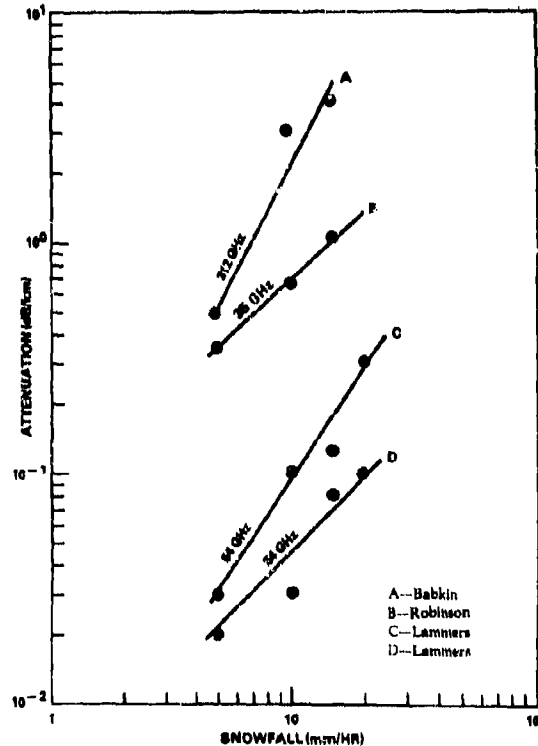


Figure III-15. Measured attenuation in snow versus snowfall rate. V. W. Richard, TTCP Ad-Hoc Study Group 102, *Electro-Optical Low Angle Tracking* (December 1976).

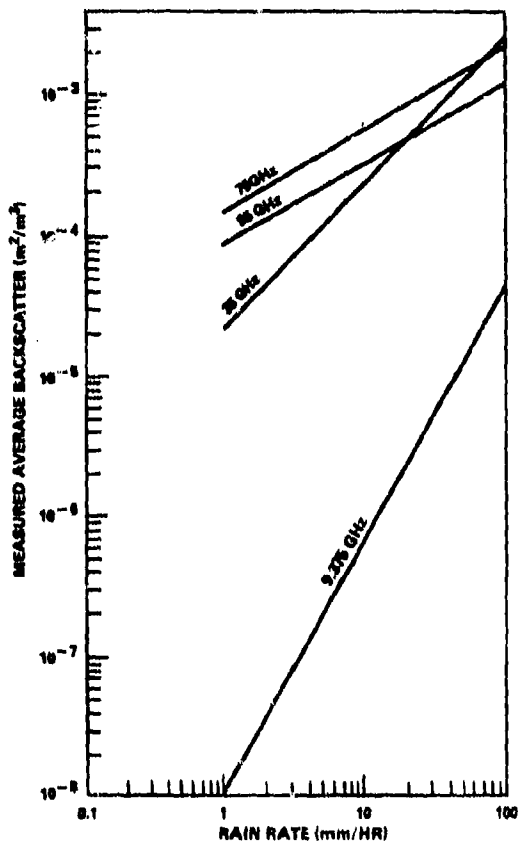


Figure III-16. Measured average backscatter coefficient of rain versus rain rate. V. W. Richard, Ballistic Research Laboratories, Memorandum Report 2631 (June 1976).

Reasonable estimates of the size and the dielectric properties of dusts would almost preclude significant attenuation, except possibly at the shortest NMM wavelengths (300  $\mu\text{m}$ ) where dust particles in the 50- to 100- $\mu\text{m}$  size range might scatter significantly. The larger particles, present immediately following ground bursts of munitions, might possibly break NMM tracking links for very short periods of time, however. Only experiments can answer such questions.\*

\*Editor's Note: Research tests have confirmed this assumption; e.g., DIRT-1, ASL-TR-0021 (January 1979), ASL-CR-79-0026-1 (June 1979), and Graf II, test results to be published.

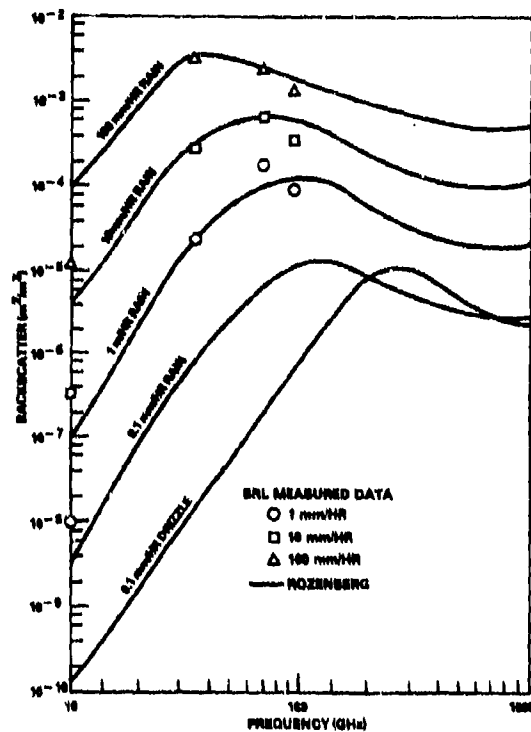


Figure III-17. Calculated and measured rain backscatter coefficient versus frequency. V. W. Richard, Ballistic Research Laboratories, Memorandum Report 2631 (June 1976).

### III-5. CLOUDS

Clouds are composed of water and/or ice particles with a condensed water content ranging from 0.1 to 1  $\text{g}/\text{m}^3$  for altitudes greater than 2 km and can range up to 10  $\text{g}/\text{m}^3$  for low-altitude ( $\sim 0.5$  to 5 km) precipitating clouds.<sup>9,10</sup> The temperature of clouds depends on both altitude and local conditions and is a very important determinant of NMMW attenuation. Typical particle-size distributions and liquid water content can be calculated using figure III-18.<sup>11</sup> Very high (>5 km) clouds fre-

<sup>9</sup>B. J. Mason, *Cloud Physics*, 2nd edition, Clarendon Press (1971).

<sup>10</sup>E. Bauer, *The Scattering of Infrared Radiation from Clouds*, *Applied Optics*, vol. 3 (1964), 197.

<sup>11</sup>L. W. Carrier, G. A. Cato, and K. J. von Esen, *The Backscattering and Extinction of Visible and Infrared Radiation by Selected Major Cloud Models*, *Applied Optics*, vol. 6 (1967), 1209-1216.

quently may contain larger ice crystals with typical dimensions of 30 to 200  $\mu\text{m}$ . It will be shown below that NMMW absorption effects due to the water contents typical of ice clouds are negligible compared to those of liquid water clouds. Scattering could become very significant for large ice crystals. Since these crystals are often preferentially aligned by aerodynamic drag forces, such scattering may be quite anisotropic with respect to polarization.

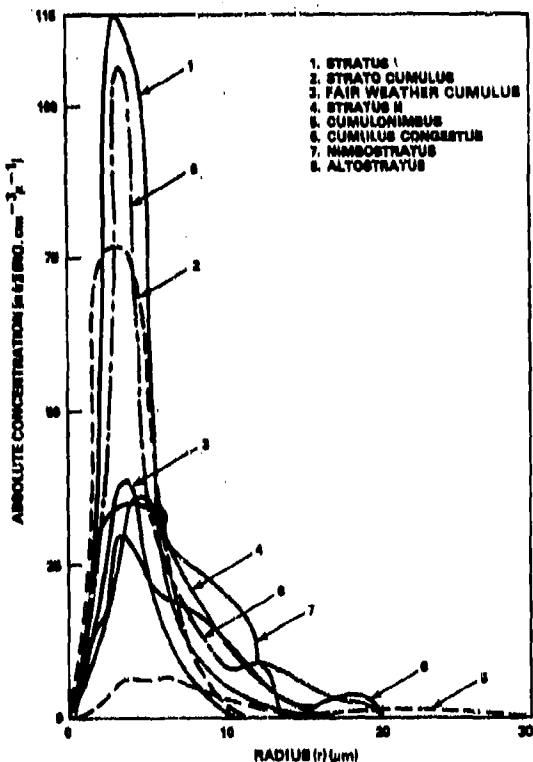


Figure III-18. Model cloud drup spectra. L. W. Carrier et al, *The Backscattering and Extinction of Visible and Infrared Radiation by Selected Major Cloud Models*, *Applied Optics*, vol. 6 (1967), 1209-1216.

An assessment of the attenuation of NMMW radiation by high-altitude large-particle clouds would require some detailed information on particle sizes, shapes, and concentrations and is beyond the scope of this report. However, for those clouds consisting simply of particles with sizes comparable to

those of figure III-18, absorption is the dominant loss mechanism and may be simply calculated from the total water content (liquid or ice) of the cloud. Table III-3 is a tabulation of refraction indices for water (from Rozenberg). From these, the absorption or attenuation in  $(\text{dB}/\text{km})/(\text{g}/\text{m}^3)$  has been computed in the Rayleigh limit; i.e., scattering effects neglected and attenuation proportional to  $\text{Im}(K)W$  as in equation (13). These data, normalized to unity precipitable water content, are plotted as a function of temperature and wavelength in figures III-19 and -20, respectively. For condensed water concentrations ranging from 0.1 to 1  $\text{g}/\text{m}^3$ , attenuations will range from 0.2 to 5  $\text{dB}/\text{km}$  for water clouds with temperatures between -20 C and -40 C. Figure III-21 is a plot of attenuation versus wavelength for ice at -20 C in  $(\text{dB}/\text{km})/(\text{g}/\text{m}^3)$ , based on Ray's data<sup>7</sup> for the complex index of refraction of ice. Note that absorption will be negligible for both ice clouds and ice fogs so that scattering will dominate, and grow in importance with increasing particle size.

TABLE III-3. TABULATION OF ROZENBERG'S COMPLEX REFRACTIVE INDICES OF LIQUID WATER

$\lambda$ mm	Temperature (C)		
	-40	-30	-20
0.8	2.35 - 10.08	2.35 - 10.13	2.35 - 10.20
1	2.35 - 10.10	2.35 - 10.16	2.36 - 10.25
2	2.36 - 10.20	2.37 - 10.32	2.41 - 10.49
3	2.37 - 10.29	2.40 - 10.47	2.48 - 10.72
$\lambda$ mm	Temperature (C)		
	-10	0	10
0.8	2.37 - 10.30	2.39 - 10.41	2.43 - 10.54
1	2.38 - 10.37	2.42 - 10.52	2.47 - 10.67
2	2.48 - 10.71	2.59 - 10.95	2.73 - 11.20
3	2.61 - 11.01	2.81 - 11.31	3.04 - 11.60
$\lambda$ mm	Temperature (C)		
	20	30	40
0.8	2.47 - 10.67	2.53 - 10.80	2.59 - 10.93
1	2.53 - 10.82	2.61 - 10.97	2.70 - 11.11
2	2.90 - 11.42	3.09 - 11.62	3.29 - 11.79
3	3.31 - 11.84	3.58 - 12.04	3.86 - 12.20

<sup>7</sup>P. S. Ray, *Broadband Complex Refractive Indices of Ice and Water*, *Applied Optics*, vol. 11 (1972), 1839.

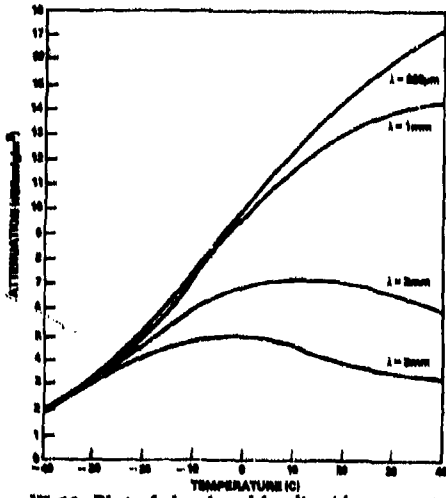


Figure III-19. Plot of cloud and fog liquid water attenuation versus temperature for the indicated wavelength.

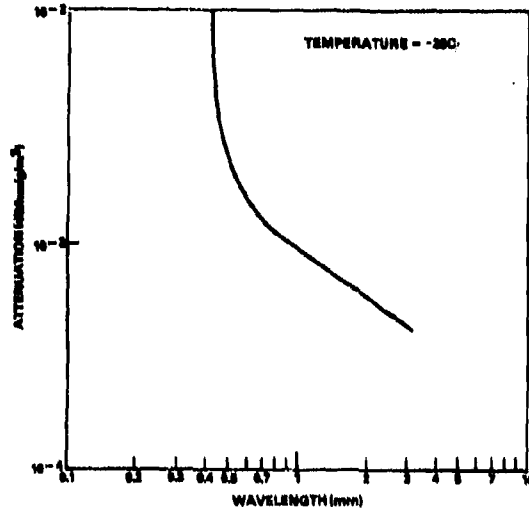


Figure III-21. Plot of ice cloud or ice fog attenuation versus wavelength.

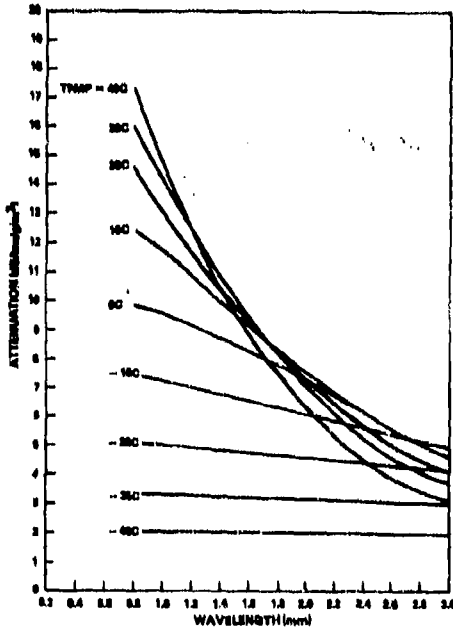


Figure III-20. Plot of cloud and fog liquid water attenuation versus wavelength.

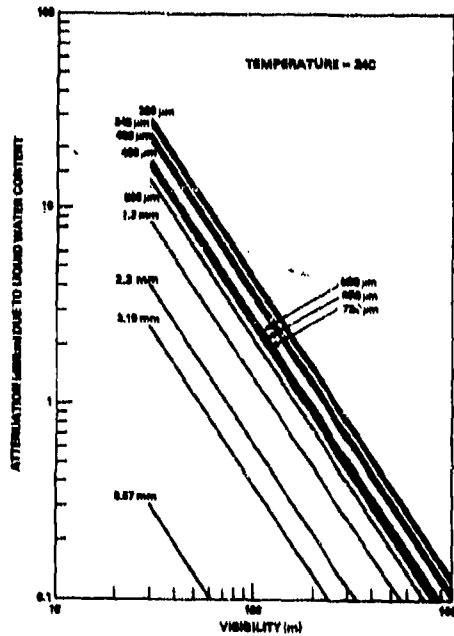


Figure III-22. Attenuation due to liquid water content of radiation fog versus visibility.

### III-6. SUMMARY

From the discussions, references, and data presented in this chapter it is possible to prepare a comparative summary of aerosol attenuation effects from the optical/infrared region to frequencies in the millimeter wave domain. Table III-4 provides such a comparison. It should, however, be recognized that because

of the rather limited data base for near-millimeter wave propagation, the principal utility of this table resides in the approximate comparisons rather than the absolute accuracy of each value. Table III-5 provides a more detailed look at the important case of fogs for wavelengths in the near-millimeter wave region. Figure III-22 is a graphical representation of table III-5.

TABLE III-4. COMPARATIVE SUMMARY OF AEROSOL ATTENUATION (dB/km) EFFECTS

Aerosol	Optical	Infrared 10.6 $\mu\text{m}$	400 GHz 730 $\mu\text{m}$	340 GHz 880 $\mu\text{m}$	220 GHz 1.3 mm	140 GHz 2.1 mm	100 GHz 3 mm	35 GHz 8.6 mm
Fog T = 10 C V ~ 100 m W = 0.3 g/m <sup>3</sup>	~204	~200	~4	~3.6	3	2.25	1.4	~0.1
Vehicular dust	Large (L)	Significant (S)	Negligible (N)	N	N	N	N	N
Rain 10 mm/hr	5.2	~5.2	7.4	7.8	8.3	8.7	8.7	2.6
Snow 10 mm/hr (H <sub>2</sub> O)	>>5.2	>>5.2	~3.7 dry ~7.4 wet	~3.9 dry ~7.8 wet	~4.1 dry ~8.3 wet	~4.4 dry ~8.7 wet	~4.4 dry ~8.7 wet	~1.3 dry ~2.6 wet

TABLE III-5. ATTENUATION (dB/km) DUE TO LIQUID WATER IN A RADIATION FOG AT 24 C

V (m)	W (g/m <sup>3</sup> )	Wavelength											
		320 $\mu\text{m}$	345 $\mu\text{m}$	450 $\mu\text{m}$	490 $\mu\text{m}$	620 $\mu\text{m}$	650 $\mu\text{m}$	720 $\mu\text{m}$	880 $\mu\text{m}$	1.3 mm	2.3 mm	3.19 mm	8.57 mm
1000	0.0032	0.128	0.125	0.109	0.102	0.080	0.077	0.075	0.062	0.039	0.018	0.011	0.001
900	0.0038	0.152	0.148	0.129	0.122	0.095	0.091	0.089	0.074	0.047	0.022	0.013	0.002
800	0.0045	0.180	0.176	0.153	0.144	0.113	0.108	0.100	0.088	0.055	0.026	0.015	0.002
700	0.0056	0.224	0.218	0.190	0.179	0.140	0.134	0.130	0.109	0.069	0.032	0.020	0.002
600	0.0071	0.284	0.277	0.241	0.227	0.178	0.170	0.170	0.138	0.090	0.040	0.025	0.003
500	0.0094	0.376	0.367	0.320	0.301	0.235	0.226	0.220	0.183	0.120	0.054	0.033	0.004
400	0.013	0.520	0.507	0.442	0.416	0.325	0.312	0.300	0.250	0.160	0.074	0.046	0.005
300	0.020	0.800	0.780	0.680	0.640	0.500	0.480	0.470	0.390	0.246	0.11	0.070	0.008
200	0.036	1.52	1.482	1.292	1.216	0.950	0.912	0.893	0.741	0.467	0.22	0.13	0.015
100	0.111	4.44	4.329	3.774	3.552	2.775	2.660	2.61	2.16	1.36	0.63	0.39	0.047
90	0.131	5.24	5.109	4.454	4.192	3.275	3.140	3.08	2.55	1.61	0.75	0.46	0.056
80	0.157	6.28	6.123	5.34	5.02	3.92	3.770	3.69	3.06	1.93	0.89	0.55	0.067
70	0.193	7.72	7.53	6.56	6.18	4.80	4.60	4.54	3.76	2.37	1.10	0.68	0.082
60	0.244	9.8	9.5	8.3	7.81	6.10	5.80	5.73	4.76	3.00	1.39	0.85	0.104
50	0.323	12.9	12.6	11.0	10.3	8.08	7.75	7.60	6.30	3.97	1.84	1.13	0.137
40	0.456	18.2	17.8	15.5	14.6	11.4	10.9	10.70	8.89	5.61	2.59	1.60	0.194
30	0.710	24.4	27.7	24.1	22.7	17.8	17.0	16.70	13.8	8.73	4.05	2.49	0.302

### CHAPTER III.—LITERATURE CITED

1. J. A. Stratton, *Electromagnetic Theory*, McGraw-Hill Book Company, New York (1941), 554-573.
2. H. C. Van de Hulst, *Light Scattering by Small Particles*, John Wiley and Sons, New York (1957).
3. D. E. Kerr, ed., *Propagation of Short Radio Waves*, McGraw-Hill Book Company, New York, Ch 7-8 (1951).
4. D. Diermendjian, *Far Infrared and Submillimeter Wave Attenuation by Clouds and Rain*, Rand Corporation Report AD-A021-947 (April 1975).
5. V. I. Rozenberg, *Scattering and Attenuation of Electromagnetic Radiation by Atmospheric Particles*, Hydrometeorological Press, Leningrad, USSR (1972).
6. G. D. Lukes, *Penetrability of Haze, Fog, Clouds, and Precipitation by Radiant Energy over the Spectral Range 0.1 Micron to 10 Centimeters*, The Center for Naval Analyses of the University of Rochester, Report No. 61 (May 1968).
7. P. S. Ray, *Broadband Complex Refractive Indices of Ice and Water*, *Applied Optics*, vol. 11 (1972), 1839.
8. M. Davies, G. W. F. Pardoe, J. Chamberlain, and H. A. Gebbie, *Submillimeter- and Millimeter-wave Absorption of Some Polar and Non-polar Liquids Measured by Fourier Transform Spectroscopy*, *Transactions of the Faraday Society*, vol. 66 (1970), 273.
9. B. J. Mason, *Cloud Physics*, 2nd edition, Clarendon Press (1971).
10. W. E. K. Middleton, *Vision Through the Atmosphere*, University of Toronto Press (1963).
11. R. G. Eldridge, *Haze and Fog Aerosol Distributions*, *Journal of Atmospheric Science*, vol. 23 (1966), 608.
12. O. Essenwanger, *On the Duration of Widespread Fog and Low Ceiling in Central Europe and Some Aspects of Predictability*, *Missile Research and Development Command TR-RR-73-9* (1 August 1973).
13. D. G. Bauer, R. A. McGee, J. E. Know, and H. B. Wallace, *140-GHz Beamrider Feasibility Experiment*, *Ballistic Research Laboratories, Interim Memorandum Report No. 538* (January 1977).
14. A. V. Sokolov and Ye. V. Sukhonin, *Attenuation of Submillimeter Radio Waves in Rain*, *Radio Engineering and Electronic Physics*, vol. 15, no. 12 (1970), 2167.
15. V. W. Richard, *Low Angle Tracking at Millimeter Wavelengths*, *TTCP Ad-Hoc Study Group 102, Electro-Optical Low Angle Tracking* (December 1976).
16. V. W. Richard, *Millimeter Wave Radar Applications to Weapon Systems*, *Memorandum Report No. 2631, Ballistic Research Laboratories* (June 1976).
17. B. D. Hinds and G. D. Hordale, *Boundary Layer Dust Occurrence IV, Atmospheric Dust Over Selected Geographic Areas, USA Electronics Command, ECOM-DR-77-3* (June 1977).
18. E. Bauer, *The Scattering of Infrared Radiation from Clouds*, *Applied Optics*, vol. 3 (1964), 197.
19. L. W. Carrier, G. A. Cato and K. J. von Essen, *The Backscattering and Extinction of Visible and Infrared Radiation by Selected Major Cloud Models*, *Applied Optics*, vol. 6 (1967), 1209-1216.

**CHAPTER IV.—ADDITIONAL METEOROLOGICAL INFORMATION**

**by Stanley M. Kulpa and Edward A. Brown**

From the previous chapters it should be clear that the utility of near-millimeter technology depends very strongly on the various weather parameters. Though a significant amount of meteorological data is provided in Chapters I through III, it is appropriate to provide some additional information. The following tables should prove useful to the reader in discussions and calculations of NMMW propagation characteristics. In addition, for those who wish to explore more thoroughly the meteorological/climatological aspects, a Selected Bibliography is included for Chapter IV (p.81).

**TABLE IV-4. REPRESENTATIVE ABSOLUTE HUMIDITY LEVELS**

Environment	Absolute humidity (g/m <sup>3</sup> )
Tropical	19
Midlatitude summer	14
Midlatitude winter	3.5
Subarctic summer	9.1
Subarctic winter	1.2

*R. A. McClatchey, Optical Properties of the Atmosphere (Revised), U.S. Air Force Cambridge Research Laboratories, AFCRL-71-0279 (May 1971).*

**TABLE IV-2. SEA-LEVEL TEMPERATURE DEPENDENCE OF WATER VAPOR CONCENTRATION**

Temperature (C)	Water vapor concentration (g/m <sup>3</sup> )	
	50 percent relative humidity	100 percent relative humidity
-20	0.51	1.0
-15	0.79	1.5
-10	1.1	2.1
-5	1.6	3.0
0	2.3	4.3
5	3.2	6.2
10	4.4	8.9
15	6.0	12.
20	8.0	16.
25	11.	22.
30	16.	30.

**TABLE IV-3. HAZE AND FOG CHARACTERISTICS**

Parameter	Haze	Radiation fog	Advection fog
Drop diameter range, $\mu\text{m}$	0.01 - 3	5 - 35	7 - 65
Typical drop concentration, per $\text{m}^3$	$10 \times 10^4$	$200 \times 10^9$	$40 \times 10^9$
Typical maximum water content, $\text{g}/\text{m}^3$	—	1	0.4
Water content for 200 m visibility, $\text{g}/\text{m}^3$	—	0.04	0.18
Visibility at $0.1 \text{ g}/\text{m}^3$ , m	—	110	280

V. W. Richard, J. E. Kammerer, and R. G. Reitz, *140 GHz Attenuation and Optical Visibility Measurements of Fog, Rain and Snow*, Ballistic Research Laboratories, ARBRL-MR-2800 (December 1977).

**TABLE IV-4. STANDARD VISIBILITY CONDITIONS (International Visibility Code)**

Conditions	Visibility
Dense fog	<50 m
Thick fog	50 - 200
Moderate fog	200 - 500
Light fog	500 - 1000 m
Thin fog	1 - 2 km
Haze	2 - 4
Light haze	4 - 10
Clear	10 - 20
Very clear	20 - 50
Exceptionally clear	>50 km

TABLE IV-5. DROPLET SIZES AND DENSITIES FOR RAIN

	Light (r = 1 mm/hr)	Moderate (r = 4 mm/hr)	Heavy (r = 25 mm/hr)	Cloudburst (r = 100 mm/hr)
Size range ( $\mu\text{m}$ )	7 - 100	10 - 300	10 - 500	50 - 700
Droplet density ( $\text{m}^{-3}$ )	350	500	700	1,250
Water density ( $\text{g}/\text{m}^3$ )	0.04	0.17	1.0	4.0

R. G. Shackelford and J. J. Gallagher, Millimeter Wave Beamrider System, U.S. Army Missile Research and Development Command, TE-CR-77-7 (August 1977).

TABLE IV-6. PROPERTIES OF STANDARD CLOUD MODELS

Name	Base (m)	Top (m)	Density ( $\text{g}/\text{m}^3$ )	Mode radius ( $\mu\text{m}$ )	Comp.
Cirrostratus, arctic, 12-18 kft	4000.	6000.	0.10	40.0	Ice
Cirrostratus, mid-lat., 15-21 kft	5000.	7000.	0.10	40.0	Ice
Cirrostratus, tropical, 18-24 kft	6000.	8000.	0.10	40.0	Ice
Altostratus 8000-9650 ft	2400.	2900.	0.15	10.0	Water
Altostratus 8000-9650 ft	2400.	2900.	0.15	10.0	Water
Low-lying stratus 500-2000 ft	150.	650.	0.25	10.0	Water
Low-lying stratus 1500-3000 ft	500.	1000.	0.25	10.0	Water
Fog layer, ground to 150 ft	0.	50.	0.15	20.0	Water
Haze, heavy	0.	1500.	$10^{-3}$	0.05	Water
Drizzle, 0.2 mm/hr	0.	500.	1.00	20.0	Rain
	500.	1000.	2.00	10.0	Water
	1000.	1500.	1.00	10.0	Water
Steady rain, 3 mm/hr	0.	150.	0.20	200.0	Rain
	150.	500.	1.00	10.0	Water
	500.	1000.	2.00	10.0	Water
	1000.	1500.	1.00	10.0	Water

TABLE IV-6. PROPERTIES OF STANDARD CLOUD MODELS (Cont'd)

Name	Base (m)	Top (m)	Density (g/m <sup>3</sup> )	Mode radius (μm)	Comp.
Steady rain, 15 mm/hr	0.	300.	1.00	200.	Rain
	300.	1000.	2.00	10.0	Water
	1000.	2000.	3.00	10.0	Water
	2000.	4000.	2.00	10.0	Water
Stratocumulus 1000-2000 ft	330.	660.	0.25	10.0	Water
Stratocumulus 2000-4000 ft	660.	1320.	0.25	10.0	Water
Fair weather cu. 1500-6000 ft	500.	1000.	0.50	10.0	Water
	1000.	1500.	1.00	10.0	Water
	1500.	2000.	0.50	10.0	Water
Cumulus with rain 2.4 mm/hr	0.	500.	0.10	400.	Rain
	500.	1000.	1.00	20.0	Water
	1000.	3000.	2.00	10.0	Water
Cumulus with rain 12 mm/hr	0.	400.	0.50	400.	Rain
	400.	1000.	2.00	20.0	Water
	1000.	4000.	4.00	10.0	Water
Cumulus congestus, 3000-9000 ft	1000.	1200.	0.30	10.0	Water
	1200.	1600.	0.50	15.0	Water
	1600.	2000.	0.80	20.0	Water
	2000.	2500.	1.00	20.0	Water
	2500.	3000.	0.50	20.0	Water
Cumulonimbus with rain 150 mm/hr	0.	300.	6.30	400.	Rain
	300.	1000.	7.00	20.0	Water
	1000.	4000.	8.00	10.0	Water
	4000.	6000.	4.00	10.0	Water
	6000.	8000.	3.00	10.0	Water
	8000.	10,000.	0.20	40.0	Ice

*N. E. Gaut and E. C. Reifenzstein, III, Interaction Model of Microwave Energy and Atmospheric Variables, NASA Report CR-61348 (20 April 1971), AD N71-25079.*

#### CHAPTER IV.—SELECTED BIBLIOGRAPHY

- F. A. Berry, Jr., E. Bollay, and N. R. Beers, *Handbook of Meteorology*, McGraw-Hill Book Co., New York (1945).
- O. M. Essenwanger, *Estimation of Absolute Humidity During Morning Fog in Central Europe*, U.S. Army Missile Research and Development Command, TR-77-10 (1 July 1977).
- O. M. Essenwanger, *On the Duration of Widespread Fog and Low Ceiling in Central Europe and Some Aspects of Predictability*, U.S. Army Missile Command, RR-73-9 (1 August 1973), AD 771 934.
- O. M. Essenwanger, *On Spatial Distribution of Visibility and Clouds in Central Europe*, U.S. Army Missile Command, RR-73-10 (28 December 1973), AD 780 723.
- R. W. Fairbridge, *The Encyclopedia of Atmospheric Sciences and Astrogeology*, Reinhold Publishing Corp., New York (1967).
- Handbook of Geophysics (Revised Edition)*, U.S. Air Force Research and Development Command, Geophysics Research Directorate, The Macmillan Company, New York (1960).
- D. H. Low, *Considerations in the Optical Characterization of the Atmosphere*, U.S. Army Atmospheric Sciences Laboratory, ASL-CR-79-0100-3 (July 1979).
- E. J. McCartney, *Optics of the Atmosphere*, John Wiley and Sons, New York (1976).
- B. J. Mason, *The Physics of Clouds*, Clarendon Press, London (1957).
- W. E. K. Middleton, *Vision through the Atmosphere*, University of Toronto Press (1952).
- A. Miller and J. C. Thompson, *Elements of Meteorology*, Charles E. Merrill Publishing Co., Columbus, OH (1970).
- R. G. Pinnick, S. G. Jennings, P. Chylek, and H. J. Auvermann, *Relationships between IR Extinction, Absorption, and Liquid Water Content of Fogs*, U.S. Army Atmospheric Sciences Laboratory, ASL-TR-0037 (August 1979).
- N. Sissenwine and R. V. Cormier, *Synopsis of Background Material for MIL-STD-210B, Climatic Extremes for Military Equipment*, U.S. Air Force Cambridge Research Laboratories, AFCRL-TR-0052 (24 January 1974).
- S. L. Valley, ed., *Handbook of Geophysics and Space Environments*, McGraw-Hill Book Co., New York (1965).

**CHAPTER V.—PROPAGATION IN SMOKE AND CHAFF**

**by Dominick A. Giglio**

Since this chapter contains classified information, it will be published as part of volume IV of this report.

**CHAPTER VI.—TARGETS AND BACKGROUNDS**

**by Gwynn H. Suits and Bobby D. Gueather**

## CONTENTS

	Page
VI-1. INTRODUCTION .....	89
VI-2. DEFINITIONS, NOMENCLATURE, AND BASIC RELATIONS .....	89
VI-2.1 Definition of Incident and Scattering Angles .....	89
VI-2.2 Defining Relations for Radar Cross Sections .....	89
VI-2.3 Cross Section Statistics .....	90
VI-2.4 Polarization Nomenclature .....	91
VI-2.5 Bistatic Radar Cross Sections .....	91
VI-2.6 Relationship between Radar and Electro-Optical Descriptors .....	91
VI-2.7 Radiometric Relations .....	92
VI-3. DISCRETE TARGETS DATA .....	93
VI-3.1 Tactical Targets .....	93
VI-3.2 Strategic Targets .....	95
VI-4. DATA ON BACKGROUNDS .....	99
VI-4.1 Terrain .....	99
VI-4.2 Atmospheric Emission Data .....	107
VI-5. MATERIAL PROPERTIES AND TRENDS INDICATED BY SIMPLE MODELING .....	109
VI-5.1 Liquid and Solid Water .....	109
VI-5.2 Metals .....	112
VI-5.3 Experimental Backscatter from Painted Surfaces and Wood .....	116
VI-5.4 Atmospheric Emission Model .....	117
VI-6. SUMMARY .....	120
VI-6.1 Discrete Targets .....	120
VI-6.2 Background .....	120
VI-6.3 Material Properties and Modeling .....	121
LITERATURE CITED .....	122

## VI-1. INTRODUCTION

The NMMW radiative properties of targets and of the backgrounds with which they may be associated are fundamental data required to begin the assessment of the probable performance of a large number of applications of NMMW systems. In the following sections, the definitions and nomenclature used as data descriptors are explained and the available data for discrete targets and extended backgrounds are tabulated and described. Where data are insufficient, the trends of data as a function of frequency from adjacent bands are described. In all cases for this spectral region, it has been necessary to draw conclusions by extrapolation from other frequency regions or by modeling.

A large part of this chapter contains information and extensive excerpts from a report of the Environmental Research Institute of Michigan.<sup>1</sup>

## VI-2. DEFINITIONS, NOMENCLATURE, AND BASIC RELATIONS

### VI-2.1 Definition of Incident and Scattering Angles

The incident and scattering angles are shown schematically in figure VI-1. The radar transmitter is located at P above the XY plane representing the plane of local terrain. The angle of incidence,  $\theta_i$ , is the polar angle from vertical at the illuminated area to the line of propagation of transmitted power. The grazing angle is the angle of elevation,  $\theta_g$ , of the radar from the horizontal plane with apex at the illuminated area. The depression angle,  $\theta_d$ , is equal to the grazing angle for a flat earth approximation and is the angle from the horizontal plane to the line

of propagation, with apex at the transmitter. The polar angle of scattering,  $\theta_s$ , is the angle between vertical at the illuminated area to the line of propagation to the receiver with apex at the illuminated area.

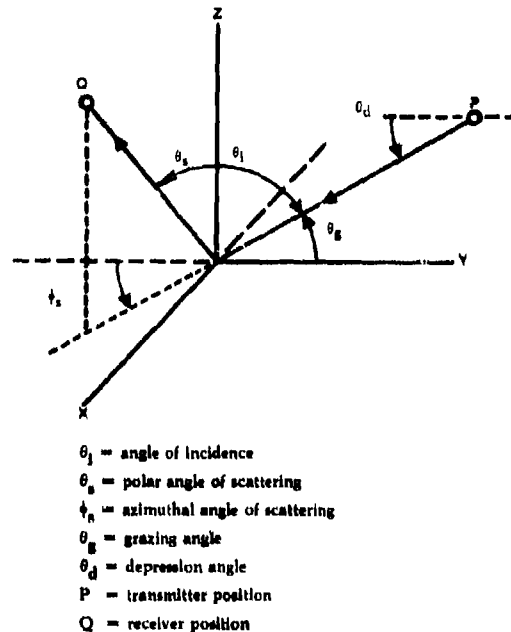


Figure VI-1. Definition of angles.

The azimuth of scattering,  $\phi_s$ , is the angle in the XY plane between the specular reflection direction and the direction to the receiver with apex at the illuminated area. The monostatic condition is obtained when  $\theta_i = \theta_s$ , and  $\phi_s = 180$  deg.

### VI-2.2 Defining Relations for Radar Cross Sections

The radar cross section,  $\sigma$ , of a target fully illuminated by a radar operating in the monostatic mode is defined by the relation

$$P_r = \frac{P_t G \sigma A_r r^{-4}(r)}{(4\pi)^2 r^4} \quad (1)$$

<sup>1</sup>J. R. Maxwell, Environmental Research Institute of Michigan, ERIM 123800-2-L (18 November 1976). (CONFIDENTIAL)

where

$P_r$  = received power,

$P_t$  = transmitted power,

$G$  = transmitter antenna gain relative to an isotropic source,

$A_r$  = effective receiver antenna aperture area,

$r$  = range from radar to target, and

$\tau(r)$  = transmittance of the separating medium over a range,  $r$ .

If  $\eta$  is the attenuation of the atmosphere in decibels/kilometer, then the transmittance is given by

$$\tau(r) = 10^{-\left(\frac{\eta}{10} \cdot \frac{r}{1000}\right)} \quad (2)$$

with  $r$  in meters.

The cross section of a fully illuminated, perfectly reflecting sphere, whose radius,  $r_s$ , is much greater than a wavelength,  $\lambda$ , is  $\pi r_s^2$ . Such spheres can be used for field experiment calibration standards. The radar cross section for more complex shapes can be expressed as

$$\sigma = \rho G' A \quad (3)$$

where  $\rho$  = reflectivity of target surface material,

$A$  = the projected area of the target, and

$G'$  = the gain of the target relative to an isotropic scatterer.

The three factors in relation (3) separate the influence of material properties, geometrical shape, and size. The target gain,  $G'$ , may be approximated by

$$G' = \frac{A_c}{4\pi\lambda^2} \quad (4)$$

where  $A_c$  is the target area of coherent reflection.

A target which is smooth relative to the wavelength will exhibit an increasing gain for decreasing wavelength. For most targets, a wavelength limit will be found for which the target appears rough and scatters incoherently so that target gain will not increase with further decreasing wavelength.

Two radar cross sections— $\sigma_0$ , the cross section per unit illuminated area, and  $\gamma$ , the cross section per unit projected illuminated area—are defined for terrain. These cross sections are defined by the relations

$$P_r = \frac{P_t G \sigma_0 A_i A_r \tau^2(r)}{(4\pi)^2 r^4} \quad (5)$$

and

$$P_r = \frac{P_t G \gamma \cos \theta_i A_i A_r \tau^2(r)}{(4\pi)^2 r^4} \quad (6)$$

where  $A_i$  is the area of terrain illuminated by the radar pulse. Both  $\sigma_0$  and  $\gamma$  are cross sections per unit area and are dimensionless quantities. The area,  $A_i$ , increases as the square of the range, resulting in an inverse square law for received power.

### VI-2.3 Cross-Section Statistics

Terrestrial cross sections,  $\sigma_0$  and  $\gamma$ , are often specified by average values. The scattering of coherent radiation from random scattering centers adds vectorially at random at the receiver so that a statistical variation in received signals may be expected. According to Long,<sup>2</sup> one may assume that land and sea scattering is Rayleigh distributed as a first approximation; however, field experiments in the microwave range result in a distribution between Rayleigh and log normal. The Rayleigh distribution density,  $p(\sigma_0)$ , is given by

<sup>2</sup>M. W. Long, *Radar Reflectivity of Land and Sea*, Lexington Books, Lexington, MA (1975)

$$p(\sigma_0) = \frac{1}{\bar{\sigma}_0} e^{-\sigma_0/\bar{\sigma}_0} \quad (7)$$

where  $\bar{\sigma}_0$  is the mean value of the point-by-point measured  $\sigma_0$  values. One may deduce that 50 percent of  $\sigma_0$  values will fall in a range from 5.4 dB below  $\bar{\sigma}_0$  to 1.43 dB above  $\bar{\sigma}_0$  for the Rayleigh distribution.

In the case of NMMW wavelengths, one may anticipate conditions where a target, such as a vehicle, will not be fully illuminated by the radar beam. The illuminated area,  $A_i$ , of the target may not be known so that neither  $\sigma$  nor  $\sigma_0$  is a convenient cross-section descriptor. However,  $\gamma$  is the cross section per unit projected illuminated area,  $A_i \cos \theta_i$ . The projected illuminated area should be approximately the area of the radar beam normal to the direction of propagation within the half-power contour of the range of the target. Consequently, the radar cross section of illuminated regions of a partly illuminated target can be described conveniently by  $\gamma$ . Reports of the statistical distribution of  $\gamma$  for NMMW waves for artifacts have not been found.

#### VI-2.4 Polarization Nomenclature

Radar cross section also depends upon the polarization of transmitted and received radiation. The commonly used designations, H and V for polarization, are used in this report. Horizontally polarized radiation, H, is that portion of the radiation for which the electric field vector is parallel to the horizontal reference plane (the XY plane in fig. VI-1). Vertically polarized radiation, V, is that portion of the radiation for which the electric field vector is orthogonal to the horizontally polarized field and orthogonal to the direction of propagation. Circularly polarized radiation is designated by the letter C. Cross-section values are qualified by letter pairs—such as HH, VH, HV, or VV—where the first letter specifies the polarization of the transmitted radiation and the second letter specifies the polarization of received radiation. The thermal emission of radiation is often

randomly polarized. Randomly polarized radiation will be specified by the letter R.

#### VI-2.5 Bistatic Radar Cross Sections

NMMW cw designators used in guidance systems may operate in the bistatic mode. The extension of the defining relations for  $\sigma$  and  $\sigma_0$  for the bistatic mode is straightforward. For the fully illuminated target, relation (1) becomes

$$P_r = \frac{P_t G_0 A_r \tau(r_t) \tau(r_r)}{(4\pi)^2 r_t^2 r_r^2} \quad (8)$$

where  $r_t$  = range from transmitter to target, and

$r_r$  = range from receiver to target.

Relation (5) becomes

$$\gamma_r = \frac{P_t G_0 A_i A_r \tau(r_t) \tau(r_r)}{(4\pi)^2 r_t^2 r_r^2} \quad (9)$$

The cross sections  $\sigma$  and  $\sigma_0$  must be qualified by the specification of the angles  $\theta_i$ ,  $\theta_s$ , and  $\phi_s$  as well as by the transmitted and received polarizations.

#### VI-2.6 Relationship between Radar and Electro-Optical Descriptors

The paucity of published data on the electromagnetic properties of materials in the NMMW spectral range may require interpolation between infrared and microwave properties. The nomenclature used in the infrared spectral range implies that measurements are done on plane sections of material, the dimensions of which are large compared to a wavelength, and that cw random polarization and bistatic conditions are used unless otherwise specified.

Bidirectional reflectance,  $q'$ , is defined by

$$P_r = \frac{P_t G_0' \cos \theta_i \cos \theta_s A_i A_r \tau(r_t) \tau(r_r)}{4\pi r_t^2 r_r^2} \quad (10)$$

Equations (9) and (10) yield the relationship between bistatic  $\sigma_0$  and  $q'$  as

$$\sigma_0 = 4\pi q' \cos \theta_1 \cos \theta_s \quad (11)$$

Data may be specified as reflectance relative to the reflectance of the ideal diffusely reflecting Lambertian panel; that is, the equivalent reflectance of a Lambertian panel which would result in the same received power, so that,

$$q_{rel} = \pi q' \quad (12)$$

and

$$\sigma_0 = 4q_{rel} \cos \theta_1 \cos \theta_s \quad (13)$$

where  $q_{rel}$  is the relative bidirectional reflectance or equivalent Lambertian reflectance.

A related reflectance is most often reported in the literature for diffusely reflecting materials. This reflectance—the directional hemispherical reflectance, or more commonly diffuse reflectance, and sometimes just reflectance (without modifiers)—is related to the bidirectional reflectance by integration over all scattering angles,

$$q_{dh} = \int_0^{2\pi} \int_0^{\pi/2} q'(\theta_1, \theta_s, \phi_s) \cos \theta_s \sin \theta_s d\theta_s d\phi_s \quad (14)$$

where  $\theta_1$  is tacitly some angle about 5 to 15 deg from sample normal and  $q_{dh}$  is the directional hemispherical reflectance.

If  $q'$  varies only slightly with  $\theta_s$  and  $\phi_s$ , then

$$q_{dh} \approx \overline{q'(\theta_1)} \quad (15)$$

where  $\overline{q'(\theta_1)}$  is the mean value of  $q'$  for all angles of scattering for incident angle  $\theta_1$ .

Specular reflectance for smooth material,  $q_{spec}$ , is defined as the ratio of flux reflecting at the specular angle to the flux inci-

dent. Rayleigh's criterion for specularity of a surface is

$$\Delta h_{rms} \cos \theta_1 < \lambda/8 \quad (16)$$

where  $\Delta h_{rms}$  is the root mean square random deviation of a surface from a plane section.

For a perfectly smooth reflecting surface,

$$q_{spec} = q_{dh} \quad (17)$$

### VI-2.7 Radiometric Relations

The rate of conversion of heat energy into radiant energy in the NMMW range is proportional to the absolute temperature of the emitter. A blackbody surface is an ideal thermal emitter, which converts heat energy into radiant energy at the maximum rate allowed by thermodynamic laws. The radiated flux per unit frequency interval emitted from a blackbody is

$$M_\nu = \frac{8\pi kT}{\lambda^2} \quad (18)$$

where  $M_\nu$  = the spectral flux density emitted,

$T$  = absolute surface temperature, and

$\lambda$  = wavelength at the band center.

Any real material emits with less efficiency than the ideal blackbody. The ratio of real body emission to blackbody emission at a specified wavelength is the spectral emissivity  $\epsilon(\lambda)$  of the real material. The emissivity in a specified direction,  $\theta_e$ , from surface normal for opaque material is given by Kirchoff's law:

$$\epsilon(\lambda, \theta_e) = 1 - \epsilon_{dh}(\theta_1 = \theta_e) \quad (19)$$

If  $q_{dh}(V) \neq q_{dh}(H)$ , then emission will not be completely randomly polarized.

For a nonscattering gas, the emissivity of a layer of gas depends upon the transmittance through the layer.

$$\epsilon(\lambda) = 1 - \tau(\lambda) \quad (20)$$

Since the thermal emission of a material in the NMMW range is proportional to the absolute temperature of the material, a common practice is to use the temperature as a descriptor of flux density. In addition, the mean-square noise current fluctuation in electrical circuits is also proportional to the absolute temperature of the circuit components, so that the temperature is a substitute descriptor for circuit noise power. In this way, an antenna temperature of  $T^{\circ}\text{K}$  means that the feed line at the antenna is receiving noise power equivalent to that of a purely resistive load at temperature  $T^{\circ}\text{K}$ . Such noise power may come from a combination of received flux and from local antenna circuit elements.

### VI-3. DISCRETE TARGETS DATA

#### VI-3.1 Tactical Targets

In general, the data base for discrete tactical targets is not extensive, for NMMW frequencies. Until the last few years, there have been few systems operating near 95 GHz; consequently, there have been few measurements. Recently, there has been increased emphasis on the 95-GHz window, and more measurements are being made. Hughes Aircraft Company and the Environmental Research Institute of Michigan (ERIM)<sup>1</sup> have been making 95-GHz measurements from the ground and from the air.\*

<sup>1</sup>J. R. Maxwell, Environmental Research Institute of Michigan, ERIM 123800-2-L (18 November 1976). (CONFIDENTIAL)  
\*Editor's Note: see Selected Bibliography (Ch IX) for additional references on target measurements. Note particularly the work of Currie et al at the Georgia Institute of Technology.

In a recent paper, Johnston<sup>2</sup> investigated the availability of radar data in the NMMW region. He found no full-scale radar measurements between 140 GHz and 10  $\mu\text{m}$ .

The millimeter wave data which have been found in the present literature search are all for the monostatic mode and primarily for frequencies of 94 GHz and below. These data allow estimation of NMMW cross sections by extrapolation. The polarization for most available data is either horizontal or vertical, although some of the measurements by Hughes were made with circular polarization.

Hughes<sup>4</sup> reported measurements at 94 GHz with three military vehicles as targets. The measurements are summarized in table VI-1. The three target vehicles presented similar intercept areas to the illuminating radar beam. As is usual for metallic objects, their effective radar scattering areas are larger than their intercept areas. Both the truck and the personnel carrier have some flat surfaces and some perpendicular intersections of surfaces that reflect strongly toward the illuminating radar. The tank surfaces are nearly all curved, so that reflection from the tank is more nearly isotropic. This probably accounts for the lower peak and lower mean values for the tank.

The measured peak scattering areas at 94 GHz are not significantly larger than is commonly found at X-band. Specularly reflecting plane surfaces, dihedrals, and corners would be expected to exhibit gains of about 100 times larger at 94 GHz than at 9.4 GHz, if they remained fully specular and diffraction limited at the higher frequency. Since the measurements show no appreciable increase of target gains with frequency, the reflecting surfaces can be assumed to be too rough and too inaccurately aligned to

<sup>2</sup>S. L. Johnson, *Submillimeter Wave Radar Technology (U)*, 22nd Annual Tri-Service Radar Symposium, Colorado Springs, CO (6-8 July 1976). (CONFIDENTIAL)

<sup>4</sup>M. F. Beebe, J. Salzman et al, *94 GHz Sensor Tower Test Program: Final Report, Report NO. MSG 6507R, Missile Systems Group, Hughes Aircraft Company (February 1976).*

remain specular and diffraction limited at the higher frequency. Measurements made by the Ballistic Research Laboratories (BRL)<sup>6</sup> at 94 GHz show effective scattering areas as a function of target aspect angle. Large effective areas were found at broadside aspects. Measurements that avoided aspects associated with these large values show scattering areas about equal to the projected areas of these targets, or slightly less. This characteristic variation with aspect angle should be present at higher frequencies.

Near-monostatic measurements by Redstone Arsenal<sup>6</sup> at 95 GHz were made on several types of military vehicles. The narrow illuminating beam was scanned across the vehicle and background terrain. Histograms of signal values from an M-48 tank are shown in figures VI-2(a) and (b). A 2-in. diameter gold-plated sphere was used as a reference. The large narrow

peak at about -50 dB is due to distant terrain. The wider and lower peak is due to the tank and foreground terrain.

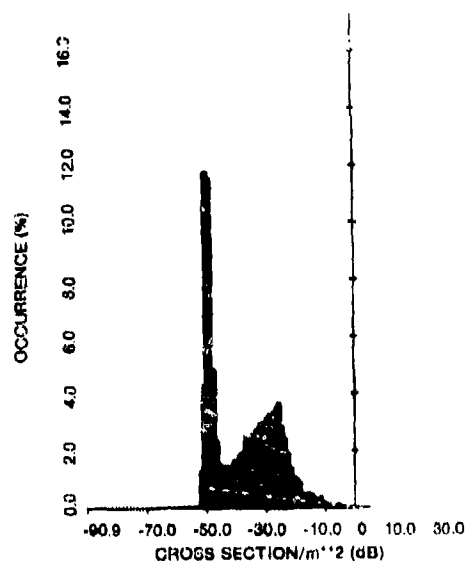


Figure VI-2(a). Histogram of M-48 tank and surrounding terrain, HH polarization.

<sup>6</sup>K. A. Richer, D. G. Bauerle, and J. E. Knox, 94 GHz Radar Cross Section of Vehicles (U), Ballistic Research Laboratories BRL-MR-2491 (June 1975), AD C002 505L. (CONFIDENTIAL)

<sup>6</sup>B. D. Guenther, Submillimeter Wave Research: Index of 3.2 mm and 10.6  $\mu$ m Image Data Tapes, U.S. Army Missile Research and Development Command TR-77-2 (1 February 1977).

TABLE VI-1. OVERALL SUMMARY OF TARGET CROSS SECTIONS— $m^2$  at 94 GHz

Measurement by Beebe, Salzman, et al, Hughes Aircraft Company, Missile Systems Group Report MSG 65075R (February 1976).

Target	Extreme values		Cross-section distribution				Comments
	Min	Max	Mean	Median (50%)	80th percentile	Standard deviation	
2½ ton truck	15.2	1229.	130.	80.	120.	116.	25 Data points; Dep angles: 3 to 9 deg Relative humidity: 70 to 81%
Armored personnel carrier	18.9	1546.	130.	40.	115.	113.	45 Data points; Dep angles: 3 to 6.5 deg Relative humidity: 58 to 95%
M-41 tank	16.	116.	64.	30.	60.	48.	48 Data points; Dep. angles 3 to 6.5 deg Relative humidity: 48 to 81%

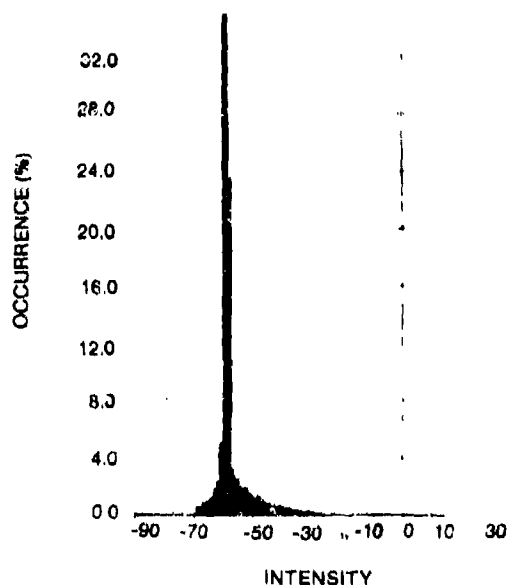


Figure VI-2(b). Histogram of M-48 tank and surrounding terrain, HV polarization.

The scanned data were level sliced and reconstituted in image form. Figures VI-3(a) and (b) show the locations of the scattering regions at signal levels relative to the signal level of a fully illuminated 1-m<sup>2</sup> cross section at a 14.6-m range—the approximate range of the tank.

There are additional small amounts of classified data on high-frequency measurements of military targets. Such information will be found in Volume IV of this study.

### VI-3.2 Strategic Targets

No report of NMMW radar cross sections of strategic targets was found. Calibrated scanned images of reentry vehicles were made by Hughes Research Laboratories<sup>7</sup> at 94 GHz. Analysis of the data has not been reported. Strategic targets—such as military ships, supply ships, military aircraft, intercon-

<sup>7</sup>J. M. Bair, *Millimeter and Infrared Image Scans of Reentry Vehicle Targets*, Technical Report Calspan 23953, Hughes Research Laboratories (September 1976).

tinental ballistic missiles, storage tanks, motor pools, airports, and ammunition dumps—may be large compared to radar spatial resolution. Some strategic targets are composites of many smaller components placed in some characteristic spatial arrangement so that the geometrical shape of the composite is often the key to their detection rather than the radar cross section of the composite.

Calibrated high spatial resolution images of these composites are suitable for estimating system performance in the detection and identification of strategic targets for systems having less spatial resolution than that of the image data. Without such images, one must estimate the target characteristics by mathematical modeling of the radiative properties of the components.

Expected Radiometric Contrast between Large Military Ships and the Sea.—The following reasoning is illustrative of the mathematical modeling approach for estimating the radiometric contrasts between large ships and the sea for a nadir view. One may expect that the emissivity,  $\epsilon$ , of sea water viewed at normal incidence is  $1 - \rho$  (sea), where the reflectance is given by

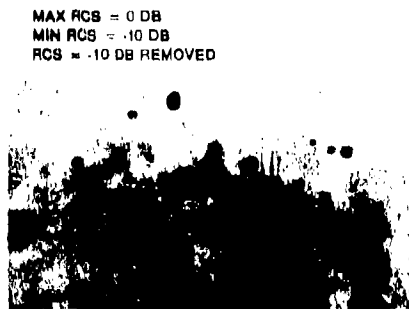
$$\rho(\text{sea}) \approx \left( \frac{n_r - 1}{n_r + 1} \right)^2 \quad (21)$$

where  $n_r$  is the real part of the index of refraction of the water.

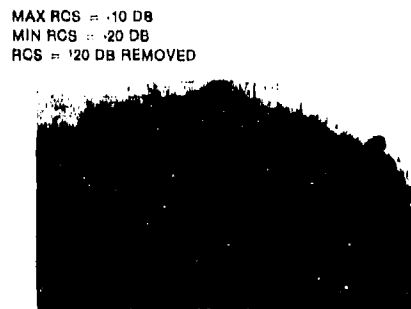
According to P. S. Ray,<sup>8</sup>  $n_r$  varies as shown in table VI-2. The reflectance and normal emissivity are calculated.

According to the Manual of Remote Sensing<sup>9</sup> (166, fig. 4-134), the emissivity for normal incidence changes only very slightly for different sea states (see fig. VI-4). The emissivity for microwaves (X- and K-bands) is about 0.47.

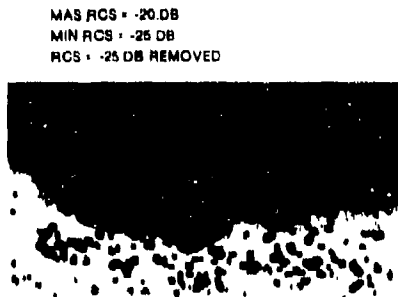
<sup>8</sup>P. S. Ray, *Applied Optics*, vol. 11, no. 8 (August 1972), 1836-1844.  
<sup>9</sup>Manual Remote Sensing, vol. 1, American Society of Photogrammetry (1975).



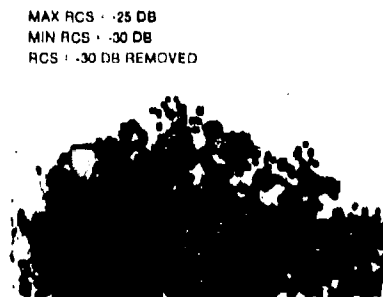
$-10 \leq I$



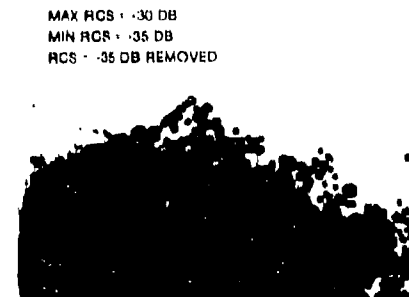
$-20 \leq I < -10$



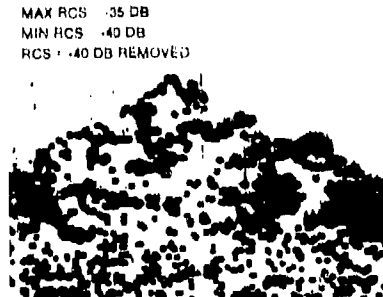
$-25 \leq I < -20$



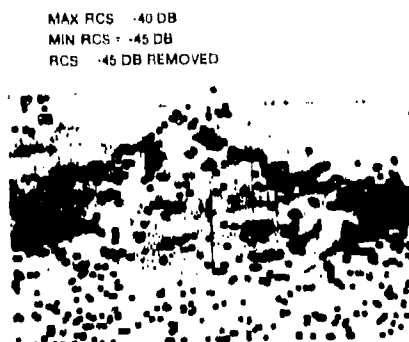
$-30 \leq I < -25$



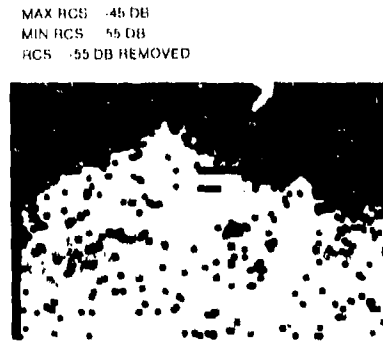
$-35 \leq I < -30$



$-40 \leq I < -35$



$-45 \leq I < -40$



$I \leq -45$

Figure VI-3(a). Level-sliced images of M-48 tank, and surrounding terrain (level-slicing intervals in dB), HH polarization.

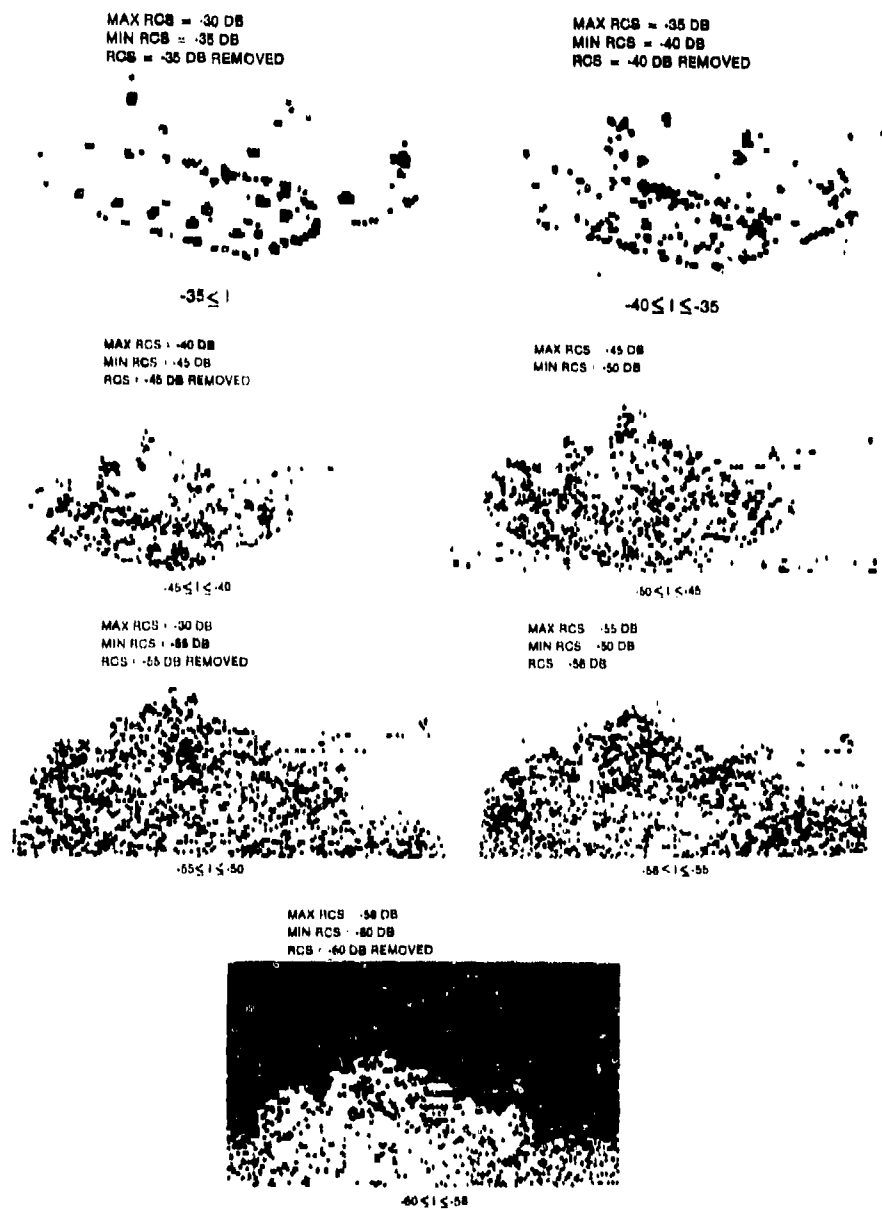


Figure VI-3(b). Level-sliced images of M48 tank and surrounding terrain (level-slicing intervals in dB), HV polarization.

TABLE VI-2. PROPERTIES OF SEA WATER

Wavelength $\lambda$ (mm)	Real part of index of refraction $n_r$	Reflectance $\rho$	Emissivity $\epsilon$
0.3	2.3	0.15	0.65
1.0	2.7	0.21	0.79
2.0	3.9	0.35	0.65
10.0	5.9	0.50	0.50
30.0	8.6	0.63	0.37
100.0	9.0	0.64	0.36

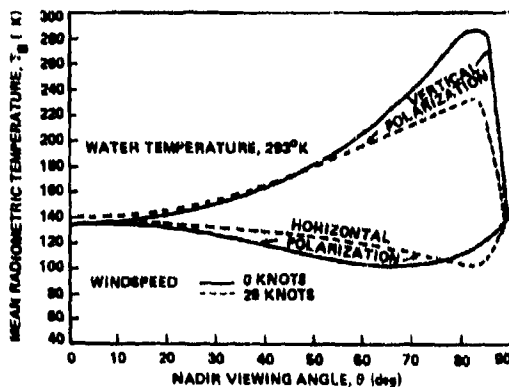


Figure VI-4. Theoretical antenna temperatures for sea state as functions of nadir viewing angles and wind velocity.

The temperature of large ships at sea results from the natural heat exchange between solar radiation, sky radiation, and convective heat transfer with the air. The effect of water contact is only secondary, except at the water line. The internal heat generated and exhaust stacks are insignificant contributors. Stacks are small compared to the entire projected deck area, and contributions of such hot parts are only in proportion to absolute temperature and the fraction of beam fill.

Naturally, the temperature of deck material will change from above water temperature during clear days to below water temperature at night. Under overcast conditions, the day to night temperature variation will be signifi-

cantly less. Under high winds, the temperature of the ship will approach air temperature, becoming slightly greater than air temperature during the day and slightly lower than air temperature at night.

During clear sunlit days with little wind, the deck temperature can rise as much as 20 to 30 C above air temperature. On clear calm nights, the deck temperature could reach the dew point.

The large heat capacity of deck materials will make the surface temperature lag behind the maximum thermal income by 2 to 3 hours. A corresponding delay in cooling off can be expected after sundown. The lowest temperature should be reached just before dawn. One may normally expect ship deck temperature and sea temperature to be equal twice equal day.

The emissivity of painted deck material is not known for the NMMW region. At 25  $\mu\text{m}$ ,  $\epsilon \sim 0.90$  and at X-band,  $\epsilon \sim 0.01$ . Obviously, the contrast between ship and sea will depend upon this value. If the emissivity at 1 mm is still very small, then ship temperature will be inconsequential in the signature. One should assume that  $\epsilon$  is very small for wavelengths as short as 1 mm until proven otherwise. The reflectance can be greatly affected by paint cover when the "optical" thickness of the paint approaches  $\lambda/4$ . Assuming  $n_r$  of paint of 1.5 and paint thickness of 0.2 mm (thick coating), one could achieve  $\lambda/4$  conditions at 1.2 mm. Absorption bands in the paint could appear, however.

One can see from table VI-2 that the emissivity of the sea will increase with decreasing wavelengths. If the emissivity of the ship is much smaller, as assumed, then the contrast will be due entirely to metallic reflection of sky radiation from the ship and the combined thermal emission and sky reflectance from the sea. Contrast should increase substantially. On the other hand, an estimation of the reflectance of painted steel is made in section VI-5.2. It is evident that significant spectral variation in the

emissivity of painted steel could occur in the NMMW range due only to the Debye relaxation effect in dielectrics. Such variations could make the difference between a successful application and an unsuccessful one.

Large Aircraft and Ballistic Missiles.—In lieu of measured data on large aircraft and ballistic missiles in the NMMW range, one must resort to simple mathematical modeling of components for estimating radiometric properties. Just as for ships at sea, the emissivity of the exposed materials of aircraft and missiles is the central issue in radiometry. The expected metal coating is either paint or an anodization of the metal. The spectral properties of anodization coatings are completely unknown in the NMMW range. One may surmise that the effects might be negligible until proven otherwise. However, a trend towards the use of nonmetallic substrates—such as graphite-epoxy—adds further complications to estimations, since the electromagnetic properties of graphite-epoxy materials are also unknown in this spectral range. If the coating is transparent, then the properties of the substrate will govern the radiative properties of the vehicle.

Atmospheric emissions caused by high-altitude vehicles may occur in two ways.

(1) The exhaust plume may emit thermally or absorb radiation due to transient chemical species.

(2) Exhaust products may cause catalytic reactions with *in situ* photochemically excited gases, yielding larger emissions than would be expected from the same concentration of simple Planckian thermal radiators. The recent concern with Freon gas catalytic reactions with ozone indicates that the understanding of such processes in the upper atmosphere is far from complete. For such a complex environment, neither mathematical modeling nor laboratory experiments are likely to lead to convincing results. There appears to be no other recourse than to make high-altitude measurements to acquire data.

## VI-4. DATA ON BACKGROUNDS

### VI-4.1 Terrain

Two basic types of measurements have been used to determine the radar scattering properties of terrain. One type consists of measurements from an airborne platform where data from a wide variety of different terrains are recorded; the frequencies for most of these data are less than 10 GHz. The other type consists of ground and laboratory measurements where a significant amount of data have been collected at 35 GHz, with some data at 94 and 140 GHz.\* Modeling is employing to estimate terrain  $\sigma_0$  up to 300 GHz. The interpolation of low-frequency data to higher frequencies can be seriously in error if the electromagnetic properties of vegetative materials change significantly in the NMMW range. Such a possibility is described in section VI-5.

The polarizations for  $\sigma_0$  measurements are usually VV, HH, and HV. The cross-polarized  $\sigma_0$  (HV) is usually 6 to 8 dB lower than the parallel-polarized  $\sigma_0$ . In the monostatic case, the return from the ground is highest at depression angles near 90 deg because of specular reflectance from the ground.

Monostatic Cross Sections of Terrain.—Aerospace Corporation<sup>10</sup> measurements of a number of horizontal surfaces show a normalized radar cross section,  $\sigma_0$ , essentially independent of frequency from 40 to 90 GHz at depression angles from 90 to 45 deg. Reflections from concrete, asphalt, and wood all appear to be nearly specular. Surfaces of gravel, sod, and weeds appear to reflect more nearly isotropically. Measured values are shown in figures VI-5 through VI-11. The large  $\sigma_0$  values at normal incidence are typical of specular reflectors. The three nonspecular surfaces exhibit backscatter nearly independent of depression angle. These measurements indicate a little larger backscatter

<sup>10</sup>H. E. King and C. J. Zamites, *Terrain Backscatter Measurements at 40 and 90 GHz*, Aerospace Corporation, SAMS-TR-70-220 and TR-0066 (3816-41)-1 (June 1970).

\*Editor's Note: see Selected Bibliography (Ch IX) for additional references on terrain measurements. Note particularly the work of Currie et al at the Georgia Institute of Technology.

at these frequencies than has been found at X- and K-band frequencies, in agreement with theoretical considerations regarding surface backscatter.

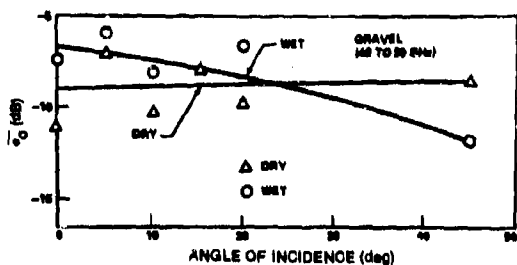


Figure VI-5. Mean  $\sigma_0$  for wet and dry gravel, 40 to 90 GHz.

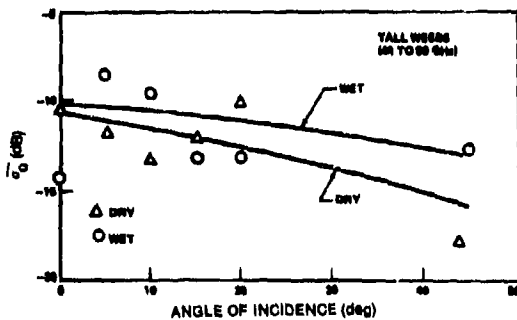


Figure VI-6. Mean  $\sigma_0$  for wet and dry tall weeds, 40 to 90 GHz.

Values of  $\sigma_0$  at 94 GHz, published by Hughes Aircraft Company, are shown in figure VI-12 and are in general agreement with the Aerospace data. The data are for low-depression angles rather than the high-depression angles of the Aerospace data. Radar  $\sigma_0$  measurements published by the System Planning Corporation<sup>11</sup> are shown in figures VI-13 through VI-17. The  $\sigma_0$  of concrete and asphalt is shown rising with frequency from 10 to 120 GHz in figure VI-17. Plowed fields show some increase of  $\sigma_0$  with radar frequency. Crop and tree  $\sigma_0$

<sup>11</sup>L. D. Strom, *Applications for Millimeter Radars (U)*, Report No. 108, System Planning Corporation (December 1973), AD 529 566. (CONFIDENTIAL)

values appear to be nearly independent of frequency.

Measurements by BRL<sup>12</sup> at 140 GHz indicate that the  $\sigma_0$  of vegetation is 10 dB greater with leaves than without leaves. BRL measurements at 94 GHz indicate that  $\sigma_0$  from "dirt and weeds" at  $\theta_d$  less than 1 deg is -22 dB. This small value of  $\theta_0$  correspond to a  $\gamma$  of -5 dB. The  $\gamma$  for dirt and weeds is similar to the  $\gamma$  found by Ohio State University<sup>13</sup> for tall oats in head.

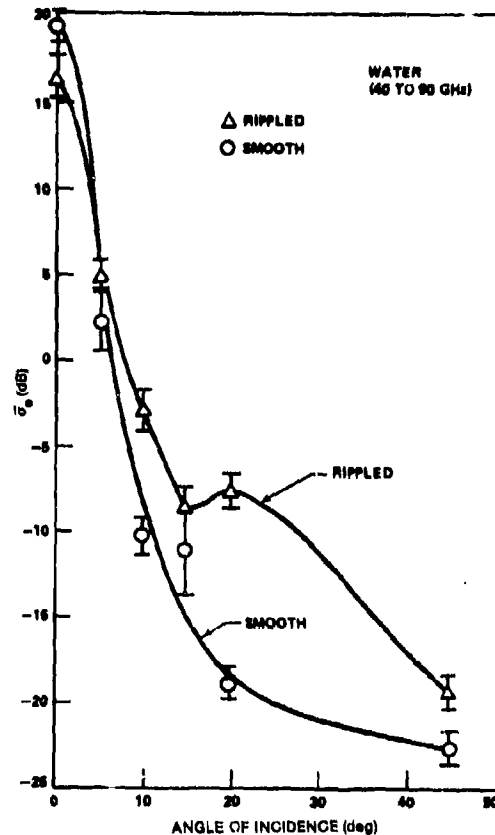


Figure VI-7. Mean  $\sigma_0$  for smooth and rippled water, 40 to 90 GHz.

<sup>12</sup>E. Kammerer and K. A. Richer, *Cross Section Measurements of U.S. Army Targets by 140 GHz Radar (U)*, Ballistic Research Laboratories BRL-MR-1785 (August 1966), AD 378 097. (CONFIDENTIAL)

<sup>13</sup>W. H. Peake and T. L. Oliver, *The Response of Terrestrial Surfaces at Microwave Frequencies*, Ohio State University AFAL-TR-70-301 and ESL-2440-7 (May 1971), AD 884 106.

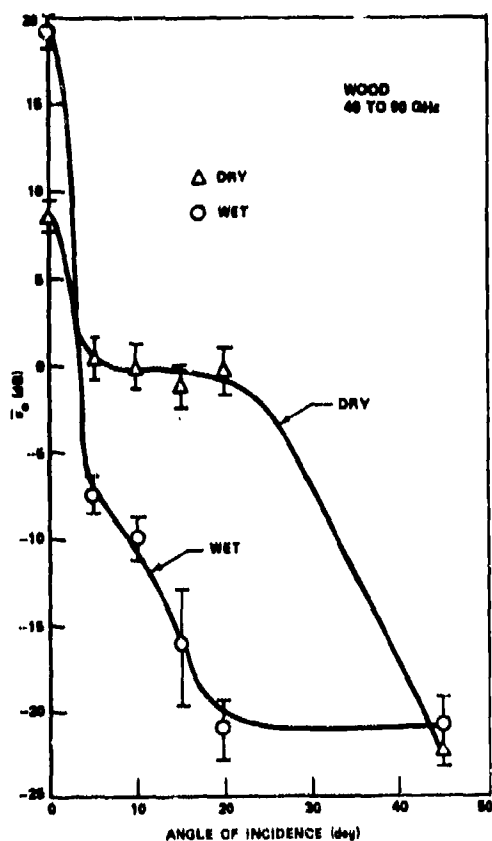


Figure VI-8. Mean  $\sigma_0$  for wet and dry wood, 40 to 90 GHz.

A publication by the Norden Division of United Aircraft<sup>14</sup> contains 70-GHz data. The  $\sigma_0$  from a macadam surface is given as -40 dB at  $\theta_d = 9.2$  deg.

To investigate the signal-to-noise ratio in the Overland Radar Technology Program, the Illinois Institute of Technology Research Institute (IITRI) developed models of the behavior of  $\sigma_0$  with depression angle; the models developed were for broad terrain classes,

<sup>14</sup>L. Chansit, L. Kosowsky, K. Koester, and I. Goldmacher, *Study of Airborne Millimeter Radar Techniques*, United Aircraft Corporation ECOM-02125-F (June 1970), AD 373 641.

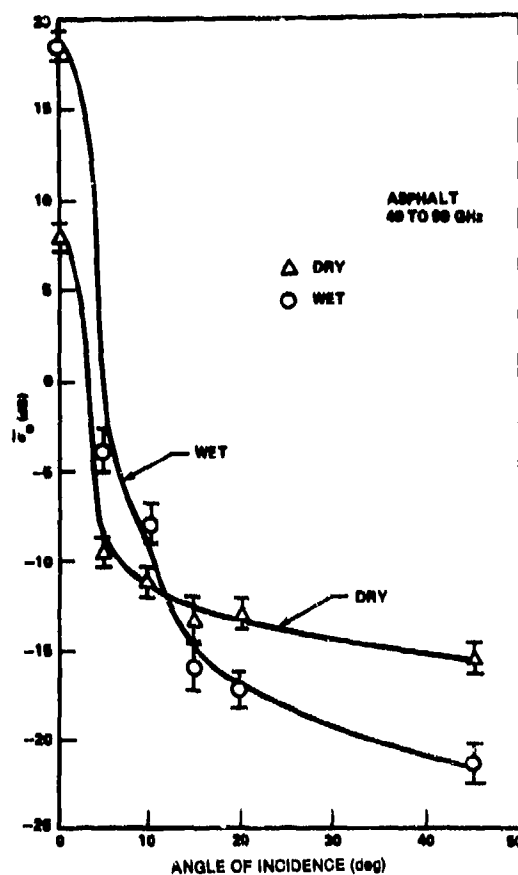


Figure VI-9. Mean  $\sigma_0$  for wet and dry asphalt, 40 to 90 GHz.

lake/sea, farmland, woodland, and desert.<sup>15</sup> The dashed lines in figure VI-18 show the median value of  $\sigma_0$  and the median  $\pm$  the standard deviation for farmland clutter. The models for the other terrain types are similar.

During their examination of experimental data, IITRI found that the difference between horizontal (HH) and vertical (VV) polarizations was less than variations in the meas-

<sup>15</sup>L. J. Gruenstein et al, *A Comprehensive Ground Clutter Model for Airborne Radars*, IIT Research Institute, Chicago, IL (September 1969), AD 861 913L.

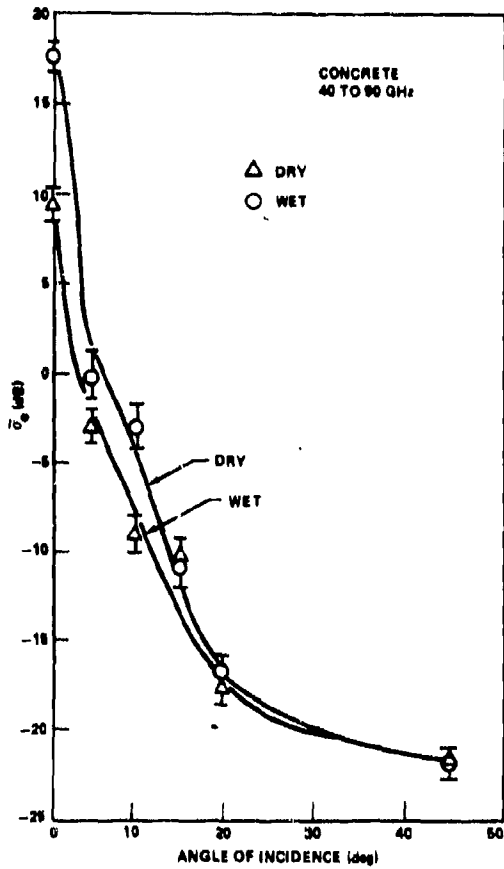


Figure VI-10. Mean  $\sigma_0$  for wet and dry concrete, 40 to 90 GHz.

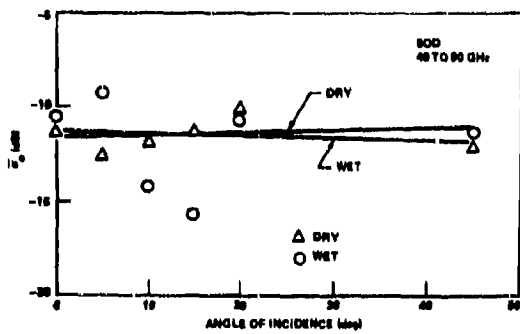


Figure VI-11. Mean  $\sigma_0$  for wet and dry sod, 40 to 90 GHz.

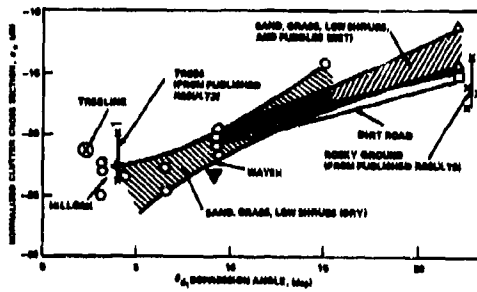


Figure VI-12. Clutter characteristics at 94 GHz.

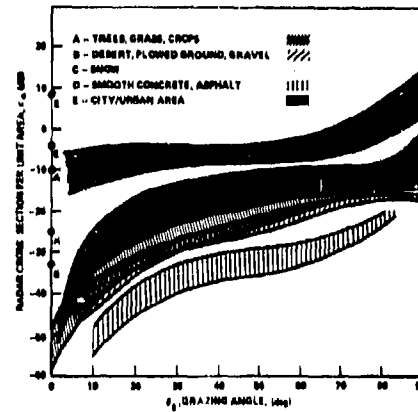


Figure VI-13. Radar cross section of natural ground targets at X-band.

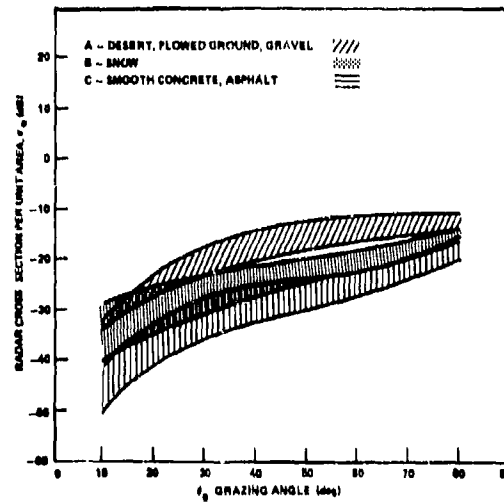


Figure VI-14. Radar cross section of natural ground targets at  $K_u$ -band.

urements; consequentially, horizontal and vertical polarizations were lumped together in the measurements. IITRI also concluded that there was no significant variation of  $\sigma_0$  with frequency from 0.3 to 10 GHz (except for desert), and the models cover this frequency range.

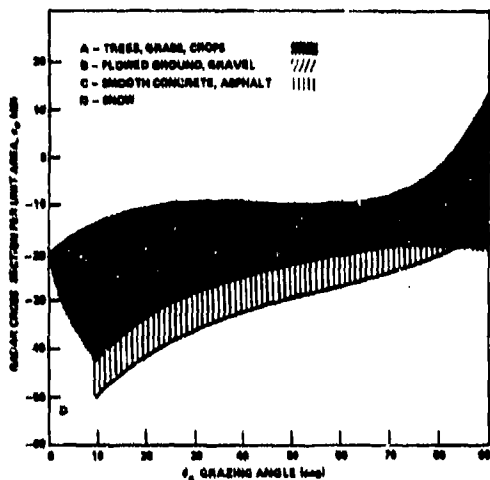


Figure VI-15. Radar cross section of natural ground targets at K<sub>u</sub>-band.

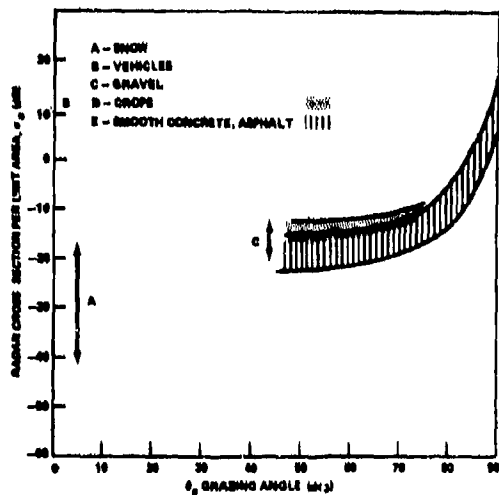


Figure VI-16. Radar cross section of natural ground targets at 40 to 90 GHz.

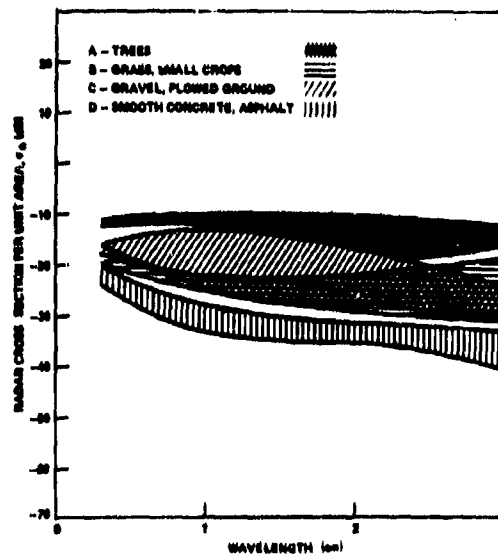


Figure VI-17. Clutter  $\sigma_0$  between 70 and 20 deg grazing angle as a function of wavelength.

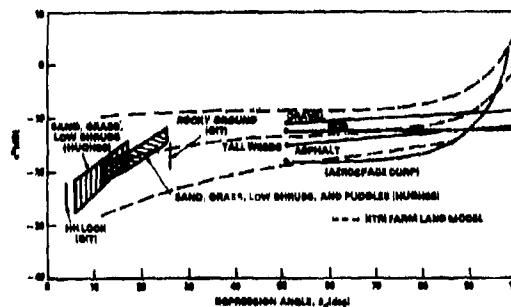


Figure VI-18. Monostatic millimeter measurements plotted with IITRI Farmland Model.

According to Long, the experimental results are not in agreement as to the variation of  $\sigma_0$  with wavelength.<sup>3</sup> He indicates that  $\sigma_0$  varies as  $\lambda^{-n}$ , where  $n$  is between zero and one. Nathanson also indicates that  $\sigma_0$  increases with frequency but usually not faster than linearly.<sup>16</sup>

<sup>3</sup>M. W. Long, *Radar Reflectivity of Land and Sea*, Lexington Books, Lexington, MA (1973).

<sup>16</sup>F. Nathanson, *Radar Design Principles*, McGraw-Hill Book Company, New York (1969), 264.

The conclusions in these references are based on airborne data taken at frequencies of 10 GHz or less and ground data taken at 35 GHz or less. To determine how  $\sigma_0$  behaves at higher frequencies, millimeter back-ground measurements from three sources<sup>10,17,18</sup> were plotted on figure VI-18. The two vertical lines near 4- and 25-deg depression angles represent data from the Georgia Institute of Technology (GIT) at 94 GHz. The cross-hatched areas are Hughes data, also taken at 94 GHz. The solid lines from 45 to 90 are Aerospace data from averaged measurements in the 40- to 90-GHz band. The figure lists the backgrounds measured. The dashed lines in the figure represent the IITRI farmland model.

The millimeter measurements agree with the IITRI model; hence, this model appears to be a reasonable estimate of terrain reflectivity at 300 GHz. Figure VI-19 is an estimate of  $\sigma_0$  for typical terrain with horizontal and vertical polarizations at frequencies of 10- to 350-GHz. The solid line in the center is the estimated median value of  $\sigma_0$ , and the dashed lines

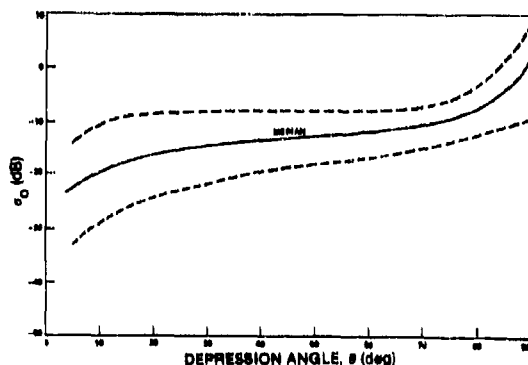


Figure VI-19. Estimated  $\sigma_0$  values, 10 to 350 GHz, for H and V polarizations, monostatic operation (IITRI) farmland model extended to 5-deg depression angle.

<sup>10</sup>H. E. King and C. J. Zamites, *Terrain Backscatter Measurements at 40 to 90 GHz*, Aerospace Corporation SAMSO-TR-70-220 and TR-0066 (5816-41)-1 (June 1970).

<sup>17</sup>N. C. Currie et al, *Radar Land Clutter Measurement at Frequencies of 9.5, 16, 35, and 94 GHz*, Georgia Institute of Technology (April 1975).

<sup>18</sup>M. E. Buebe et al, *94 GHz Sensor Tower Test Program*, Hughes Report No. MSG 65075R (February 1976).

represent the upper and lower extremes within which  $\sigma_0$  is expected to lie for a monostatic radar. This figure is the IITRI farmland model extended to a 5-deg depression angle.

Images of snow-covered terrain have been made at 35 GHz with the use of the airborne AN/APQ-97 radar.<sup>19</sup> Measurements of  $\gamma$  for various snow-covered terrains were also measured by OSU.<sup>20</sup> The influence of nominal depths of new snow is reported to be negligible compared to the influence of the underlying terrain.<sup>19</sup> However, the old snow mixed with ice may result in significantly higher values of  $\gamma$ . A 2-in. ( $\sim 50$  mm) snow and ice layer covering concrete is shown by OSU to yield 10 to 15 dB greater  $\gamma$  than for bare concrete. Also, images of regions of old snow display an anomalously high return.<sup>19</sup> The cause for the higher returns is not known, but a possible mechanism is intimated to be the retroreflecting power of ice crystals in old snow with dimensions of the order of a wavelength.<sup>19</sup> If that is the cause, then these "anomalous" returns may be expected to become more frequent in the NMMW range, due to the increasing frequency of occurrence of small ice crystals.

#### Bistatic Cross Sections of Terrain

—The amount of available bistatic terrain  $\sigma_0$  data is evidently quite small; only six references were located and only four of these provide independent data. No data have been located for the 0.3 to 3.2-mm wavelength region. In fact, the shortest wavelength for bistatic  $\sigma_0$  data appears to be  $\sim 3$  cm. BRL has published bistatic scattering measurements.<sup>21</sup> These data indicated that forward scattering decreases as the illuminating frequency increases and as the grazing angle increases, not entirely consistent with data presented below.

<sup>19</sup>Manual of Remote Sensing, vol. 11, American Society of Photogrammetry (1975).

<sup>20</sup>R. L. Cosgriff et al, *Terrain Scattering Properties for Sensor System Design*, Engineering Experiment Station Bulletin, Ohio State University, Columbus, OH (May 1960).

<sup>21</sup>K. A. Richer, *4.4 mm Wavelength Near Earth Propagation Measurements*, Ballistic Research Laboratories BRL-MR-1403 (May 1962), AD 331 098.

Figure VI-20 shows the envelope of data points measured by the Royal Canadian Air Force<sup>13</sup> using a two-aircraft measurement system. For all these measurements, the transmitting antenna radiated straight down ( $\theta_i = 0$  deg). The receiver aircraft flew abreast of the transmitter aircraft at various distances in order to receive at different values of  $\theta_s$  between 21 and 83 deg. Since the results for flat farmland and hilly terrain are quite similar, they are lumped together in the figure. Note that  $\sigma_0$  ranges between -20.5 and -6.5 dB.

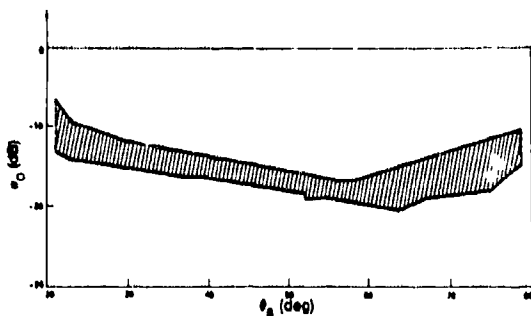


Figure VI-20.  $\sigma_0$  versus  $\theta_s$  for HH polarization,  $\theta_i = 0$  deg and  $\phi_s = 0$  deg,  $\lambda = 3$  cm (flat farmland and hilly terrain).

The next four figures show the results of measurements made by OSU<sup>13,23,24,\*</sup> on small controlled terrain patches using ground instrumentation. Figure VI-21 shows  $\sigma_0$  versus  $\theta_s$  for  $\theta_i = 20$  deg and  $\phi_s = 0$  deg. Observe how  $\sigma_0$  for smooth sand peaks at the specular angle ( $\theta_s = 20$  deg). Note also that  $\sigma_0$  for smooth sand exhibits the widest variation; its  $\sigma_0$  values range

<sup>13</sup>W. H. Peake and T. L. Oliver, *The Response of Terrestrial Surfaces at Microwave Frequencies*, Ohio State University, AFAL-TR-70-301 and ESL-2440-7 (May 1971), AD 884 106.

<sup>23</sup>B. J. Starkey, *Bi-Static Ground Scatter Measurements in X-Band and the Ground Scatter Jammer Parameters (U)*, Directorate of Electronic Warfare S957-104-3 (DEW), Air Force Headquarters, Ottawa, Canada (September 1963). (SECRET)

<sup>24</sup>S. T. Cost, *Measurements of the Bistatic Echo Area of Terrain at X-Band*, Ohio State University Report No. 1822-2 (May 1965).

<sup>25</sup>J. A. Rupke and G. S. Kasweller, *Investigation of Ground Illumination at Radar Frequencies (U)*, AFAL-TR-65-204 and 6148-17-F, The University of Michigan, Willow Run Laboratories (September 1965), AD 366 232. (SECRET)

\*References 23 and 24 each provide a complete set of the data. Reference 13 presents much, but not all, of the same data.

from -37 to +12 dB. The  $\sigma_0$  for rough sand and dry grass terrain patches exhibits much less variation.

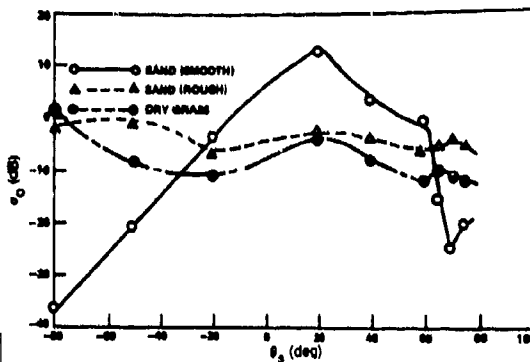


Figure VI-21.  $\sigma_0$  versus  $\theta_s$  for HH polarization,  $\theta_i = 20$  deg and  $\phi_s = 0$  deg,  $\lambda = 3$  cm.

Figures VI-22 and -23 show OSU plots of  $\sigma$  versus  $\phi_s$  for relatively large incidence and scattering angles ( $\theta_i = \theta_s = 70$  deg and  $\theta_i = \theta_s = 80$  deg, respectively). Note that, in most cases, there is a significant peaking for specular reflection ( $\theta_s = 0$ ). Note also that  $\sigma_0$  values for the smooth sand vary more widely than those for the loam or soybean foliage, although the differences are not as pronounced for  $\theta_i = 80$  deg as for  $\theta_i = 70$  deg. For  $\theta_i = 70$  deg,  $\sigma_0$  for smooth sand ranges from -43 to +21 dB.

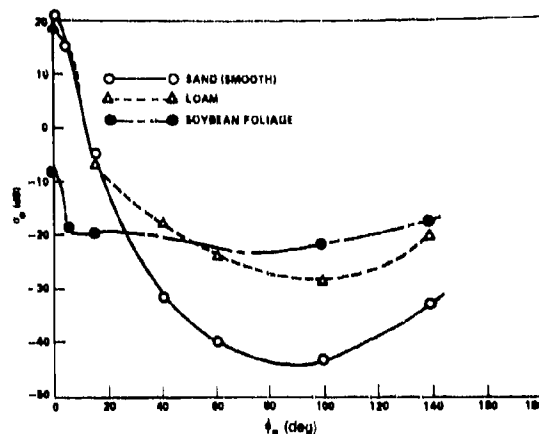


Figure VI-22.  $\sigma_0$  versus  $\phi_s$  for HH polarization,  $\theta_i = \theta_s = 70$  deg,  $\lambda = 3$  cm.

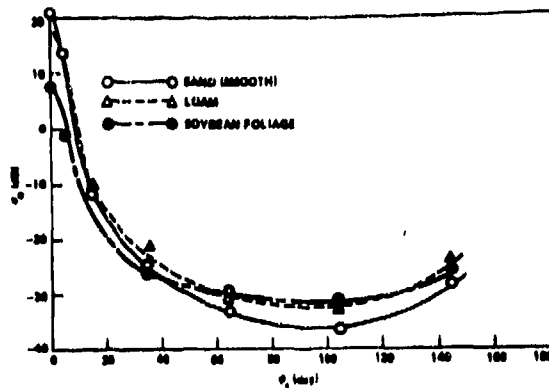


Figure VI-23.  $\sigma_0$  versus  $\phi_s$  for HH polarization,  $\theta_i = \theta_s = 80$  deg,  $\lambda = 3$  cm.

All the previously discussed  $\sigma_0$  data were for HH polarization. Figure VI-24 compares OSU data taken at HH, VV, and crossed HV polarizations for smooth sand and at  $\theta_i = 85$  deg. Note that HH polarization gives the strongest response for most values of  $\phi_s$ . Also, HV values are the smallest much of the time, especially in the near-specular ( $0 \text{ deg} < \phi_s < 10 \text{ deg}$ ) directions and the backscattering ( $\phi_s > 90 \text{ deg}$ ) directions.

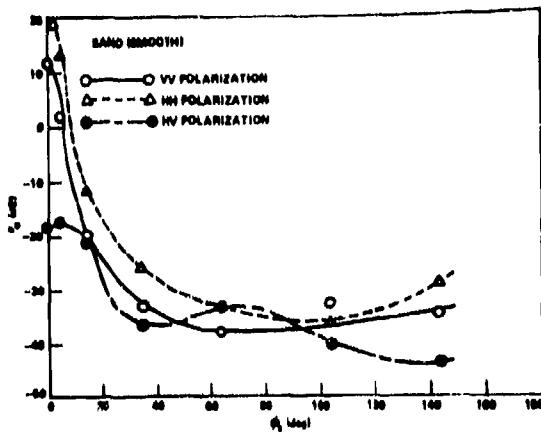


Figure VI-24.  $\sigma_0$  versus  $\phi_s$  for  $\theta_i = \theta_s = 85$  deg for various polarizations,  $\lambda = 3$  cm.

Recent bistatic  $\sigma_0$  measurements have been made by ERIM.<sup>28</sup> The next two figures show typical results. Like most of the previously discussed data, a 3-cm wavelength and HH polarization were used; the incidence and scattering angles are relatively large, ranging between  $\sim 67$  and  $85$  deg.

Figure VI-25 shows  $\sigma_0$  versus  $\phi_s$  (0 to 55 deg) for flat terrain (grass and a cement ramp). Note that the data points range between -17 and -7 dB. Note also that there is no significant variation in  $\sigma_0$  as a function of  $\phi_s$ . This is believed to be due to considerably less homogeneity in the terrain area as compared to that measured in the OSU program.

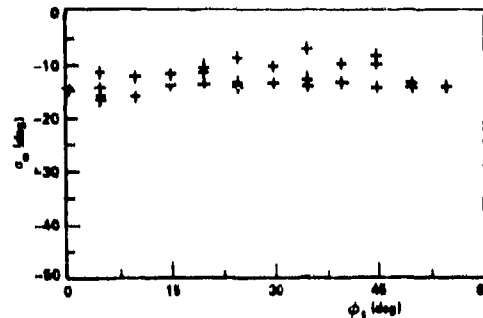


Figure VI-25.  $\sigma_0$  versus  $\phi_s$  for HH polarization,  $\theta_i \sim 79$  deg and  $\theta_s = 85$  deg,  $\lambda = 3$  cm (grass and cement ramp).

Figure VI-26 provides the envelope of the ERIM data points collected for an area of tall weeds and scrub trees. Here again, there does not appear to be any clear trend with  $\phi_s$ . The abrupt level change in the vicinity of  $\phi_s = 85$  deg is believed to be due to experimental errors related to the fact that the first and second

<sup>28</sup>R. W. Larson et al., *Measurements of Bistatic Scattering Coefficients Using Air-Ground Coherent Instrumentation*, Environmental Research Institute of Michigan Report 118200-14-F (April 1977).

halves of the data curves were measured on separate passes. It is shown that  $\sigma_0$  values range from -27 to -0.5 dB.

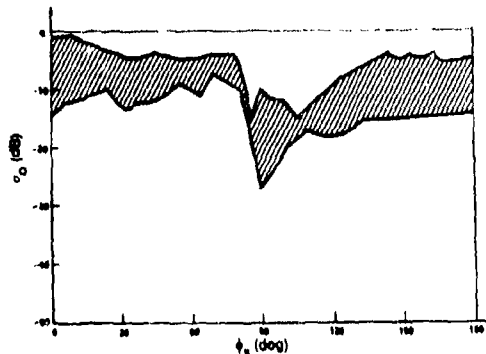


Figure VI-26.  $\sigma_0$  versus  $\phi_s$  for HH polarization,  $\theta_i \sim 67$  to 78 deg,  $\theta_s = 80$  deg,  $\lambda = 3$  cm (tall weeds and scrub trees).

**Target-Background Contrast Data.**—Target-background contrast measurements have been made at 35 and 70, as well as a few measurements at 94 GHz in support of the terminal homing data bank at the U.S. Army Missile Research and Development Command. Some of the types of measurements are described in table VI-3.

It seems clear from the data discussed in the previous paragraphs that bistatic  $\sigma_0$  values can vary widely, depending on the particular measurement parameters. In the absence of other information, we shall assume that the bistatic return—like the monostatic—is constant with frequency above 10 GHz so that measurements made from 9 to 10 GHz will indicate the order of magnitude of bistatic  $\sigma_0$  for radars operating from 10 to 350 GHz. With smooth surfaces at angles near specular,  $\sigma_0$  is likely to be -5 to 5 dB; the values for rough surfaces are likely to be -10 dB near specular. Away from the specular point,  $\sigma_0$  values for terrain will be -15 to -10 dB.  $\sigma_0$  can drop to -30 dB or less far from the plane of the incident field. The data

curves should be helpful in making estimates for particular situations.

**Radiometric Obscuration by Fore-ground Foliage.**—According to McGee,<sup>26</sup> the obscuration by foliage of a target thermally emitting 35-GHz radiation is related to the visual obscuration. He offers the empirical relation

$$B \approx 0.103 + 1.59B' - 0.700(B')^2, \quad (22)$$

where B is the apparent radiometric blockage; i.e.,

$$T = BT(\text{foliage}) + (1 - B)T(\text{target}), \text{ and}$$

B' is the visual blockage, i.e., the fraction of the target covered by foliage as viewed from the receiver and T is the radiometric temperature.

McGee's relation will probably hold true for shorter wavelengths as long as  $\gamma$  for vegetation is approximately constant. It may fail for wavelengths near 1 mm due to possible changes in the electromagnetic properties of vegetation (see sect. VI-5.1) and painted steel (see sect. VI-5.2).

#### VI-4.2 Atmospheric Emission Data

NMMW background radiation at high altitude (144 km) for space-ward viewing radiometers is reported by J. R. Houck et al.,<sup>27</sup> as  $1.5 \mu\text{W}/\text{m}^2\text{sr}$  in the band from 0.4 to 1.3 mm and about  $0.3 \mu\text{W}/\text{m}^2\text{sr}$  in the band from 1.2 to 1.8 mm. The anticipated radiation from a 2.7 K blackbody residual radiation from space due to an expanding universe would be about  $0.4 \mu\text{W}/\text{m}^2\text{sr}$  in the 0.4 to 1.3 mm band.

For further discussion of atmospheric emission measurements the reader is referred to Chapter I and numerous references in the Selected Bibliography (Ch IX) (Gibbins, Sokolov, Künzi, Staelin, and Aganbekeyan).

<sup>26</sup>R. A. McGee, Millimeter Wave Radiometric Detection of Targets Obscured by Foliage, Ballistic Research Laboratories BRL-MR-1901 (January 1969), AD 667 962.

<sup>27</sup>J. R. Houck et al., The Far Infrared and Submillimeter Background, Cornell University (1 September 1972), A1) 763 139.

TABLE VI-3. MILLIMETER TARGET AND BACKGROUND MEASUREMENTS

Frequency	Target	Background	Contract support	Remarks	Location
35-GHz, passive and fm/cw	M60, M48, M4, tanks, mortars, howitzer, rocket launcher, trucks, convoys	Dense brush, woods	Sperry Microwave	Joint MICOM-Eglin AFB effort; <sup>a</sup> tower-mounted sensors	Eglin AFB, FL
35 GHz, fm/cw	M48, M41, tanks	Grass, brush, woods	—	Joint MICOM-BRL effort; <sup>b</sup> helicopter-mounted sensor	Redstone Arsenal, AL
35 GHz, pulsed	M41 tank, truck, M113 APC	Dense brush, woods	General Dynamics	Joint MICOM-Eglin AFB effort; <sup>c</sup> tower seeker	Eglin AFB, FL
35 GHz, fm/cw	M48 tank, M113 APC	Grass, trees wet soil, airport runway, roads	Sperry Microwave	Helicopter-mounted sensor <sup>d</sup> primarily wet backgrounds	Redstone Arsenal, AL
35 GHz, pulsed	M48 tank, M113 APC	Grass, brush, woods	Martin-Marietta	Tower and helicopter mounted <sup>e</sup>	Redstone Arsenal, AL
70 GHz, pulsed	M48 tank, M113 APC	Grass, woods	Norden/United Technology	Joint MICOM-ECOM effort; <sup>f</sup> tower-mounted sensor; polarization diversity; variable pulse width	Redstone Arsenal, AL
95 GHz	M60 tank	—	Honeywell	—	TARADCOM, Warren, MI
35- and 94-GHz, pulsed	Foreign armored targets	Grass	Georgia Inst. of Technology Sperry Microwave	Joint Army-AF effort; tower-mounted sensors; simultaneous 35- and 94-GHz measurements	Aberdeen PG, MD
35- and 94-GHz, pulsed	M48 tank, M113 APC	Grass	Sperry Microwave	Joint Army-DARPA tower; helicopter-mounted sensors; simultaneous 35- and 94-GHz; monostatic and bistatic data on targets and backgrounds	Redstone Arsenal, AL
17, 35, and 94 GHz	M48 tank, M113 APC cargo trucks	Grass, brush, woods	Georgia Inst. of Technology	Investigate polarization and frequency agility; target/background characteristics; tower-mounted sensors; initiated May 77	Redstone Arsenal, AL

<sup>a</sup>Air Force Armament Laboratory, K<sub>a</sub> Band Radiometer Tower Test (U), Eglin AFB, FL (June 1972) AFATL-TR-72-123, RE-TR-72-3, (CONFIDENTIAL)

<sup>b</sup>Army Terminal Homing Symposium Proceedings, Millimeter Wave Measurements for Terminal Homing (U), U.S. Army Missile Command (24-25 April 1973). (CONFIDENTIAL)

<sup>c</sup>U.S. Army Missile Command, Millimeter Target Measurements and Seeker Effort (U), Technical Report RE-76-23 (January 1976). (CONFIDENTIAL)

<sup>d</sup>Sperry Microwave Electronics, fm/cw Millimeter Sensor Target-Background Measurements (U), SJ 242-7914-1, Final Report, Contract DAAH01-74-C-0682 (August 1975). (CONFIDENTIAL)

<sup>e</sup>Martin Marietta, D<sup>o</sup> Range Processor Test Program, MICOM Test Program (U), Report No. OR 14,147 (Final Report from 26 January to 26 March 1976). (CONFIDENTIAL)

<sup>f</sup>Norden Division of United Technologies Corporation, Millimeter Radar Test Program, Report No. TE-CR-77-6 (Final Report from May 1976 to February 1977).

## VI-5. MATERIAL PROPERTIES AND TRENDS INDICATED BY SIMPLE MODELING

Even though target and background scattering and emission may not be measured at the desired wavelengths, it may be possible to estimate what reasonably could be expected from a knowledge of the constituent material properties and from applying simple modeling concepts. If one uses relation (3), which separates the material properties, the geometrical shape, and the size factors, one may estimate trends in  $\sigma$  and  $\sigma_0$  on the basis of the expected trends of each factor.

### VI-5.1 Liquid and Solid Water

P. S. Ray<sup>9</sup> published values of the real and imaginary index of refraction for liquid and solid water as shown in figures VI-27 and VI-28. The complex dielectric constant may be derived from these data by use of the relations

$$\epsilon' = n_r^2 - n_i^2, \quad (23)$$

$$\epsilon'' = 2n_r n_i, \quad (24)$$

where  $\epsilon'$  = real part of the complex dielectric constant,

$\epsilon''$  = imaginary part of the complex dielectric constant,

$n_r$  = real part of the index of refraction, and

$n_i$  = imaginary part of the index of refraction.

A portion of the spectrum of the complex dielectric constant is shown in figure VI-29.

Plane sections of materials containing water, such as leaves of vegetation and soil, will exhibit a reflectance and transmittance

which should vary in frequency in accordance with the complex dielectric constant of water. An empirical relation between the complex dielectric constant of water and the complex dielectric constant of corn and grass leaves at a frequency of 8.5 GHz is given in the Manual of Remote Sensing<sup>9</sup> as

$$\epsilon'(\text{leaf}) = 1.5 + \frac{m\epsilon'(\text{water})}{2},$$

$$\epsilon''(\text{leaf}) = 0.001 + \frac{m\epsilon''(\text{water})}{3},$$

where  $m$  = weight fraction of water in the leaf ( $0 \leq m \leq 0.6$ ).

The leaf thickness of many temperate-zone plants is about 0.3 mm so that one may compute the leaf specular transmittance and reflectance for a leaf plane section at normal incidence using Stratton's relation.<sup>10</sup> The results of such a computation are shown in figure VI-30. Since  $\sigma_0 \approx \rho G' A/A_i$ , one may argue that since  $G'$  appears to remain constant with decreasing wavelength for other targets, then  $G'$  should remain constant for foliage. The projected area of the foliage is not wavelength dependent; thus,  $\sigma_0$  should vary as canopy reflectance. In turn, canopy reflectance should vary with the specular reflectance for single surface scattering and as specular transmittance and reflectance for multiple scattering. One may observe from figure VI-30 that decreasing wavelength should yield no significant change until  $\lambda < 2$  mm where some possible surprises in  $\sigma_0$  might be observed. For wavelengths below 0.1 mm, the canopy  $\sigma_0$  should merge with observations at 10.6  $\mu\text{m}$ .

Blue and Perkowitz<sup>11</sup> made relative reflectance measurements  $\rho_{\text{rel}} = \pi q'$  of grass blades and leaves for  $\theta_i = 12$  deg,  $\theta_s = 12$  deg, and  $\phi_s = 0$  deg, the specular angle conditions.

<sup>9</sup>Manual of Remote Sensing, Vol. I, American Society of Photogrammetry (1975).

<sup>10</sup>J. A. Stratton, *Electromagnetic Theory*, McGraw-Hill Book Company (1941).

<sup>11</sup>M. D. Blue and S. Perkowitz, *Reflectivity of Common Materials in the Submillimeter Region*, *IEEE Trans. Microwave Theory and Tech.*, vol. MTT-25 (1977), 491-493.

<sup>9</sup>P. S. Ray, *Applied Optics*, vol. 11, no. 8 (August 1972), 1836-1844.

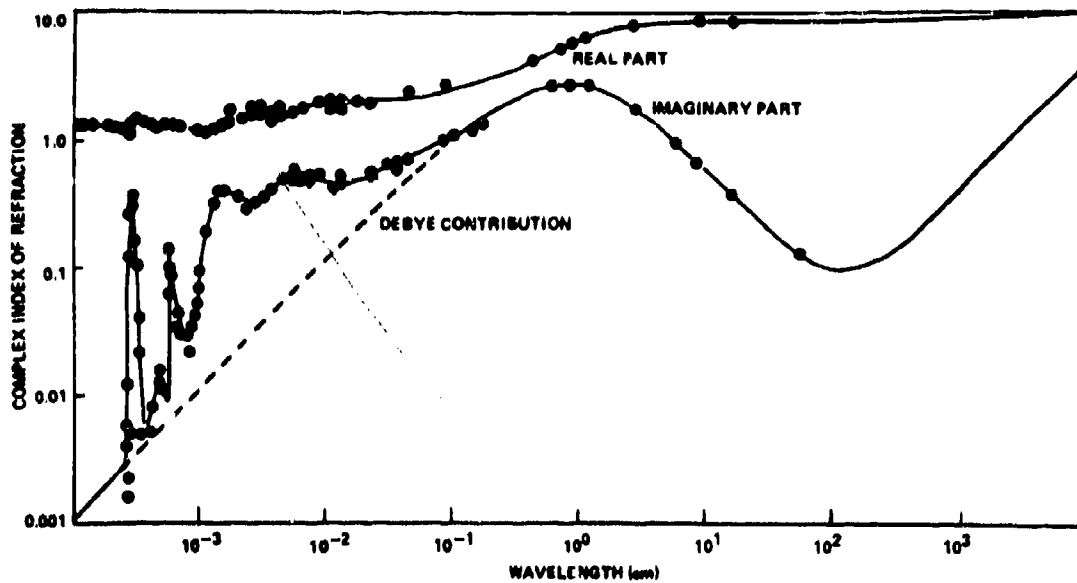


Figure VI-27. Analytic model of complex index of refraction for liquid water with a sample of experimental data to illustrate fit. The temperature is 25 C.

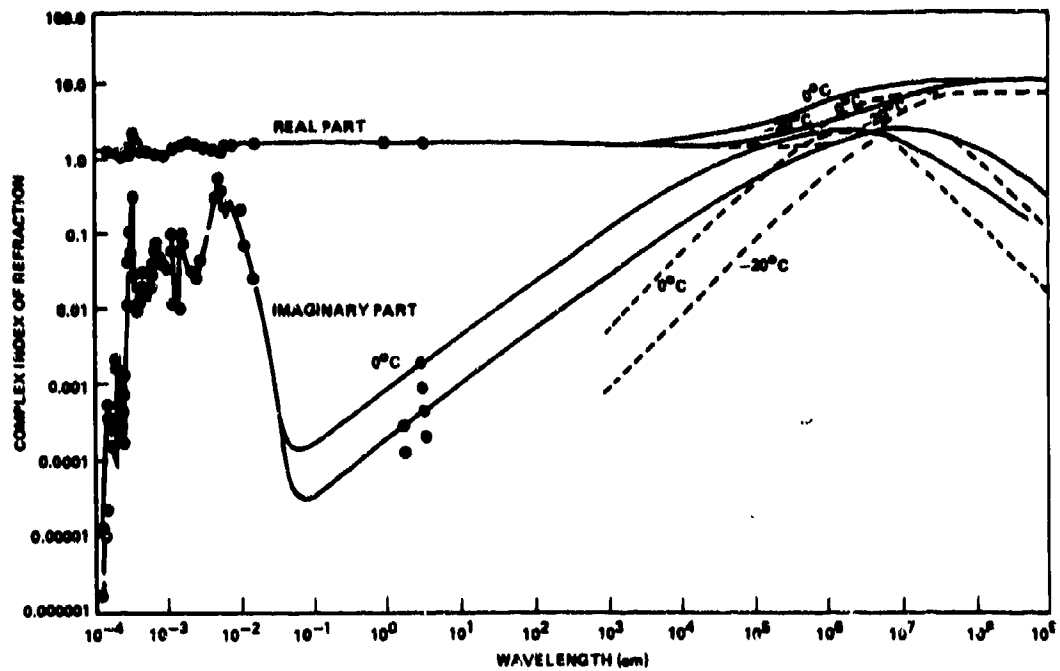


Figure VI-28. Analytic model of complex index of refraction for ice with a sample of data to illustrate fit. Dashed line represents Worz-Cole Model.

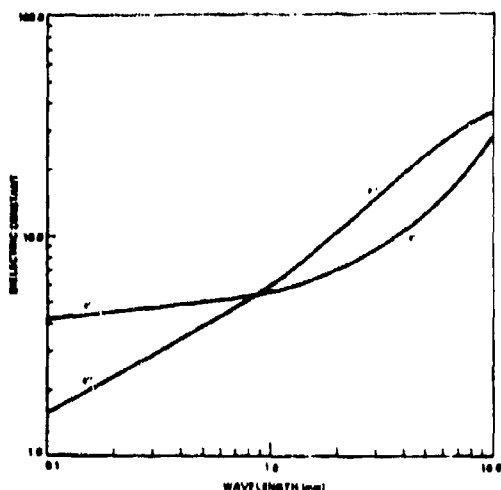


Figure IV-29. Complex dielectric constant, calculated from Ray's curve for water at 25 C ( $\epsilon' = n_T^2 - n_I^2$ ,  $\epsilon'' = 2n_T n_I$ ).

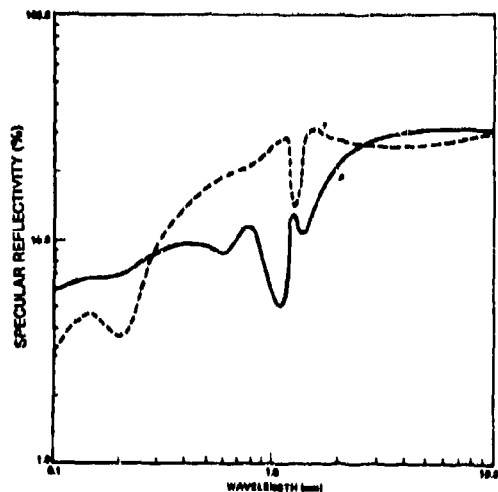


Figure VI-30. Normal specular reflectance,  $Q$ , and transmittance,  $\tau$ , of healthy green leaf ( $d = 0.3$  mm,  $m = 0.6$ ).

The results are shown in figure VI-31. The magnitude of  $Q_{dh}$  must be greater than  $Q_{rel}$  so that the values shown are minimum values of  $Q_{dh}$ . The roughness of surface will determine the degree of scattering into angles other than specular angle.

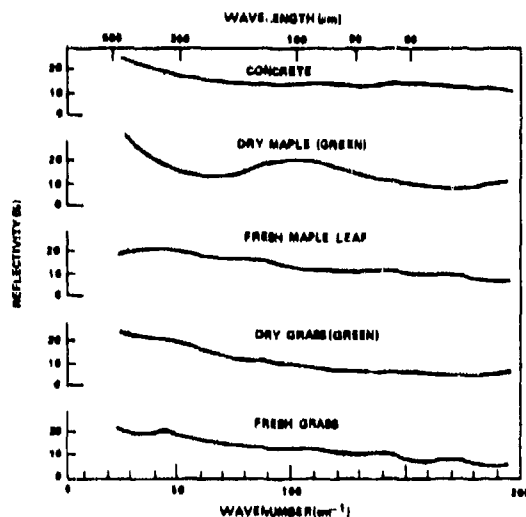


Figure VI-31. Normal reflectivity in percent for typical organic materials, and concrete surface for comparison.

Perkowitz and Bean<sup>30</sup> have shown that molecular absorption bands of chlorophyll also occur in the NMMW range. Figure VI-32 shows relative absorption as a function of wavenumber for chlorophyll (a) and (b). The short wavelength limit of NMMW range is 0.3 mm, or 33  $\text{cm}^{-1}$ .

Work on material properties and spectroscopy in the NMMW region has been underway since 1892.<sup>31</sup> During most of this

<sup>30</sup>S. Perkowitz and B. L. Bean, *Far Infrared Absorption of Chlorophyll in Solution*, *Journal of Chemical Physics*, vol. 66 (1977), 2231-2232.

<sup>31</sup>K. D. Möller and W. G. Rothchild, *Far-Infrared Spectroscopy*, Wiley-Interscience (1971).

period, fewer than 10 papers a year were published, and only since 1965 have the number of papers per year approached 100. Because of the lack of adequate experimental data, material properties and trends must be estimated through simple modeling. Important parameters such as the temperature dependence of the complex dielectric constant of liquid water are not certain at present.

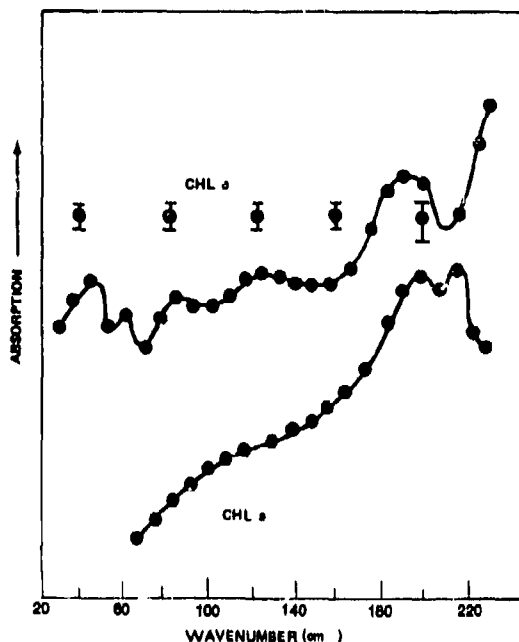


Figure VI-32. Far-infrared absorption spectra of chlorophyll (a) and (b) in cyclohexane solution at concentrations of 1 mg/ml. The solid lines are drawn on smooth curves through the data points. Typical errors are indicated.

A computation for soil materials that was similar to the one for healthy green leaves indicates that the specular reflectance for moist soils is not significantly wavelength dependent. Any change in  $\sigma_0$  for soils should be due only to  $G'$  variations due to changes in the degree of specularity, unless molecular absorption bands appear.

The very low values of the imaginary part of the index of refraction of ice and the nearly constant real part will lead to very little change due to frost cover. No surprises are expected for frost-covered surfaces.

One may expect an increase in emissivity for thermal radiation when metals are coated with water drops or water films at least 0.2 mm thick. Using Stratton's relation, one may calculate the absorptance of a water layer. The emissivity,  $\epsilon$ , for random polarization normal to the surface should be approximately equal to the absorptance,  $\alpha = 1 - \tau - \rho$ .

#### VI-5.2 Metals

According to Stratton,<sup>28</sup> the macroscopic electromagnetic theory is valid for metals for all wavelengths greater than 10  $\mu\text{m}$  (all frequencies less than 30 THz). For almost all angles of incidence, the specular reflectance,  $\rho$ , of a metal for radiant flux is given by the relation

$$\rho = 1 - 2\sqrt{2\omega K_m \epsilon_0 / \sigma} \quad (27)$$

where  $\omega = 2\pi\nu$ ,

$\nu$  = radiation frequency,

$K_m$  = relative magnetic permeability,

$\epsilon_0 = 8.854 \times 10^{-12}$  farad/meter, and

$\sigma$  = conductivity of the metal.

Evaluation of relation (27) for  $K_m = 1$  yields the relation

$$\rho = 1 - 2.11 \times 10^{-4} \sqrt{\nu/\sigma} \quad (28)$$

in MKS units.

<sup>28</sup> A. Stratton, *Electromagnetic Theory*, McGraw-Hill Book Company (1941).

A comparison of the calculated and observed values of  $1 - \rho$  for various metals measured by Hagen and Rubens is also presented by Stratton. However, using conductivity values in the Handbook of Chemistry and Physics, a better fit to observed values of Hagen and Rubens is obtained using the relation

$$\rho = 1 - 2.64 \times 10^{-8} \sqrt{K_m \nu / \sigma} \quad (29)$$

Table VI-4 shows the results of using relation (29) for predicting the normal spectral emissivity of metals ( $1 - \rho$ ), at 2.5 mm, 0.3 mm, and 25  $\mu\text{m}$ . The observed values of thermal emissivity<sup>22</sup> are compared to the predicted spectral values at 25  $\mu\text{m}$ . In general, the observed thermal emissivity values at room temperature ( $\sim 95$  percent of blackbody radiation is between 2.5 and 40  $\mu\text{m}$ ) tend to agree adequately with the predicted values at 25  $\mu\text{m}$ . The major source of variation in thermal emissivity measurements is the variation in the surface preparation. Emissivity values for iron and steel metals indicate that the magnetic permeability may be a significant factor, even at 25  $\mu\text{m}$ . Titanium also appears to deviate considerably from the calculated value for  $K_m = 1$ .

The common metals used in construction of military equipment are aluminum, iron, steel, and titanium. Except for aluminum, these are the metals for which the reflectance may be significantly frequency dependent.

Although polished metals should not reveal any new or surprising reflectance properties in the NMMW spectral range, practically no polished metal surfaces will appear in a battle area. Some other form of surface characteristics can be expected—rust and oxidation, paints and anodizations, along with rough surface finishes. The thermal emissivity variations due to such surface characterizations are quite large, indicating that surface reflectance in the 25- $\mu\text{m}$  spectral range is strongly influenced by surface properties. The thermal emissivity of

iron<sup>22</sup> varies from 21 percent for a polished surface to 63 percent for an oxidized surface, to 69 percent for a red rusted surface. These values should approximate the spectral emissivity at 25  $\mu\text{m}$  for iron. The addition of dust, mud, dew, frost, grease, and oil to such iron surfaces should alter the spectral emissivities also.

Figure VI-33 shows the influence of various surface finishes of aluminum on the infrared spectral reflectivity. At 25- $\mu\text{m}$ , the emissivity ( $1 - \rho$ ) may be anywhere from 10 to 80 percent, depending upon the anodization process. Figure VI-34 shows the influence of painted surfaces.

Clearly, there must be a transition between the emissivities at 25  $\mu\text{m}$  to the emissivities at 2.5 mm. The question is, "What is the nature of this transition and at what wavelength does a significant change occur?"

A vital issue in the detection of thermal emission from strategic targets such as large ships at sea is the value of thermal emissivity of painted steel in this spectral range. A computation can be made using classical electromagnetic theory<sup>23</sup> and Debye relaxation time<sup>24</sup> to obtain the probable normal spectral reflectance of a plane section of a sheet of painted steel. The emissivity for a direction normal to the plate should be

$$\epsilon(\text{normal}) = 1 - \rho(\text{specular}), \quad (30)$$

if scattering due to roughness of surface is not excessive. The results of the computation indicate that very important reflectance variations could occur at wavelengths of 1.0 mm and less.

The computation employs the expected real and imaginary dielectric constants for paint with the Debye relaxation time,  $t$ , as a parameter. The assumption is made that no

<sup>22</sup>J. A. Stratton, *Electromagnetic Theory*, McGraw-Hill Book Company (1941).

<sup>23</sup>Charles Kittel, *Introduction to Solid State Physics*, John Wiley and Sons (1956).

<sup>24</sup>W. Wolfe (ed.), *Handbook of Military Infrared Technology*, Office of Naval Research (1965), 797.

TABLE VI-4. NORMAL SPECTRAL EMISSIVITIES OF METALS AND OBSERVED THERMAL EMISSIVITIES AT ROOM TEMPERATURE

Metal	Resistivity $\mu\text{ohm-cm}$	Normal spectral emissivity (%)			Room temperature thermal emissivity (%)
		Wavelength			
		2.5 mm	0.3 mm	25 $\mu\text{m}$	
Aluminum	2.824	0.15	0.44	1.54	2 to 5
Antimony	41.7	0.59	1.70	5.91	3 to 6
Arsenic	33.3	0.53	1.52	5.28	—
Bismuth	120	1.00	2.89	10.02	—
Brass	7	0.24	0.70	2.42	—
Cadmium	7.6	0.25	0.73	2.52	2 to 3
Climax	87	0.85	2.46	8.53	—
Copper	1.771	0.12	0.35	1.22	1.5 to 3
Gold	2.44	0.14	0.41	1.43	1 to 2
Iron $K_m=1$	10	0.29	0.83	2.89	21 cast iron, polished
Iron $K_m=100$	10	2.9	8.3	29	21 cast iron, polished
Lead	22	0.43	1.24	4.29	5
Magnesium	4.6	0.20	0.57	1.96	—
Manganin	44	0.61	1.75	6.07	7.6
Mercury	95.783	0.90	2.58	8.95	—
Molybdenum	5.7	0.22	0.63	2.18	5
Monel metal	42	0.59	1.71	5.93	15 to 20
Nickel	7.8	0.26	0.74	2.55	2.2
Palladium	11	0.30	0.86	3.03	3
Phosphor bronze	7.8	0.26	0.74	2.55	—
Platinum	10	0.29	0.83	2.89	1.6 to 3
Silver	1.59	0.13	0.33	1.15	2.2
Steel, E.B.B. $K_m=1$	10.4	0.29	0.85	2.95	19 Stainless type 302
$K_m=100$		2.9	8.5	29.5	19 Stainless type 302
Steel, B.B. $K_m=1$	11.9	0.32	0.91	3.15	19 Stainless type 302
$K_m=100$		3.2	9.1	31.5	19 Stainless type 302
Steel, manganese $K_m=1$	70	0.77	2.21	7.65	—
Tantalum	15.5	0.36	1.04	3.60	5
Tin	11.5	0.31	0.90	3.10	1.2
Titanium	5.5	0.22	0.63	2.18	16 to 20
Tungsten, drawn	5.6	0.22	0.62	2.16	5
Zinc	5.8	0.22	0.64	2.20	5

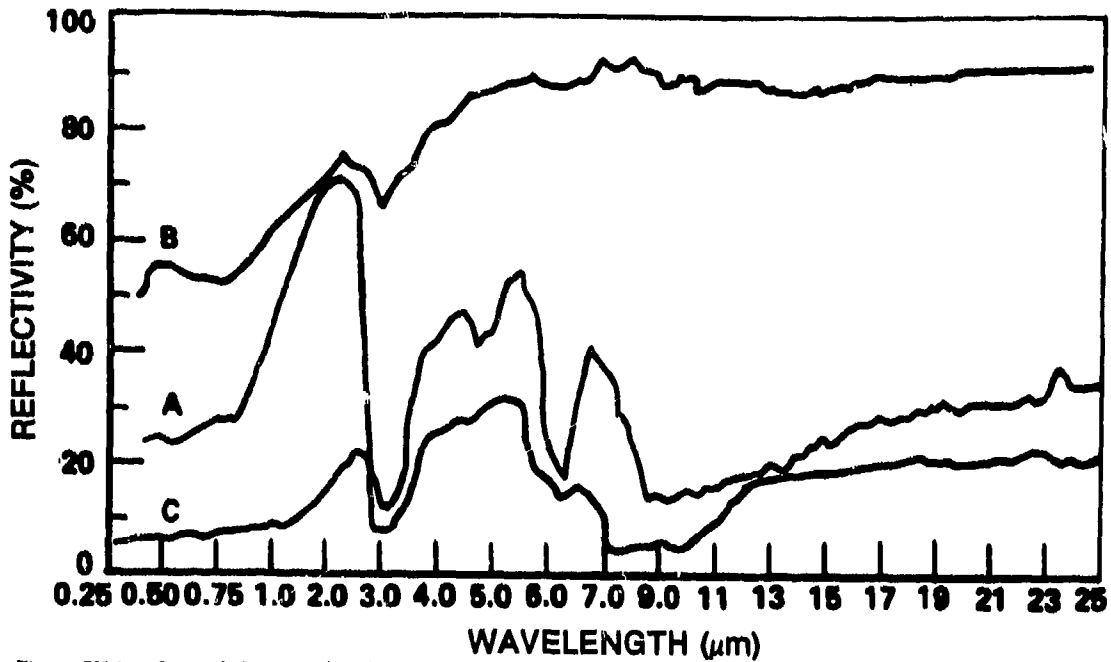


Figure VI-33. Compiled spectral reflectivities. A = chromic acid anodize on 24S-T61 aluminum. B = sulfuric acid anodize on 24 S-T61 extruded aluminum, chemically milled. C = hard anodize (1 mil) on 6061-T6 aluminum (35 A/ft<sup>2</sup>, 45 V, 20 F).

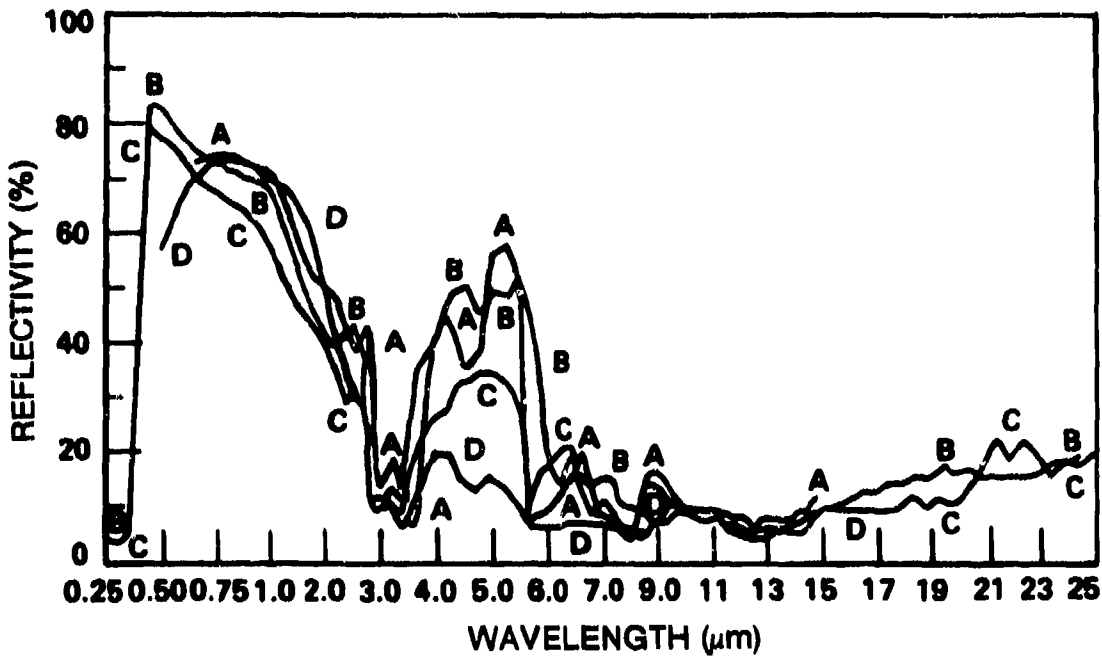


Figure VI-34. Compiled spectral reflectivities. A = flat white paint, Fuller No. 2882 on 2-mil polished aluminum. B = white epoxy resin paint of Mg. C = flat white acrylic resin, Sherwin-Williams M49WC8-CA-10144; MIL-C-15328-A Pretreatment wash coating on 22-mil 301 stainless steel 1/2 hard. D = white paint mixed with powdered glass, 7 mil on polished aluminum.

molecular absorption bands are encountered in this spectral range.

Using data from the Handbook of Chemistry and Physics for dielectric properties as a guide, one may assume that the probable relaxation time for paints may be anywhere in the range of  $10^{-10}$  to  $10^{-14}$  s. The relaxation times for good insulating materials such as Lucite, Teflon, etc.<sup>28</sup> are about  $10^{-14}$  to  $10^{-16}$  s, according to von Hippel's measurements at 25 GHz. At any given frequency, the relaxation time,  $t$ , may be determined from measurements of the complex dielectric constant, so that

$$t = \epsilon_2 / \omega(\epsilon_1 - 1), \quad (31)$$

where  $\epsilon_1$  = real part of the complex dielectric constant,

$\epsilon_2$  = imaginary part, and

$\omega = 2\pi\nu$ , the angular frequency of incident electromagnetic radiation.

The relations given by Stratton<sup>29</sup> (pp. 511-513) are used for computation of reflectance. The following parameters are used as input:

$d$  = paint thickness of 0.1 mm,

$\epsilon_2$  = relative paint dielectric constant at zero frequency, 3.35,

$\mu_2$  = relative paint magnetic permeability, 1.0,

$\epsilon_1$  = relative air dielectric constant, 1.0,

$\mu_1$  = relative air magnetic permeability, 1.0,

$\mu_3$  = relative magnetic permeability of steel, 100.0

$\sigma_3$  = conductivity of steel,  $10^7$  mho/m,

$t$  = Debye relaxation time of paint,  $10^{-10}$  to  $10^{-14}$  s, and

$\lambda$  = wavelength of radiation 0.1 to 10 mm.

The results are shown in figure VI-35. The range of reflectance values at 0.3 mm is from 13 to 92 percent. The temperature of large painted steel ships will vary about sea temperature with the time of day. As long as the emissivity of the ship is much less than the emissivity of the sea, the temperature variation will not influence contrast. For wavelengths of 1.0 mm and shorter, it is possible for the emission from painted ships to nearly match the radiation from the sea so that little contrast would be observed for detection purposes.

#### VI-5.3 Experimental Backscatter from Painted Surfaces and Wood

Laboratory measurements\* have been made of the reflectance of painted plane sections of aluminum at 0.89 mm. Only the monostatic case was measured ( $\theta_1 = \theta_s$ ,  $\phi_s = 180$  deg) as a function of  $\theta_1$ . The results (fig. VI-37 to -39) show the variation in  $Q_{rel} = \pi q'$  for these samples at various incident angles.

Figure VI-36 is for an aluminum substrate with a first paint coating of zinc chromate primer and a second coat of camouflage forest green (MIL-E-52798). Figure VI-37 is for an aluminum substrate with a first coat of epoxy primer and second coat of lusterless white enamel. Figures VI-38 and VI-39 are for all-weather plywood. The grain direction is that of the exposed surface.

The fact that nonzero reflectance values are observed for  $\theta_1 \neq 0$  indicates either

<sup>29</sup>J. A. Stratton, *Electromagnetic Theory*, McGraw-Hill Book Company (1941).

\*Private communication from B. D. Guenther, Redstone Arsenal (1977).

that nonspecular scattering occurs from these plane sections or that there are effects of beam divergence of the source. Paint thickness and surface roughness are not specified. The low value of normal reflectance ( $\theta_i = 0$ ) on painted metal could be due, at least in part, to losses in the paint layer from Debye relaxation of the dielectric; however, surface roughness could also be responsible for losses through nonspecular scattering. Measurements of  $\rho_{dh}$  by gonireflectometer instruments are needed to determine the loss mechanisms.

Blue and Perkowitz<sup>29</sup> have measured the reflectivity of several common

<sup>29</sup>M. D. Blue and S. Perkowitz, *Reflectivity of Common Materials in the Submillimeter Region*, IEEE Trans. on Microwave Theory and Tech., vol. MTT-25 (1977), 491-493.

materials at near normal incidence ( $\theta_i = 12$  deg) for wavelengths of 50 to 500  $\mu\text{m}$ . The results are shown in figure VI-40. Large differences are seen to occur in the 500- $\mu\text{m}$  range.

#### VI-5.4 Atmospheric Emission Model

One may expect nonscattering gases to emit NMM waves in accordance with thermodynamic laws. Let the spectral transmittance through a homogeneous gas be given by

$$\tau(\lambda, z) = e^{-a(\lambda)z}, \quad (32)$$

where  $a(\lambda)$  = spectral absorption coefficient and

$z$  = distance through the gas.

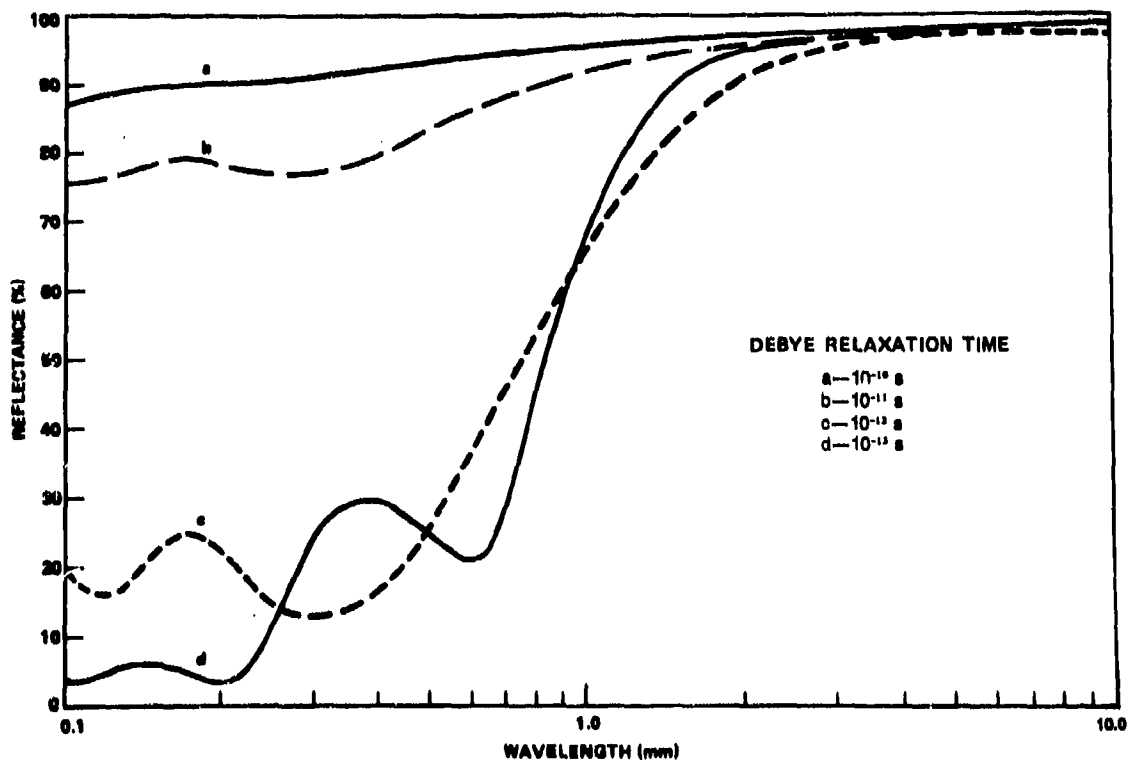


Figure VI-35. Spectral specular reflectance of painted steel calculated with Debye relaxation time as parameter. Paint thickness of 0.1 mm.

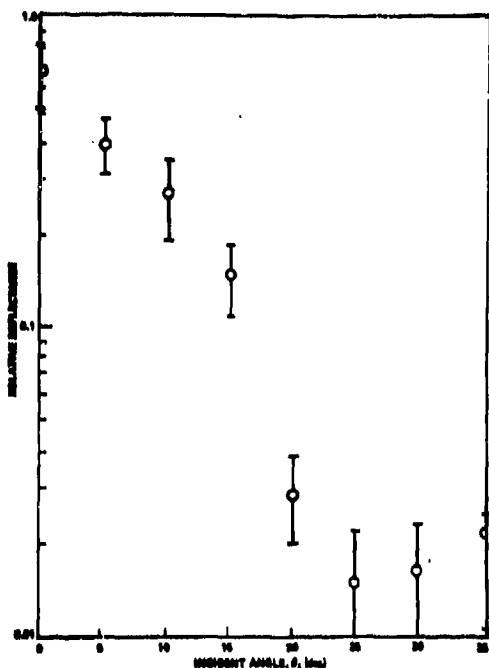


Figure VI-36. Relative reflectance versus incident angle,  $\lambda = 0.89$  mm.

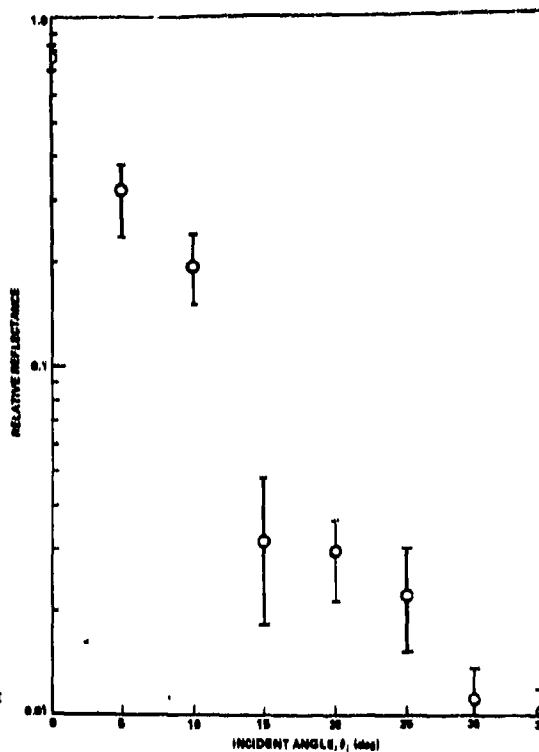


Figure VI-37. Relative reflectance versus incident angle,  $\lambda = 0.89$  mm.

The transmittance through a very thin layer of such gas is

$$\tau(\lambda, \Delta z) = 1 - a(\lambda)\Delta z . \quad (33)$$

Since no scattering occurs, the emissivity of the thin gas layer must be by Kirchoff's law,

$$\epsilon(\lambda, \Delta z) = 1 - \tau(\lambda, z) = a(\lambda)\Delta z . \quad (34)$$

The contribution to upward and downward flowing spectral flux density,  $\Delta E_{\nu}$  ( $W/m^2 \cdot Hz$ ), is given by Planck's radiation law,

$$\Delta E_{\nu}(z) = \epsilon(\lambda, \Delta z) M_{\nu}(\lambda, T(z)) , \quad (35)$$

where  $M_{\nu}(\lambda, T(z))$  = Planck's radiation formula for the temperature,  $T$ , at altitude  $z$ . The radiation from such a layer, which contributes to exoatmospheric upward spectral flux density,  $\Delta E_{\nu}(\text{exo})$ , is then

$$\Delta E_{\nu}(\text{exo}) = \Delta E_{\nu}(z) \cdot \tau(z, \infty) , \quad (36)$$

where  $\tau(z, \infty)$  is the transmittance from altitude,  $z$ , to an exoatmospheric altitude. The radiation from such a layer, which contributes to downward spectral flux density  $\Delta E_{\nu}(\text{sea})$  at sea level is

$$\Delta E_{\nu}(\text{sea}) = \Delta E_{\nu}(z) \cdot \tau(0, z) , \quad (37)$$

where  $\tau(0, z)$  is the transmittance from sea level to  $z$ .

The sum of the contributions of all such layers at all altitudes,  $z$ , yields the expected atmospheric emission observed either moving upward at an exoatmospheric altitude or downward at sea level.

Thus,

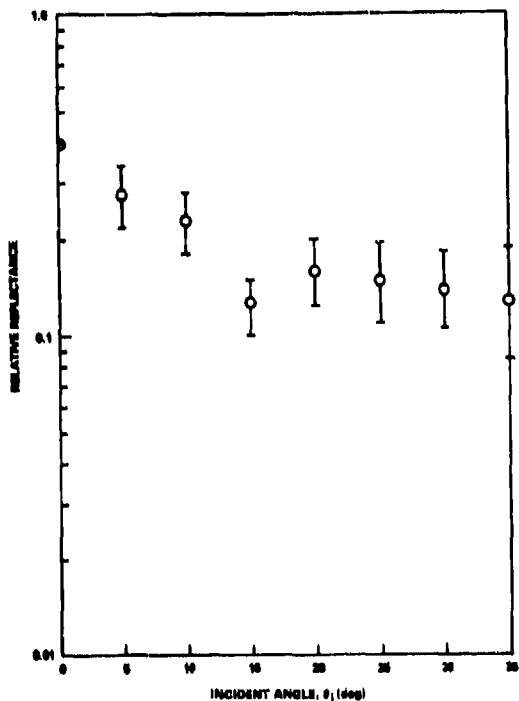


Figure VI-38. Relative reflectance versus incident angle,  $\lambda = 0.89$  mm—wood with grain perpendicular to rotation axis.

$$E_y(\text{exo}) = \int_0^{\infty} a(\lambda) dz M_y(\lambda, T(z)) \tau(z, \infty) \quad (38)$$

and

$$E_y(\text{sea}) = \int_0^{\infty} a(\lambda) dz M_y(\lambda, T(z)) \tau(0, z) \quad (39)$$

The total upward spectral flux density observed at an exoatmospheric altitude must include radiation from the earth's surface so that

$$\begin{aligned} E_y(\text{exo, total}) = & E_y(\text{exo}) \\ & + \tau(0, \infty) [a(\lambda, \text{terrain}) M_y(\lambda, T_{\text{terrain}}) \\ & + \rho(\lambda, \text{terrain}) E_y(\text{sea})] \quad (40) \end{aligned}$$

The data required to determine the spectral flux density include the temperature profile of the atmosphere which changes from time to time and

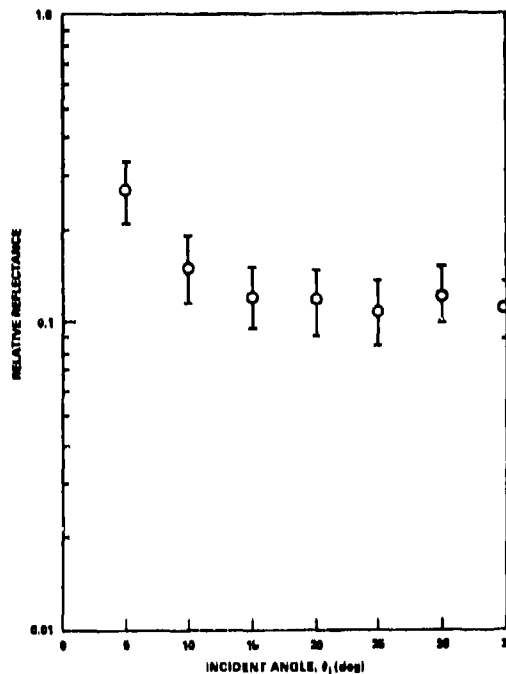


Figure VI-39. Relative reflectance versus incident angle,  $\lambda = 0.89$  mm—wood with grain parallel to rotation axis.

place to place, and a measurement of  $a(\lambda)$  as a function of altitude.

It is common practice for a first approximation to assume  $a(\lambda)$  to be independent of pressure and temperature and to assume uniform mixing of atmospheric constituents at all altitudes; however, spectral absorption lines do undergo pressure and doppler (temperature-dependent) broadening, and neither water vapor nor ozone are uniformly mixed. Furthermore, the assumption that only Planck's radiation formula applies ignores the possibility of nonthermal causes of radiation such as photochemical processes in the upper atmosphere and transient decay of metastable chemical species produced, for example, by high-temperature exhausts. The source of possible surprises in atmospheric emission lies in the possible existence of such "non-Planckian" sources.

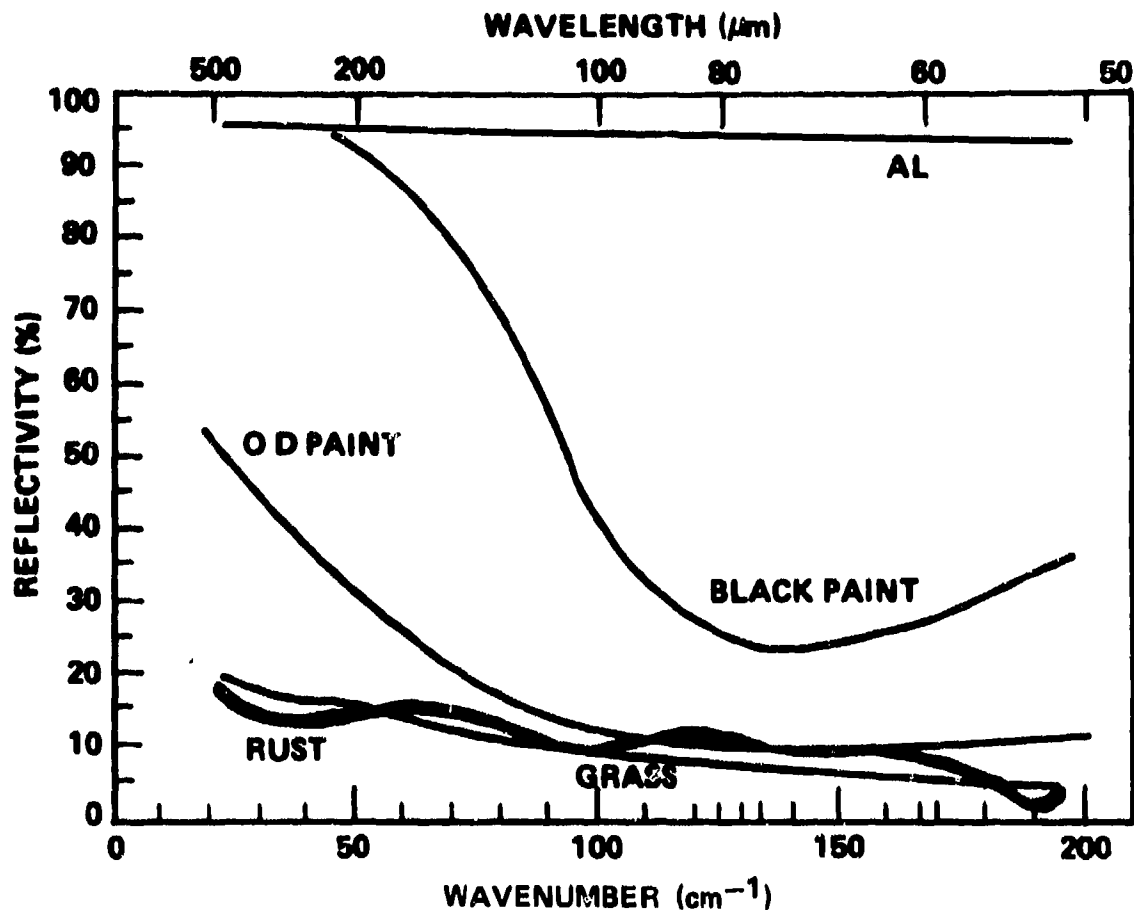


Figure VI-40. Normal reflectivity (in percent) for common materials. Included are normally oxidized aluminum surface (Al), aluminum sprayed with flat-black paint (black paint), olive drab paint on brass (OD paint), freshly cut blade of grass (grass) and rusty iron surface (rust).

## VI-6. SUMMARY

### VI-6.1 Discrete Targets

The only NMMW target cross-section data available are for the monostatic case for tactical targets at 94 GHz and for selected targets at 140 GHz. (These latter data, which are classified, have not been included in this volume.) Conclusions about other target cross sections at NMMW frequencies can be obtained at this time only by extrapolation from the 35- to 94-GHz region and by mathematical modeling.

The measured peak scattering areas at 94 GHz are not significantly larger than those found at X-band. Since the measurements show no appreciable increase with frequency, the roughness of the targets can be seen to be assuming a more important role as the frequency increases. This behavior is expected to continue into the NMMW region.

### VI-6.2 Background

Monostatic measurements of background cross sections have been made up to

94 GHz. A small amount of data has been reported by BRL at 140 GHz. A model developed for measurements taken at less than 10 GHz was extended to obtain agreement with data taken at 94 GHz. Because no other information is available, this model was extended to 350 GHz to give an estimate of  $\sigma_0$  as a function of depression angle.

The only data available for bistatic measurements are four independent measurements made at a wavelength of 3 cm. In the absence of data, one must assume that the bistatic data are wavelength independent in order to obtain order of magnitude estimates of  $\sigma_0$ . Making this assumption gives approximate values of  $\sigma_0$  of -5 to 5 dB for smooth surfaces near specular and -10 dB for rough surfaces near specular. In the NMMW range, one must expect most surfaces to appear rough. The extrapolation of  $\sigma_0$  values for terrain may be seriously in error if the Debye relaxation phenomenon and

molecular absorption appear in the NMMW range.

### *VI-6.3 Material Properties and Modeling*

Modeling techniques that have been applied with some success at lower frequencies are unconfirmed in the NMMW region. The attempts made in this report at modeling material properties suggest that significant variations in electromagnetic properties can occur in the near-millimeter range. Few experimental measurements on materials are available, thus preventing confirmation of the modeling predictions made in this report.

The emission of the standard atmosphere can be predicted with available models; however, the understanding of emission due to plumes and their interaction with the upper atmosphere will require considerable effort.

## CHAPTER VI.—LITERATURE CITED

1. J. R. Maxwell, Environmental Research Institute of Michigan, ERIM 123800-2-I (18 November 1976). (CONFIDENTIAL)
2. M. W. Long, Radar Reflectivity of Land and Sea, Lexington Books, Lexington, MA (1975).
3. S. L. Johnston, Submillimeter Wave Radar Technology (U), 22nd Annual Tri-Service Radar Symposium, Colorado Springs, CO (6-8 July 1976). (CONFIDENTIAL)
4. M. E. Beebe, J. Salzman, et al, 94 GHz Sensor Tower Test Program: Final Report, No. MSG 65075, Missile Systems Group, Hughes Aircraft Company (February 1976).
5. K. A. Richer, D. G. Bauerle, and J. E. Knox, 94 GHz Radar Cross Section of Vehicles (U), Ballistic Research Laboratories BRL-MR-2491 (June 1975), AD C002 505L. (CONFIDENTIAL)
6. B. D. Guenther, Submillimeter Wave Research: Index of 3.2 mm and 10.6  $\mu$ m Image Data Tapes, U.S. Army Missile Research and Development Command TR-77-2 (1 February 1977).
7. J. M. Bair, Millimeter and Infrared Image Scans of Reentry Vehicle Targets, Technical Report Calspan 23963, Hughes Research Laboratories (September 1976).
8. P. S. Ray, Applied Optics, vol. 11, no. 8 (August 1972), 1836-1844.
9. Manual of Remote Sensing, vol. I, American Society of Photogrammetry (1975).
10. H. E. King and C. J. Zamites, Terrain Backscatter Measurements at 40 to 90 GHz, Aerospace Corporation, SAMSO-TR-70-220 and TR-0066 (5816-41)-1 (June 1970).
11. L. D. Strom, Application for Millimeter Radars (U), Report No. 108, System Planning Corporation (December 1973), AD 529 566. (CONFIDENTIAL)
12. J. E. Kammerer and K. A. Richer, Cross Section Measurements of U.S. Army Targets by 140 GHz Radar (U), Ballistic Research Laboratories BRL-MR-1785 (August 1966), AD 378 097. (CONFIDENTIAL)
13. W. H. Peake and T. L. Oliver, The Response of Terrestrial Surfaces at Microwave Frequencies, Ohio State University AFAL-TR-70-301 and ESL-2440-7 (May 1971), AD 884 106.
14. L. Chanzit, L. Kosowsky, K. Koester, and I. Goldmacher, Study of Airborne Millimeter Radar Techniques, United Aircraft Corporation ECOM-02125-F (June 1970), AD 373 641.
15. L. J. Greenstein et al, A Comprehensive Ground Clutter Model for Airborne Radars, IIT Research Institute, Chicago, IL (September 1969), AD 861 913L.
16. F. Nathanson, Radar Design Principles, McGraw-Hill, New York (1969), 264.

CHAPTER VI.—LITERATURE CITED (Cont'd)

17. N. C. Currie et al, Radar Land Clutter Measurement at Frequencies of 9.5, 16, 35, and 94 GHz, Georgia Institute of Technology (April 1975).
18. M. E. Beebe et al, 94 GHz Sensor Tower Test Program, Hughes Report No. MSG 65075R (February 1976).
19. Manual of Remote Sensing, vol. II, American Society of Photogrammetry (1975).
20. R. L. Cosgriff et al, Terrain Scattering Properties for Sensor System Design, Engineering Experiment Station Bulletin, Ohio State University, Columbus, OH (May 1960).
21. K. A. Richer, 4.4 mm Wavelength Near Earth Propagation Measurements, Ballistic Research Laboratories BRL-MR-1403 (May 1962), AD 331 098.
22. B. J. Starkey, Bi-Static Ground Scatter Measurements in X-Band and the Ground Scatter Jammer Parameters (U), Directorate of Electronic Warfare S957-104-3 (DEW), Air Force Headquarters, Ottawa, Canada (September 1963). (SECRET)
23. S. T. Cost, Measurements of the Bistatic Echo Area of Terrain at X-Band, Ohio State University Report No. 1822-2 (May 1965).
24. J. A. Rupke and G. S. Rassweiler, Investigation of Ground Illumination at Radar Frequencies. (U), AFAL-TR-65-204 and 6148-17-F, The University of Michigan, Willow Run Laboratories (September 1965), AD 366 232. (SECRET)
25. R. W. Larson et al, Measurements of Bi-static Scattering Coefficients Using Air-Ground Coherent Instrumentation, Environmental Research Institute of Michigan Report 118200-14-F (April 1977).
26. R. A. McGee, Millimeter Wave Radiometric Detection of Targets Obscured by Foliage, Ballistic Research Laboratories BRL-MR-1901 (January 1968), AD 667 962.
27. J. R. Houck et al, The Far Infrared and Submillimeter Background, Cornell University (1 September 1972), AD 763 139.
28. J. A. Stratton, Electromagnetic Theory, McGraw-Hill Book Company (1941).
29. M. D. Blue and S. Perkowitz, Reflectivity of Common Materials in the Submillimeter Region, IEEE Trans. on Microwave Theory and Tech., vol. MTT-25 (1977), 491-493.
30. S. Perkowitz and B. L. Bean, Far Infrared Absorption of Chlorophyll in Solution, Journal of Chemical Physics, vol. 66 (1977), 2231-2232.
31. K. D. Möller and W. G. Rothchild, Far-Infrared Spectroscopy, Wiley-Interscience (1971).
32. W. Wolfe (ed.), Handbook of Military Infrared Technology, Office of Naval Research (1965), 797.
33. Charles Kittel, Introduction to Solid State Physics, John Wiley and Sons (1956).

**CHAPTER VII.--MEASUREMENT TECHNIQUES AND CAPABILITIES**

**by David C. Hogg and Dominick A. Giglio**

## CONTENTS

	Page
VII-1. INTRODUCTION.....	129
VII-2. INSTRUMENTATION.....	129
VII-2.1 Propagation Measurements.....	129
VII-2.2 Meteorological Measurements.....	131
VII-2.3 Radiometric and Radar Measurements.....	133
VII-3. RECOMMENDATIONS.....	134
VII-4. FACILITIES.....	135
VII-4.1 Laboratory Facilities.....	135
VII-4.2 Field Facilities.....	136
VII-4.3 Addendum—Facilities Listing.....	139
LITERATURE CITED.....	144

## VII-1. INTRODUCTION

This chapter briefly discusses some of the methods, technology, and current capabilities for obtaining data on propagation and target/background characteristics. Included are detailed descriptions of several laboratory and field facilities which have major experimental programs. In addition, the editors have provided a detailed listing of institutions involved in the experimental aspects of NMMW propagation and target/background characterization. Areas of investigation and points of contact are included.

## VII-2. INSTRUMENTATION

### VII-2.1 Propagation Measurements

The measurement of attenuation at NMM wavelengths, as influenced by gases and aerosols in the open atmosphere, is not a task to be approached with abandon; this applies to measurements on both terrestrial and earth-space paths. Accurate measurements are difficult to obtain because of

(1) Errors involved in the system used to observe the attenuation itself, since this is a variable quantity that depends on the amount of water vapor, fog, snow, rain, or clouds on the propagation path. It is knowledge of both the variability and the absolute value that is necessary for system design.

(2) Errors in measurement of the parameters of the gases and aerosols (e.g., density, etc.) that give rise to the attenuation.

On a terrestrial path, it is tempting simply to instrument a transmitter and receiver for observing attenuation. However, stability of the electronics and variability in the performance of the antennas under various weather conditions are factors that seriously limit the accuracy and, therefore, the credibility of the data. Further, measurement of the ab-

solute value (rather than just the variability) of the attenuation is even more challenging. Of course, within the laboratory, these factors are, to a great extent, under control.

An accurate technique of outdoor measurement is illustrated in figure VII-1(a), which shows two trihedral corner-cube reflectors,  $R_1$  and  $R_2$ , at ranges  $d_1$  and  $d_2$  from an antenna. The antenna is equipped with a simple small radar. Initially,  $R_1$  and  $R_2$  are located beside each other and their relative reflecting efficiencies are calibrated by alternately covering the reflectors, with a totally absorbing material. For well-constructed reflectors, this calibration can be obtained to an accuracy within 0.1 dB. The reflectors are then located as shown in figure VII-1, at a separation of about 1 km. Since the separation can be measured accurately, and the relative free-space attenuation to the two reflectors can be calculated, the absolute value of the attenuation on the path ( $d_2 - d_1$ ) between  $R_1$  and  $R_2$  is obtained by alternately interrogating the reflectors with the radar and measuring the ratio of the received powers.

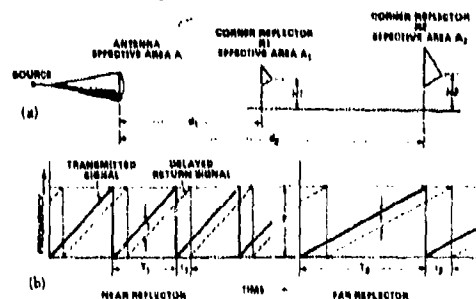


Figure VII-1. (a) Siting arrangement for atmospheric absorption measurements and (b) transmitted and reflected frequency-modulated signal. A. B. Crawford and D. C. Hogg, *Bell System Technical Journal*, vol. 35 (July 1956), 907-916.

The radar can be efficiently operated with a single cw low-power oscillator, using the sawtooth frequency-modulation technique illustrated in figure VII-1(b). Part of the transmitted signal is used as the local-oscillator pump at the converter; the delayed

signal reflected from  $R_1$  and  $R_2$  (shown dashed in the figure) results in an intermediate frequency,  $f$ , as shown. In changing from one reflector to the other, the amplitude of the frequency modulation is kept constant to ensure no change in transmitted power. Only the period of the sweep is changed in the ratio of  $d_1$  to  $d_2$ , which results in the same intermediate frequency for the two cases. This method has been used<sup>1</sup> successfully to measure absorption by oxygen over the 50- to 60-GHz band. An example of the measurement of atmospheric attenuation at 70 and 80 GHz (wavelengths of 4.3 and 3.8 mm) is shown in figure VII-2. About one year is needed to take such data (from the cool dry days of early winter through humid summer conditions). The dependence of attenuation on water-vapor content appears to have a strong quadratic component, as indicated by the curves in figure VII-2. The intercepts of the curves at zero water vapor are the attenuations by oxygen. Attenuation by

fog, rain, and snow can also be measured with this method.

Outdoor measurements using frequency-modulated lasers and trihedral corner reflectors are being extended to the far infrared at Redstone Arsenal (information from W. L. Gamble, MIRADCOM). Basically, this technique for measuring absorption involves modulating the wavelength of the incident radiation while slowly sweeping the average frequency over an absorption line. Synchronous detection is then used, with the modulation essentially differentiating the absorption line. With this technique, relative spectral attenuation can be measured with very high precision over short paths. This eliminates such effects as atmospherically induced scintillation, diffraction corrections, and detector nonlinearity, which limit the precision of propagation measurements. Even detector spectral sensitivity effects and source amplitude fluctuations correlated with the frequency modulation can be eliminated by using the same receiver (with a suitable switching arrangement) for monitoring both the transmitted and propagated beam. Unfortunately, continuously tunable, frequency modulatable sources are not available with reasonable amplitude stability over significant portions of the NMMW spectral region.

The abundance of single spectral lines obtainable from NMMW lasers does allow such measurement techniques. MIRADCOM has set up the following experimental apparatus for accomplishing the above. Two ordinary FIR lasers have been fabricated in the same Invar stabilized optical structure. Such a system as that shown in figure VII-3 (using different gases with NMMW laser lines differing by only a few percent in wavelength) will allow high-precision measurements over short paths with very small errors due to correction for diffraction effects. There are adequate known laser lines in the atmospheric windows to render this technique very useful.

Interferometric techniques have been employed for absorption measurements

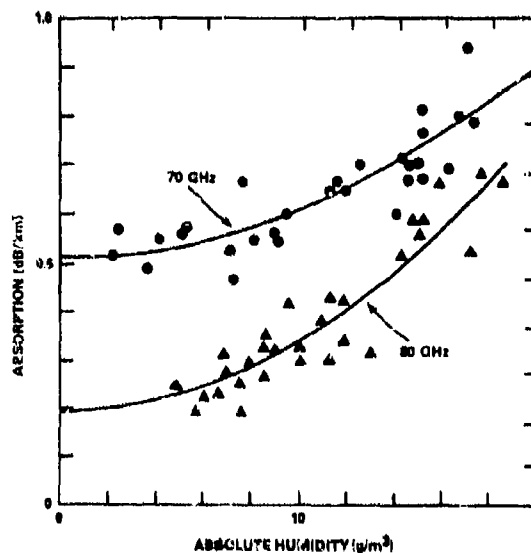


Figure VII-2. Measured dependence of terrestrial path (1.5 km) absorption on absolute humidity.

<sup>1</sup>A. B. Crawford and D. C. Hogg, *Measurement of Atmospheric Attenuation at Millimeter Wavelengths*, Bell System Technical Journal, vol. 35 (July 1956), 907-16.

both in the laboratory and in the field. Burch<sup>2</sup> describes H<sub>2</sub>O absorption measurements between approximately 12.6 and 36.0 cm<sup>-1</sup>. Samples of either pure H<sub>2</sub>O, H<sub>2</sub>O + N<sub>2</sub>, or air were contained in a multiple-pass absorption cell in which the optical path length varied from 121 to 469 m. Total pressure varied from approximately 2.3 torr to 1 atm, with values of H<sub>2</sub>O absorber thickness between 0.03 and 0.6 g/cm<sup>2</sup>. By employing the different samples, it was possible to investigate the self-broadening of the H<sub>2</sub>O lines as well as the broadening of N<sub>2</sub> and air.

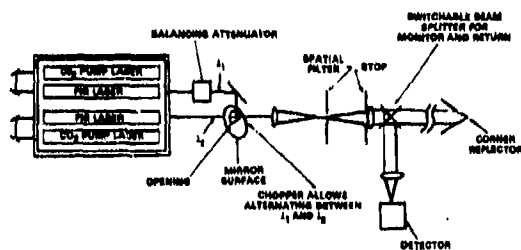


Figure VII-3. Absorption measuring system.

A high-pressure Hg-arc lamp with the glass envelope removed served as the radiation source. A chopper blade that consisted of a 12-mm thick crystal of NaCl chopped the energy beam at 13 Hz. The NaCl was nearly transparent for  $\nu > 600 \text{ cm}^{-1}$  and, therefore, only slightly modulated the energy at these high wavenumbers. Screens and polyethylene filters further reduced the sensitivity of the instrument to high wavenumbers energy so that it would not interfere with the measurement of the low-level energy of interest at low wavenumbers. A gallium-doped germanium bolometer cooled by liquid helium detected the chopped energy. The detector output was amplified and demodulated by a synchronous demodulator and displayed on a strip-chart recorder.

After passing through the sample cell, the energy beam was incident on a Michelson interferometer with a Mylar beam splitter. One of the interferometer mirrors was moved in steps by a precision screw. An interfer-

<sup>2</sup>D. E. Burch, *Absorption of Infrared Radiant Energy CO<sub>2</sub> and H<sub>2</sub>O. III. Absorption between 0.5 and 36 cm<sup>-1</sup> (278  $\mu\text{m}$  to 2 cm)*, *Journal of the Optical Society of America*, vol. 58, no. 10 (1968), 1362-1394.

ogram consisting of a plot of amplifier output versus mirror position was recorded for each sample and for the sample cell evacuated. A computer was used to calculate the Fourier transform of each interferogram to obtain a spectrum proportional to energy versus wavenumber. The transmittance of a sample at a given wavenumber was determined from the ratio of the energy observed at the wavenumber with the sample cell to that observed with the cell evacuated.

The spectrum of each sample was compared with calculated spectra based on theoretical positions, strengths, and widths of the H<sub>2</sub>O lines. The absorption observed in the windows was greater than that predicted by theory.

On earth-space paths, the best quantitative propagation measurements are made using beacons operating at the desired wavelength mounted in an earth-synchronous satellite. Attenuation measurements can also be made using the sun, but these result in questionable statistics of attenuation because of the ever-changing angle.<sup>3</sup> Passive radiometers can also be used to measure attenuation on fixed earth-space paths by virtue of the natural emission of any absorbing constituent on the path. To obtain truly quantitative results, such measurements are compared with independent measurements of temperature and water vapor taken by radiosonde<sup>4</sup> and, for clouds and rain, by radar.<sup>5</sup>

#### VII-2.2 Meteorological Measurements

Measurement of water vapor in the free atmosphere has long been a challenge to meteorologists and physicists. The main difficulty has not been to construct a device that is sensitive to water vapor. Rather it is a matter of producing a device that will measure over the com-

<sup>3</sup>D. C. Hogg and T. S. Chu, *The Role of Rain in Satellite Communications*, *IEEE Proceedings*, vol. 63, 9 (September 1975), 1308-1331.

<sup>4</sup>M. T. Decker, E. R. Westwater, and F. O. Guiraud, *Microwave Sensing of Atmospheric Temperature and Water*, *Navy Workshop on Remote Sensing of Marine Boundary Layer*, Vall, CO (9-11 August 1976).

<sup>5</sup>B. J. Mason, *The Physics of Clouds*, Clarendon Press, Oxford (1957).

plete range from 0- to 100-percent relative humidity, independent of temperature and other environmental effects, and maintain calibration over long periods. Economy is also a significant factor in applications such as radiosondes. For terrestrial monitoring of water-vapor content, the so-called dew-point hygrometer is perhaps the best compromise in the context of outdoor propagation measurements. It operates on the principle of equilibrium between a saturated gas and condensation on a cooled surface. These devices now incorporate thermoelectric cooling, optical sensing of condensation, and electronic feedback circuitry, resulting in high reliability, infrequent need for calibration, and good accuracy and sensitivity. For earth-space propagation, the comparisons are made with data obtained by radiosonde, the conventional humidity-measuring instrument being the hygistor; these are fairly accurate at medium to high relative humidities, but more research is needed to provide a device covering the entire range.

Measurement of fog involves monitoring of two major parameters: the drop-size distribution and the number of drops per volume. For direct measurement of particle sizes in clouds, various impact and photographic methods have been used, and the density of water is commonly measured by transmission.

The sizes of clouds and their relatively short lives demand the use of an airplane as a sampling platform. The following are some of the more acceptable methods of liquid-water-content measurement.

Impaction and Replication Instruments .—A suitable exposed surface records the impressions of shapes of the particles; data reduction is time-consuming. Problems arise with determination of the collection efficiency of the sampler and calibration of the impressions. Slide coatings can be from oil, magnesium oxide, and carbon film, to gelatin. Cloud samplers such as the modified (now two-stage) May impactor

described by Garland can be used to measure the liquid water content by summing the total number of droplets captured in a measured volume of air.

The above are not suitable for collecting larger droplets. Foil impactors are used to measure large droplets, such as raindrops, with radius greater than 100  $\mu\text{m}$ .

Replicating instruments use the Formvar technique to capture the droplets permanently. Details on samplers and replicators are given by Spyers-Duran.<sup>6</sup>

Knollenberg Optical Probes .—The liquid water content is calculated through the measurement of the number of particles over the specified size ranges of the instrument. The theory of operation of this device is given by Knollenberg.<sup>7</sup> The instrument should be calibrated with water drops of known size before accurate measurements of liquid water content can be determined from the particle-size counts.

Hot-Wire Liquid Water Content Instruments .—The most common device for measuring liquid water content, the Johnson-Williams hot-wire device described by Neel,<sup>8</sup> is accurate for cloud droplets less than about 20  $\mu\text{m}$  in radius, but it becomes saturated for a liquid water content greater than about 3  $\text{g}/\text{m}^3$  and has a lower limit of about 0.05  $\text{g}/\text{m}^3$ . A disadvantage of most hot-wire devices is the change in calibration because of cooling when they are operated in mixed-phase clouds. Cooling due to rapid fluctuations in air speed caused by turbulence will also cause errors in calibration.

<sup>6</sup>P. Spyers-Duran, *Measuring the Size, Concentration, and Structural Properties of Hydrometeors in Clouds with Impactor and Replicating Devices*, Atmospheric Technology, 8, NCAR (1976), 3-9.

<sup>7</sup>R. G. Knollenberg, *The Optical Array: An Alternative to Scattering or Extinction for Airborne Particle Size Determination*, Journal of Applied Meteorology, vol. 9 (1970), 86-103.

<sup>8</sup>C. B. Neel, *A Heated-Wire Liquid-Water Content Instrument and Results of Initial Flight Tests in Icing Conditions*, NASA Research Memorandum RM 454123 (1955).

Lyman-Alpha Liquid Water Content Evaporation Instrument.—Wexler and Ruskin<sup>9</sup> and Ruskin<sup>10</sup> discuss a liquid water content meter based on evaporation, which employs a vapor density sensor in which water vapor causes light absorption in the spectral line of atomic hydrogen at  $\lambda = 121.56$  nm. These devices provide a direct measure of water content in all three phases. However, operation with a dew point hygrometer is necessary in order to subtract the vapor density. Thus, the instrument will operate most accurately at a relatively low temperature (near 0 C) where the liquid water content probably exceeds that of the vapor. An instrument with a single sensor which time shares the response due to the liquid water and the vapor is currently being developed at the Naval Research Laboratory. The Lyman-Alpha evaporation instrument has been manufactured<sup>11</sup> for aircraft measurement of total liquid water content. The response time of the instrument as given by Ruskin is a few hundredths of a second, which is an obvious advantage for flight measurements through clouds.

Rain Characterization.—Good technique exists for measurement of point rain rate. Even the classical collecting rain gauge can be used to derive rain rate fairly accurately by simply taking the derivative of the recorded amount with respect to time. Tipping-bucket gauges are reliable, but become increasingly inaccurate at high rates. Flow gauges which measure electrical capacitance as a function of rain intensity have a rapid response time and can measure high rain rates, but frequent calibration is required. Knollenberg, photographic<sup>12</sup> and optical transmission<sup>13</sup> methods can be used to measure drop-size distribution of rain.

<sup>9</sup>A. Wexler and R. E. Ruskin, *Humidity and Moisture, vol. 1, Principles and Methods of Measuring Humidity in Gases*, Reinhold Publishing Corporation, New York (1965).

<sup>10</sup>R. E. Ruskin, *Liquid Water Content Devices, Atmospheric Technology*, 8 (1976), 38-42.

<sup>11</sup>E. A. Mueller and A. L. Sims, *The Influence of Sampling Volume on Raindrop-Size Spectra, Proceedings of the 12th Conference on Radar Meteorology* (October 1966), 135.

<sup>12</sup>Ting-i Wang and S. F. Clifford, *Use of Rainfall-Induced Optical Scintillations to Measure Path-Averaged Rain Parameters*, *Journal of the Optical Society of America*, vol. 65, 8 (August 1975), 927-37.

<sup>13</sup>NRL Lyman-Alpha instrument manufactured by General Eastern Corp., 50 Hunt St., Watertown, MA 02172.

### VII-2.3 Radiometric and Radar Measurements

As early as 1956,<sup>14</sup> an extensive set of measurements was reported at 8.5 mm on the emitting and reflecting properties of common surfaces such as grass, gravel, blacktop, shrub growth, and water, along with millimeter-wave photographs of large metal objects such as ships. The technique involved use of a traditional Dicke radiometer which measured brightness temperatures on an antenna scanned over a solid angle several degrees squared. These data contain the characteristics of radiometric backgrounds.

In measuring either radiometric or radar backgrounds, rather than scanning an antenna beam mechanically, it is tempting to investigate phased arrays which provide a change in the direction of the beam by the introduction of appropriate phase shifts in the transmission lines feeding the elements of the array. However, in the millimeter and NMMW bands, the high losses and low antenna efficiencies presently achieved make arrays unsuitable for radiometry. But significant advances have been made recently on beam scanning using dual-reflector antenna systems; in that case, motion of a relatively small feed may provide scanning over a significant solid angle for either radiometric or radar systems.

The direct field measurement method of determining the radar cross sections of discrete targets and backgrounds is often costly, and the results for one target or background may not be readily extended to others. A supplementary method involves development of a mathematical model of the interaction of NMM waves with the common material components which make up the target or background. The interaction of NMM waves with components is measured in the laboratory. The appropriate cross sections are then calculated by computer.

A limited set of field measurements is required to verify the model. Once the model

<sup>14</sup>D. H. Ring, *Bell Telephone Laboratories, Final Report AF-19-(122)-458 to Lincoln Laboratories (released 1962)*.

has been verified, the model may be applied to targets and backgrounds which fall within the extremes of the verification tests. An additional advantage is accrued in the use of the mathematical models in that they may be utilized to arrive at much more general statements concerning the cross sections of a class of targets and backgrounds.

### VII-3. RECOMMENDATIONS

Laboratory measurements of water vapor attenuation with emphasis on window regions of low attenuation are needed to determine basic physical properties:

(a) Pure  $H_2O$  at different pressures to determine self-broadening

(b)  $H_2O$  mixed with dry air at different pressures to determine broadening

(c) Both (a) and (b) over a wide range of temperatures typical of the atmosphere

(d) Careful measurements of samples of pure  $H_2O$  and of  $H_2O + N_2$  with  $H_2O$  partial pressure at and near saturation

Accurate field measurements on attenuation in the lower atmosphere are vital. These measurements are needed to provide comparison with the laboratory measurements. The priority assigned to each type of measurement will depend on its impact of potential applications. For example, if laboratory measurements at a wavelength of interest indicate significant anomalous absorption near saturation, field measurements designed to check this should be given high priority. Also, single-frequency measurements might be made with a particular source or detector that shows promise in a system. Such measurements would provide a check for absorption mechanisms that may have been overlooked. However, tests of this sort should be assigned low priority because of the large number of laser and other single-frequency

sources, unless the source is powerful enough and particularly adaptable to a specific application of interest.

Analytical and theoretical work based on the above measured results and previous measurements of attenuation by water vapor is needed to

- Develop an empirical model that accounts for effects of self-broadening, nitrogen broadening, and temperature variations so that different atmospheric conditions can be accounted for reliably.
- Develop a theoretical model based on the strengths, positions, widths, and shapes of the  $H_2O$  lines. Most attention should be given to the shapes because they are least understood. Contributions by any anomalous absorption factors should also be considered in this theoretical treatment.

Laboratory measurements on attenuation by minor constituents can be made, but these are of low priority in view of most of the applications of interest to the study panel.

Field measurements at NMM wavelengths of interest need to be made under adverse weather conditions, in particular, fog, snow, dust, and light rain. It is preferable that these measurements be made continuously so that statistics of attenuation can be obtained in climates of interest; appropriate instrumentation for measurement of meteorological parameters form part of these observations.

For earth-space applications, NMMW radiometric systems are required to determine atmospheric thermal background and attenuation. These measurements should be accompanied by radiosonde data for comparison and interpretation. With appropriate improvement in technology, a NMMW source could be launched to provide a synchronous satellite beacon.

Quantitative field measurements are needed on both radiometric and radar backgrounds during various weather conditions.

#### VII-4. FACILITIES

The following list of laboratory and field facilities represents a sampling of the more significant national facilities that are currently available for the study of the NMMW atmospheric, target, background, and radar technology.

##### VII-4.1 Laboratory Facilities

Various laboratory facilities exist for the investigation of NMMW absorption in gases. Some of the better equipped of these are discussed in the following paragraphs.

Ford Aerospace and Communications Corporation .—This facility has a well-equipped laboratory for the investigation of infrared and NMMW absorption by gases. Among the facilities is a multiple-pass absorption cell that can be used at path lengths up to more than 1 km. Samples of a pure absorbing gas (such as pure H<sub>2</sub>O) or of a mixture of gases can be contained in the cell at pressures from less than 10<sup>-3</sup> atm to more than 2 atm. The cell can be heated and controlled at any desired temperature up to 65 C. A variety of windows makes it possible to investigate the absorption from the visible to the NMMW region.

Ford also has a set of versatile computer programs to calculate the infrared and NMMW transmission of all permanent atmospheric gases. The listing of line parameters compiled by AFGL forms the basis for the calculations. Various parameters such as temperature, total pressure, partial pressure of H<sub>2</sub>O or other absorbing gases, and path length are accounted for. Effects of continuum absorption or attenuation by particulates can also be included. Transmission spectra can be calculated

and plotted as they would be observed, with infinite resolving power or with any desired spectral resolution.

Institute for Telecommunications Sciences .—Measurements using a microwave Fabry-Perot resonator have been made under closely controlled temperature (<0.10 C) and pressure conditions to investigate several gases, including water vapor and oxygen. The cell is presently operated at 22, 30, 60, 94, and 120 GHz. For example, both absorption and dispersion of pure water vapor have been measured at 30 and 60 GHz from 0 to 40 torr,<sup>14</sup> and empirical relationships have been developed for the pressure and temperature dependence, the former evidencing the strong anomalous quadratic behavior. However, measurements on air of various relative humidities have not yet been made, although the equipment is sensitive enough for such measurements. Measurements at 230 GHz, would require implementation of the cell with 1.3-mm waveguide circuitry.

The Environmental Research Institute of Michigan (ERIM) .—A microwave anechoic chamber the size of a small auditorium and operational up to K<sub>a</sub> band is available; it is suitable for total cross-section measurements of parts of vehicles. A gonioreflectometer—an automated system for measuring the bidirectional reflectance of small plane sections of materials—is also available. Both coherent and incoherent sources are bench mounted and directed toward the rotatable goniometer plate. The receiver is mounted on a rotating arm so that bistatic reflection may be measured and recorded on a punched tape. This system has been used at 10.6 μm and shorter wavelengths, but could be extended to wavelengths as long as 2 mm with suitable sources.

<sup>14</sup>H. J. Liebe, *Studies of Oxygen and Water Vapor Microwave Spectra under Simulated Atmospheric Conditions*, Office of Telecommunications Report OT 75-65 (June 1975); available from U.S. Government Printing Office, Washington, DC 20402.

Night Vision and Electro-Optics Laboratory, ERADCOM.—In conjunction with its own laser propagation programs, the laser technical area has developed a 3-m index-of-refraction cell for turbulence simulation. Such a cell might be used for laboratory simulation of turbulence effects for NMMW systems. A 4-D computer code has been used for supporting Army laser systems which are adversely affected by turbulence. This code could be readily available for the NMMW regime.

A 6-m, 152.4-mm diameter test cell used for laser propagation measurements is available and has been designed for circulating aerosols or smokes. Supporting instrumentation includes Royco and Whitley particle counters as well as a Thermo-System mono-disperse particle generator. Sources of NMMW radiation include an Apollo optically pumped cw or chopped NMMW laser and multi-pulsed optically pumped NMMW laser capable of both laboratory and field tests. Both sources can operate throughout the 100- $\mu$ m to 3-mm band by changing the pump gas. High-power optically pumped NMMW sources are currently under construction for both laboratory and field use.

Smoke Facilities.—Laboratory work with smoke has been conducted in a test chamber at Edgewood Arsenal (now the Chemical Systems Laboratory—CSL). The chamber is instrumented for smoke characterization and optical propagation studies. Measurements at millimeter wavelengths have been started in conjunction with the Georgia Institute of Technology.

Atmospheric Sciences Laboratory, ERADCOM.—Facilities at the Atmospheric Sciences Laboratory at White Sands, include:

- A 21-m White cell is used to obtain absorption coefficients for gaseous trace pollutants by obtaining transmittance values for two cell conditions—one with a nonabsorbing

medium and the other with the absorbing trace pollutant of interest. Absolute transmittance, the ratio of these two relative transmittance measurements, yields an absorption coefficient for the absorbing medium.

Temperature range—ambient to +100 C (useful working range)

Pressure range—0 torr to 2 atm absolute

Path length—84 m to 2.0 km

This cell may be suitable for NMMW use—provided the beam divergence on an 84-m path could be controlled.

- Also available is a 2-m White cell with the following characteristics.

Temperature range—20 to 100 C (useful working range)

Pressure range—from the torr range to 2 atm absolute

Path length—8 to 168 m

A NMMW beam divergence over 8 m should be no problem.

- Aerosol analyzers are available for classification and sizing of atmospheric aerosol concentrations.

#### VII-4.2 Field Facilities

Various facilities are available for making NMMW measurements in the field. Some of these are listed in the following paragraphs.

ERIM.—ERIM maintains facilities for making microwave images, measurements of discrete target cross section, back-

grounds, and material properties of plane sections for modeling purposes. A ground-based radar platform is available that is large enough to range military vehicles lighter than a tank. The radar is roof mounted so that one may measure either total cross section as a function of azimuth angle or, by operating in the synthetic aperture mode, high resolution images of the target.

An airborne multiband system has been completed. It operates in a mechanical scanning mode with passive visible and near infrared, thermal infrared, 1.06- and 10.6- $\mu\text{m}$  lasers, and 94-GHz millimeter wave, all bore-sighted. The beam width of the 94-GHz system is about 10 mrad. The system should be able to make quantitative field measurements over large areas.

Electrical Engineering Research Laboratory (EERL).—The EERL at the University of Texas has a nucleus of personnel with strong experience in the propagation of millimeter waves. This laboratory has sufficient expertise to perform accurate outdoor measurements on attenuation by water vapor at a NMM wavelength using, for example, the calibrated corner-reflector technique discussed in section VII-2.1.

Wave Propagation Laboratory, National Oceanic and Atmospheric Administration (NOAA).—WPL has an on-going program for ground-based, millimeter wave radiometric measurement of total water vapor content on a zenith path. Measurements are also made directly by radiosondes. This facility accommodates inversion of measured data to retrieve both temperature and water-vapor profiles of the atmosphere. Noise temperature and attenuation are measured and computed.

Night Vision and Electro-optics Laboratory, ERADCOM.—The 3.2-km Wayside Laser Range (about 10 min from Ft. Monmouth) is instrumented and used for various laser and radar tests. This facility can easily be made available for NMMW system testing for tur-

bulence, attenuation, or other propagation programs.

Supporting instrumentation includes Royco and Whitley particle counters. Particle sizing is available from 0.015 to 50  $\mu\text{m}$  with a dilution capability for heavy concentrations such as smokes. Turbulence measurements are available with both hot-wire anemometer or optical techniques. Present plans include testing and use of a field-portable 0- to 3-km transmissometer using a real-world aerosol concentration centrifuge and transmission cell developed in cooperation with the Naval Research Laboratory. A high scan rate Block Engineering Fourier transform spectrometer is available for obtaining broadband 2- to 14- $\mu\text{m}$  transmission.

Range facilities also include the 400 ft Oakhurst Tower, which is roughly 5 km from the laser range and is visible to each part of the range. In addition, the Wayside range has several single point targets at distances up to 8 km and up to 13 km utilizing the Oakhurst tower.

MIRADCOM.—MIRADCOM's capabilities in the near-millimeter spectral region include:

Propagation measurements at NMMW laser wavelengths are currently underway on a range which is, at present, nearly completely instrumented. Propagation measurements are being made serially at 744, 890, 1020, and 1200  $\mu\text{m}$ .

A cw heterodyne system is currently under construction which will use two FIR lasers, frequency locked approximately 1 MHz apart. One will be a master oscillator and the other a local oscillator. The system will also be able to operate in the pulsed mode. It will be basically an optical mixer using mirrors and beam-splitters. The pulsed system will be used for backscatter measurements; the cw system which is currently in operation will be used for

simultaneous attenuation measurements. Operation will be possible in the windows at 730, 880, and 1300  $\mu\text{m}$ .

MIRADCOM also has an airborne test facility which consists of a gyro-stabilized platform mounted on a helicopter. Extensive instrumentation is mounted in the helicopter. This facility is available for NMMW measurement programs.

In addition to the range devoted solely to NMMW propagation tests, MIRADCOM has the following ranges.

- A 5-km laser test range.
- A 12-km, clear view, point-to-point transmission test range.
- A 210-ft tower (F1 Facility) (formerly a Saturn test tower) which has approximately a 1-km path from the foot of the tower. Most of the 5-km laser test range is available from this tower for small depression angles. There is no practical weight limit on equipment that can be placed on this tower. Measurements at 3.2 mm are now underway on this tower to obtain target and background signatures.
- A tower 100 ft above the 5-km range (radar tower) is available for tests. It has a working area of 300  $\text{ft}^2$ .

Harry Diamond Laboratories ERADCOM.—Harry Diamond Laboratories is developing a capability for providing the data base required for design of NMMW systems. A mobile measurement facility (MMF) is being constructed for this purpose under a contract with the Engineering Experiment Station of the Georgia Institute of Technology. This system will allow simultaneous measurements at 94, 140, and 220 GHz of radar cross sections of targets and background clutter in both the

monostatic and bistatic modes. The antennas will be adjustable and have sufficiently narrow beamwidths for making measurements independent of multipath effects. It will also be possible to make measurements with this facility of attenuation a backscatter in clear air, fog, rain, smoke, and chaff. The 1-kHz PRFs, 100-ns pulsewidths, and positionable range gates of the system will allow investigations of temporal and spatial fluctuations of measured parameters for ranges of 0.5 km or more at 220 GHz and 1.0 km or more at 94 and 140 GHz.

The MMF will be housed in two large trailers that will receive electric power from a portable generating station. A second mobile station is being constructed by the Atmospheric Sciences Laboratory to provide complete meteorological characterization of the environmental conditions during the measurements. Data acquisition and processing systems in the NMMW and meteorological vans will allow real-time monitoring and field evaluation of experimental results. The system is scheduled to begin operation in the fall of 1980.

Follow-on plans for improvement of the MMF capability include addition of a Fourier transform spectrometer for broadband attenuation measurements in the 90- and 400-GHz frequency range, and conversion of the system for coherent operation.

Smoke Facilities.—The quality of smoke (and dust) test instrumentation and methodology has improved rapidly, over the last few years. A variety of Army facilities exist for open-air smoke tests that employ the appropriate munitions detonated either dynamically or statically. The Office of the Project Manager for Smoke/Obscurants periodically stages tests in which well-characterized smoke (or dust, or both) environments are produced, and many investigators are invited to gather propagation or system performance data in these environments. Such tests, termed "Smoke Weeks," have been held at White Sands Missile Range and Eglin AFB with future plans to be determined by

community-wide data requirements. Data resulting from these tests (Smoke Weeks I and II) as well as that from many others which the PM Office has supported, are available from that office. Future requirements for NMMW smoke and dust propagation data should be integrated into the many ongoing and planned activities. This integration can be accomplished through the PM Office, which is the Army's single focal point for such activities.

Georgia Institute of Technology (GIT) .--GIT Engineering Experiment Station has facilities for the performance of propagation measurements. A campus facility, meteorologically instrumented for short ranges of 600 and 1200 ft (~182 and 366 m) is capable of simultaneous measurements at wavelengths from 0.48  $\mu\text{m}$  to 3 cm. Sources available include lasers (argon, CO<sub>2</sub>, HCN, NMMW optically pumped), a 300-GHz carcinotron, and microwave sources at 230, 140, and 94 GHz and lower frequencies. A 5000-ft (1524-m) extension of this range exists. Rain backscatter measurements, radiometric measurements at 183 GHz, turbulence measurements, and adverse weather propagation are current areas of interest. Off-campus facilities include a range in northwest Atlanta, GA, and a facility at Boca Raton, FL (for sea-state studies and propagation over water). Instrumented vans provide the means for propagation and target/background measurements at sites of interest. For example, snow-return measurements have been made with apparatus mounted in one of these vans.

#### VII-4.3 Addendum—Facilities Listing

The organizations discussed above were known to the members of the Propagation Subpanel as being involved in experimental programs concerned with the propagation and target/background characteristics of NMMW radiation. While they certainly represent a good portion of the work being done in the field today, a number of other institutions are also involved. This has been demonstrated by the number of journal papers appearing in the last few years and in the talks given at such international symposia as, for example, the 2nd and 3rd International Submillimeter Wave Conferences and the 1977 NATO Millimeter/Submillimeter Conference.

As a service to the reader, the editors have provided the following listing (table VII-1) of institutions involved in the experimental aspects of NMMW propagation and target/background characterization. The organizations listed were drawn from the authorships of presentations and publications in the field over the past few years, as well as from the personal contacts made by the editors and the subpanel members. Names have been provided of individuals who might be used as points of contact for their respective institutions. Such a listing is destined to be incomplete and highly time dependent; however, it should provide several entry points for the reader who seeks contact with workers in some particular area. The editors offer their apologies for any errors or omissions, and hope that this listing of facilities and points of contact will prove useful.

**TABLE VII-1. EXPERIMENTAL FACILITIES—NMMW PROPAGATION AND  
TARGET/BACKGROUND CHARACTERIZATION**

Institution	Area of Investigation	Point of contact
<b>I. Department of the Army</b>		
Armaments R&D Command (ARRADCOM): Ballistic Research Laboratory (BRL) Aberdeen Proving Ground, MD	Propagation through aerosols (particularly smokes and obscurants) target/background signatures	Arthur LaGrange Richard McGee
Army Research Office Research Triangle Park, NC	Sponsor of basic research	Leo Alpert
Electronics R&D Command (ERADCOM): Atmospheric Sciences Labora- tory (ASL) White Sands Missile Range, NM	Propagation through clear and obscured atmospheres; measurement techniques; propagation data base; atmospheric modeling	Donald Snider Kenneth White
Combat Surveillance & Target Acquisition Laboratory (CSTAL) Ft. Monmouth, NJ	Stationary target classification	William Fishbein
Harry Diamond Laboratories (HDL) Adelphi, MD	Mobile Measurement Facility (MMF), operations and maintenance; material reflectivities; multipath measurements	Joseph Nemarich Gregory Cirincione
Night Vision & Electro-optics Laboratory (NVEOL) Fort Belvoir, VA	Propagation through aerosols; propagation through artillery barrages; turbulence studies; battle- field aerosol modeling	John Johnson
Missile R&D Command (MIRADCOM): Redstone Arsenal, AL Missile Research Director- ate (MRD)	Propagation through clear air and aerosols; target and background signatures; target material properties	Richard Hartman
Advanced Sensors Director- ate (ASD)	Target and background signatures and target classification	George Emmons
Tank-Automotive R&D Command (TARADCOM) Warren, MI	Vehicle signatures	G. J. McInnes
Project Manager for Smoke/ Obscurants Aberdeen Proving Ground, MD	Conducts Smoke Week field tests	Anthony Vanderwall

**TABLE VII-1. EXPERIMENTAL FACILITIES—NMMW PROPAGATION AND  
TARGET/BACKGROUND CHARACTERIZATION (Cont'd)**

<b>Institution</b>	<b>Area of investigation</b>	<b>Point of contact</b>
<b>II. Department of the Navy</b>		
Naval Research Laboratory (NRL) Washington, DC	Radiometry; high-altitude signatures	Ben Yaplee James P. Hollinger
Office of Naval Research) (ONR) Boston, MA	Atmospheric physics	J. Hughes
<b>III. Department of the Air Force</b>		
AF Geophysical Laboratory (AFGL) Hanscomb AFB, MA	Aircraft measurements	J. Garing
Rome Air Development Center Hanscomb AFB, MA and, Griffis AFB, NY	Vertical propagation; measurements; scattering over snow; atmospheric physics	E. E. Altschuler D. T. Hayes E. A. Lewis
Air Force Armament Laboratory Eglin AFB, FL	Target/background signatures	Davut Ebeoglu
<b>IV. Other Government Agencies</b>		
National Aeronautics and Space Administration Goddard Space Flight Center Greenbelt, MD	Propagation through clear atmosphere; snow backscatter; radiometry	Nelson McAvoy J. L. King
National Oceanic and Atmos- pheric Administration Wave Propagation Laboratory Boulder, CO	Propagation through atmosphere	David C. Hogg
<b>V. Private Industry</b>		
Block Engineering	Broadband propagation measurements	G. Wyntjes
Environmental Research and Technology, Inc.	Near-field effects	R. K. Crane
Environmental Research Insti- tute of Michigan (ERIM) Ann Arbor, MI	Target signatures; material properties; near-field tests	E. L. Johanson Gwynn H. Suits

TABLE VII-1. EXPERIMENTAL FACILITIES--NMMW PROPAGATION AND  
TARGET/BACKGROUND CHARACTERIZATION (Cont'd)

Institution	Area of investigation	Point of contact
Ford-Aeronutronic Division Newport Beach, CA	Laboratory propagation and backscatter measurements	D. E. Burch
Georgia Institute of Technology Engineering Experiment Station Atlanta, GA	Propagation measurements through clear atmosphere and aerosols; sea clutter; reflectivity of targets and backgrounds; reflectivity and emissivity of snow and ice	J. J. Gallagher N. C. Currie R. D. Hayes
Hughes Research Laboratories Malibu, CA	Target/background signatures; multispectral imaging	D. Lynch
Institute of Telecommunication Sciences Boulder, CO	Laboratory measurements of gases	H. J. Liebe
Jet Propulsion Laboratory (JPL) Pasadena, CA	High-altitude studies; atmospheric composition	J. W. Waters
Sperry Research Center	Target classification	—
University of California at Berkeley Berkeley, CA	Propagation	R. L. Plambeck
University of Florida	Reflectance of snow	R. C. Anderson
University of Texas Electrical Engineering Research Laboratory	Propagation measurements	A. Straiton

VI. Foreign sector

Canada

University of British Columbia Vancouver, BC	Rain measurements	M. M. Kharadly
University of Calgary	High-altitude measurements	D. J. W. Kendall
Federal Republic of Germany		
DFVLR Oberpfaffenhofen Wessling	Radar signatures	M. Vogel
FGAN Wachtberg-Werthoven	Transmission and backscatter	E. Barrs

**TABLE VII-1. EXPERIMENTAL FACILITIES—NMMW PROPAGATION AND  
TARGET/BACKGROUND CHARACTERIZATION (Cont'd)**

<b>Institution</b>	<b>Area of investigation</b>	<b>Point of contact</b>
German Military Geophysics Office	Propagation	K. E. Fisher
<b>Italy</b>		
Institute di Fisica	High-altitude measurements	E. Bassoletti
<b>Netherlands</b>		
TNO—Physical Laboratory of the National Defense The Hague	Propagation and scattering in rain	J. Sneider
<b>Switzerland</b>		
University of Berne	Atmospheric studies	K. F. Künzi
<b>United Kingdom</b>		
Admiralty Surface Weapons Establishment Portsmouth Hants	Propagation; sea reflectivity	R. J. Sherwell
Appleton Laboratories Slough, Ditton Park	Zenith measurements	C. Gibbons
Imperial College London	Propagation; anomalous effects	H. Alastair Gebbie
BMI Weston super mare	Target signatures and modeling	Sid Woolcock Les Cram
National Physical Laboratory Teddington	High-altitude studies	J. E. Harries
University of Bradford Bradfordshire	Near field effects	D. P. Haworth
University of Cambridge	Absolute atmospheric measurements	R. E. Hills
University College, London	Turbulence	R. S. Cole
<b>USSR</b>		
USSR Academy of Science	Millimeter/submillimeter propagation	A. V. Sokolov

## CHAPTER VII.— LITERATURE CITED

1. A. B. Crawford and D. C. Hogg, Measurement of Atmospheric Attenuation at Millimeter Wavelengths, *Bell System Technical Journal*, vol. 35 (July 1956), 907-16.
2. D. E. Burch, Absorption of Infrared Radiant Energy  $\text{CO}_2$  and  $\text{H}_2\text{O}$ . III. Absorption between 0.5 and  $36 \text{ cm}^{-1}$  ( $278 \mu\text{m} - 2 \text{ cm}$ ), *Journal of the Optical Society of America*, vol. 58, 10 (1968), 1383-1394.
3. D. C. Hogg and T. S. Chu, The Role of Rain in Satellite Communications, *IEEE Proceedings*, vol. 63, 9 (September 1975), 1308-1331.
4. M. T. Decker, E. R. Westwater, and F. O. Guiraud, Microwave Sensing of Atmospheric Temperature and Water, Navy Workshop on Remote Sensing of the Marine Boundary Layer, Vail, CO (9-11 August 1976).
5. B. J. Mason, *The Physics of Clouds*, Clarendon Press, Oxford (1957).
6. P. Spyers-Duran, Measuring the Size, Concentration, and Structural Properties of Hydrometeors in Clouds with Impactor and Replicating Devices, *Atmospheric Technology* 8, NCAR (1976), 3-9.
7. R. G. Knollenberg, The Optical Array: An Alternative to Scattering or Extinction for Airborne Particle Size Determination, *Journal of Applied Meteorology*, vol. 9 (1970), 86-103.
8. C. B. Neel, A Heated-Wire Liquid-Water Content Instrument and Results of Initial Flight Tests in Icing Conditions, NASA Research Memorandum RM 454123 (1955).
9. A. Wexler and R. E. Ruskin, *Humidity and Moisture*, vol. I, Principles and Methods of Measuring Humidity in Gases, Reinhold Publishing Corporation, New York (1965).
10. R. E. Ruskin, Liquid Water Content Devices, *Atmospheric Technology*, 8 (1976), 38-42.
11. E. A. Mueller and A. L. Sims, The Influence of Sampling Volume on Raindrop-Size Spectra, *Proceedings of the 12th Conference on Radar Meteorology* (October 1966), 135.
12. Ting-i Wang and S. F. Clifford, Use of Rainfall-Induced Optical Scintillations to Measure Path-Averaged Rain Parameters, *Journal of the Optical Society of America*, vol. 65, 8 (August 1975), 927-37.
13. D. H. Ring, Bell Telephone Laboratories, Final Report AF-19-(122)-458 to Lincoln Laboratories (released 1962).
14. H. J. Liebe, Studies of Oxygen and Water Vapor Microwave Spectra under Simulated Atmospheric Conditions, Office of Telecommunications Report OT 75-65 (June 1975); available from U.S. Government Printing Office, Washington, DC 20402.

**CHAPTER VIII.—CONCLUDING REMARKS**

**by Stanley M. Kulpa, Edward A. Brown, and Dominick A. Giglio**

*"Those who can't remember the past are condemned to repeat it."*

George Santayana's prophetic words bear, in many ways, directly upon the current interest in near-millimeter wave technology. Perhaps nowhere does this become more apparent than when one investigates the World War II activities of Division 14 (Radar) of the National Defense Research Committee.<sup>1</sup> H. E. Guerlac, in his comprehensive history<sup>2</sup> of Division 14, provides background on the activities leading to the development of K-band (~1 cm) technology. One of the most significant decisions in this effort was made at a meeting held at Columbia University on 7 August 1942.

The purpose of this meeting was to coordinate the K-band work of various American groups and to prepare for eventual cooperation with the British. The principal problem before the conferees<sup>3</sup> was to suggest a standard wavelength so that a coordinated attack could be made to open up the new band. In brief, the result of this meeting was the adoption of 1.25 cm (24 GHz) as the wavelength at which K-band work would proceed. The British had preferred 1.6 cm (18.8 GHz) mainly because it was the second harmonic of an established X-band frequency. However, they bowed to the choice of the 1.25-cm wavelength as a "compromise" between 1.6 cm and the other most-considered wavelength of 1 cm.

<sup>1</sup>Summary Technical Report of Division 14-- National Defense Research Committee, Volume 1--Radar, Washington, DC (1946).

<sup>2</sup>H. E. Guerlac, *Radar in World War II*, available from Library of Congress Photoduplication Service, PB 93618 through PB 93621 (May 1947).

<sup>3</sup>Present at the meeting were J. Kellog and A. Nordwick of Columbia, E. M. Purcell, N. F. Ramsey, H. V. Neher, C. G. Montgomery, and D. Montgomery of MIT, E. L. Ginxton of Sperry Gyroscope, G. C. Southworth, S. Robertson, and T. M. Odarenko of Bell Laboratories.

As discussed in Chapter I, a wavelength of 1.25 cm unfortunately corresponds closely to the 22-GHz water absorption line, thus leading to limited range capabilities for radar applications. The stage was thus set for the long controversy as to the utility of millimeter waves. Had the alternative 1.6 cm wavelength proposed by the British been chosen, round-trip atmospheric transmission over a typical target range of 20 miles would have been nearly 400 percent greater and the history of millimeter wave technology might have been quite different.

The editors have had the opportunity to discuss the Columbia meeting and its implications for K-band research effort with Professors E. M. Purcell and J. H. Van Vleck of Harvard University. Professor Purcell, then head of the Fundamental Development Group (Group 41) at the Massachusetts Institute of Technology (MIT) recalled the meeting:

The committee (in choosing 1.25 cm) was oblivious to the theoretical predictions of water vapor absorption. We should have been aware had we done our homework, but we were not."

Professor Purcell then went on to describe his group's efforts with a breadboard, 1.25-cm radar atop MIT's Bldg. 6, beginning in the fall of 1942:

"We were somewhat mystified since, as work proceeded for the next several months, the performance of various components of the radar was improved, yet the operating range steadily decreased. What in fact we eventually found was that we were observing the onset of spring in New England and its associated increase in absolute humidity."

In the spring of 1942, Professor Van Vleck, then a consulting member of the Radiation Laboratory Theory Group, had done preliminary calculations on the intensity and position of the water absorption line near 1 cm. Results of some of his work were published in a 1943 classified report calling attention to the fact that the absorption peak occurred near 1.5 cm. Communications, however, with the K-band experimental group, especially in the early stages of Van Vleck's work, were not timely and, as Professor Van Vleck said,

"Had I been more persuasive, the physicists and engineers at MIT might have been more careful about their choice of wavelength—one might have been selected that didn't have the water trouble."

Little really need be said as to the relevance of this past history to the current thrust in near-millimeter wave technology. The reader, having digested the contents of each of the previous chapters, should clearly see that our current knowledge of NMMW propagation and target/background effects could easily lead to the fulfillment of Santayana's prophecy.

Proper attention to NMMW atmospheric and target/background effects obviously requires a careful balance between aggressive attempts at systems development and a many-faceted, long-range, basic research effort to characterize effects first. One purpose of this volume is to assist the research community in obtaining this sort of balance and devising a well-directed, productive program of research and development. In this regard, two factors might profitably be kept in mind.

First, a number of technologies have produced elegant and proven systems with relatively modest prior knowledge of atmospheric and target effects. An outstanding example is the very successful forward-looking infrared system (FLIR), operating in the 8- to 14- $\mu\text{m}$  band. Though research is still continuing on many

aspects of propagation in that region, it is unlikely that these detailed results together with more complex modeling efforts will significantly affect the utility of FLIR. In a similar fashion, the NMMW atmospheric and target/background community should be careful to focus on those areas which are most likely to directly impact the application of the technology. As a result of this study, several of these areas have been identified and are presented in summary form later in this chapter.

Second, from the study it is abundantly clear that the current understanding of basic atmospheric and target/background phenomena is quite limited. At a recent MIRADCOM workshop on these effects, some of the observed phenomena were even classified as "spooky." Another worker at ARRADCOM has expressed his frustration at attempted 200-GHz measurements saying, "Every time we turned the equipment on, we saw something different." The point here is that the real data base is extremely limited and first-order engineering-type estimates using a simple extension from microwave observations do not appear to be sufficient. In addition, the various atmospheric and target/background effects are so strongly dependent upon meteorological variables, that unless one specifies quite clearly the environment within which operation is required, the arguments pro and con as to the utility of NMMW technology become moot. The general solution for attenuation, backscatter, target return, etc. represents an extremely complex problem which can only be reduced to certain tractable common elements of physics after deciding on the desired range of operational weather environment.

The relative importance of system development as opposed to further research to expand the current data base can be illustrated by a simple example. Consider the propagation data base requirements for the design of a high-resolution, 220 GHz, ground-to-ground tracking radar. Typically, the specifications guideline might be

that the system operate to ranges of 2.5 km in a 100-m visibility fog or a 4-mm/hr rain. Obviously, an immediate requirement exists for reliable estimates of one-way transmission losses through these environments.

As the study of this volume will reveal, proper response to this requirement depends on a number of important factors:

(a) At what geographic location is operation required? Geographic as well as seasonal variations in humidity and temperature can drastically (by 10 to 15 dB/km) affect clear air attenuation.

(b) What type of fog is to be encountered? Though visibility is an appealing characterization from perhaps the radar operator's point of view, it is insufficient for design purposes. The only reliable characterization in the NMMW region is liquid water content. Fog with a visibility of 100 m can, depending on its type, contain varying amounts of liquid water leading to attenuation factors (dB/km) differing by a factor of four.

(c) What is the temperature during the fog or rain? The effects of lower temperature with near-saturation conditions have not been well-characterized and there is evidence to indicate that such conditions may yield higher attenuations than expected. In addition, only very limited data exist for the temperature dependence of liquid water dielectric constants necessary in the calculations of fog absorption.

(d) What types of rain and wind conditions are to be encountered? Depending on conditions (drop size, wind, spatial distribution, etc.) the attenuation for a given rain rate can fluctuate several dB/km.

To provide a perspective on the danger of simplified predictions which do not account for these various factors, it is illustrative to attempt an estimate of the attenuation values based on currently available data. Assume for the moment

that the 220-GHz radar design problem has been narrowed by specifying an environment whose temperature is 273 K, thus yielding, at saturation, a water vapor content of  $4.85 \text{ g/m}^3$  (fig. II-1, Ch II). In addition, for a 100-m visibility fog the water density,  $\rho_L$ , can range approximately from 0.1 to  $0.4 \text{ g/m}^3$  (fig. III-6, Ch III) depending on the type of fog. As indicated in Chapter I, water vapor attenuation appears to be related to the presence of liquid water in or near the transmission path. However, for lack of a more quantitative relation to describe these effects, we assume that the effects of vapor and liquid in fog or rain are simply additive.

Table VIII-I lists the best estimates obtainable for the clear air water vapor attenuation from the discussion in Chapters I and II. The limited calculations, chamber experiments, and field tests<sup>2-4</sup> yield attenuation values (dB/km) varying by nearly a factor of seven.

In Chapter III, fog attenuation was calculated based upon Rozenberg's<sup>4</sup> dielectric constant data at 273 K. For a liquid water content varying between 0.1 and  $0.4 \text{ g/m}^3$ , the predicted fog attenuation varies between approximately 0.8 and 3.5 dB/km. As indicated in Chapter III, there is some question as to the reliability of Rozenberg's data. The temperature-dependent measurements recently published by Afsar<sup>7</sup> yield, when extrapolated to 220 GHz and 273 K, a slightly different range of values, 0.4 to 4.7 dB/km. However, the principal factor responsible for the uncertainty is still the variation of liquid water content of the 100-m visibility fog.

<sup>2</sup>J. W. Waters, *Absorption and Emission by Atmospheric Gases, Methods of Experimental Physics*, Vol. 12, Part B, Chapter 2.3, Academic Press (1976).

<sup>3</sup>D. T. Llewellyn-Jones et al, *Absorption by Water Vapour at  $7.1 \text{ cm}^{-1}$  and its Temperature Dependence*, *Nature*, Vol. 274 (August 1978), 876-878.

<sup>4</sup>R. J. Emery et al, *Measurements of Anomalous Absorption in the Wave Number Range  $4 \text{ cm}^{-1} - 15 \text{ cm}^{-1}$* , *Journal of Atmospheric and Terrestrial Physics*, Vol. 37 (1975), 587-594.

<sup>5</sup>V. I. Rozenberg, *Scattering and Attenuation of Electromagnetic Radiation by Atmospheric Particles*, Hydrometeorological Press, Leningrad, USSR (1972).

<sup>7</sup>M. N. Afsar and J. B. Hasted, *Submillimeter Wave Measurements of Optical Constants of Water at Various Temperatures*, *Infrared Physics*, Vol. 18 (1978), 835-841.

TABLE VIII-1. CLEAR AIR ATTENUATION

Data source	$\nu$ (GHz)	$q_{H_2O}$ (g/m <sup>3</sup> )	$\alpha$ (dB/km)
1. Model—Gross line shape (T = 300 K) calculation plus Gaut and Reiferstein correction term (273 K); linear scaling with $q_{H_2O}$ . (Chapter I)	220	4.85	1.9
2. Model—Van Vleck/Weiskopf line shape plus empirical correction (T = 288 K); linear scaling with $q_{H_2O}$ only. (Chapter II)	220	4.85	1.6
3. Chamber measurements (T = 270 K). (Chapter I)	213	~4.0 4.85	9.2 11.2 <sup>a</sup>
4. Field measurements (T = 275 K) scaled from 216-m path to 1 km. (Chapter I)	210	~4.0 4.85	7.2 8.7 <sup>a</sup>

<sup>a</sup>Values for  $q_{H_2O} = 4.85$  g/m<sup>3</sup> obtained by linear scaling.

As regards the effects of rain, the data in Chapters I and III clearly show that for a given rain rate, attenuation can differ significantly, depending on various factors (drop size distribution, wind, etc.). Comparing available measurements and calculations,<sup>9-11</sup> the best estimate for 220-GHz attenuation by a 4-mm/hr rain vary between approximately 1 and 7 dB/km.

Table VIII-2 summarizes the resultant variations of total one-way attenuation during the fog and rain conditions specified for operation of the radar. Considering the fact that for radars, typical total system error budgets are at worst approximately  $\pm 10$  dB, uncertainties of 10 to 15 dB/km in the one-way transmission loss are clearly unacceptable. The wide variations demonstrate the relatively immature status of knowledge of propagation phenomena in the

NMMW region and the importance of precise specification of the various meteorological variables. This example is but one of many which could be tabulated from this volume to demonstrate the relatively meager technology base for NMMW propagation and target/background effects.

TABLE VIII-2. BEST ESTIMATE OF 220-GHz ATTENUATION BY A 100-m VISIBILITY FOG AND A 4-mm/hr RAIN (T = 0 C)

Condition	One-way attenuation (dB/km)	1-km transmission (%)
Clear air	1.6 to 11.2	—
100-m fog	0.4 to 4.7	—
Total	2.0 to 15.9	63 to 3
Clear air	1.6 to 11.2	—
4-mm/hr rain	1 to 7	—
Total	2.6 to 18.2	55 to 2

<sup>9</sup>J. Sander, Rain Attenuation of Millimeter Waves at  $\lambda = 5.77, 3.3,$  and 2 mm, IEEE Transactions on Antennas and Propagation, Vol. AP-23, No. 2 (March 1975), 213-220.

<sup>10</sup>V. W. Richard, J. E. Kummerer, and R. G. Raltz, 140 GHz Attenuation and Optical Visibility Measurements of Fog, Rain, and Snow, U.S. Army Ballistic Research Laboratory Memorandum Report ARBRL-MR-2800 (December 1977).

<sup>11</sup>D. T. Llewellyn-Jones and A. M. Zavody, Rainfall Attenuation at 110 and 890 GHz, Electronics Letters, Vol. 7, No. 12 (1971), 321-322.

<sup>12</sup>W. P. M. N. Keiser, J. Shields, and C. D. de Haan, Rain Attenuation Measurements at 94 GHz: Comparison of Theory and Experiment, NATO AGARD Conference Proceedings No. 245 (February 1979).

Anticipation of this state of affairs was, of course, one of the principal factors which motivated the entire Near-Millimeter Wave Technology Base Study. The various panel meetings, visits, discussions, and literature studies have allowed for the identification of key

factors for providing program guidance in the further study of NMMW propagation and target/background effects. These factors may be summarized in two basic categories. Table VIII-3 lists those areas of a general nature which have been highlighted as a result of the study. These general areas are accompanied in table VIII-4 by important, specific issues (not in order of priority) which must be addressed in future efforts to develop a more mature technology base. The reader may find appropriate expansion of these various thrusts and issues in the preceding chapters and the numerous references provided throughout the volume.

**TABLE VIII-3. GENERAL AREAS OF EMPHASIS FOR DEVELOPMENT OF THE NMMW PROPAGATION AND TARGET/BACKGROUND TECHNOLOGY BASE**

- 
- \* 94, 140, 230, 345 GHz
  - \* Field studies under statistically significant meteorological conditions
  - \* Adequate meteorological support
  - \* Apparatus portability for site variability
  - \* Broadband Fourier Transform measurements simultaneously with single frequency measurements.
  - \* System-specific measurements
- 

**TABLE VIII-4. RECOMMENDED RESEARCH THRUSTS**

- 
- \* Origin of anomalous absorption—line shapes, impact assumptions, polymolecular complexes
  - \* Temperature and pressure dependence of empirical correction term
  - \* Comparison with infrared effects

**TABLE VIII-4. RECOMMENDED RESEARCH THRUSTS (Cont'd)**

- 
- \* Structured absorption in windows
  - \* Quadratic density dependencies
  - \* Low temperature and high humidity effects
  - \* Fog/cloud attenuation and backscatter—liquid and ice
  - \* Rain attenuation and backscatter
  - \* Separation of water vapor and liquid effects
  - \* Temperature/frequency dependence of liquid water dielectric constants—varying salinity
  - \* Near ground turbulence—intensity and angle of arrival fluctuations, power spectra
  - \* Temperature and humidity structure constants
  - \* Sky temperature comparisons
  - \* High-altitude nadir radiometric studies of clutter backgrounds and target returns
  - \* Material reflectivities—varied surface conditions and coatings
  - \* Snow attenuation and backscatter
  - \* Snow and moisture cover effects on target/background returns
  - \* Target scintillation due to changing aspect angle
  - \* Plume emissions, backscatter, and attenuation
  - \* Coherent signature phenomena
  - \* Meteorological statistics
  - \* Near field effects
  - \* Screening techniques—smoke, dust, etc.
-

## CHAPTER VIII.—LITERATURE CITED

1. Summary Technical Report of Division 14—National Defense Research Committee, Volume 1—Radar, Washington, DC (1946).
2. H. E. Guerlac, Radar in World War II, available from Library of Congress Photoduplication Service, PB 93618 through PB 93621 (May 1947).
3. J. W. Waters, Absorption and Emission by Atmospheric Gases, Methods of Experimental Physics, Vol. 12, Part B, Chapter 2.3, Academic Press (1976).
4. D. T. Llewellyn-Jones et al, Absorption by Water Vapour at  $7.1 \text{ cm}^{-1}$  and its Temperature Dependence, Nature, Vol. 274 (August 1978), 876-878.
5. R. J. Emery et al, Measurements of Anomalous Absorption in the Wave Number Range  $4 \text{ cm}^{-1} - 15 \text{ cm}^{-1}$ , Journal of Atmospheric and Terrestrial Physics, Vol. 37 (1975), 587-594.
6. V. I. Rozenberg, Scattering and Attenuation of Electromagnetic Radiation by Atmospheric Particles, Hydrometeorological Press, Leningrad, USSR (1972).
7. M. N. Afsar and J. B. Hasted, Submillimeter Wave Measurements of Optical Constants of Water at Various Temperatures, Infrared Physics, Vol. 18 (1978), 835-841.
8. J. Sander, Rain Attenuation of Millimeter Waves at  $\lambda = 5.77, 3.3,$  and  $2 \text{ mm}$ , IEEE Transactions on Antennas and Propagation, Vol. AP-23, No. 2 (March 1975), 213-220.
9. V. W. Richard, J. E. Kammerer, and R. G. Reitz, 140 GHz Attenuation and Optical Visibility Measurements of Fog, Rain, and Snow, U.S. Army Ballistic Research Laboratories Memorandum Report ARBRL-MR-2800 (December 1977).
10. D. T. Llewellyn-Jones and A. M. Zavody, Rainfall Attenuation at 110 and 890 GHz, Electronics Letters, Vol. 7, No. 12 (1971), 321-322.
11. W. P. M. N. Keizer, J. Shields, and C. D. de Haan, Rain Attenuation Measurements at 94 GHz: Comparison of Theory and Experiment, NATO AGARD Conference Proceedings No. 245 (February 1979).

**CHAPTER IX.—SELECTED BIBLIOGRAPHY**

Although each of the preceding chapters contains numerous references for particular specialty areas, the overall tone and content of the discussions is obviously based upon a greater body of published literature. This section constitutes an attempt to provide a comprehensive listing of such material. Although a detailed description of each publication would be desirable, such a task would require an inordinate effort. Therefore, the references are simply listed by year, with titles and appropriate indexing information. Upon review, the included texts, conference proceedings, and individual reports have been found to contain material of significant technical or historical value in evaluating near-millimeter wave propagation and target/background effects. Some minor duplication of the chapter references may exist, but the bulk of the material has not otherwise been listed previously.

S. M. Kulpa  
E. A. Brown

#### 1979

- E. Spitz (ed.) *Millimeter and Submillimeter Wave Propagation and Circuits*, NATO-AGARD Conference Proceedings, No. 245 (February 1979).
- J. D. Lindberg, *Measured Effects of Battlefield Dust and Smoke on Visible, Infrared, and Millimeter Wavelength Propagation: A Preliminary Report on Dusty Infrared Test-I (DIRT-I)*, U.S. Army Atmospheric Sciences Laboratory, ASL-TR-0021 (January 1979).
- J. C. Wiltse, R. W. McMillan, and D. E. Snider, *Atmospheric Effects on Millimeter Wave Systems*, Georgia Institute of Technology report for U.S. Army Atmospheric Sciences Laboratory, Contract No. DAAG29-76-10-0100 (18 May 1979).
- A *Roadmap for Tactical Millimeter Wave Technology (U)*, Systems Planning Corporation Log No. 79-0717, (February 1979). (CONFIDENTIAL)
- O. M. Essenwanger and M. Thompson, Jr., *Workshop Proceedings on Millimeter and Submillimeter Atmospheric Propagation Applicable to Radar and Missile Systems*, U.S. Army Missile Research and Development Command (20 to 22 March 1979) (to be published).
- 1979 *Microwave Theory and Techniques—Symposium*, Orlando, Florida, Session Y—Active and Passive Remote Sensing (30 April to 2 May 1979).
- A. H. Green, Jr., *Analysis of Linear FM-CW Millimeter Seeker Performance at 35 and 94 GHz (U)*, U.S. Army Missile Command Technical Report RE-75-39 (15 June 1979), AD-C003711. (CONFIDENTIAL)
- R. W. McMillan, R. Rogers, R. Platt, D. Guillory, J. J. Gallagher, and D. E. Snider, *Millimeter Wave Propagation Through Battlefield Dust—Final Report*, U.S. Army Atmospheric Sciences Laboratory, ASL-CR-79-0026 -1 (June 1979).
- C. J. Gibbins et al, *Atmospheric Emissions Measurements Between 22 and 150 GHz*, Appleton Laboratory Report, England (to be published) (1979).

#### 1978

- A. V. Jelalian et al, *Low Probability of Intercept Multifunctional Tactical Sensors*, Air Force Avionics Laboratory, Final Report, AFAL-TR-77-77 (January 1978), AD-B029461.
- S. A. Collins, Jr., *Scientific Services on the Effects of Atmospheric Turbulence on Millimeter Transmissions*, The Ohio State University Electroscience Laboratory, Final Report 7108681 (August 1978).
- Third International Conference on Submillimeter Waves and their Applications*, Guildford, U. K., 29 March to 1 April 1978; Conference Digest published by The Institute of Physics; Proceedings published in *Infrared Physics*, 18, 5/6 (December 1978).

SELECTED BIBLIOGRAPHY (Cont'd)

- D. M. Brown and M. B. Wells, *A Literature Review of Millimeter and Submillimeter Radiation Absorption and Scattering in the Atmosphere*, Radiation Research Associates, Fort Worth, Texas, Report No. RRA-T7804-1 (October 1978).
- O. M. Essenwanger and D. A. Stewart, *Fog and Haze in Europe and their Effects on Performance of Electro-Optical Systems*, U.S. Army Missile Research and Development Command (June 1978), AD-A056431.
- G. F. Dionne et al, *Radiometer Requirements for High Altitude Rocket Plume Observation at Submillimeter Wavelengths*, Lincoln Laboratory Technical Note 1978-3 (31 January 1978), AD-B029247.
- R. Hofer and E. Schanda, *Signatures of Snow in the 5 to 94 GHz Range*, Radio Science, 13, 2 (March-April 1978), 365.
- D. H. Staelin and P. W. Rosenkranz, *High Resolution Passive Microwave Satellites*, The Massachusetts Institute of Technology Research Laboratory of Electronics Report (14 April 1978).
- H. B. Wallace, *140 GHz Captive Antenna Multipath Experiment*, Ballistic Research Laboratories Memorandum Report ARBRL-MR-02855 (August 1978).
- L. G. Mundie and N. E. Feldman, *The Feasibility of Employing Frequencies Between 20 and 300 GHz for Earth-Satellite Communication Links*, RAND Report R-2275-DCA (May 1978), AD-A056100.
- A. E. Salomonovich et al, *Investigation of the Sub-Millimeter Earth Atmosphere Radiation from a Satellite*, P. N. Lebedev Physical Institute Preprint No. 99, Moscow (1978).
- H. J. Liebe and G. G. Gimmetad, *Calculation of Clear Air EHF Refractivity*, Radio Science, 13, 2 (March-April 1978), 245.
- J. H. Rainwater, *Radiometers: Electronic Eyes that "See" Noise*, Microwaves, 17, 9 (September 1978), 58.
- F. E. Goodwin and A. T. Villeneuve, *Geosynchronous Microwave Atmospheric Sounding Radiometer (MASR) Feasibility Studies*, Hughes Aircraft Co. Report, D8647/D9236 (January 1978) National Aeronautics and Space Administration NASA CR-156804.
- D. O. Stringfellow, *Annual Report—Millimeter-Wavelength Discrimination Technology (U)*, Calspan Report No. KH-5751-S-6 (March 1978), AD-C014171. (SECRET)
- R. D. Brewer, *Final Report—Combined Active/Passive Radar (CAPAR) Volume II (U)*, Spectra Research Systems Report SRS-2082-78N (3 August 1978), AD-C016027. (CONFIDENTIAL)
- R. J. Polge and A. Sinh, *Reduction and Analysis of Cross Section Measurement Data at 35 GHz and 94 GHz, Volume III (U)*, The University of Alabama at Huntsville (July 1978), AD-C015411. (CONFIDENTIAL)
- R. L. Olsen et al, *the  $aR^b$  Relation in the Calculation of Rain Attenuation*, IEEE Transactions on Antennas and Propagation, AP-26, 2 (March 1978), 318.
- V. J. Corcoran, *Speckle and Specular Effects in Active Infrared and Submillimeter Imaging Systems*, Institute for Defense Analyses Paper P-1294 (June 1978), AD-A058355.
- R. K. Crane and H. K. Burke, *The Evaluation of Models for Atmospheric Attenuation and*

### SELECTED BIBLIOGRAPHY (Cont'd)

- Backscatter Characteristic Estimation at 95 GHz*, Environmental Research and Technology, Inc. Report No. P-3606 (February 1978).
- G. D. Weathers et al, *Glint at Millimeter Wavelengths*, Proceedings of SOUTHEASTCON, Region 3 Conference, Atlanta (10 to 12 April 1978) (IEEE Cat No 78CHO-1314-4), 405.
- 1977
- W. L. Gamble and T. D. Hodgens, *Propagation of Millimeter and Submillimeter Waves*, U.S. Army Missile Research and Development Command, Technical Report No. TE-77-14 (June 1977).
- M. M. Wisler and J. P. Hollinger, *Estimation of Marine Environmental Parameters Using Microwave Radiometric Remote Sensing Systems*, Naval Research Laboratory Memorandum Report 3661 (November 1977).
- W. H. Pepper et al, *Limited Visibility Operations Assessment (Phases I and II) (U)*, Harry Diamond Laboratories Technical Memorandum HDL-TM-77-16 (December 1977). (SECRET)
- Second International Conference and Winter School on Submillimeter Waves and Their Applications*, San Juan, Puerto Rico (6 to 11 December 1976); Proceedings published in the following journals: *J. Optical Soc. Am.*, 67, 7 (July 1977); *IEEE Transactions on Microwave Theory and Techniques*, MTT-25, 6 (June 1977); *J. Quantum Elect.*, QE-13, 6 (June 1977); *Conference Digest*, IEEE Cat. No. 76-CH-1152-9MTT.
- N. E. Feldman and S. J. Dudzinsky, Jr., *A New Approach to Millimeter-Wave Communications*, RAND Report-1936-RC (April 1977).
- J. D. Harrop et al, *Surface Navy Applications of Millimeter Wave Sensors, Vol. I: Design Trade-Off Study*, Naval Surface Weapons Center Report NSWC/DL TR-3748 (November 1977).
- Ye. P. Dombrovskaya et al, *Investigation of Submillimeter Radiation of Convective Cloud Systems of the Tropical Region From Aboard the "KOSMOS-669" Artificial Earth Satellite*, *Izvestiya Akademii Nauk SSR Seriya Fizika Atmosfery i Okeana*, 13, 4 (1977), 391-398.
- D. A. Stewart, *Infrared and Submillimeter Extinction by Fog*, U.S. Army Missile Research and Development Command Technical Report TR-77-9 (14 July 1977).
- J. H. Rainwater, *Weather Affects MM-Wave Missile Guidance Systems*, *Microwaves* (September 1977), 62.
- R. G. Shackelford and J. J. Gallagher, *Millimeter Wave Beamrider System*, U.S. Army Missile Research and Development Command, Redstone Arsenal, Alabama, Report No. TE-CR-77-7 (August 1977).
- R. G. Reitz, *An Analysis of Smoke Transmittance Measurements and Techniques*, Ballistic Research Laboratories Memorandum Report No. 2798 (November 1977).
- J. D. Weisz, *Climatology Handbook for V Corps Forward Areas*, U.S. Army Human Engineering Laboratory Technical Memorandum 35-77 (December 1977).
- H. B. Holl, *Fundamentals in Visibility*, U.S. Army Missile Research and Development Command Technical Report, TR-77-1 (February 1977).

SELECTED BIBLIOGRAPHY (Cont'd)

- B. N. Harden et al, *Measurements of Rainfall for Studies of Millimetric Radio Attenuation, Microwaves, Optics and Acoustics*, 1, 6 (November 1977), 197.
- T. F. Divine et al, *Adverse Weather Test Range Development (Phase I)*, U.S. Air Force Armament Laboratory Report AFATL-TR-77-121 (October 1977), AD-B029445.
- T. S. Hartwick and D. T. Hodges (eds.), *Far Infrared/Submillimeter Wave Technology/Applications*, Proc. SPIE, 105 (18 to 21 April 1977).
- G. Weathers and E. R. Graf, *Design of Experiment to Characterize the Propagation of Millimeter Waves in Aerosols*, U.S. Army Missile Research and Development Command Technical Report TE-CR-77-10 (30 September 1977), AD-B021851.
- G. Skahill, *A Study of Millimeter Wavelength Radars (U)*, Riverside Research Institute Report F-1/370-4-20 (8 April 1977), AD-C010125. (SECRET)
- G. F. Dionne and J. A. Weiss, *Submillimeter-Wave Spectroradiometry: A Proposed Technique for High-Altitude Rocket Plume Observation (U)*, Lincoln Laboratory Report RMP-88 (27 January 1977). (SECRET)
- J. M. Loomis et al, *Millimeter Wave Beamrider Tests*, U.S. Army Missile Research and Development Command Technical Report, T-78-27 (September 1977), AD-C014238. (CONFIDENTIAL)
- R. K. Crane, *Prediction of the Effects of Rain on Satellite Communications Systems*, Proceedings of the IEEE, 65, 3 (March 1977), 456.
- Proceedings of the Sixth DARPA/Tri-Service Millimeter Wave Conference (U)*, Systems Planning Corporation Log No. 78-0095 (29 to November 1977). (SECRET)
- N. C. Currie et al, *Radar Millimeter Backscatter Measurements from Snow*, Air Force Armament Laboratory Report AFATL TR-77-4 (January 1977), AD-B021148.
- N. C. Currie et al, *Radar Millimeter Backscatter Measurements on Hard Targets (U)*, Air Force Armament Laboratory Report AFATL-TR-77-13 (January 1977), AD-C011261. (CONFIDENTIAL)
- N. C. Currie et al, *Radar Millimeter Backscatter Measurements, Vol I: Snow and Vegetation*, Air Force Armament Laboratory Report AFATL-TR-77-92 (July 1977), AD-B030190.
- N. C. Currie et al, *Radar Millimeter Backscatter Measurements, Vol II: Target Signatures (U)*, Air Force Armament Laboratory Report AFATL-TR-77-92, Vol. II (July 1977), AD-C015118. (CONFIDENTIAL)
- 1976
- A. R. Downs, *A Review of Atmospheric Transmission Information in the Optical and Microwave Spectral Regions*, Ballistic Research Laboratories Memorandum Report No. 2710 (December 1976).
- K. F. Künzi and E. Schanda, *Passive Microwave Remote Sensing at the University of Berne, Switzerland*, Presentation to the European Association of Remote Sensing Laboratories, Lyngby, Denmark (24 to 25 September 1976).
- H. E. King et al, *90 GHz Radiometric Imaging*, U.S. Air Force Space and Missile Systems Organization Report, SAMSO-TR-76-37 (19 February 1976), AD-A022241.
- C. R. Christensen and A. Kozma, *The Effects of Speckle on Resolution of High Contrast and*

SELECTED BIBLIOGRAPHY (Cont'd)

- Continuous Tone Objects*, U.S. Army Missile Command Technical Report RR-77-2 (14 December 1976).
- E. J. McCartney, *Optics of the Atmosphere*, John Wiley and Sons, New York (1976).
- Proceedings of the Optical-Submillimeter Atmospheric Propagation Conference, Executive Summary and Volume II (U)*, The Office of the Director, Defense Research and Engineering Log No. 77-139 (6 to 9 December 1976). (SECRET)
- R. W. Nelson, *Millimeter Target Measurements on Seeker Effort (U)*, U.S. Army Missile Command Technical Report RE-76-23 (January 1976). (CONFIDENTIAL)
- R. O. Hundley and C. G. Gabbard, *Strategic Technology Final Technical Report (U)*, R&D Associates Report RDA-TR-1900-007 (October 1976), AD-C008628. (SECRET)
- J. W. Mink, *A Technique for Simultaneous Measurement of Attenuation and Bistatic Scatter Due to Rainfall at Millimeter Waves*, Radio Science, 11, 11 (November 1976), 915.
- M. N. Kaidanovskii et al, *Experimental Characteristics of the Fluctuations in the Radio Emission From Clouds at Millimeter Wavelengths*, Izvestiya Vysshikh Uchebnykh Zavendenii, Radiofizika, 19, 11 (November 1976), 1644.
- V. W. Richard, *Millimeter Wave Radar: Applications to Weapons Systems*, Ballistic Research Laboratories, Report No. 2631 (June 1976), AD-B012103.
- D. C. Hogg, *Millimeter Wave Propagation Through Rain on Short Terrestrial Paths*, DoD Workshop on Millimeter Wave Terminal Guidance Systems (Second), Rome Air Development Center, Report No. RADC-TM-76-9 (May 1976), AD-A026270.
- R. D. Hayes et al, *Backscatter from Ground Vegetation at Frequencies Between 10 and 100 GHz*, AP-S International Symposium (1976), 93-96.

1975

- C. C. Chen, *Attenuation of Electromagnetic Radiation by Haze, Fog, Clouds, and Rain*, Rand Corporation, Report No. R-1694-PR (April 1975), AD-A011642.
- J. Sander, *Rain Attenuation of Millimeter Waves at  $\lambda = 5.77, 3.3,$  and 2 mm*, IEEE Transactions on Antennas and Propagation, AP-23, 2 (March 1975), 213.
- L. Lo et al, *Attenuation of 8.6 and 3.2 mm Radio Waves by Clouds*, IEEE Transactions on Antennas and Propagation, AP-23, 6 (November 1975), 792.
- R. O. Hundley, *Strategic Technology Final Technical Report (U)*, R&D Associates Report RDA-TR-4600-018 (July 1975). AD-C002541. (SECRET)
- R. O. Hundley, *Strategic Technology Quarterly Technical Report (U)*, R&D Associates, Report RDA-TR-4600-17 (May 1975), AD-C002185. (SECRET)
- S. C. Woolcock, *Report of the W5 Subgroup of the TTC Panel on the U.K. Radio Modeling Facilities at EMI Electronics Limited (U)*, EMI Document DMP.6317 (November 1975). (CONFIDENTIAL)
- M. A. Kolosov (ed.), *Radiowave Propagation*, Izd-vo Nauka, Moscow (1975). AD-B022487.
- H. J. Liebe, *Studies of Oxygen and Water Vapor Microwave Spectra Under Simulated Atmospheric Conditions*, Office of Telecommunications Report 75-65 (June 1975).

SELECTED BIBLIOGRAPHY (Cont'd)

- D. C. Hogg and T. Chu, *The Role of Rain in Satellite Communications*, Proc. IEEE, 63, 9 (September 1975).
- S. J. Dudzinsky, Jr., *Atmospheric Effects on Terrestrial MM-Wave Communications*, Microwave Journal (December 1975), 39.
- P. W. Kruse and V. Garber, *Technology for Battlefield Target Recognition in Inclement Weather*, Proceedings of the Third International IRIS Conference (1975).
- R. B. Dybdal and H. E. King, *93 GHz Radar Cross Section Measurements of Satellite Elemental Scatterers*, U.S. Air Force Space and Missile Systems Organization Report SAMSO-TR-75-127 (10 April 1975).
- N. C. Currie et al, *Radar Foliage Penetration Measurements at Millimeter Wavelengths*, Georgia Institute of Technology, Engineering Experiment Station Technical Report No. 4 (December 1975).
- N. C. Currie, *Analysis of Radar Rain Return at Frequencies of 9.375, 35, 70 and 95 GHz*, Georgia Institute of Technology, Engineering Experiment Station Technical Report No. 2 (1 February 1975).
- N. C. Currie, *Radar Land Clutter Measurements at Frequencies of 9.5, 16, 35 and 95 GHz*, Georgia Institute of Technology, Engineering Experiment Station Technical Report No. 3 (2 April 1975).
- J. J. Gallagher et al, *Applications of Submillimeter Wave Gigawatt Sources*, Georgia Institute of Technology Final Report GT/EES A-1717 (1975).
- K. Aganbekyan et al, *Propagation of Submillimeter, Infrared and Optical Waves in the Earth's Atmosphere*, Institute Radiotekhniki i Elektroniki, Nauka (1975), 187.
- 1974
- A. Barrow, *Radar Images of a Cherry Picker Obtained at 80 GHz*, EMI Electronics Ltd. Report DMP.6257 (December 1974). (FOR OFFICIAL USE ONLY).
- First International Conference on Submillimeter Waves and Their Application*, Atlanta (5 to 7 June 1974), Conference Digest, IEEE Cat. No. 74-CHO-856-6MTT; Proceedings published in IEEE Transactions on Microwave Theory and Techniques, MTT-22 (12 December 1974).
- K. Tomiyasu, *Remote Sensing of the Earth by Microwaves*, Proc. IEEE, 62, 1 (January 1974), 86.
- G. Schaerer, *Passive Sensing Experiments and Mapping at 3.3 mm Wavelength*, Remote Sensing of Environment, 3 (1974), 117.
- A. S. Khaykin, *Optical Systems of Submillimeter Telescopes Carried Above the Earth*, Works of the Order of Lenin Physics Institute imeni P. N. Lebedev, 77, Radiotelescopes (in Russian) (1974), 56.
- A. Ye. Salomonovich and A. S. Khaykin, *Outer Atmospheric Research in the Submillimeter Band Using On-board Telescopes*, Moscow Radiotelescopes (in Russian), 77 (1974), 33.
- R. K. Crane, *The Rain Range Experiment—Propagation Through a Simulated Rain Environment*, IEEE Transactions on Antennas and Propagation, AP-22, 2 (March 1974), 321.
- 1973
- L. D. Strom, *Applications for Millimeter Radars (U)*, Systems Planning Corporation Report 108 (31 December 1973). AD-529566. (CONFIDENTIAL)

### SELECTED BIBLIOGRAPHY (Cont'd)

- R. D. Hayes and F. B. Dyer, *Land Clutter Characteristics for Computer Modeling of Fire Control Radar Systems*, Georgia Institute of Technology Engineering Experiment Station, Technical Report No. 1 (May 1973), AD-912490.
- D. W. Webster, *Military Potential of the Extreme Infrared—Technology and Applications*, Naval Weapons Center Report NWC TP 5565 (November 1973), AD-915347.
- L. G. Mundie, *Passive Millimeter-Wave Radiometry and Some Possible Applications (I)*, RAND Report R-1175-ARPA (April 1973), AD-528057. (CONFIDENTIAL)
- F. P. Wilcox et al, *Analysis and Definition of Millimeter-Wave Radars*, Goodyear Aerospace Corporation, Report No. AFAL-TR-73-232 (July 1973), AD-526669L.
- J. P. Hollinger, *Microwave Properties of a Calm Sea*, Naval Research Laboratory Report No. 7110-2 (15 August 1973).
- 1972
- L. E. Volger et al, *Bibliography on Propagation Effects from 100 GHz to 1000 THz*, Office of Telecommunications, Report OT/TRER 30 (March 1972).
- R. N. Trebits et al, *MM-Wave Reflectivity of Land and Sea*, *Microwave Journal*, 21, 8 (August 1972), 49.
- 1971
- N. E. Gaut and E. C. Reifstein, III, *Interaction Model of Microwave Energy and Atmospheric Variables*, National Aeronautics and Space Administration NASA Report No. CR-61348 (20 April 1971), AD-N7125079.
- W. J. Brinks and R. D. Hayes, *A Study of Factors Basic to the Development of Millimeter Wave Radiometric Terminal Tracking*, Harry Diamond Laboratories Report R-110-71-5 (15 September 1971).
- R. A. McClatchey, *Optical Properties of the Atmosphere (Revised)*, Air Force Cambridge Research Laboratories, Report No. AFCRL-71-0279 (May 1971).
- A. G. Kislyakov, *Radioastronomical Investigation in the Millimeter and Submillimeter Bands*, *Sov. Phys. Uspekhi*, 13, 4 (Jan-Feb 1971), 495.
- 1970
- J. Fox (ed.), *Proceedings of the Symposium on Submillimeter Waves*, Polytechnic Press, Brooklyn, NY (31 March to 2 April 1970).
- V. I. Rozenberg, *Radar Characteristics of Rain in Submillimeter Range*, *Radio Engineering and Electronic Physics*, 15, 12 (1970), 2157.
- Yu. S. Babkin et al, *Measurement of Attenuation in Rain over 1 km Path at a Wavelength of 0.96 mm*, *Radio Engineering and Electronic Physics*, 15, 12 (1970).
- A. Miller and J. C. Thompson, *Elements of Meteorology*, Charles E. Merrill Publishing Co., Columbia, Ohio (1970).
- V. J. Falcone and R. Dyer, *Refraction, Attenuation, and Backscattering of Electromagnetic Waves in the Troposphere*, Air Force Cambridge Research Laboratories, Report No. AFCRL-70-0007 (January 1970).
- D. E. Setzer, *Computed Transmission Through Rain at Microwave and Visible Frequencies*, *Bell System Technical Journal* (October 1970), 1873-1892.

## SELECTED BIBLIOGRAPHY (Cont'd)

1969

R. A. Valitov, *Submillimeter Wave Technology, Soviet Radio, Moscow (1969).*

F. G. R. Warren, *Millimeter Investigations—Volume 2: Millimeter Wave Propagation and its Prediction, Project Mallard Final Report, RCA Ltd., Montreal (January 1969), AD-857433.*

W. J. Lese, Jr., et al, *An Application of Pattern Recognition to Radiometric Target Detection, Ballistic Research Laboratories Memorandum Report No. 1962 (February 1969), AD-684904.*

1968

E. E. Alshuler, *Atmospheric Effects on Propagation at Millimeter Wavelengths, IEEE Spectrum (July 1968).*

R. A. McGee, *Millimeter Wave Radiometric Detection of Targets Obscured by Foliage, Ballistic Research Laboratories Memorandum Report No. 1901 (January 1968), AD-667962.*

T. F. Rogers, *Propagation in the Neutral Atmosphere, Chapter 2, Part I of "Radar Astronomy,"* edited by J. V. Evans and T. Hagfors, McGraw-Hill Book Company, New York (1968).

*Microwave Journal, Special Issue on State-of-the-Art—Millimeter Wave Communications, 11, 11 (November 1968).*

1967

J. E. Kammerer and K. A. Richer, *Wide-Angle Bistatic Measurements of Reflections from Periodic Surfaces and Dielectric Camouflage at 140 GHz (U), Ballistic Research Laboratories Memorandum Report 1820 (May 1967), AD 383424. (SECRET)*

C. L. Wilson, *Camouflage Against Millimeter Waves (U), Ballistic Research Laboratories Memorandum Report 1836 (April 1967), AD-381886. (SECRET)*

*Microwave Journal, Special Issue on Millimeter Wave Technology—Present and Future Status, 10, 12 (November 1967).*

1966

J. E. Kammerer and K. A. Richer, *140 GHz Millimetric Bistatic Continuous Wave Measurements Radar, Ballistic Research Laboratories Memorandum Report No. 1730 (January 1966), AD-484693.*

J. E. Kammerer and K. A. Richer, *Cross Section Measurements of U.S. Army Targets by 140 GHz Radar (U), Ballistic Research Laboratories Memorandum Report 1785 (August 1966), AD-378097. (CONFIDENTIAL)*

L. A. Hoffman, *Propagation Observations at 3.2 Millimeters, Proceedings of the IEEE, 54, 4 (April 1966), 449.*

*Proceedings on the IEEE, Special Issue on Millimeter Waves and Beyond, 54, 4 (April 1966).*

L. A. Morgan and C. A. Ekdahl, *Millimeter Wave Propagation, Smyth Research Associates, San Diego, Report No. RADC-TR-76-342 (August 1966), AD-489424.*

Pre-1966

C. W. Tolbert, A. W. Straiton, and J. R. Gerhardt, *A Study and Analysis of Anomalous Atmospheric Water Vapor Absorption of Millimeter Wavelength Radiation, Report 117, EBRL, University of Texas (October 1960), AD-246528.*

SELECTED BIBLIOGRAPHY (Cont'd)

- L. Frenkel and E. P. Valkenburg, *Propagation of Millimeter and Submillimeter Waves*, Martin-Marietta Corp. Final Report OR 6607 (July 1965).
- J. E. Kammerer and K. A. Richer, *4.4 m Near-Earth Antenna Multipath Pointing Errors*, Ballistic Research Laboratories Memorandum Report No. 1559 (March 1964), AD-443211.
- E. S. Rosenblum, *Atmospheric Absorption of 10-400 KMCPS Radiation*, *Microwave Journal* (March 1961), 91-96.
- D. C. Hogg and W. W. Mumford, *The Effective Noise Temperature of the Sky*, *The Microwave Journal* (March 1960), 80.
- T. L. Booth and E. Weger, *Feasibility Study of Target Location and Charting by Passive Microwave Radiometry*, Rome Air Development Center Report RADC-TR-59-125 (25 June 1959).
- S. S. Penner et al, *Relations Between Molecular Gas Absorptivities and Emissivities*, Jet Propulsion Laboratory Technical Report No. 29 (October 1958), AD-204286.
- B. J. Mason, *The Physics of Clouds*, Oxford University Press, London (1957).
- D. E. Kerr (ed.), *Propagation of Short Radio Waves*, MIT Radiation Laboratories Series, Vol. 13, McGraw-Hill Book Co., Inc., New-York (1951).